Article

Discovery and Preclinical Development of IIIM-290, an Orally Active Potent Cyclin-Dependent Kinase Inhibitor

Sandip B. Bharate,[*,†,‡,O] Vikas Kumar,[‡,§,O] Shreyans K. Jain,[§,O] Mubashir J. Mintoo,[‡,⊥,O]
Santosh K. Guru,[⊥] Vijay K. Nuthakki,[†] Mohit Sharma,[†] Sonali S. Bharate,[§] Sumit G. Gandhi,[‡,#]
Dilip M. Mondhe,[‡,⊥] Shashi Bhushan,[‡,∇] and Ram A. Vishwakarma[*,†,‡]

[†]Medicinal Chemistry Division, CSIR-Indian Institute of Integrative Medicine, Canal Road, Jammu-180001, India

[‡]Academy of Scientific & Innovative Research, CSIR-Indian Institute of Integrative Medicine, Canal Road, Jammu-180001, India

[§]Preformulation Laboratory, PK–PD Toxicology & Formulation Division, CSIR-Indian Institute of Integrative Medicine, Canal Road, Jammu-180001, India

[§]Natural Products Chemistry Division, CSIR-Indian Institute of Integrative Medicine, Canal Road, Jammu-180001, India

[⊥]Cancer Pharmacology Division, CSIR-Indian Institute of Integrative Medicine, Canal Road, Jammu-180001, India

[#]Plant Biotechnology Division, CSIR-Indian Institute of Integrative Medicine, Canal Road, Jammu-180001, India

[∇]Indian Pharmacopeia Commission, Sec-23, Raj Nagar, Ghaziabad 201002, India
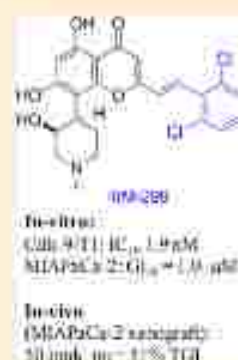
S Supporting Information

ABSTRACT: Rohitukine (1), a chromone alkaloid isolated from Indian medicinal plant *Dysoxylum binectariferum*, has inspired the discovery of flavopiridol and riviciclib, both of which are bioavailable only via intravenous route. With the objective to address the oral bioavailability issue of this scaffold, four series of rohitukine derivatives were prepared and screened for Cdk inhibition and cellular antiproliferative activity. The 2,6-dichloro-styryl derivative IIIM-290 (11d) showed strong inhibition of Cdk-9/T1 (IC$_{50}$ 1.9 nM) kinase and Molt-4/MIAPaCa-2 cell growth (GI$_{50}$ < 1.0 μM) and was found to be highly selective for cancer cells over normal fibroblast cells. It inhibited the cell growth of MIAPaCa-2 cells via caspase-dependent apoptosis. It achieved 71% oral bioavailability with in vivo efficacy in pancreatic, colon, and leukemia xenografts at 50 mg/kg, po. It did not have CYP/efflux pump liability, was not mutagenic/genotoxic or cardiotoxic, and was metabolically stable. The preclinical data presented herein indicates the potential of 11d for advancement in clinical studies.

INTRODUCTION

Cell division is one of the basic requirements for survival of all living cells. Classically, the cell growth occurs via four distinct phases, namely G1, S, G2, and M phases. Progression through each of these phases is tightly controlled by the interaction of cyclin-dependent kinases (Cdks) and cyclins. Cdks are a family of serine threonine protein kinases that interact with associated cyclins to activate their function. Cdk-1, 2, 3, 4, and 6 directly interfere with cell cycle, and Cdk-8, 9, and 7 play a crucial role as regulator of transcription.[1,2] A number of cancers are associated with hyperactivation of Cdks as a result of mutation of Cdk genes or Cdk inhibitory genes.[3] Therefore, in recent

years, Cdk inhibitors have elicited great interest in oncology to discover novel anticancer therapeutics.[4] Two Cdk inhibitors have reached the market; palbociclib (Pfizer) was the first one to enter the market (2015) for treatment of breast cancer.[5–8] In 2017, second Cdk inhibitor ribociclib (Novartis) received FDA approval for HER2-negative advanced breast cancer in combination with an aromatase inhibitor.[9] Eli Lilly's abemaciclib (LY2835219) is another Cdk-4/6 inhibitor that has recently completed Phase III trial.[10–12] There are several

Figure 1. Structures of rohitukine (1) and its inspired anticancer candidates 2 and 3.

Figure 2. Design of four different series A–D of rohitukine derivatives.

follow-on Cdk inhibitor candidates in the clinical pipeline (with >100 clinical studies ongoing) including rigosertib sodium, FLX925, dinaciclib, P276-00 (riviciclib), etc.[13]

In addition to the Cdks (Cdk-2,4,6) involved in cell cycle regulation, the inhibition of transcriptional Cdks (particularly, Cdk-9) are also gaining great interest for effective anticancer therapy because of their role in controlling short-lived mitotic regulatory kinases and apoptosis regulators such as Mcl-1 for their survival.[14–16] Among the transcriptional Cdks, the Cdk-9 has been investigated as a therapeutic target by many groups.[17–20] Flavopiridol (alvocidib), the first Cdk inhibitor to enter clinical trials, is the most active Cdk-9 inhibitor reported so far, with IC$_{50}$ value of 20 nM.[21,22]

Rohitukine (1) is a chromone alkaloid, initially isolated from *Amoora rohituka* (Roxb.),[23] and later from *Dysoxylum binectariferum* Hook. (Meliaceae).[24–26] This alkaloid is present in abundance in all parts of *Dysoxylum binectariferum*,[27] and therefore, it is being used as a primary source for isolation of this precious natural product. Inspired from rohitukine, two clinical candidates have been discovered, *viz.* flavopiridol (2) and riviciclib (P276-00, 3; structures are shown in Figure 1). Flavopiridol inhibits a number of Cdks and other kinases; however, its primary mechanism of action is believed to be through Cdk-9 inhibition, leading to down-regulation of the transcription of antiapoptotic proteins in cancer cells.[11,22,28] It was evaluated in a number of clinical trials as a single agent[29–31] as well as in combination[32,33] with other anticancer agents, and recently, it received orphan drug status from FDA for treatment of AML and CLL.[34,35] Riviciclib (P276-00)[36–41] is another potent inhibitor of Cdks (IC$_{50}$ for Cdk-4/D1 = 63 nM, Cdk-9/T1 = 20 nM) discovered from this scaffold, which has recently completed phase II clinical trials in patients with relapsed or refractory mantle cell lymphoma.[42] However, both these clinical candidates are administered in preclinical and clinical studies as a daily intravenous (IV) infusion and have no oral bioavailability. In the present work, we set out to address the issue of oral bioavailability of rohitukine scaffold, and we now report a discovery of the first preclinical candidate IIIM-290[43] with 71% oral bioavailability from this scaffold.

The synthesis strategy employed to prepare new derivatives was semisynthetic modifications on rohitukine, as this approach
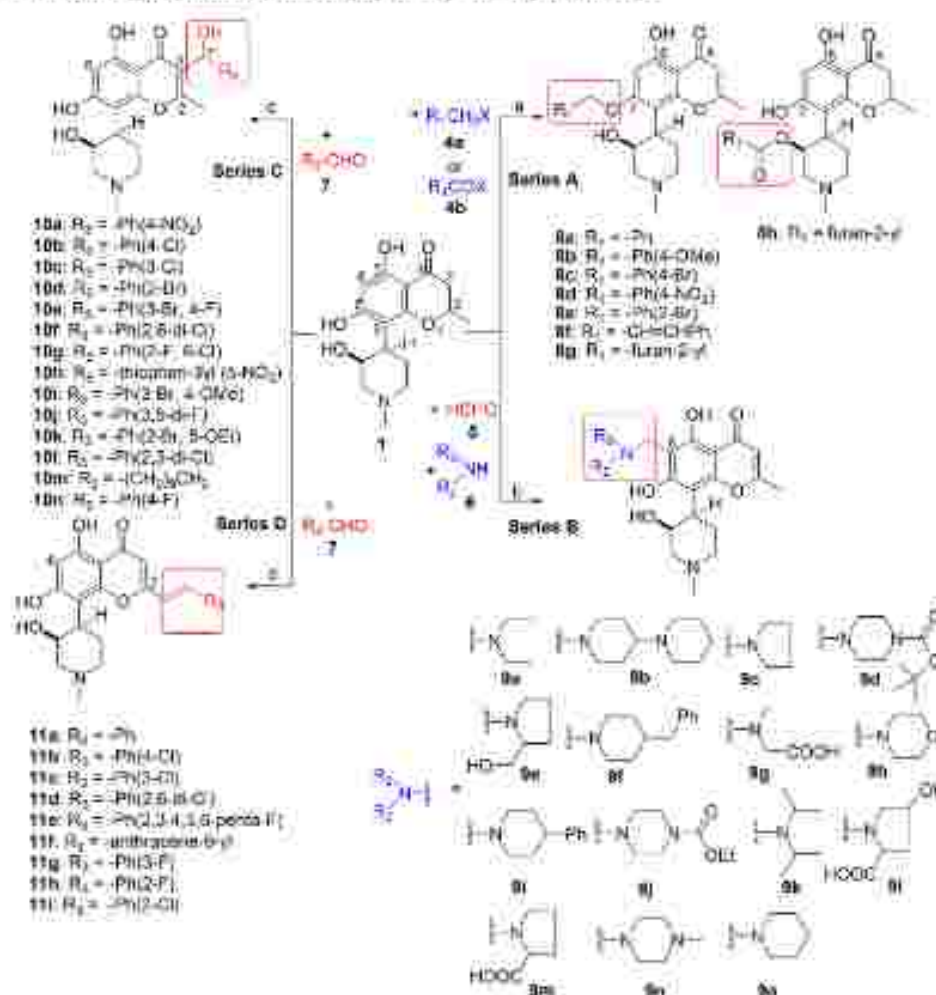
was never explored in prior medicinal chemistry efforts on this scaffold. Four series of rohitukine derivatives were designed based on the known structural information[44,45] and reported structure–activity relationship (SAR) on flavopiridol.[46] All synthesized compounds were screened for Cdk inhibition and cellular antiproliferative activity in a panel of cancer cell lines. The best-identified lead IIIM-290 (11d) was subjected to complete preclinical characterization.

RESULTS AND DISCUSSION

Design and Synthesis of Rohitukine Derivatives. To design new derivatives of rohitukine, we utilized prior structural information on the cocrystal structure of Cdk-2 with deschloroflavopiridol[47] and flavopiridol[48] and previous work of Murthi,[49] Kim,[46] Schoepfer,[50] and Ahn[51] on this scaffold. On comparing the lipophilicity of rohitukine and flavopiridol, it was observed that the additional 2-chlorophenyl ring present in the later compound provided extra lipophilicity, which was translated into its cytotoxic properties (cLogP of rohitukine, 1.01; flavopiridol, 3.42; MCF-7 of rohitukine, GI$_{50}$ = 15 μM; flavopiridol GI$_{50}$ = 26 nM[51]). This observation prompted us to incorporate lipophilic substituents on rohitukine to fine-tune its Cdk inhibition and cellular activity. Taking the advantage of easy isolation of natural alkaloid rohitukine from any part of the *D. binectariferum* tree in good quantity,[28] it was decided to follow a semisynthetic approach for creating structurally diverse compounds within this scaffold. Four series of modifications were planned, as shown in Figure 2. This includes (a) preparation of C7-O-ether derivatives (series A), (b) Mannich reaction at C6 active hydrogen (series B), (c) Baylis–Hillman reaction with aldehydes (series C), and (d) Claisen–Schmidt condensation (styrylation at C2-methyl) with aryl aldehydes (series D).

The powdered leaves or barks of *Dysoxylum binectariferum* were subjected to cold maceration with methanol. The obtained methanolic extract was loaded on a silica gel column chromatography, eluting with DCM/MeOH to get rohitukine (1) in bulk quantity. Rohitukine was obtained in 0.8–3% w/w from both parts of the plant.

The isolated rohitukine was subjected to four series of semisynthetic modifications (Scheme 1). To synthesize series A

Scheme 1. Synthesis of Rohitukine Derivatives 8a–h, 9a–o, 10a–o, and 11a–i[a]

Series C

Series A

Series D

Series B

10a: R₂ = -Ph(4-NO₂)
10b: R₂ = -Ph(4-Cl)
10c: R₂ = -Ph(3-Cl)
10d: R₂ = -Ph(2-Br)
10e: R₂ = -Ph(3-Br, 4-F)
10f: R₂ = -Ph(2,6-di-Cl)
10g: R₂ = -Ph(2-F, 6-Cl)
10h: R₂ = -thiomen-3-yl (5-NO₂)
10i: R₂ = -Ph(2-Br, 4-OMe)
10j: R₂ = -Ph(3,5-di-F)
10k: R₂ = -Ph(2-Br, 5-OEt)
10l: R₂ = -Ph(2,3-di-Cl)
10m: R₂ = -(CH₂)₃CH₃
10n: R₂ = -Ph(4-F)

8a: R₁ = -Ph
8b: R₁ = -Ph(4-OMe)
8c: R₁ = -Ph(4-Br)
8d: R₁ = -Ph(4-NO₂)
8e: R₁ = -Ph(2-Br)
8f: R₁ = -CH=CHPh
8g: R₁ = -furan-2-yl

8h: R₁ = furan-2-yl

11a: R₂ = -Ph
11b: R₂ = -Ph(4-Cl)
11c: R₂ = -Ph(3-Cl)
11d: R₂ = -Ph(2,6-di-Cl)
11e: R₂ = -Ph(2,3,4,5,6-penta-F)
11f: R₂ = -anthracen-9-yl
11g: R₂ = -Ph(3-F)
11h: R₂ = -Ph(2-F)
11i: R₂ = -Ph(2-Cl)
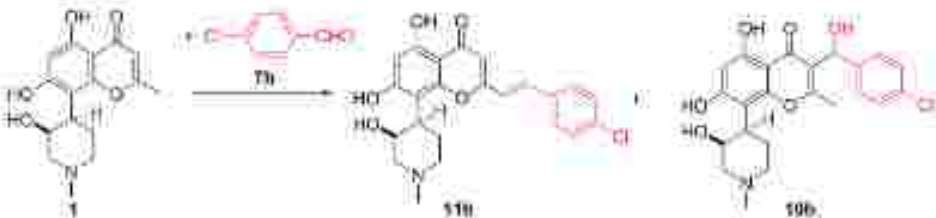
9a 9b 9c 9d
9e 9f 9g 9h
9i 9j 9k 9l
9m 9n 9o

compounds, various base catalyzed O-benzylation methods were attempted. Initially, a mixture of mono-, di-, and tri-O-benzylation products were observed, under different basic conditions (K₂CO₃, NaH, NaOH, CH₃ONa, etc.) and solvents (acetone, THF, dioxane, DCM, etc.). Subsequent attempts discovered that the treatment of rohitukine with alkyl or benzyl halide in the presence of KF-alumina using grind-stone chemistry results in the regioselective formation of 7-O-ethers.[a] Our motivation to synthesize this series (series A) was to check the tolerance of 7-hydroxyl group with respect to the biological activity. In series A compounds (e.g., 8a), the presence of a peak at δ 12.78 ppm in the ¹H NMR spectrum represents the presence of free phenolic OH at position C-5, which is H-bonded with C-4 carbonyl oxygen. This also indicated that benzylation occurred regioselectively at 7-OH position. This series of derivatives also showed characteristic additional peaks for -O-CH₂-Ph at δ 5.15 and 4.44 ppm in the ¹H NMR spectrum. Next, one esterification reaction was also attempted, using furoyl chloride in similar reaction conditions. Interestingly, in contrast to the etherification, furoylation occurred at piperidinyl OH group. This was revealed from the ¹H NMR spectrum of compound 8h wherein there is a significant downfield shift in the chemical shift value of O-

linked CH proton of piperidine ring. The δ value was shifted from 4.14 to 5.58 ppm.

Mannich products (series B) at position C-6 in rohitukine (1) were synthesized by conventional Mannich reaction protocol. The reaction was performed with different secondary amines in the presence of formalin solution and DMSO as a solvent under the heating (60–70 °C, 5 h) condition. In this series, the ¹H NMR spectrum showed that the C6 aromatic proton of rohitukine disappears with the appearance of additional expected peaks (for R₂R₃-N-CH₂-Ar) of Mannich product.

Based on the known SAR,[44] it was understood that the substitution at the 2-position of chromone nucleus helps in gaining selectivity within Cdks and improves its Cdk inhibition activity. The flavopiridol possesses 2-chlorophenyl substituent, whereas rohitukine has 2-methyl substituent. The flavopiridol is at least a 10-fold more potent Cdk-9 inhibitor than rohitukine. Therefore, it was decided to investigate substitution at the C-2 methyl of rohitukine. For this, the Claisen–Schmidt condensation with aryl aldehydes was planned. A model reaction of rohitukine (1) with 4-chlorobenzaldehyde (7b) was investigated. Various weaker to stronger bases were investigated for

Table 1. Reaction Conditions for Condensation of Rohitukine (1) with 4-Chlorobenzaldehyde (7b)[a]

entry	base (equiv)	solvent	temp (°C)	time	11b, % yield	10b, % yield
1	DABCO (1)	MeOH	25	24 h	0	20
2[b]	DABCO (1)	MeOH	25	15 days	0	65
3	DABCO (1)	MeOH	25	20 days	0	70
4	DABCO (10)	MeOH	25	15 days	0	72
5[b]	KOH (10)	MeOH	25	15 days	0	30
6[b]	KOH (10)	MeOH	110	15 days	65	5
7[b]	KOH (10)	MeOH	110	20 days	65	5
8[b,d]	KOH (10)	MeOH	110	10 h	81	5

[a]Rohitukine (0.328 mmol) and aldehyde (0.394 mmol). [b]KOH solution was made in water, and then it was added to the reaction mixture (containing a substrate in methanol). [c]Optimized reaction condition for synthesis of Baylis–Hillman products. [d]Optimized reaction condition for synthesis of styryl products.

this reaction. Reaction optimization results are summarized in Table 1.

In an effort toward the synthesis of styryl derivative **11b**, the reaction of rohitukine (1) with 4-chlorobenzaldehyde (7b) was performed in the presence of DABCO as a base at room temperature for 24 h. It was observed that a Baylis–Hillman reaction was followed and that the corresponding 3-substituted Baylis–Hillman product **10b** was formed in 20% yield (entry 1 of Table 1). Further optimization efforts with respect to time indicated that longer duration of reaction (up to 15–20 days) results in the formation of Baylis–Hillman product **10b** in >70% yield (entries 3–4). To get styryl derivative **11b**, further variation in the base and reaction temperature was studied. It was observed that in the presence of KOH as a base at reflux temperature, styryl derivative **11b** was formed as the primary product, along with **10b** as a minor product. Thus, the reaction conditions 2 and 8 (Table 1) were optimal for the synthesis of products **10b** and **11b**, respectively. Interestingly, when product **10b** was further refluxed under reaction conditions mentioned in entry 8, styryl product **11b** was formed. Results presented in Table 1 indicate that when rohitukine was treated with aryl aldehyde in the presence of a weak base in methanol, it undergoes Baylis–Hillman reaction (Series C) at room temperature while under reflux condition in the presence of a strong base, it follows Claisen–Schmidt condensation (Series D). The Baylis–Hillman reaction proceeded with slow kinetics, and full conversion was not observed even after 20 days. Typical reaction time for this was 15 days at room temperature. Using optimized reaction conditions, a series of derivatives were prepared. In total, 14 Baylis–Hillman adducts **10a–n** and nine styryl products **11a–i** were synthesized (Scheme 1). In case of all styryl products, trans-isomer was formed as a major product, with traces of cis-product in few cases.

The ^{1}H NMR of Baylis–Hillman product **10a** showed a multiplet of 2H at δ 5.9 ppm, for one aromatic proton (H-6) and another proton (7'-H), confirming the formation of Baylis–Hillman adduct at the C-3 position of rohitukine. The position of the newly formed bond was confirmed by HMBC correlations wherein the 7'-H is correlated with 2-CH₃ and C=O. The ^{1}H NMR spectra (series D) of styryl derivative **11a** showed the presence of a typical doublet at δ 6.92 and 7.44

ppm with trans-coupling ($J = 16$ Hz) corresponding to the newly constructed styryl bond. As depicted in Scheme 1, a total of 46 derivatives of rohitukine were synthesized and characterized based on their spectral properties.

In Vitro Inhibition of Cdk-2/A and Cdk-9/T1. Rohitukine (1) along with all four series of rohitukine derivatives **8a–h**, **9a–o**, **10a–n**, and **11a–i** were screened for in vitro inhibition of Cdk-2/A and Cdk-9/T1. The initial screening was performed at a single concentration of 0.5 μM, followed by the determination of IC₅₀ values of active compounds. At 0.5 μM, rohitukine showed strong inhibition (75%) of Cdk-9/T1; however, only 10% inhibition of Cdk-2/A was observed. On determination of IC₅₀ values, it was observed that rohitukine inhibits Cdk-2/A and Cdk-9/T1 with IC₅₀ values of 7.3 and 0.3 μM, respectively. The single concentration results of all derivatives are shown in Table 2. Among 7-O-ether derivatives **8a–h** (series A), none of the compounds was active, indicating that substitution at the 7-hydroxy position is not favorable for Cdk inhibition. Series B compounds **9a–o** also showed weak activity against Cdk-2/A and Cdk-9/T1 at 0.5 μM, indicating that introduction of any hydrophilic (nitrogen containing) functional group at this position is not tolerable probably because of the change in the orientation of the molecule in enzyme cavity (interaction of **9a** with Cdk-9 is shown in section S4 of the Supporting Information). Among Baylis–Hillman adducts (series C), again most of the compounds showed weak or no activity, the best among this series was compound **10d** (29% inhibition of Cdk-9/T1 at 0.5 μM). Like C7-OH and C-6 positions, the substitution at C-3 position was also not tolerated with respect to Cdk-2/A and Cdk-9/T1 inhibition activity. In series D, the modification at the 2-methyl position of rohitukine was found to be most favorable and tolerable.

The Cdk screening results shown in Table 2 indicated that most of the compounds of series D (**11a–i**) showed >50% inhibition of Cdk-9/T1 at 0.5 μM. Therefore, the IC₅₀ values were determined for all compounds from series D, and results are presented in Table 3. The 2,6-dichloro styryl derivative **11d** was found to be the most potent Cdk-2/A and Cdk-9/T1 inhibitor with IC₅₀ values of 16 and 1.9 nM, respectively.

Table 2. In Vitro Inhibition of Cdk-2/A and Cdk-9/T1 and Cellular Antiproliferative Activity of Rohitukine Derivatives at Single Concentration

entry	enzyme inhibition % inhibition (±SD) at 0.5 μM[a]		cellular activity % growth inhibition (±SD) at 10 μM[b]				
	Cdk-2/A	Cdk-9/T1	HL-60	PC-3	MIAPaCa-2	MCF-7	Caco-2
1	10 ± 2.3	75 ± 2.3	85 ± 3.4	33 ± 3.5	2 ± 0.4	15 ± 1.2	12 ± 0.5
8a	10 ± 0.7	0	24 ± 1.2	41 ± 0.6	14 ± 0.8	1 ± 2.3	18 ± 0.5
8b	10 ± 0.9	0	23 ± 1.3	35 ± 2.1	15 ± 0.4	16 ± 1.5	8 ± 0.4
8c	0	0	27 ± 0.3	17 ± 0.6	13 ± 1.2	14 ± 1.9	13 ± 2.8
8d	0	5 ± 1.5	18 ± 0.7	23 ± 0.9	12 ± 0.5	39 ± 1.3	14 ± 1.9
8e	6 ± 1.1	0	3 ± 0.1	32 ± 1.3	30 ± 2.1	43 ± 2.5	15 ± 3.9
8f	7 ± 0.4	8 ± 0.5	21 ± 2.5	16 ± 1.4	11 ± 0.7	7 ± 0.2	9 ± 0.3
8g	7 ± 1	8 ± 0.2	32 ± 1.2	14 ± 0.2	7 ± 0.3	8 ± 0.5	17 ± 1.7
8h	10 ± 1.2	0	22 ± 0.3	33 ± 1.3	13 ± 1.2	28 ± 0.7	33 ± 0.4
9a	0	4 ± 0.9	47 ± 1.4	2 ± 0.3	27 ± 2.5	14 ± 1.9	17 ± 0.6
9b	10 ± 1.4	5 ± 4.5	34 ± 2.5	17 ± 0.9	23 ± 3.3	25 ± 2.6	33 ± 1.3
9c	7 ± 1.3	5 ± 0.5	38 ± 1.4	10 ± 0.8	28 ± 2.6	12 ± 0.7	32 ± 2.9
9d	2 ± 1.0	0	13 ± 2.5	1 ± 0.3	6 ± 2.5	16 ± 0.8	23 ± 2.1
9e	0	5 ± 0.6	33 ± 2.5	15 ± 1.3	13 ± 1.5	22 ± 1.8	19 ± 3.1
9f	6 ± 0.9	0	28 ± 2.6	16 ± 1.9	18 ± 2.5	17 ± 2.7	21 ± 0.6
9g	0	0	23 ± 1.9	20 ± 4.5	44 ± 1.9	37 ± 2.6	18 ± 2.4
9h	0	0	8 ± 0.4	21 ± 2.4	4 ± 0.5	22 ± 0.5	11 ± 0.2
9i	0	6 ± 0.8	26 ± 0.7	22 ± 2.9	44 ± 0.6	13 ± 2.0	21 ± 0.5
9j	5	0	36 ± 0.9	1 ± 0.5	4 ± 1.9	34 ± 2.7	18 ± 4.3
9k	4 ± 0.2	12 ± 0.5	21 ± 0.4	0	11 ± 0.3	33 ± 0.4	22 ± 2.3
9l	10 ± 0.4	8 ± 0.6	28 ± 1.9	0	25 ± 0.3	25 ± 0.6	19 ± 0.4
9m	17 ± 1.2	0	16 ± 0.3	0	10 ± 0.5	21 ± 2.9	30 ± 0.7
9n	0	2 ± 0.8	15 ± 0.9	0	6 ± 0.7	10 ± 3.9	30 ± 0.6
9o	10 ± 1.5	10 ± 1.5	32 ± 0.8	18 ± 3.0	14 ± 0.4	15 ± 2.0	22 ± 0.3
10a	6 ± 1.7	8 ± 1.2	0	24 ± 2.0	2 ± 0.3	4 ± 0.7	5 ± 0.9
10b	0	0	2 ± 0.4	41 ± 2.8	15 ± 0.8	6 ± 0.7	3 ± 0.4
10c	0	4 ± 0.5	22 ± 1.2	31 ± 1.9	2 ± 0.4	5 ± 0.5	4 ± 0.4
10d	0	29 ± 1.5	52 ± 1.8	45 ± 0.9	10 ± 0.5	21 ± 0.6	7 ± 0.3
10e	2 ± 0.5	2 ± 0.3	25 ± 2.1	72 ± 0.8	9 ± 1.6	19 ± 0.9	6 ± 0.4
10f	0	0	14 ± 1.0	0	0	33 ± 2.6	24 ± 1.4
10g	0	0	49 ± 1.9	0	41 ± 1.9	41 ± 2.9	18 ± 0.5
10h	7 ± 0.7	0	45 ± 3.9	0	41 ± 0.5	28 ± 0.4	3 ± 0.7
10i	3 ± 0.4	0	23 ± 0.4	0	3 ± 3.5	41 ± 0.5	0
10j	2 ± 0.8	10 ± 1.2	30 ± 3.3	0	6 ± 2.7	25 ± 0.8	10 ± 0.4
10k	0	2 ± 0.5	2 ± 0.1	0	4 ± 0.5	9 ± 1.9	5 ± 0.3
10l	0	0	42 ± 0.3	30 ± 3.5	2 ± 0.3	7 ± 0.3	3 ± 1.1
10m	5 ± 1.1	11 ± 0.8	9 ± 1.2	0	4 ± 0.6	7 ± 0.5	10 ± 4.5
10n	13 ± 1.5	13 ± 1.6	30 ± 3.4	0	17 ± 0.9	9 ± 0.6	11 ± 2.4
11a	5.2 ± 0.5	66 ± 2.1	91 ± 2.4	10 ± 2.4	87 ± 1.8	8 ± 0.8	72 ± 2.5
11b	2 ± 0.9	71 ± 1.9	58 ± 1.2	12 ± 2.0	88 ± 2.1	10 ± 1.3	70 ± 1.9
11c	5 ± 0.2	53 ± 2.8	35 ± 1.9	53 ± 1.8	52 ± 3.0	82 ± 1.9	55 ± 2.9
11d	90 ± 0.2	94 ± 0.8	90 ± 2.3	84 ± 2.9	88 ± 3.2	80 ± 1.9	68 ± 2.7
11e	42 ± 1.6	92 ± 1.2	90 ± 1.4	82 ± 2.6	89 ± 2.8	64 ± 1.8	59 ± 3.5
11f	43 ± 2.5	80 ± 2.4	78 ± 1.5	75 ± 2.0	77 ± 5.2	78 ± 3.4	44 ± 2.3
11g	55 ± 0.2	85 ± 1.5	88 ± 1.9	87 ± 1.6	87 ± 2.4	83 ± 3.2	61 ± 3.7
11h	9 ± 1.9	80 ± 5.3	82 ± 0.7	25 ± 1.8	68 ± 0.5	62 ± 2.7	68 ± 2.7
11i	10 ± 1.8	75 ± 2.4	61 ± 0.8	22 ± 1.1	59 ± 0.9	63 ± 3.2	65 ± 2.5

[a]Values are reported as average of two independent determinations. [b]Values are reported as average of three independent determinations.
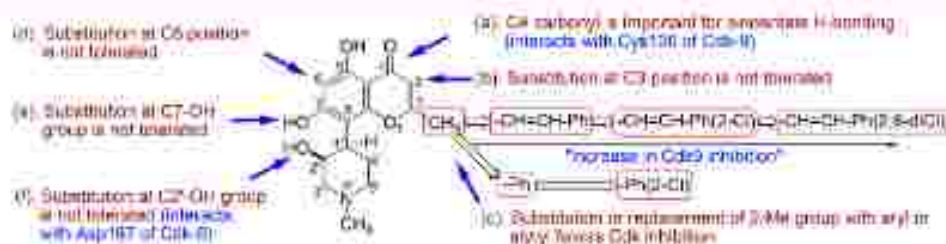
Structure–Activity Relationship and Molecular Modeling for Cdk-9/T1 Inhibition.

The substitution of various possible positions of rohitukine provided four series of compounds. The substitution at C3, C6, C7-OH, and C2′-OH positions resulted in the loss of Cdk inhibition activity, particularly the Cdk-9/T1 inhibition. However, substitution of C2-methyl with styryl moiety resulted in improvement of activity. Literature precedence also indicated that C2-position is the most tunable position for favorable modulation of Cdk inhibition activity. The replacement of C2-methyl with 2-chlorophenyl group provided flavopiridol (2), which possesses 15-fold improvement in Cdk-9/T1 inhibition activity (IC$_{50}$ of rohitukine, 300 nM; flavopiridol, 20 nM). Similarly, the substitution of C2-methyl with styryl group (compound 11a, IC$_{50}$ 66 nM) led to ~5-fold improvement in the Cdk-9/T1 inhibition activity. The styryl moiety was further substituted

Table 3. IC$_{50}$ Values for in Vitro Inhibition of Cdk-2/A and Cdk-9/T1 and GI$_{50}$ Values for Cellular Antiproliferative Activity by Styryl Derivatives 11a–i

entry	enzyme inhibition IC$_{50}$ (nM) ± SD[a]		cellular activity GI$_{50}$ (μM) ± SD[b]				
	Cdk-2/A	Cdk-9/T1	HL-60	PC-3	MIAPaCa-2	MCF-7	Caco-2
1	7300 ± 89	300 ± 15	19 ± 0.8	19 ± 1.3	19 ± 2.9	28 ± 3.3	25 ± 2.1
11a	925 ± 12	66 ± 12	1 ± 0.2	58 ± 1.5	3 ± 0.4	31 ± 2.1	17 ± 1.4
11b	3300 ± 31	310 ± 14	8 ± 0.3	51 ± 2.1	2 ± 0.4	49 ± 2.4	5.6 ± 1.5
11c	3000 ± 34	200 ± 3	20 ± 1.2	10 ± 0.3	10 ± 1.4	2 ± 0.4	9 ± 0.8
11d	16 ± 1	1.9 ± 1	0.9 ± 0.3	1 ± 0.1	1 ± 0.4	4 ± 0.6	7 ± 1.1
11e	608 ± 13	11.5 ± 4	3 ± 0.5	2 ± 0.2	1 ± 0.4	8 ± 0.9	8 ± 0.8
11f	1800 ± 67	350 ± 14	8 ± 0.2	>100	8 ± 0.6	5 ± 0.3	8 ± 0.5
11g	666 ± 31	29 ± 1	8 ± 1.1	7 ± 1.4	2 ± 1.1	3 ± 0.5	8 ± 0.7
11h	1520 ± 13	260 ± 21	8 ± 0.4	20 ± 2.1	3 ± 1.2	8 ± 3.2	7 ± 1.1
11i	1410 ± 14	160 ± 9	9 ± 0.8	17 ± 1.4	8 ± 1.3	9 ± 1.4	9 ± 1.0

[a]Values are reported as average of two independent determinations. [b]Values are reported as average of three independent determinations.

**Figure 3.** Structure–activity relationship of rohitukine scaffold for Cdk inhibition.

with "Cl" at the ortho position, resulting in a marginal decrease (by 2.4-fold) in activity; however, introduction of another "Cl" at other ortho position (compound 11d, IC$_{50}$ 1.9 nM) resulted in tremendous improvement in the Cdk-9/T1 inhibition potency. This 2,6-dichloro derivative 11d possesses ~160-fold improvement in Cdk-9/T1 potency over parent natural product rohitukine.

In particular, the position and type of halogen substituent on styryl ring was found to play crucial role in selectivity for Cdk-9/T1 versus Cdk-2/A. The penta-fluorobenzyl derivative 11e showed higher selectivity (52-fold) for Cdk-9/T1 (IC$_{50}$ 11.5 nM) versus Cdk-2/A (IC$_{50}$ 608 nM). The 2,6-dichlorostyryl derivative 11d was found to be the most potent inhibitor of Cdk-9/T1 (IC$_{50}$ 1.9 nM) with 7-fold selectivity over Cdk-2/A (IC$_{50}$ =15.5 nM). Furthermore, the 2-chlorostyryl derivative 11i (Cdk-9: IC$_{50}$ = 160) nM) is more active than 3-chlorostyryl derivative 9c (Cdk-9/T1: IC$_{50}$ =280 nM), which is more active than 4-chlorostyryl derivative 11b (Cdk-9/T1: IC$_{50}$ = 310 nM). The similar trend of activity was also seen for Cdk-2/A inhibition, indicating that chloro-substitution at the ortho position of the styryl ring is more favorable. Furthermore, the presence of two chloro substituent's at both ortho positions resulted in the highly active Cdk-9/T1 and Cdk-2/A inhibitor 11d (IC$_{50}$ = 1.9 and 15.5 nM for Cdk-9/T1 and Cdk-2/A, respectively). In general, the activity of chloro-substituted analogues has ~10× higher activity against Cdk-9/T1 over Cdk-2/A. Overall, these results indicated that series D compounds are potent Cdk-9 and Cdk-2 inhibitors with better selectivity toward Cdk-9; however, other three series of compounds were weakly active or completely inactive. Figure 3 depicts the key features of the SAR of rohitukine scaffold for Cdk inhibition.

Next, the molecular modeling studies were performed to understand the interaction pattern of styryl derivative 11d with the active site of Cdk-9. The docking of styryl derivative 11d

and flavopiridol was performed using Cdk-9/flavopiridol crystal structure (PDB: 3BLR). The compound 11d was found to occupy the ATP binding cavity of the Cdk-9 enzyme exactly in a similar fashion like flavopiridol. The surface view of the ATP binding pocket showing orientation of 11d inside the cavity is shown in Figure 4a, and the overlay of 11d with flavopiridol in the binding cavity is displayed in Figure 4c. The key interactions of 11d with ATP binding site residues are shown in the Figure 4b,d. The chromenone moiety of both these compounds orients toward the bottom of the cavity, forming an important bidentate H-bonding interaction with the Cys 106 residue. In addition, compound 11d forms two other important H-bonds with Ala 153 and Asp 167. The protonated NH of the piperidine ring forms H-bond with the carbonyl oxygen of Ala 153, and the oxygen of C-7 hydroxyl forms H-bond with NH of Asp 167. Apart from these H-bond interactions, two important π–π interactions were observed, viz. the ring A (a ring which is connected with piperidine) of 11d shows π–π interaction with Phe 103, and protonated NH of piperidine interacts with Phe 30 via π–π interaction. The surface view of the binding pocket also revealed that the dichlorophenyl moiety orients toward the solvent, i.e., outside the front specificity pocket of Cdk-9. This computational information indicated that three functionalities, viz. keto–enol of chromenone ring, piperidinyl moiety, and ortho-chloro substituted styryl ring, are important functionalities for binding to Cdk-9 enzyme (Figure 4a–d).

Screening of IIIM-290 (11d) in a Panel of Cdks and Kinase Profiling. As depicted in Table 3, the promising Cdk inhibition profile and cellular antiproliferative activity of 11d prompted us to further explore its potential as an anticancer agent. The 11d was screened in a panel of 13 Cdk enzymes, viz. Cdk-1/cyclin A, Cdk-1/cyclin E, Cdk-2/cyclin O, Cdk-2/cyclin A, Cdk-3/cyclin E, Cdk-4/cyclin D3, Cdk-5/cyclin p25, Cdk-5/cyclin p35, Cdk-6/cyclin D1, Cdk-6/cyclin D3, Cdk-7/cyclin H, Cdk-9/cyclin K, and Cdk-9/cyclin T1. It inhibited strong
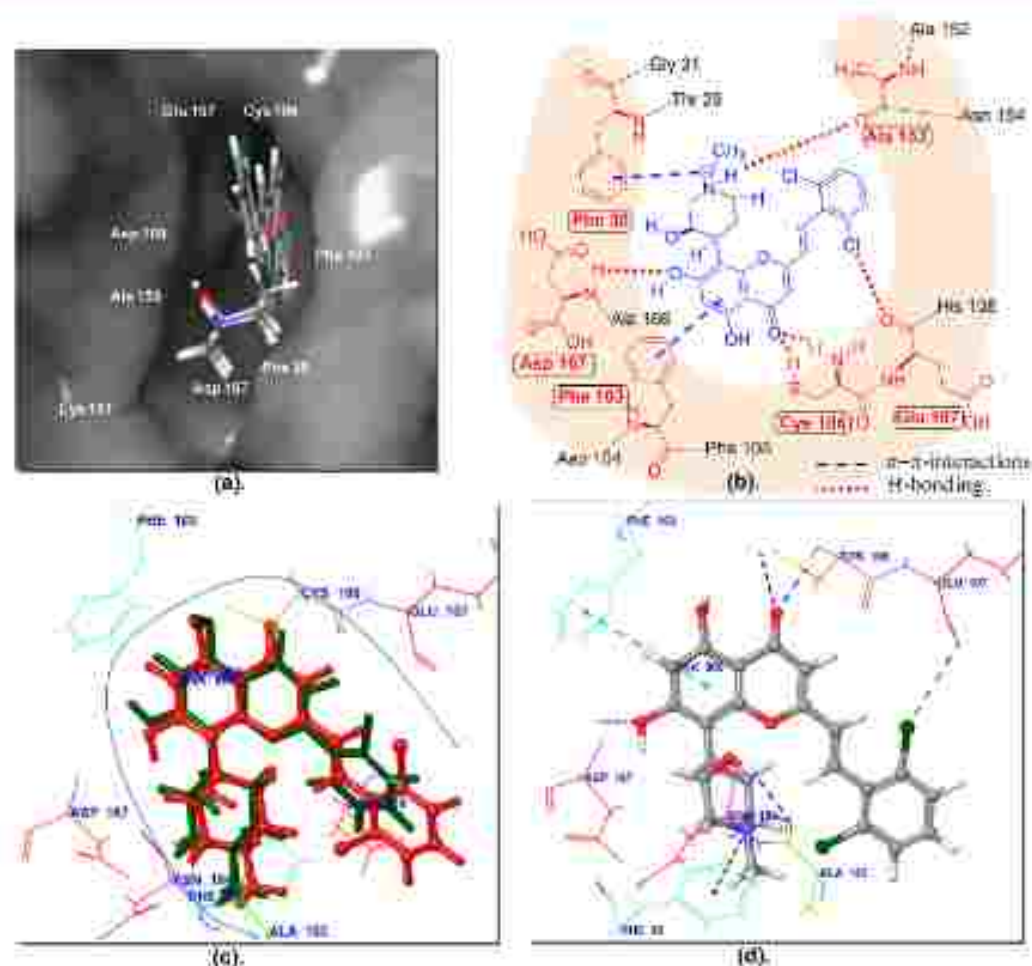
Figure 4. Interactions of 11d with the ATP binding site of Cdk-9 kinase (PDB code: 3BLR). (a) Surface view of the ATP binding site of Cdk-9 showing orientation of 11d inside the cavity; (b) two-dimensional view of the key interactions of 11d with active site residues; (c) overlay of flavopiridol (green) with 11d (red) in the active site; (d) key interactions of 11d with binding site residues in the 3D view.

inhibition of Cdk-1/cyclin A and Cdk-9/cyclin T1 with IC$_{50}$ values of 4.9 and 1.9 nM, respectively. It also showed promising activity against Cdk-4/D3 and Cdk-6/D1 with IC$_{50}$ values of 22.5 and 45 nM, respectively. IIIM-290, like flavopiridol and riviciclib, belongs to the flavone class of compounds. However, unlike flavopiridol and riviciclib, it shows better selectivity toward Cdk-1/A and Cdk-9/T1 as compared with Cdk-7/H. The Cdk screening results are shown in Table 4.

The kinase selectivity of 11d was then studied in a panel containing 468 kinases (scanMAX KINOMEscan, DiscoverX) at a compound concentration of 0.5 μM. A set of 468 kinases covers AGC, CAMK, CMGC, CK1, STE, TK, TKL, lipid, and atypical kinase families, plus important mutant forms. The kinome profiling indicated that the compound 11d is somewhat promiscuous by inhibiting some of the Ser/Thr and Tyr kinases. The most prominent kinases, other than Cdk-9/T1, which were also inhibited (>98% inhibition) by 11d, includes ABL1 mutants (E255 K, H396P, Q252H), BLK, Cdk4/D1, Cdk4/D3, CIT, ERBB3, ICK, KIT A829P mutant, MEK5, PRKCE, and Tyk2. The complete profiling data on 468 kinases is provided in section S5 of the Supporting Information, and the TREEspot Interaction Map showing the percent inhibition profile is shown in Figure 5. The percent inhibition values for kinases (with >65% inhibition) are displayed in the TREEspot interaction map, wherein the bigger circles are indicative of the stronger inhibition of particular kinase by compound 11d.

PRKCE (protein kinase C, epsilon) is an AGC group of wild-type human kinase, which plays a role in cardioprotection.[55] As 11d inhibits PRKCE, it was investigated for its potential cardiotoxic effect, using hERG channel binding assay. This assay involved a competitive radioligand binding assay in HEK293 cells expressing the hERG K$^+$ channel. The IC$_{50}$ of 11d for inhibition of hERG K$^+$ channel was found to be >50 μM, indicating that the compound does not have liability for cardiac toxicity.

The selectivity scores (S-score) provide a quantitative method of describing compound selectivity to facilitate comparison of different compounds. The S(35), S(10), and

Table 4. Profiling of 11d in a Panel of Cdks[a]

Cdk	IC$_{50}$ (nM) ± SD	Cdk	IC$_{50}$ (nM) ± SD
Cdk-1/cyclin A	4.91 ± 0.5	Cdk-5/cyclin p35	15.7 ± 2.5
Cdk-1/cyclin E	75.9 ± 12	Cdk-6/cyclin D1	45 ± 4.2
Cdk-2/cyclin O	138 ± 14	Cdk-6/cyclin D3	599 ± 5.7
Cdk-2/cyclin A	15.5 ± 1.8	Cdk-7/cyclin H	711 ± 13.2
Cdk-3/cyclin E	>1000	Cdk-9/cyclin K	412 ± 22.1
Cdk-4/cyclin D3	22.5 ± 2.5	Cdk-9/cyclin T1	1.9 ± 0.2
Cdk-5/cyclin p25	15.5 ± 1.2		

[a]Values are reported as average of two independent determinations.
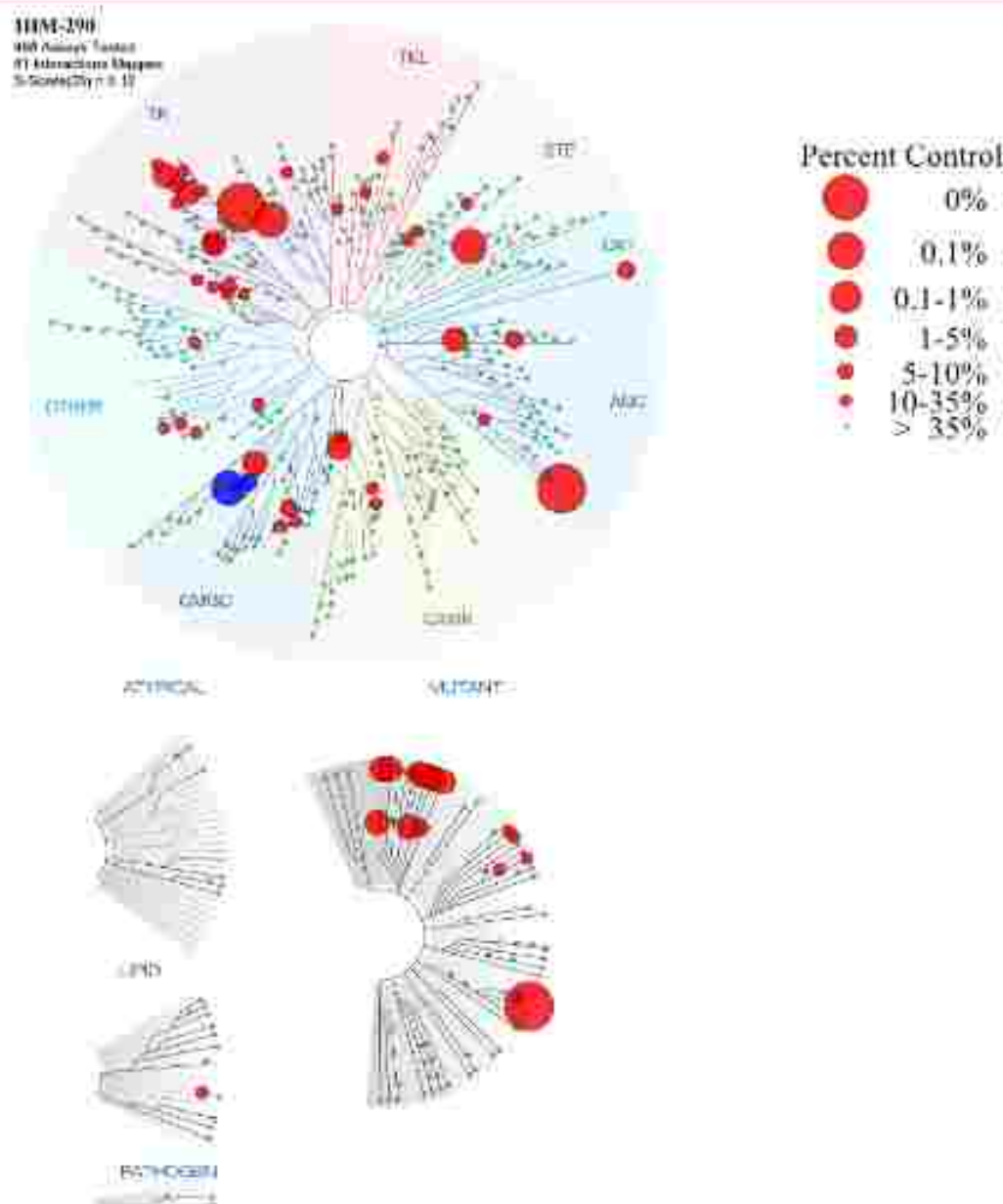
Figure 5. Percent inhibition profile (TREEspot Interaction Map) in the DiscoverX ScanMax kinome scan for compound 11d. The kinase groups and number of kinases in the panel: TK, tyrosine kinases (87); TKL, tyrosine kinase like (31); STE, STE kinases (43); CK1, cell kinase 1 (8); AGC, PKA, PKG, PKC kinases (46); CAMK, calcium and calmodulin regulated kinases (46); CMGC, Cdk, MAP, GSK, Cdk like kinases (54); other, other kinases (54); mutant kinases (60); atypical kinases (8); lipid kinases (13); pathogen kinases (3). The red (and blue) circles indicate the kinases where compound 11d has reduced the kinase activity to less than 35% of control. Two blue circles indicate Cdk-4 and Cdk-9 kinases.

S(1) scores for 11d were computed from the kinase profiling results and these scores were found to be 0.114, 0.04, and 0.012, respectively. The comparison of the S(35) score of 11d with kinase inhibitor clinical candidates and drugs indicated that 11d has superior S-score over several of these candidates (details are provided in section S5 of the Supporting Information). In particular, the selectivity score [S(35) = 0.114] of 11d was found to be better than several clinically approved kinase inhibitors erlotinib, sorafenib, dasatinib, and sunitinib.

Cellular Antiproliferative Activity in a Panel of Cancer Cell Lines. The cellular antiproliferative activity of all four series of compounds was evaluated in a panel of cancer cell lines including HL-60 (leukemia), PC-3 (prostate), MIAPaCa-2 (pancreatic), MCF-7 (breast), and Caco-2 (colon) using

tetrazolium-based calorimetric antiproliferation assay (MTT assay). The initial screening was performed at a single concentration of 10 μM, followed by determination of GI_{50} values for the best compounds. Like Cdk inhibition results, series A–C were weak to moderately active in a panel of five cell lines tested (Table 2). None of the compounds from these three series showed >50% growth inhibition of cancer cell lines at 10 μM. However, several compounds from series D showed >50% inhibition of the cell growth, the most promising among them were compounds 11d and 11e, which were active against all five cell lines. Therefore, the GI_{50} values were determined for series D compounds (Table 3). Compound 11d from series D, which was most active in Cdk screening, displayed promising cellular antiproliferative activity in HL-60 and MIAPaCa-2 cells with GI_{50} values of 0.9 and 1 μM, respectively.

Further, compound **11d** was studied for its cellular antiproliferative activity in a panel of 27 cancer and three normal cell lines. Results are shown in Table 5. The

Table 5. Cellular Antiproliferative Activity (IC$_{50}$ Values) of 11d in a Panel of Cancer Cell Lines[a]

cell line (tissue)	GI$_{50}$ µM (±SD)	cell line (tissue)	GI$_{50}$ µM (±SD)
HL60 (leukemia)	0.9 ± 0.3	NCIH522 (lung)	2 ± 0.4
MOLT-4 (leukemia)	0.5 ± 0.2	NCIH522 (lung)	5 ± 0.5
MIAPaCa-2 (pancreatic)	1.0 ± 0.4	HOP62 (lung)	7 ± 0.3
Panc-1 (pancreatic)	4 ± 0.6	HOP92 (lung)	3 ± 0.4
PC-3 (prostate)	6 ± 0.5	NCIH226 (lung)	4 ± 0.4
DU145 (prostate)	5 ± 0.3	786-O (renal)	6 ± 0.5
MCF-7 (breast)	4 ± 0.4	A431 (skin)	4 ± 0.3
MDAMB-231 (breast)	4 ± 0.3	LOXIMVI (skin)	4 ± 0.7
MDAMB-468 (breast)	4 ± 0.4	OVCAR-3 (ovarian)	4 ± 0.5
BT-549 (breast)	5 ± 0.2	OVCAR-4 (ovarian)	9 ± 0.8
T47D (breast)	6 ± 0.3	OVCAR-5 (ovarian)	7 ± 1.0
Caco-2 (colon)	7 ± 0.4	mouse adenocarcinoma	1.2 ± 0.4
SW620 (colon)	0.3 ± 0.04	HGF (normal)	18 ± 1.3
Colo-205 (colon)	7 ± 0.8	f92 (normal)	19 ± 1.5
HCT116 (colon)	5 ± 1.0	HEK293 (normal)	22 ± 2.1
A549 (lung)	4 ± 1.0		

[a]Cellular antiproliferative activity is average of three independent determinations and is performed at 48 h of incubation time.

representative dose–response curves for antiproliferative activity of **11d** are shown in section S2 of the Supporting Information. It exhibited significant cellular activity across the panel; however, the most prominent activity was observed in leukemia and pancreatic cancer cell lines. Compound **11d** displayed strong antiproliferative activity in leukemia cells, which could be because of the higher expression of Cdks and cyclins in these cells.[54,55] In contrast, the cell cycle proteins are less expressed in Caco-2 cells,[56] resulting in comparatively low cellular antiproliferative activity of **11d** in this cell line. In addition to the panel of human cancer cell lines, compound **11d** was also tested for cellular antiproliferative activity in mouse adenocarcinoma cell line, wherein the GI$_{50}$ was found to be 1.2 µM. Compound **11d** showed significantly low toxicity to normal cell lines (GI$_{50}$ values of 18–22 µM), indicating a good cellular therapeutic window of the compound.

It has been reported that the inhibition of Cdk-9 selectively targets survival proteins and reinstates apoptosis in cancer cells. Therefore, for compound **11d**, which is a highly potent Cdk-9 inhibitor, the mechanistic studies were performed in MIAPaCa-2 (pancreatic cancer) cell line, and results are shown in Figure 6. The compound was studied for cell cycle analysis (Figure 6a), by apoptosis study via scanning electron microscopy (Figure 6b), by DAPI staining (Figure 6c), and for mitochondrial membrane potential loss (Figure 6d). The cell cycle analysis indicated that there is a marginal cell cycle arrest by **11d** in G1 phase. This may be because of the higher selectivity of the compound for Cdk-9/T1 inhibition, the Cdk, which is not a cell cycle regulator. However, in apoptosis study, there is an increased formation of apoptotic bodies and chromatin condensation in nuclei of cells treated with **11d**, which suggests that this compound inhibits the growth of

MIAPaCa-2 cells by inducing apoptosis. The scanning electron microscopy of treated cells showed vesicle formation inside the cells, while the control cells were healthy. The untreated cells showed healthy and round nuclei with no DNA fragmentation. The compound **11d** was also found to trigger mitochondrial membrane potential (MMP) loss in MIAPaCa-2 cells (Figure 6d). Further, we studied the effect of compound **11d** on important apoptosis markers, viz. PARP, caspase-3, and caspase-7. Western-blot studies (Figure 7) indicated the concentration-dependent cleavage of PARP, caspase-3, and caspase-7 by compound **11d**, confirming the apoptosis mediated cell death of MIAPaCa-2 cells.

Physicochemical Properties and ADME Profile of 11d. The experimental physicochemical parameters such as thermodynamic equilibrium solubility in water and biological medias (PBS, SGF, and SIF), log P, and pK$_a$ values were determined using our established protocols.[57,58] Compound **11d** was found to possess moderate solubility in water (20 µg/mL). The experimental log P, log D, and pK$_a$ of compound **11d** were found to be 3.09, 1.65, and 5.4, respectively. The compound was also studied for pH-dependent solution stability and stability in various biorelevant medias and in mouse plasma. It was found to be stable at all the conditions tested. Furthermore, the compound **11d** also follows the Lipinski Rule of Five (passes 4/4 rules). The physicochemical parameters of **11d** are summarized in Table 6.

Human serum protein binding affinity affects the drug distribution in the body, and it also has an impact on the drug–drug interaction. In plasma, drug exists in bound ↔ unbound form. The percent protein binding of **11d** in human plasma was found to be 96.7%. The plasma protein binding in other species, viz. rat, mouse, and dog plasma, was also determined, which was found to be in a similar range (95–97.2% binding). The human serum albumin (HSA) and α1-acid glycoprotein (AAG) are the most relevant drug carriers in blood plasma, and it is generally accepted that basic drugs mainly bind to these two proteins. Therefore, the binding of **11d** with AAG and HSA was also assessed, which showed that the compound also possess higher binding to these two proteins (98.3 and 96.7%).

The in vitro metabolism of compound **11d** was investigated using pooled liver microsomes, hepatocytes, and S9 liver fraction of mouse, rat, human, dog, and monkeys. First, the microsomal stability was studied to investigate phase I metabolism using NADPH as the enzyme cofactor. The half-life ($t_{1/2}$) value was measured by monitoring substrate disappearance over time. Intrinsic clearance (CL$_{int}$) was also determined, which helps to confirm whether metabolism is the main clearance pathway when it is compared with the total body clearance in vivo. The compound showed $t_{1/2}$ > 30 min in mouse, rat, and human liver microsomes, whereas this value was <30 min in dog and monkey liver microsomes. It has low intrinsic clearance in mouse, rat, and human liver microsomes, whereas medium CL$_{int}$ in monkey and high CL$_{int}$ in dog liver microsomes. Next, the metabolic stability was assessed in hepatocytes of all five species in order to investigate the phase II metabolism. Compound **11d** showed higher $t_{1/2}$ value in hepatocytes compared with microsomes. The $t_{1/2}$ in human hepatocytes was found to be 12 h, as the corresponding intrinsic clearance was very low. Overall, **11d** falls in medium clearance category in all the species of hepatocytes. The S9 liver fractions contain both microsomal (CYPs) and cytosolic enzymes (SULT, GST, XO, ADHs, NATs), and therefore, it offers a more complete representation of the metabolic profile
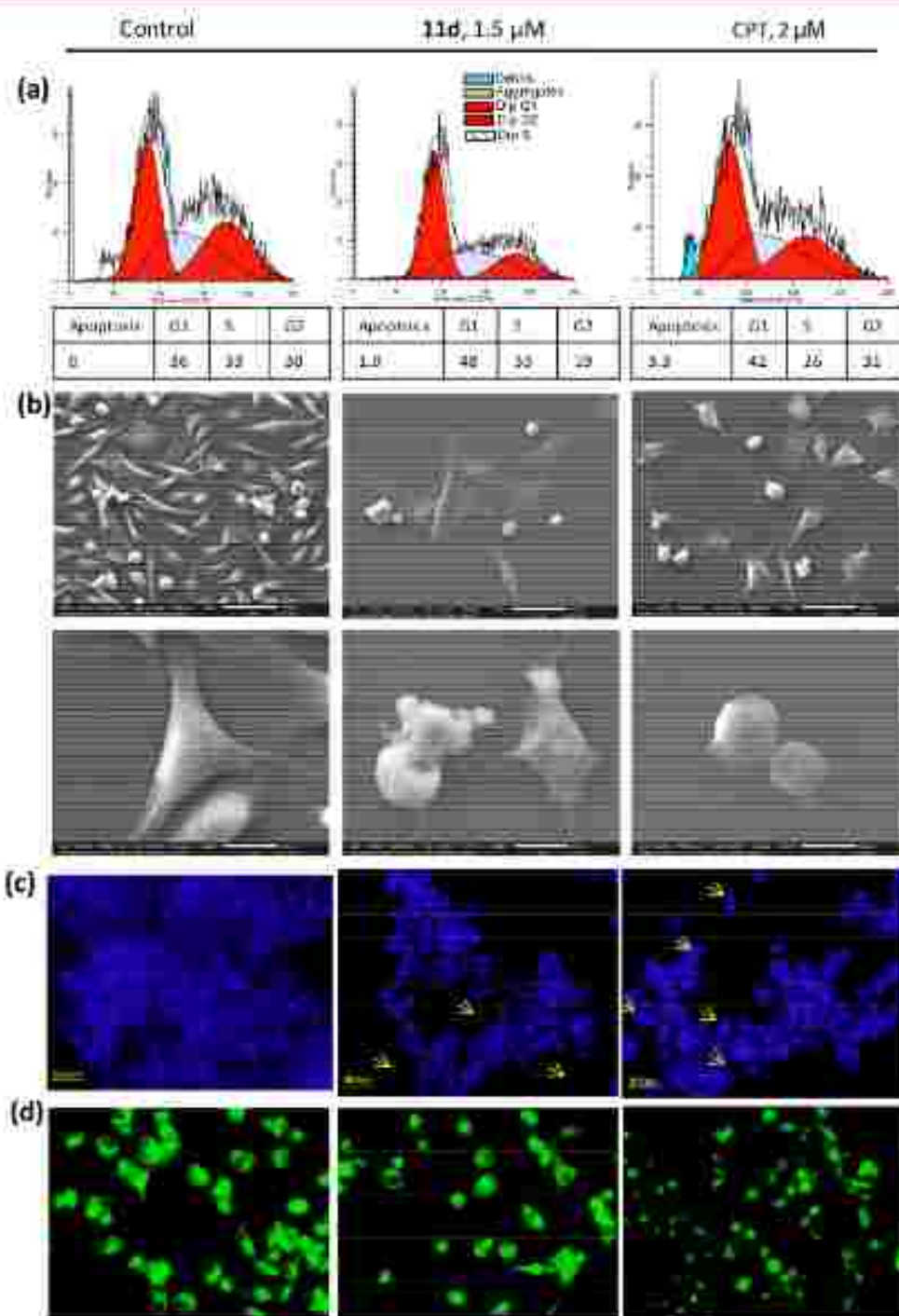
Figure 6. Effect of compound **11d** on cell cycle (a), apoptosis via scanning electron microscopy (b), and DAPI staining (c), and mitochondrial membrane potential loss (using Rh123 dye) (d) in MIAPaCa-2 cells.

compared with microsomes and cytosolic fractions. Compound **11d** was also studied for metabolic stability in S9 liver fraction of all five species, wherein it displayed moderate half-life and intrinsic clearance. In a nutshell, compound **11d** undergoes metabolic degradation in all three matrices with varied half-lives and intrinsic clearance, and it has acceptable metabolic stability profile (Table 6).

Pharmacokinetics of 11d. The pharmacokinetics of compound **11d** was evaluated in BALB/c mice following a single 10 mg/kg dose administration by oral route and 1.0 mg/ kg dose administration by IV route. Following oral admin-

istration, elimination half-life ($t_{1/2,\beta}$) was found to be 4.65 h and AUC_{0-t} was found to be 4503 nM·h. Following IV administration, elimination half-life ($t_{1/2,\beta}$) was found to be 5.46 h, and clearance was ~55 mL/min/kg. The absolute oral bioavailability was 71% (Figure 8). The data presented in Table 6 and Figure 8 indicated that compound **11d** has optimal ADME parameters for anticancer therapeutics.

Next, the dose-dependent pharmacokinetics of **11d** was studied in BALB/c mice and also in SD rats. Results are shown in Table 7. Compound **11d** displayed a dose-dependent increase in the plasma exposure upon oral administration, both

Figure 7. Effect of compound **11d** on PARP, caspase-3, and caspase-7 using western blot analysis in MIAPaCa-2 cells.

in mice and rats. In a tissue-distribution study performed in SD rats (at 30 mg/kg, po) to find the exposure of the compound to organs of interest (pancreas, the targeted cancer), it was observed that the compound has good tissue distribution in the pancreas. The pancreas/plasma ratio (kp) of compound **11d** was found to be 5.3, 4.1, and 10.5 at 0.5, 1, and 8 h. Similarly, in the tissue distribution study in BALB/c mice (at 30 mg/kg, po), the pancreas/plasma ratio (kp) of compound **11d** was found to be 14.2, 24.4, and 6.79 at 0.5, 1, and 8 h, indicating a good exposure of drug to the pancreas. Other tissues where compound showed good exposure include lung, liver, and kidneys.

In Vivo Anticancer Activity of 11d in Murine and Xenograft Models. The preliminary anticancer activity investigation of styryl derivative **11d** was performed in Ehrlich solid tumors, a murine mice model to understand the effective dose range in a 15-day study. The purpose of this study was 2-fold, first to determine the maximum tolerated dose in mice, and second to determine the effective dose-range. Initial dose-optimization studies involved various doses ranging from 10 to 100 mg/kg. Compound **11d** at 70 and 100 mg/kg p.o. showed 31 and 39% tumor growth inhibition without causing any mortality (mortality: 0/7). The doses above 100 mg/kg resulted in mortality. The detailed results of anticancer activity in murine models are shown in section S3 of the Supporting Information. This study indicated that the maximum tolerated dose of **11d** by oral route in mice is 100 mg/kg.

After getting indication of the anticancer activity of **11d** in the murine mice model via oral route, further we tested the compound **11d** in three human xenograft models, viz. pancreatic, colon, and leukemia cancer at 25 and 50 mg/kg doses via peroral route. The selection of these tumor types for xenograft study was based on cellular antiproliferative activity results. Compound **11d** possesses the most prominent in vitro cellular antiproliferative activity in Molt-4 and MIAPaCa-2 cells with GI_{50} values of <1 μM; therefore, these cell lines were selected for xenograft studies. In all these models, compound **11d** was found to display promising tumor growth inhibition, showing up to 40–52% TGI at 50 mg/kg p.o. dose, without causing any mortality. Results are shown in Figure 9. There was no significant change in the body weight of animals during these studies. Results obtained from the in vivo study confirmed the anticancer potential of the compound **11d**, indicating its potential for detailed preclinical characterization.

In order to have a look at the in vitro/in vivo efficacy correlation, the tissue distribution pharmacokinetics data was analyzed. The single dose tissue distribution PK study (30 mg/kg, po) in BALB/c mice as well as in SD rats indicated that drug reaches to the target tissue, pancreas, significantly, with the highest concentration within 0.5 h; however, after 8 h, the concentration drops by 5–10-fold because of the rapid elimination of compound. This is also evidenced from the metabolic stability data of the compound in liver microsomes and hepatocytes ($t_{1/2}$ less than 4 h). As shown in Table 7, the C_{max} of the compound at 30 mg/kg, p.o. is 4.1 μM, which is ~4-fold higher than the average GI_{50} of **11d** in leukemia/pancreatic cancer cell lines. However, the equivalent dose (25 mg/kg) in the in vivo xenograft study does not show significant antitumor activity, which could be due to the permeability and metabolic inactivation barriers. However, the statistically significant in vivo antitumor activity was obtained at 50 mg/kg in all three xenograft models, without causing any mortality.

Safety Pharmacology Studies of 11d. After obtaining interesting in vitro and in vivo anticancer activity for compound **11d**, a thorough investigation of the safety profile of this lead was carried out. Various studies that are performed include CYP inhibition liability, efflux pump substrate liability, cardiac toxicity (hERG channel binding), mutagenicity (Ames test), in

Table 6. Physicochemical Characterization of 11d and Metabolic Stability in Liver Microsomes, Hepatocytes, and in the S9 Liver Fraction

solubility (μg/mL ± SD)	log P/pKa	chemical stability	PPB, % bound	CYP inhibition, IC_{50} (μM)
water: 20.34 ± 4.04	log P: 3.04	% drug remaining (after h)	mouse: 97.2	1A2: >20
PBS (pH 7.4): 2.39 ± 0.07	log D: 1.65	pH 1.2: 100 (24)	rat: 95.4	2D6: >20
SGF (pH 1.2): 8.81 ± 0.38	pKa: 5.4	pH 4.0: 100 (24)	dog: 95	2C9: >20
SIF (pH 6.8): 2.18 ± 0.16		pH 6.8: 81 (24)	human: 96.7	2C19: >20
		pH 7.4: 100 (24)	HSA: 96.7	3A4: >20
		SGF: 100 (8)	AAG: 98.3	
		SIF: 100 (8)		
		mouse plasma: 94 (8)		

	metabolic stability				
	liver microsomes		hepatocytes		S9 liver fraction	
species	$t_{1/2}$ (min)	CL_{int} (μL/min/mg protein)	$t_{1/2}$ (min)	CL_{int} (μL/min/10^6 cells)	$t_{1/2}$ (min)	CL_{int} (μL/min/mg protein)
mouse	>30	<5.8	186	15.9	88	16
rat	>30	<11	576	9.2	31	45
human	>30	<5.8	726	6.8	72	19
dog	24	>29	281	12.3	117	12
monkey	25	54.8	326	10.6	56	25

PK parameter	PO, 10 mg/kg[b]	IV, 1 mg/kg[c]
$t_{1/2}$ (h)	4.63	3.46
C_{max} (nM)	1286	677
T_{max} (h)	0.25	-
C_{0} (ng/mL)	-	859
AUC_{0-t} (nM.h)	4303	323
$AUC_{0-\infty}$ (nM.h)	4399	683
CL (mL/min/kg)	-	35.4
V_{z} (L/kg)	-	26.2
V_{ss} (L/kg)	-	14.1
Bioavailability	79.7 %	-
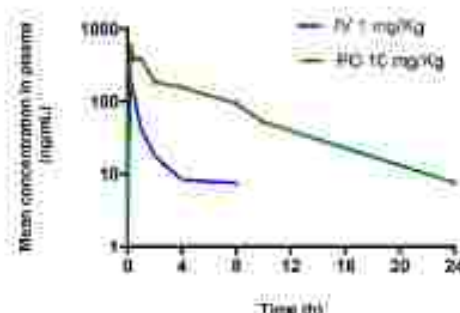
Figure 8. Pharmacokinetic analysis of 11d in BALB/c mice.

Table 7. Dose-Dependent Pharmacokinetics of 11d in BALB/c Mice and SD Rats

parameters	BALB/c mice			SD rats		
	3 mpk, p.o.	10 mpk, p.o.	30 mpk, p.o.	3 mpk, p.o.	10 mpk, p.o.	30 mpk, p.o.
C_{max} (nM)	316	870	4108	316	900	3023
T_{max} (h)	0.57	1.71	0.54	0.50	1.75	1.80
$T_{1/2}$ (h)	3.89	3.61	3.62	4.67	5.18	3.23
AUC (nM.h)	642.88	2414	11266	1441	5676	15076

vitro micronucleus test (genotoxicity), and acute oral toxicity in rats. Cytochrome P450 is a group of drug metabolizing enzymes, and their induction or inhibition affects the blood level of a drug and hence can affect toxicity and efficacy. Compound 11d was studied for inhibition of five major CYP enzymes, using 10 min incubation time. It showed inhibition of CYP3A4, CYP2D6, CYP2C9, CYP1A2, and CYP2C19 with IC_{50} values of >20 μM. In order to understand the propensity of 11d for inhibition of CYP enzymes over the time, the time-dependent inhibition study was then performed against three CYP enzymes, viz. CYP3A4, CYP2D6, and CYP2C9. Compound was tested at 2 and 20 μM, at two incubation times (5 and 30 min). Compound was found to show some propensity of time-dependent inhibition of 3A4 isoform (at 2 μM, 30% and 40% inhibition after 5 and 30 min incubation time, respectively), whereas no propensity was observed for 2D6 and 2C9 isoforms.

The Caco-2 permeability is also an important parameter to predict oral absorption and cellular permeability or mechanism of transport of a drug molecule. This information indicates whether the compound is a substrate for efflux pumps. This assay is considered to be the gold standard for in vitro prediction of in vivo human intestinal permeability and bioavailability of orally administered drugs. An efflux ratio of 1 is indicative of passive diffusion, and a value less than 0.5 and greater than 2 is regarded as active influx and active efflux, respectively. The Papp values of 11d were found to be: (10⁻⁶ cm/s) A to B, 2.1; B to A, 3.9; efflux ratio = 1.8. The efflux ratio of 1.8 indicates that 11d is not a substrate of an efflux pump.

The hERG channel binding potential of compound 11d was studied using competitive radioligand binding assay in HEK293 cells expressing the hERG K⁺ channel. Astemizole was used as a positive control in the study. The IC_{50} of 11d for inhibition of the hERG K⁺ channel was found to be >50 μM (Astemizole, IC_{50} = 14 nM). This indicated that compound does not have liability for cardiac toxicity.

Ames study was performed to evaluate 11d for its possible mutagenic activity, by the bacterial reverse mutation test, using five histidine deficient (his⁻) mutant tester strains of Salmonella

typhimurium, viz. TA1537, TA1535, TA98, TA100, and TA102. This has been evaluated along with known mutagens (positive controls), sodium azide, 9-aminoacridine, 2-nitrofluorene, and mitomycin C, in the absence and presence of a metabolic activation system. Based on these cytotoxicity observations, a maximum concentration of 50 μg/plate was selected for the mutagenicity test, both in the absence and presence of the metabolic activation system, for all the tester strains. There was no statistically significant increase in the number of revertant colonies in any strain, both with (5% and 10%, v/v S9 mix) and without a metabolic activation system when compared with the concurrent negative control. This indicates that 11d is nonmutagenic in the bacterial reverse mutation test in the absence and presence of a metabolic activation system.

The in vitro mammalian cell micronucleus study was performed to evaluate the clastogenic and aneugenic activity of 11d in cells that have undergone cell division after exposure with cytokinesis blocking substance cytochalasin B in the absence and presence of a metabolic activation using human peripheral blood lymphocytes. Cyclophosphamide (30 μg/mL) and mitomycin C (1 μg/mL) were used as the positive controls in the presence and absence of metabolic activation, respectively. Human peripheral blood lymphocyte cultures were exposed to 11d at five dose-levels (two cultures/dose level) between 0.125 and 2 μg/mL of culture medium both in the absence and presence of a metabolic activation system (5% v/v S9 mix). Compound 11d did not induce statistically significant or biologically relevant increases in the number of binucleated cell micronuclei in the absence and presence of a metabolic activation in either of the two independently conducted experiments, indicating a nongenotoxic property of compound 11d. Next, the acute oral toxicity in Wistar rats indicated that the LD_{50} of the compound is 1000 mg/kg. Overall, compound 11d displayed a desirable profile in safety pharmacology studies.

■ CONCLUSION

Medicinal chemistry efforts on roluiperine have resulted in the identification of the first orally bioavailable Cdk inhibitor IIIM-
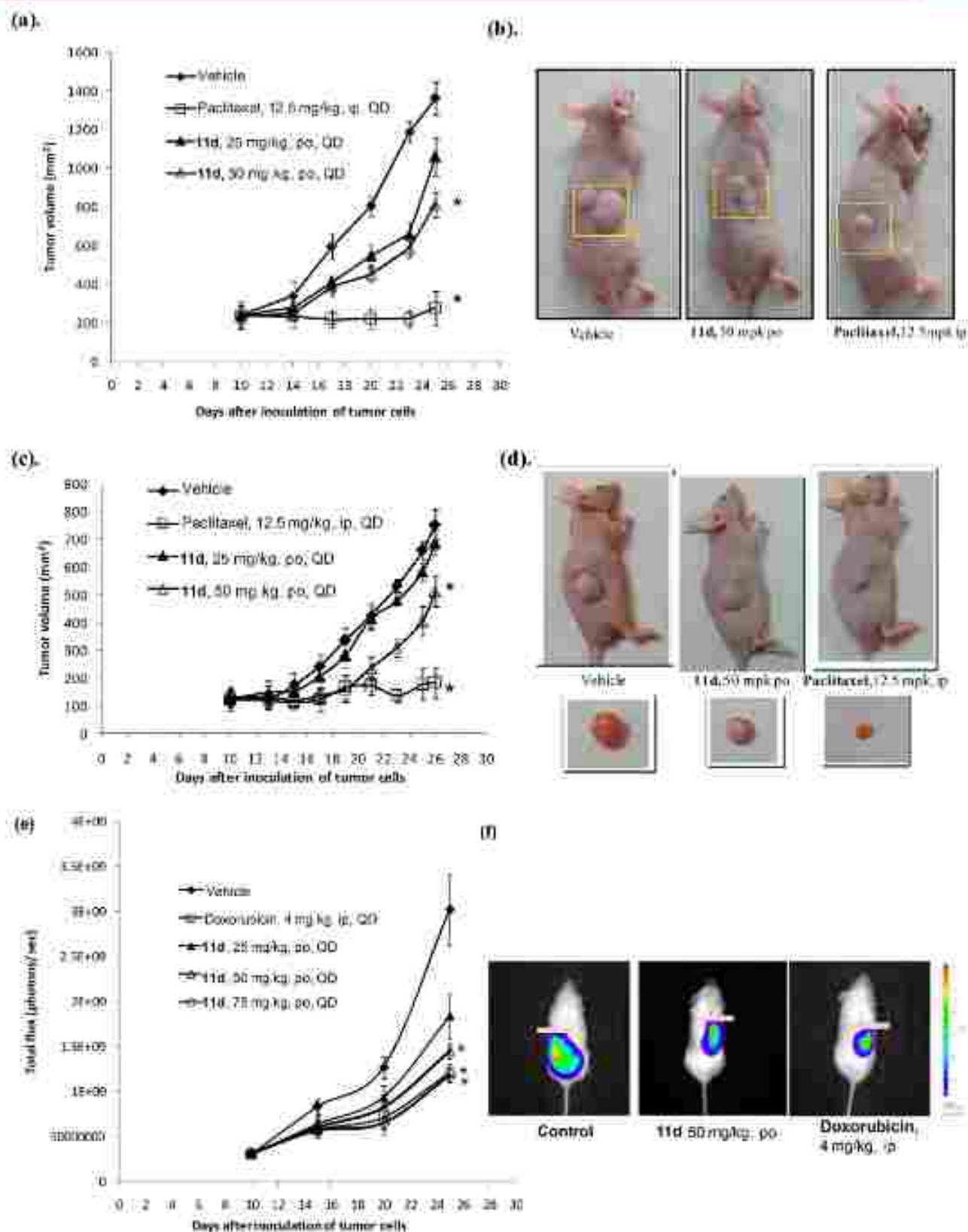
Figure 9. In vivo antitumor effect of styryl derivative 11d in human pancreatic (MIAPaCa-2), colon (HCT-116), and leukemia (Molt-4) xenograft nude mice models. (a,b) Graph showing the effect of 11d on the MIAPaCa-2 tumor growth along with representative tumor images. (c,d) Graph showing the effect of 11d on the HCT-116 tumor growth along with representative tumor images. (e,f) Graph showing the effect of 11d on the Molt-4 tumor growth along with representative images of Molt-4 xenograft studies. Data represent the mean ($n = 6$) ± SEM. Statistical significance (*$p < 0.05$) was determined by one-way analysis of variance.

290 (**11d**) from the rohitukine scaffold, exhibiting anticancer activity in cellular and animal models. Compound **11d** is a potent Cdk-9/T1 inhibitor with an IC_{50} value of 1.9 nM and exhibited promising in vivo efficacy in human xenograft models by the oral route. Compound **11d**, which targets cell cycle-related Cdk-2/4 and transcription-related Cdk-9, might contribute to the antitumor activity. It possesses drug-like properties (good aqueous solubility, Log P = 3.09, pK_a 5.4, no violation of any Lipinski rule), is stable throughout the pH range and in all biological medias, does not possess CYP inhibition liability, does not have efflux pump substrate liability, is metabolically stable in microsomes, hepatocytes, and S9 liver fraction, is nonmutagenic and nongenotoxic, does not have hERG channel binding (no cardiac toxicity), and has a good profile in acute oral toxicity in rats. The preclinical data presented herein warrants the clinical investigation of this lead compound in cancer patients.

■ EXPERIMENTAL SECTION

General. ^{1}H, ^{13}C, and DEPT and 2D NMR spectra were recorded on Bruker Avance DPX IT-NMR 500 and 400 MHz instruments. NMR experiments were carried out in the indicated solvent. Chemical data for protons are reported in parts per million (ppm) downfield from tetramethylsilane and are referenced to the residual proton in the NMR solvent [CDCl$_3$ 7.24 ppm, CD$_3$OD 3.31 ppm, DMSO-d_6 2.6 ppm, acetone-d_6 2.04 ppm]. ^{13}C NMR were recorded at 135 or 100 MHz; chemical data for carbons are reported in parts per million (ppm, δ scale) downfield from tetramethylsilane and are referenced to the carbon resonance of the solvent [CDCl$_3$ 77 ppm, CD$_3$OD 49.3 ppm, DMSO-d_6 39.7 ppm, acetone-d_6 29.8 ppm]. ESI MS and HRMS spectra were recorded on Agilent 1100 LC Q-TOF and HRMS 6540 UHD machines. All chromatographic purifications were performed on Sephadex and Dianion HP-20 resin. Thin layer chromatography (TLC) was performed on precoated silica gel 60 GF$_{254}$ aluminum sheets (Merck). All solvents used were of analytical grade and purchased from Merck. HPLC and HRMS were used to ascertain the purity of synthesized compounds. The UPLC purity analysis of all samples was carried out on a UPLC Shimadzu system (LC20ADXR) connected with a Lichrosphere RP18e (5 μ, 4.6 mm × 250 mm) column and was eluted with water (0.1% formic acid)/ACN gradient at the flow rate of 0.8 mL/min. The gradient elution was set with the increasing concentration of ACN in the following format: 5% ACN (0–3 min), 5–80% ACN (3–8 min), 80% ACN (8–12 min), 80–20% ACN (12–14 min), 5% ACN (14–16 min). The detection wavelength used was 254/280 nm.

The authentic plant material *Dysoxylum binectariferum* (leaves/bark) was collected by the Plant Biotechnology Division of Indian Institute of Integrative Medicine (CSIR), Jammu, during 2014–2016 from Forest Research Institute, Dehradun (Uttarakhand). The plant was identified and authenticated at IIIM, and herbarium sheet was prepared and submitted to Janaki Ammal herbarium, IIIM (Acronym RRLH, accession no. 22163). Dried samples of leaves were submitted to the institutional crude drug repository (accession no. 3892). The Ames test, micronucleus test, CYP inhibition, metabolic stability, pharmacokinetics, and Caco-2 permeability studies were performed at Jubilant Biosys Bangalore. MIAPaCa-2 and HCT-116 xenograft studies were performed at Sphaera Pharma Manesar and acute oral toxicity at Advinus Therapeutics Bangalore on a commercial basis. The animals used in the in vivo study were bred in-house and used. The animal facility is registered with CPCSEA vide registration no. 67/99/ CPCSEA. All of the biologically tested compounds have met the >92% purity requirement.

Isolation of Rohitukine (1) from *Dysoxylum binectariferum*. The dried and powdered leaves (2 kg) of *D. binectariferum* were defatted with hexane (3 L × 3). The obtained residue was then extracted using 3 L of MeOH/CHCl$_3$ (15:85) using a mechanical stirrer for 2 h. MeOH/CHCl$_3$ extraction was repeated five times, and combined extract was concentrated under reduced pressure to get an

extract (120 g). The obtained extract was partitioned between equal volume (500 mL each) of EtOAc and water. The aqueous layer was separated and concentrated under reduced pressure to a minimum volume (25 mL) without any precipitation. The concentrated solution was chilled in ice bath, and acetone was added slowly until complete precipitation. Upon decantation of the acetone, brown residue (stage 3) was obtained, which was further recrystallized using methanol/acetone (2 times) to obtain a cream colored powder (rohitukine 18.4 g, 0.92% yield). The compound was characterized by NMR, mass, and melting point.[24] 5,7-Dihydroxy-8-(3-hydroxy-1-methylpiperidin-4-yl)-2-methyl-4H-chromen-4-one (**1**): cream colored powder (18.4 g, 0.92% yield); mp 215–218 °C; HPLC t_R = 1.96 min (98.60% purity); [α]$_D$ −17.07 (c 0.1, MeOH). IR (CHCl$_3$): ν_{max} 3584, 3312, 2956, 2920, 2870, 1741, 1653, 1460, 1378, 1247, 1082, 1020 cm^{-1}. ^{1}H NMR (400 MHz, CD$_3$OD): δ 6.15 (s, 1H), 5.97 (s, 1H), 4.14 (s, 1H), 3.62–3.59 (m, 1H), 3.49 (d, J = 8.4 Hz, 1H), 3.38 (t, J = 4.4 Hz, 1H), 3.35 (d, J = 4 Hz, 1H), 3.22–3.20 (m, 1H), 3.15 (d, J = 12 Hz, 1H), 2.82 (s, 3H), 2.32 (s, 3H), 1.75 (d, J = 8 Hz, 1H). ^{13}C NMR (100 MHz, CD$_3$OD): δ 183, 167.7, 163.1, 160.7, 156.5, 107.4, 106.4, 104, 99.4, 66.7, 63.4, 55.4, 42.9, 35.7, 31.9, 18.9. ESI-MS: m/z 306.01 [M + H]$^+$. HR-ESIMS: m/z 306.1367 (calcd for C$_{16}$H$_{20}$NO$_5$$^+$, 306.1341).

Synthesis of 5-O-Ether/Ester Derivatives 8a–h. Rohitukine (1, 100 mg, 0.328 mmol), KF-Al$_2$O$_3$ (5 mol %), and benzyl halides/benzoyl halides (0.394 mmol) were mixed in a mortar and grinded intermittently using a pestle. The mixture was changed to a mushy state within a proper reaction time, and then it solidified itself. Formation of the product was monitored by TLC. On completion of the reaction, dichloromethane was added to the reaction mixture. After filtration of the catalyst, the filtrate was washed with aqueous NaOH (10%), and the organic phase was evaporated under reduced pressure. The crude products were purified over silica gel column chromatography (# 100–200) using hexane-ethyl acetate mobile phase, to furnish desired products 8a–h.

(1'R,2'S)-7-(Benzyloxy)-5-hydroxy-8-(3-hydroxy-1-methylpiperidin-4-yl)-2-methyl-4H-chromen-4-one (8a). Light yellowish powder (80 mg, 62% yield); mp 218–220 °C; HPLC t_R = 6.5 min (92.3% purity); [α]$_D$ −50 (c 0.1, MeOH). IR (KBr): ν_{max} 3325, 2923, 1658, 1588, 1420, 1270, 1130, 1020 cm^{-1}. ^{1}H NMR (400 MHz, CD$_3$OD + CDCl$_3$): δ 7.54–7.47 (m, 3H, ArH), 7.37–7.28 (m, 2H, ArH), 6.67 (s, 1H, ArH), 6.17 (s, 1H, ArH), 5.21 (2H, 2H), 4.31 (brs, 1H), 3.82–3.36 (m, 6H of piperidine), 2.93 (s, 3H), 2.48 (s, 3H) 1.93 (m, 1H of piperidine). ^{13}C NMR (100 MHz, CD$_3$OD): δ 184.6, 169.4, 165.0, 162.7, 157.5, 137.5, 134.6, 132.9, 129.8, 129.5, 129.0, 108.9, 97.8, 72.5, 65.9, 65.3, 63.1, 55.5, 38.4, 21.5, 20.5. HR-ESIMS: m/z 396.1802 [M + H]$^+$ (calcd for C$_{23}$H$_{26}$NO$_5$$^+$, 396.1805).

(1'R,2'S)-7-(4-Methoxybenzyloxy)-5-hydroxy-8-(3-hydroxy-1-methylpiperidin-4-yl)-2-methyl-4H-chromen-4-one (8b). White powder (81 mg, 58% yield); mp 208–210 °C; HPLC t_R = 6.39 min (93.2% purity). [α]$_D$ −29 (c 0.1, MeOH). IR (KBr): ν_{max} 3415, 2854, 1617, 1332, 1258, 1180 cm^{-1}. ^{1}H NMR (400 MHz, DMSO-d_6): δ 12.39 (s, 1H, H-bonded), 7.71 (d, J = 8.2 Hz, 2H), 7.09 (d, J = 8.2 Hz, 2H), 5.82 (s, 1H), 5.57 (s, 1H), 5.29 (d, J = 12.7 Hz, 1H), 4.73 (d, J = 12.7 Hz, 1H), 4.15 (br, 1H), 3.80 (s, 3H), 3.57–3.35 (m, 6H of piperidine), 2.83 (s, 3H), 2.27 (s, 3H), 1.54 (m, 1H). ^{13}C NMR (100 MHz, CD$_3$OD): δ 179.6, 176.4, 163.7, 159.9, 159.6, 155.3, 134.3, 120.2, 113.7, 106.8, 106.1, 102.1, 98.0, 68.3, 62.5, 62.2, 61.8, 55.8, 51.5, 35.3, 19.8, 19.3; ESIMS: m/z 448.2 [M + Na]$^+$. HR-ESIMS: m/z 426.1913 [M + H]$^+$ (calcd for C$_{24}$H$_{28}$NO$_6$$^+$, 426.1911).

(1'R,2'S)-7-(4-Bromobenzyloxy)-5-hydroxy-8-(3-hydroxy-1-methyl)piperidin-4-yl)-2-methyl-4H-chromen-4-one (8c). Off-white powder (82 mg, 53% yield); mp 208–210 °C; HPLC t_R = 6.6 min (99.2% purity); [α]$_D$ −48 (c 0.1, MeOH). ^{1}H NMR (400 MHz, CD$_3$OD): δ 7.71–7.68 (m, 4H), 6.31 (s, 1H), 6.11 (s, 1H), 5.27 (d, J = 12 Hz, 1H), 4.84 (d, J = 12 Hz, 1H, merge with moisture), 4.33 (brs, 1H), 3.73–3.30 (m, 6H of piperidine), 2.89 (s, 3H), 2.43 (s, 3H), 2.01 (m, 1H). ^{13}C NMR (125 MHz, CD$_3$OD): δ 183.8, 172.1, 167.8, 161.8, 157.6, 144.2, 139.3, 128.6, 128.2, 128.0, 108.2 (2C), 103.1, 78.4, 69.3, 65.4, 64.9, 56.8, 44.4, 37.3, 23.3, 20.7. ESIMS: m/z 476.0898 [M + H]$^+$. HR-ESIMS: m/z 476.0906 [M + H]$^+$ (calcd for C$_{23}$H$_{27}$^{79}BrNO$_5$$^+$, 476.0896).

(1′R,2′S)-7-(4-Nitrobenzyloxy)-5-hydroxy-8-(3-hydroxy-1-methyl-piperidin-4-yl)-2-methyl-4H-chromen-4-one (8d). White powder (76 mg, 53% yield), mp 218–220 °C; HPLC t_R = 12.56 min (93% purity); $[\alpha]^{20}_D$ −9.8 (c 0.1, MeOH). ^{1}H NMR (400 MHz, CD$_3$OD): δ 8.36 (d, J = 8.4 Hz, 2H), 8.07 (d, J = 8.4 Hz, 2H), 6.17 (m, 2H), 5.57 (d, J = 12.8 Hz, 1H), 4.89 (d, J = 12.8 Hz, 1H), 4.13 (bes, 1H), 3.77–3.33 (m, 6H of piperidine), 2.95 (s, 3H), 2.35 (s, 3H), 1.74 (m, 1H). ^{13}C NMR (100 MHz, CD$_3$OD): δ 183.4, 176.2, 167.3, 157.6, 151.3, 149.1, 136.5 (2C), 124.9 (2C), 107.9, 107.9, 104.3, 104.0, 101.8, 70.9, 65.1, 64.5, 62.7, 57.2, 37.7, 31.7, 20.2. HR ESIMS: m/z 441.1646 [M + H]$^+$ (calcd for C$_{23}$H$_{25}$N$_2$O$_7$$^+$, 441.1656).

(1′R,2′S)-7-(2-Bromobenzyloxy)-5-hydroxy-8-(3-hydroxy-1-methylpiperidin-4-yl)-2-methyl-4H-chromen-4-one (8e). White powder (65 mg, 42% yield), mp 214–218 °C; HPLC t_R = 6.75 min (97% purity); $[\alpha]^{20}_D$ −11.2 (c 0.1, MeOH). ^{1}H NMR (400 MHz, CD$_3$OD): δ 8.01 (d, J = 8.0, 1H), 7.83 (m, J = 8.0, 6.8 Hz, 1H), 7.55–7.43 (m, 2H), 5.97 (brs, 2H), 5.42 (d, J = 13.2 Hz, 1H), 5.17 (d, J = 13.3 Hz, 1H), 4.38 (brs, 1H), 3.95–3.59 (m, 6H of piperidine), 2.41 (s, 3H), 2.03 (s, 3H), 1.84 (m, 1H). ^{13}C NMR (100 MHz, CD$_3$OD): δ 184.4, 169.5, 164.1, 161.9, 158.3, 137.2, 136.4, 135.6, 133.7, 129.6, 128.9, 108.8, 106.2, 105.5, 100.3, 72.1, 69.8, 66.7, 64.6, 53.3, 38.0, 31.3, 20.7. HR ESIMS: m/z 474.0886 [M + H]$^+$ (calcd for C$_{23}$H$_{25}$BrNO$_5$$^+$, 474.0910).

(1′R,2′S)-7-(Cinnamyloxy)-5-hydroxy-8-(3-hydroxy-1-methylpiperidin-4-yl)-2-methyl-4H-chromen-4-one (8f). Yellow powder (65 mg, 47% yield); mp 206–210 °C; HPLC t_R = 6.64 min (98% purity); $[\alpha]^{20}_D$ −2.0 (c 0.1, MeOH). ^{1}H NMR (400 MHz, CD$_3$OD): δ 7.57 (m, 2H), 7.37 (m, 3H), 7.08 (d, J = 15.6 Hz, 1H), 6.51 (m, J = 15.6 Hz, 1H), 6.07 (s, 1H), 5.97 (s, 1H), 4.85 (m, 1H), 4.51 (m, 1H), 4.28 (brs, 1H), 3.78–3.33 (m, 6H of piperidine ring), 3.10 (s, 3H), 2.36 (s, 3H), 1.74 (m, 1H). ^{13}C NMR (100 MHz, CD$_3$OD): δ 180.7, 165.2, 164.6, 159.9, 155.8, 140.8, 135.2, 128.6 (2C), 127.0 (2C), 117.2, 106.7, 106.6, 101.6, 68.2, 64.8, 63.7, 62.4, 52.2, 36.1, 19.9, 19.7. HR ESIMS: m/z 422.1916 [M + H]$^+$ (C$_{25}$H$_{28}$NO$_5$$^+$, 422.1962).

(1′R,2′S)-7-((Furan-2-yl)methoxy)-5-hydroxy-8-(3-hydroxy-1-methylpiperidin-4-yl)-2-methyl-4H-chromen-4-one (8g). White crystalline powder (64 mg, 51% yield); mp 199–200 °C; HPLC t_R = 6.37 min (99.5% purity); $[\alpha]^{20}_D$ −6.0 (c 0.1, MeOH). IR (CHCl$_3$): ν_{max} 3400, 2923, 2359, 1661, 1558, 1410, 1362, 1272, 1186, 1082 cm^{-1}. ^{1}H NMR (400 MHz, CD$_3$OD + CDCl$_3$): δ 7.72 (d, J = 1.2 Hz, 1H), 6.92 (d, J = 3.2 Hz, 1H), 6.58 (dd, J = 3.2, 1.6 Hz, 1H), 6.07 (s, 1H), 5.94 (s, 1H), 5.26 (d, J = 14.4 Hz, 1H), 5.14 (d, J = 14.4 Hz, 1H), 4.29 (brs, 1H), 3.71–3.50 (m, 6H of piperidine), 3.10 (s, 3H), 2.36 (s, 3H), 1.84 (m, 1H). ^{13}C NMR (100 MHz, CD$_3$OD): δ 181.6, 172.2, 167.8, 162.0, 158.0, 157.9, 147.3, 144.9, 113.2, 112.5, 111.9, 108.2, 107.7, 103.1, 66.9, 65.1, 62.7, 58.3, 54.2, 37.4, 23.7, 21.5. HR ESIMS: m/z 386.1571 [M + H]$^+$ (calcd for C$_{21}$H$_{24}$NO$_6$$^+$, 386.1598).

(1′R,2′S)-5-Hydroxy-8-(3-hydroxy-1-methylpiperidin-4-yl)-2-methyl-4-oxo-4H-chromen-7-yl furan-2-carboxylate (8h). White powder (60 mg, 46% yield); mp 184–186 °C; HPLC t_R = 4.88 min (92% purity); $[\alpha]^{20}_D$ −8.0 (c 0.1, MeOH). IR (KBr): ν_{max} 3416, 2924, 1617, 1360, 1424, 1290, 1177, 1113 cm^{-1}. ^{1}H NMR (400 MHz, CD$_3$OD, ppm): 7.73 (dd, J = 0.4, 1.6 Hz, 1H), 7.49 (dd, J = 0.8, 3.6 Hz, 1H), 6.60 (dd, J = 1.6, 3.6 Hz, 1H), 6.22 (s, 1H), 5.96 (s, 1H), 5.58 (brs, 1H), 2H of piperidine ring), 3.89–3.33 (m, 6H of piperidine), 2.97 (s, 3H), 2.34 (s, 3H), 2.10 (m, 1H). ^{13}C NMR (100 MHz, CD$_3$OD, ppm): 184.2, 169.0, 164.1, 162.3, 158.7, 158.2, 148.8, 145.0, 120.9, 113.5, 108.7, 105.2, 104.6, 99.8, 70.4, 58.3, 56.9, 44.7, 36.5, 24.4, 20.5. ESI MS: m/z 400.16 [M + H]$^+$. HR ESIMS: m/z 400.1394 [M + H]$^+$ (calcd for C$_{21}$H$_{22}$NO$_7$$^+$, 400.1391).

Synthesis of Mannich Derivatives 9a–o. To the solution of rohitukine (1, 100 mg, 0.328 mmol) in methanol–water (10 mL, ratio 7:3) was slowly added a solution of formaldehyde (1 mL solution) and secondary amine (0.394 mmol). The resultant reaction mixture was then stirred at 70 °C for 5 h. Products were purified over Sephadex LH20 using methanol as eluent to get a gummy sticky mass, which was solidified in acetone.

(1′R,2′S)-6-((Diethylamino)methyl)-5,7-dihydroxy-8-(3-hydroxy-1-methylpiperidin-4-yl)-2-methyl-4H-chromen-4-one (9a). White solid (57 mg, 45% yield); mp 200–202 °C; HPLC t_R = 4.76 min

(99.1% purity), $[\alpha]^{20}_D$ −3.8 (c 0.1, MeOH). IR (CHCl$_3$): ν_{max} 3400, 2958, 2927, 2858, 1738, 1660, 1610, 1274, 1153, 1019 cm^{-1}. ^{1}H NMR (400 MHz, CD$_3$OD): δ 5.88 (s, 1H), 4.13 (m, 3H), 3.32–3.05 (m, 6H of piperidine + 4H of N-CH$_2$CH$_3$), 2.79 (s, 3H), 2.39 (s, 3H), 1.51 (m, 1H), 1.26 (m, 6H of N CH$_2$CH$_3$). ^{13}C NMR (CD$_3$OD, 125 MHz): 183.1, 174.3, 168.1, 160.8, 158.0, 108.6, 108.0, 103.3, 101.1, 69.2, 61.9, 56.6, 51.5, 44.2, 36.5, 34.8, 23.3, 20.3, 9.3. ESIMS: m/z 391.10 [M + H]$^+$. HR ESIMS: m/z 391.2229 [M + H]$^+$ (calcd for C$_{21}$H$_{31}$N$_2$O$_4$$^+$, 391.2227).

(1′R,2′S)-5,7-Dihydroxy-8-(3-hydroxy-1-methylpiperidin-4-yl)-2-methyl-6-((4-(piperidin-1-yl)piperidin-1-yl)methyl)-4H-chromen-4-one (9b). White solid (66 mg, 42% yield); mp 194–196 °C; HPLC t_R = 5.31 min (97% purity); $[\alpha]^{20}_D$ +5.6 (c 0.1, MeOH). IR (CHCl$_3$): ν_{max} 3399, 3335, 2857, 1659, 1556, 1397, 1323,1152 cm^{-1}. ^{1}H NMR (400 MHz, DMSO-d$_6$): δ 5.91 (s, 1H), 3.93 (brs, 2H), 3.85 (m, 1H), 3.25–2.47 (m, 13H), 2.47 (s, 3H), 2.23 (s, 3H), 1.78–1.34 (m, 11H). ^{13}C NMR (125 MHz, CD$_3$OD): δ 182.9, 172.6, 166.7, 159.7, 156.5, 107.1, 106.6, 102.1, 99.9, 67.7, 60.5, 60.2, 55.3, 49.8, 49.7, 43.0, 42.8, 39.0, 35.6, 24.2, 22.0, 21.9, 18.9. ESIMS: m/z 486.20 [M + H]$^+$. HR ESIMS: m/z 486.2961 [M + H]$^+$ (calcd for C$_{27}$H$_{40}$N$_3$O$_5$$^+$, 486.2968).

(1′R,2′S)-5,7-Dihydroxy-8-(3-hydroxy-1-methylpiperidin-4-yl)-2-methyl-6-((pyrrolidin-1-yl)methyl)-4H-chromen-4-one (9c). White solid (56 mg, 44% yield); mp 189–191 °C; HPLC t_R = 1.56 min (96.0% purity); $[\alpha]^{20}_D$ +11.4 (c 0.1, MeOH). IR (CHCl$_3$): ν_{max} 3400, 2958, 2924, 1738, 1658, 1394, 1151, 1021 cm^{-1}. ^{1}H NMR (400 MHz, CD$_3$OD + DMSO-d$_6$): δ 5.86 (s, 1H), 4.72 (brs, 2H), 4.16 (d, J = 8 Hz, 1H), 3.51–3.05 (m, 10H), 2.76 (s, 3H), 2.26 (s, 3H), 1.99–1.85 (m, 4H), 1.51 (d, 1H). ^{13}C NMR (CD$_3$OD, 125 MHz): δ 183.2, 175.3, 167.8, 158.0, 108.9, 107.8, 104.4, 100.5, 69.4, 62.1, 56.8, 54.6, 50.1, 44.6, 44.3, 37.0, 24.0, 20.1. ESIMS: m/z 389.2 [M + H]$^+$. HR ESIMS: m/z 389.2071 [M + H]$^+$ (calcd for C$_{21}$H$_{29}$N$_2$O$_4$$^+$, 389.2071).

(1′R,2′S)-tert-Butyl-4-((5,7-dihydroxy-8-(3-hydroxy-1-methylpiperidin-4-yl)-2-methyl-4-oxo-4H-chromen-6-yl)methyl)piperazine-1-carboxylate (9d). Cream colored solid (68 mg, 41% yield); mp 197–205 °C; HPLC t_R = 5.92 min (95.8% purity); $[\alpha]^{20}_D$ +2.0 (c 0.1, MeOH). IR (CHCl$_3$): ν_{max} 3394, 2931, 2719, 1692, 1660, 1611, 1459, 1418, 1365, 1280, 1248, 1152, 1167 cm^{-1}. ^{1}H NMR (400 MHz, DMSO-d$_6$): δ 5.92 (s, 1H), 4.09 (m, 3H), 3.56–3.00 (m, 14H), 2.79 (s, 3H), 2.28 (s, 3H), 1.61 (m, 1H), 1.21 (brs, 9H). ^{13}C NMR (CD$_3$OD, 100 MHz): δ 183.7, 168.4, 160.7, 157.7, 155.7, 108.3, 108.0, 103.3, 102.3, 82.1, 68.8, 61.9, 56.8, 52.5, 52.4, 50.3, 49.2, 44.4, 44.2, 40.5, 37.1, 28.7, 28.5, 28.5, 23.3, 20.3. ESIMS: m/z 504 [M + H]$^+$. HR ESIMS: m/z 504.2705 [M + H]$^+$ (calcd for C$_{26}$H$_{38}$N$_3$O$_7$$^+$, 504.2704).

(1′R,2′S)-5,7-Dihydroxy-8-(3-hydroxy-1-methylpiperidin-4-yl)-6-((2-(hydroxymethyl)pyrrolidin-1-yl)methyl)-2-methyl-4H-chromen-4-one (9e). White crystalline solid (50 mg, 36% yield); mp 200–202 °C; HPLC t_R = 5.24 min (99% purity); $[\alpha]^{20}_D$ −2.0 (c 0.1, MeOH). IR (CHCl$_3$): ν_{max} 3335, 2958, 1657, 1463, 1164, 1044 cm^{-1}. ^{1}H NMR (400 MHz, CD$_3$OD + DMSO-d$_6$): δ 6.04 (s, 1H), 4.56–4.03 (m, 3H), 3.99–3.25 (m, 11H, 6H of piperidine + 5H of prolinol), 2.75 (s, 3H), 2.56 (s, 3H), 2.14 (m, 2H), 2.02–1.77 (m, 2H), 1.56–1.50 (m, 1H). ^{13}C NMR (DMSO-d$_6$ + CD$_3$OD): δ 182.8, 169.1, 161.16, 157.8, 108.7, 103.9, 69.9, 68.8, 62.9, 61.5, 60.6, 56.3, 55.4, 48.8, 48.4, 40.5, 39.6, 36.1, 27.3, 24.8, 23.4, 20.4. ESIMS: m/z 419 [M + H]$^+$. HR ESIMS: m/z 419.2170 [M + H]$^+$ (calcd for C$_{22}$H$_{31}$N$_2$O$_5$$^+$, 419.2176).

(1′R,2′S)-6-((4-Benzylpiperidin-1-yl)methyl)-5,7-dihydroxy-8-(3-hydroxy-1-methylpiperidin-4-yl)-2-methyl-4H-chromen-4-one (9f). Cream colored solid (60 mg, 37% yield); mp 218–220 °C; HPLC t_R = 6.18 min (92% purity); $[\alpha]^{20}_D$ −7.3 (c 0.1, MeOH). IR (CHCl$_3$): ν_{max} 3400, 2930, 2704, 1731, 1660, 1609, 1556, 1454, 1396, 1361, 1151, 1041 cm^{-1}. ^{1}H NMR (400 MHz, CD$_3$OD): δ 7.18–7.10 (m, 5H), 5.86 (s, 1H), 4.11 (m, 3H), 3.35–2.80 (m, 10H), 2.79 (s, 3H), 2.26 (s, 3H), 1.75 (brs, 4H), 1.53–1.40 (m, 2H), 0.89 (m, 1H). ^{13}C NMR (125 MHz, CD$_3$OD): δ 184.8, 173.7, 166.5, 159.8, 156.5, 139.2, 128.8, 128.0, 125.5, 107.3, 106.6, 101.6, 99.5, 67.9, 66.2, 60.4, 55.2, 47.1, 42.8, 38.8, 38.2, 35.4, 30.21, 28.7, 22.4, 18.9. ESIMS: m/z 479.1 [M + H]$^+$. HR ESIMS: m/z 493.2694 [M + H]$^+$ (calcd for C$_{29}$H$_{37}$N$_2$O$_4$$^+$, 493.2697).

(1′R,2′S)-2-(N-((5,7-Dihydroxy-8-(3-hydroxy-1-methylpiperidin-4-yl)-2-methyl-4-oxo-4H-chromen-6-yl)methyl)-N-methylamino)-

acetic Acid (9g). White powder (45 mg, 31% yield), mp 210–212 °C; HPLC t_R = 3.82 min (99% purity); [α]$^{20}_D$ +6.0 (c 0.1, MeOH). IR (CHCl$_3$): ν$_{max}$ 3400, 2229, 2852, 1618, 1384, 1021 cm^{-1}. ^{1}H NMR (400 MHz, CD$_3$OD): δ 6.01 (s, 1H), 4.31–4.28 (m, 3H), 3.69–3.25 (m, 8H), 2.83 (s, 3H), 2.80 (s, 3H), 2.32 (s, 3H), 1.61 (d, J = 13.3 Hz, 1H). ^{13}C NMR (100 MHz, CD$_3$OD): δ 182.3, 167.5, 168.2, 159.8, 156.3, 107.2, 106.3, 102.08, 101.3, 67.0, 59.8, 54.7, 49.3, 42.6, 40.4, 34.6, 28.0, 21.4, 18.7. ESIMS: m/z 407.0 [M + H]$^+$. HR ESIMS: m/z 407.1809 [M + H]$^+$ (calcd for C$_{20}$H$_{27}$N$_2$O$_7$$^+$, 407.1812).

(1′R,2′S)-5,7-Dihydroxy-8-(3-hydroxy-1-methylpiperidin-4-yl)-2-methyl-6-(morpholinomethyl)-4H-chromen-4-one (9h). Cream colored solid (46 mg, 33% yield); mp 202–205 °C; HPLC t_R = 3.89 min (99% purity); [α]$^{20}_D$ +3.2 (c 0.1, MeOH). IR (CHCl$_3$): ν$_{max}$ 3435, 2921, 2851, 1740, 1631, 1384, 1019 cm^{-1}. ^{1}H NMR (400 MHz, CD$_3$OD + DMSO-d$_6$): δ 5.90 (s, 1H), 4.11 (m, 3H), 3.77 (brs, 4H), 3.42–3.00 (m, 14H), 2.78 (s, 3H), 2.25 (s, 3H), 1.55 (d, J = 12 Hz, 1H). ^{13}C NMR (100 MHz, CD$_3$OD): δ 183.6, 175.25, 166.43, 161.0, 157.9, 106.2, 102.8, 102.0, 65.7, 64.9, 61.8, 56.7, 52.8, 52.7, 44.7, 44.2, 24.8, 20.4. ESIMS: m/z 405.2 [M – H]$^-$. HR ESIMS: m/z 405.2028 [M + H]$^+$ (calcd for C$_{21}$H$_{29}$N$_2$O$_6$$^+$, 405.2020).

(1′R,2′S)-5,7-Dihydroxy-8-(3-hydroxy-1-methylpiperidin-4-yl)-2-methyl-6-((4-phenylpiperidin-1-yl)methyl)-4H-chromen-4-one (9i). Cream colored solid (55 mg, 35% yield); mp 197–200 °C; HPLC t_R = 5.89 min (98% purity); [α]$^{20}_D$ +9.0 (c 0.1, MeOH). IR (CHCl$_3$): ν$_{max}$ 3400, 2932, 2700, 1732, 1661, 1604, 1558, 1454, 1396, 1362, 1152, 1042 cm^{-1}. ^{1}H NMR (400 MHz, Pyr-d$_5$): δ 7.48–7.22 (m, 5H), 6.13 (s, 1H), 4.54 (s, 1H), 4.25 (s, 2H), 3.92–3.75 (m, 5H), 3.52–2.89 (m, 5H), 2.55 (s, 3H), 2.32 (s, 3H), 2.22–1.81 (m, 6H). ^{13}C NMR (100 MHz, Pyr-d$_5$): δ 186.3, 175.3, 167.9, 161.3, 158.0, 145.4, 129.7, 127.9, 127.7, 108.8, 108.0, 103.1, 100.8, 69.3, 61.9, 56.7, 47.2, 46.1, 42.0, 41.0, 37.0, 31.1, 23.1, 20.2. ESIMS: m/z 479.1 [M + H]$^+$. HR ESIMS: m/z 479.2536 [M + H]$^+$ (calcd for C$_{28}$H$_{35}$N$_2$O$_5$$^+$, 479.2540).

(1′R,2′S)-Ethyl-4-((5,7-dihydroxy-8-(3-hydroxy-1-methyl piperidin-4-yl)-2-methyl-4-oxo-4H-chromen-6-yl)methyl)piperazine-1-carboxylate (9j). White colored solid (55 mg, 35% yield); mp 218–224 °C; HPLC t_R = 6.03 min (99% purity); [α]$^{20}_D$ –4.8 (c 0.1, MeOH). IR (CHCl$_3$): ν$_{max}$ 3400, 2930, 1696, 1660, 1611, 1468, 1429, 1395, 1323, 1245, 1151, 1100, 1034 cm^{-1}. ^{1}H NMR (400 MHz, DMSO-d$_6$): δ 5.92 (s, 1H), 4.08–4.01 (m, 5H), 3.57–2.80 (m, 14H), 2.79 (s, 3H), 2.39 (s, 3H), 1.63 (m, 1H), 1.19 (m, 3H). ^{13}C NMR (101 MHz, Pyr-d$_5$): δ 184.7, 169.0, 166.1, 160.7, 158.3, 156.9, 109.7, 107.9, 105.5, 105.0, 82.4, 69.8, 63.1, 62.9, 54.2, 53.5, 52.9, 45.2, 15.0, 38.9, 21.9, 16.1. ESIMS: m/z 476.2 [M + H]$^+$. HR ESIMS: m/z 476.2400 [M + H]$^+$ (calcd for C$_{24}$H$_{34}$N$_3$O$_7$$^+$, 476.2391).

(1′R,2′S)-6-((Diisopropylamino)methyl)-5,7-dihydroxy-8-(3-hy-droxy-1-methylpiperidin-4-yl)-2-methyl-4H-chromen-4-one (9k). Cream colored solid (65 mg, 47% yield); mp 190–196 °C; HPLC t_R = 4.73 min (99% purity); [α]$^{20}_D$ –19.0 (c 0.1, MeOH). IR (CHCl$_3$): ν$_{max}$ 3400, 2932, 2852, 1618, 1384, 1022 cm^{-1}. ^{1}H NMR (400 MHz, DMSO-d$_6$): δ 6.05 (s, 1H), 4.41 (m, 1H), 4.00 (s, 2H), 4.00–3.17 (m, 8H), 2.80 (s, 3H), 2.33 (s, 3H), 1.52 (m, 1H), 1.33–1.22 (m, 12H). ^{13}C NMR (125 MHz, CD$_3$OD): δ 184.0, 169.2, 167.9, 163.2, 155.8, 113.0, 108.1, 106.8, 103.9, 68.3, 61.4, 56.5, 55.5, 43.9, 36.5, 35.1, 31.5, 22.9, 20.3. ESIMS: m/z 419.1 [M + H]$^+$. HR ESIMS: m/z 419.2543 [M + H]$^+$ (calcd for C$_{23}$H$_{35}$N$_2$O$_5$$^+$, 419.2540).

(1′R,2′S)-4-Hydroxy-1-((5,7-dihydroxy-8-(3-hydroxy-1-methylpi-peridin-4-yl)-2-methyl-4-oxo-4H-chromen-6-yl)methyl)pyrrolidine-2-carboxylic Acid (9l). Crystalline solid (55 mg, 37% yield); mp 201–205 °C; HPLC t_R = 3.80 min (92% purity); [α]$^{20}_D$ +7.0 (c 0.1, MeOH). IR (CHCl$_3$): ν$_{max}$ 3435, 2921, 2852, 1739, 1589, 1418, 1219, 1019 cm^{-1}. ^{1}H NMR (400 MHz, CD$_3$OD): δ 6.01 (s, 1H), 4.31 (brs, 2H), 4.26 (s, 1H), 3.95 (d, J = 8 Hz, 1H), 3.67 (d, J = 12 Hz, 1H), 3.50–3.25 (m, 6H), 2.81 (s, 3H), 2.80 (m, 1H), 2.52 (m, 1H), 2.37 (s, 3H), 2.13 (d, J = 12 Hz, 1H), 1.60 (d, J = 12 Hz, 1H), 1.25 (m, 1H). ^{13}C NMR (CD$_3$OD, 125 MHz): δ 184.0 (2C), 172.4, 169.2, 161.1, 157.7, 108.9, 107.8, 103.9, 103.7, 70.2, 68.6, 62.3, 61.4, 57.5, 56.3, 44.3, 39.0, 36.0, 23.3, 20.3, 17.4. ESIMS: m/z 449.1 [M + H]$^+$. HR ESIMS: m/z 449.1922 [M + H]$^+$ (calcd as C$_{23}$H$_{29}$N$_2$O$_8$$^+$, 449.1918).

(1′R,2′S)-1-((5,7-Dihydroxy-8-(3-hydroxy-1-methylpiperidin-4-yl)-2-methyl-4-oxo-4H-chromen-6-yl)methyl)pyrrolidine-2-carboxylic

Acid (9m). White crystalline solid (65 mg, 46% yield); mp 218–220 °C; HPLC t_R = 5.18 min (99% purity); [α]$^{20}_D$ –2.0 (c 0.1, MeOH). IR (CHCl$_3$): ν$_{max}$ 3436, 2923, 2852, 1742, 1616, 1418, 1019 cm^{-1}. ^{1}H NMR (400 MHz, CD$_3$OD): δ 6.04 (s, 1H), 4.69 (brs, 2H), 4.33–4.26 (m, 3H), 3.85–3.21 (m, 7H of piperidine ring and 1H of proline), 2.83 (s, 3H), 2.32 (s, 3H), 2.06 (m, 2H), 1.84 (m, 1H), 1.59 (m, 1H), 1.24 (m, 1H). ^{13}C NMR (101 MHz, Pyr-d$_5$): δ 184.39 (2C), 168.34, 160.89, 158.53, 151.96, 109.49, 108.49, 108.16, 104.04, 69.92, 69.12, 62.47, 57.40, 54.97, 51.12, 45.42, 38.58, 31.27, 25.36, 24.28, 21.81. ESIMS: m/z 433.2 [M + H]$^+$. HR ESIMS: m/z 433.1970 [M + H]$^+$ (calcd for C$_{22}$H$_{29}$N$_2$O$_7$$^+$, 433.1969).

(1′R,2′S)-5,7-Dihydroxy-8-(3-hydroxy-1-methylpiperidin-4-yl)-2-methyl-6-((4-methylpiperazin-1-yl)methyl)-4H-chromen-4-one (9n). Cream colored powder (56 mg, 41% yield); mp 210–212 °C; HPLC t_R = 4.97 min (99% purity); [α]$^{20}_D$ –3.0 (c 0.1, MeOH). IR (CHCl$_3$): ν$_{max}$ 3400, 2923, 2852, 1659, 1559, 1466, 1391, 1274, 1150 cm^{-1}. ^{1}H NMR (400 MHz, CD$_3$OD + DMSO-d$_6$): δ 5.88 (s, 1H), 4.04 (m, 3H), 3.51–2.56 (m, 14H), 2.81 (s, 3H), 2.56 (s, 3H), 2.25 (m, 3H), 1.54 (d, J = 12 Hz, 1H). ^{13}C NMR (101 MHz, DMSO-d$_6$): δ 181.2, 172.8, 165.9, 158.7, 155.6, 106.8, 106.5, 101.9, 99.8, 66.8, 59.8, 54.6, 52.2, 51.1, 50.3, 44.5, 43.2, 42.6, 35.5, 19.9. ESIMS: m/z 418.3 [M + H]$^+$. HR ESIMS: m/z 418.2341 [M + H]$^+$ (calcd for C$_{22}$H$_{32}$N$_3$O$_5$$^+$, 418.2336).

(1′R,2′S)-5,7-Dihydroxy-8-(3-hydroxy-1-methylpiperidin-4-yl)-2-methyl-6-((piperidin-1-yl)methyl)-4H-chromen-4-one (9o). Cream colored solid (68 mg, 52% yield); mp 199–205 °C; HPLC t_R = 5.15 min (99% purity); [α]$^{20}_D$ +10.0 (c 0.1, MeOH). IR (CHCl$_3$): ν$_{max}$ 3400, 2928, 2858, 1734, 1659, 1459, 1395, 1157, 1032 cm^{-1}. ^{1}H NMR (400 MHz, DMSO-d$_6$): δ 5.98 (s, 1H), 4.08–3.92 (m, 3H), 3.04–2.80 (m, 4H), 2.61 (s, 3H), 2.31 (s, 3H), 1.68 (m, 4H), 1.53 (m, 4H), 1.25 (m, 3H), 0.85 (m, 2H). ^{13}C NMR (100 MHz, CD$_3$OD): δ 180.8, 172.6, 165.4, 158.9, 155.5, 107.2, 106.5, 101.2, 98.6, 67.5, 65.7, 60.5, 55.06, 51.55, 50.6, 43.8, 43.5, 38.1, 33.1, 28.2, 20.3, 17.1. ESIMS: m/z 403.2 [M + H]$^+$. HR ESIMS: m/z 403.2232 [M + H]$^+$ (calcd for C$_{22}$H$_{31}$N$_2$O$_5$$^+$, 403.2227).

Synthesis of Baylis–Hillman Derivatives 10a–n. The solution of rohitukine (1, 100 mg, 0.328 mmol) in methanol (5 mL) was stirred with substituted aromatic and aliphatic aldehydes (0.328 mmol) in the presence of DABCO (0.328 mmol). The reaction mixture was then continuously stirred for 10–15 days; however, in none of the reactions was starting material completely consumed. The crude products were purified by preparative TLC.

(1′R,2′S)-5,7-Dihydroxy-3-(hydroxy(4-nitrophenyl)methyl)-8-(3-hydroxy-1-methylpiperidin-4-yl)-2-methyl-4H-chromen-4-one (10a). Cream colored solid (76 mg, 51% yield); mp 202–205 °C; HPLC t_R = 5.58 min (99% purity); [α]$^{20}_D$ +4.0 (c 0.1, MeOH). IR (CHCl$_3$): ν$_{max}$ 3400, 2923, 1658, 1556, 1468, 1389, 1273, 1150, 1025 cm^{-1}. ^{1}H NMR (400 MHz, DMSO-d$_6$): δ 13.57 (s, 1H), 8.32 (dd, J = 4.8, 10 Hz, 2H), 7.72 (dd, J = 4.4, 10.1 Hz, 2H), 5.94 (m, 2H), 3.94 (brs, 1H), 3.25–3.05 (m, 6H of piperidine), 2.60 (s, 3H), 1.88 (s, 3H), 1.27 (m, 1H). ^{13}C NMR (100 MHz, DMSO-d$_6$): δ 180.6, 175.2, 172.4, 164.7, 155.5, 154.6, 145.7, 126.6, 122.8, 112.4, 108.4, 105.4, 98.2, 68.5, 61.3, 55.5, 44.5, 36.4, 23.0, 21.9, 19.7. ESIMS: m/z 457.1 [M + H]$^+$. HR ESIMS: m/z 457.1604 [M + H]$^+$ (calcd for C$_{23}$H$_{25}$N$_2$O$_8$$^+$, 457.1605).

(1′R,2′S)-3-((4-Chlorophenyl)(hydroxy)methyl)-5,7-dihydroxy-8-(3-hydroxy-1-methylpiperidin-4-yl)-2-methyl-4H-chromen-4-one (10b). White solid (95 mg, 65% yield); mp 218–220 °C; HPLC t_R = 5.83 min (99% purity); [α]$^{20}_D$ –7.0 (c 0.1, MeOH). IR (CHCl$_3$): ν$_{max}$ 3400, 2926, 1659, 1556, 1468, 1361, 1127, 1014 cm^{-1}. ^{1}H NMR (400 MHz, CD$_3$OD): δ 7.38–7.30 (m, 2H), 7.14–7.10 (m, 2H), 5.92 (m, 1H), 5.84 (m, 1H), 4.03 (brs, 1H), 3.50–3.00 (m, 6H), 2.73 (s, 3H), 2.34 (s, 3H), 1.61 (m, 1H). ^{13}C NMR (126 MHz, CD$_3$OD): δ 181.9, 174.2, 165.9, 156.2, 155.3, 144.5, 131.5, 127.7, 113.1, 107.6, 106.4, 68.2, 60.7, 55.4, 42.7, 36.6, 29.3, 21.9, 18.7. ESIMS: m/z 446.1 [M + H]$^+$. HR ESIMS: m/z 446.1342 [M + H]$^+$ (calcd for C$_{23}$H$_{25}$ClNO$_6$$^+$, 446.1364).

(1′R,2′S)-3-((3-Chlorophenyl)(hydroxy)methyl)-5,7-dihydroxy-8-(3-hydroxy-1-methylpiperidin-4-yl)-2-methyl-4H-chromen-4-one (10c). White powder (66 mg, 45% yield); mp 215–217 °C; HPLC t_R = 6.74 min (99% purity); [α]$^{20}_D$ +3.0 (c 0.1, MeOH). IR (CHCl$_3$):

ν_{max} 3400, 2925, 1659, 1570, 1388, 1273, 1150, 1027 cm^{-1}. ^{1}H NMR (400 MHz, DMSO-d_6): δ 13.46 (s, 1H), 7.47–7.17 (m, 4H), 5.91 (m, 1H), 5.97 (m, 1H) 3.88 (brs, 1H), 3.30–2.78 (m, 6H of piperidine), 2.51 (s, 3H), 2.34 (s, 3H), 1.13 (m, 1H). ^{13}C NMR (100 MHz, CD$_3$OD): δ 183.6, 175.0, 167.2, 161.6, 157.7, 156.3, 149.6, 142.6, 134.2, 130.7, 127.2, 127.0, 125.8, 114.5, 108.0, 102.1, 70.6, 69.6, 62.6, 56.4, 44.2, 37.0, 23.5, 20.2. ESIMS: m/z 446.1 [M + H]$^+$. HR-ESIMS: m/z 446.1365 [M + H]$^+$ (calcd for C$_{23}$H$_{25}$ClNO$_6$, 446.1364).

(1'R,2'S)-3-((2-Bromophenyl)(hydroxy)methyl)-5,7-dihydroxy-8-(3-hydroxy-1-methylpiperidin-4-yl)-2-methyl-4H-chromen-4-one (10d). Colorless needles (58 mg, 36% yield); mp 212–215 °C; HPLC t_R = 6.51 min (99% purity); [α]^{20}$_D$ +6.3 (c 0.1, MeOH). IR (CHCl$_3$) ν_{max} 3391, 2923, 1656, 1558, 1465, 1387, 1273, 1149, 1026 cm^{-1}. ^{1}H NMR (400 MHz, CD$_3$OD): δ 7.51–7.06 (m, 4H), 6.37 (m, 1H), 5.88 (m, 1H), 4.17 (brs, 1H), 3.09–3.08 (m, 6H of piperidine), 2.86 (s, 3H), 2.32 (s, 3H), 1.60 (m, 1H). ^{13}C NMR (101 MHz, CD$_3$OD): δ 183.3, 176.6, 167.1, 158.0, 156.7, 144.8, 133.7, 130.7, 129.7, 128.3, 125.5, 112.4, 109.7, 107.7, 101.4, 72.0, 70.5, 62.8, 57.4, 45.1, 37.8, 24.3, 20.2. ESIMS: m/z 491.1 [M + H]$^+$. HR-ESIMS: 492.0848 [M + H]$^+$ (calcd for C$_{23}$H$_{25}$BrNO$_6$, 492.0845).

(1'R,2'S)-3-((3-Bromo-4-fluorophenyl)(hydroxy)methyl)-5,7-dihydroxy-8-(3-hydroxy-1-methylpiperidin-4-yl)-2-methyl-4H-chromen-4-one (10e). Light yellowish solid (60 mg, 36% yield); mp 217–221 °C; HPLC t_R = 5.49 min (96% purity); [α]^{20}$_D$ −12.0 (c 0.1, MeOH). IR (CHCl$_3$) ν_{max} 3400, 2925, 1659, 1551, 1490, 1468, 1411, 1100, 1026 cm^{-1}. ^{1}H NMR (400 MHz, DMSO-d_6): δ 7.70 (m, 1H), 7.42 (m, 1H), 7.23 (m, 1H), 5.92 (m, 1H), 5.75 (m, 1H), 4.00 (m, 1H), 3.34–2.51 (m, 6H of piperidine), 2.51 (s, 3H), 2.24 (s, 3H), 1.32 (m, 1H). ^{13}C NMR (125 MHz, CD$_3$OD): δ 183.3, 175.2, 167.2, 160.0 (d, $^1J_{CF}$ = 254 Hz), 156.8, 145.2, 132.1, 128.1, 116.4, 116.3, 109.3, 108.2, 107.9 (d, $^3J_{CF}$ = 7 Hz), 101.8, 76.6, 70.2, 62.5, 57.1, 44.7, 37.4, 23.6, 20.1. ESIMS: m/z 508.1 [M + H]$^+$. HR-ESIMS: m/z 508.0765 [M + H]$^+$ (calcd for C$_{23}$H$_{24}$BrFNO$_6$, 508.0765).

(1'R,2'S)-3-((2,6-Dichlorophenyl)(hydroxy)methyl)-5,7-dihydroxy-8-(3-hydroxy-1-methylpiperidin-4-yl)-2-methyl-4H-chromen-4-one (10f). Cream colored solid (55 mg, 35% yield); mp 216–217 °C; HPLC t_R = 6.67 min (99% purity); [α]^{20}$_D$ +12.0 (c 0.1, MeOH). IR (CHCl$_3$) ν_{max} 3400, 2922, 1651, 1561, 1465, 1386, 1260, 1032 cm^{-1}. ^{1}H NMR (500 MHz, CD$_3$OD): δ 7.89 (s, 1H), 7.30 (m, 1H), 7.17 (m, 1H), 6.91 (m, 1H), 5.95 (s, 1H), 4.20 (brs, 1H), 4.00–3.21 (m, 6H of piperidine), 3.18 (s, 3H), 2.35 (s, 3H), 1.82 (m, 1H). ^{13}C NMR (125 MHz, CD$_3$OD): δ 182.0, 172.1, 166.1, 157, 155, 144.1, 132.3, 128.7, 127.4, 110.9, 107.3, 100.7, 68.4, 68.4, 60.7, 55.4, 43.0, 35.5, 21.8, 18.2. ESIMS: m/z 480.1 [M + H]$^+$. HR-ESIMS: m/z 480.0947 [M + H]$^+$ (calcd for C$_{23}$H$_{24}$Cl$_2$NO$_6$, 480.0951).

(1'R,2'S)-3-((2-Chloro-6-fluorophenyl)(hydroxy)methyl)-5,7-dihydroxy-8-(3-hydroxy-1-methylpiperidin-4-yl)-2-methyl-4H-chromen-4-one (10g). White powder (50 mg, 40% yield); mp 214–217 °C; HPLC t_R = 5.82 min (93.7% purity); [α]^{20}$_D$ −10.0 (c 0.1, MeOH). IR (CHCl$_3$) ν_{max} 3400, 2922, 1660, 1556, 1468, 1390, 1273, 1153, 1023 cm^{-1}. ^{1}H NMR (500 MHz, DMSO-d_6): δ 13.15 (s, 1H), 7.28 (m, 2H), 7.61 (m, 1H), 6.32 (m, 1H), 5.87 (s, 1H), 4.04 (brs, 2H), 3.33–3.10 (m, 5H of piperidine), 2.75 (s, 3H), 2.27 (s, 3H), 1.44 (m, 1H). ^{13}C NMR (125 MHz, CD$_3$OD): δ 181.4, 175.5, 165.4, 156.5 (d, $^1J_{CF}$ = 115 Hz), 144.3, 130.7, 126.9, 115.1, 113, 107.7 (d, $^2J_{CF}$ = 31 Hz), 106.5, 98.8, 68.2, 68.8, 60.6, 43.3, 35.4, 22.0, 19.5. HR-ESIMS: m/z 464.1271 [M + H]$^+$ (calcd for C$_{23}$H$_{24}$ClFNO$_6$, 464.1270).

(1'R,2'S)-5,7-Dihydroxy-3-(hydroxy(5-nitrothiophen-3-yl)methyl)-8-(3-hydroxy-1-methylpiperidin-4-yl)-2-methyl-4H-chromen-4-one (10h). Brown colored solid (75 mg, 50% yield); mp 311–316 °C; HPLC t_R = 5.41 min (97% purity); [α]^{20}$_D$ −11.0 (c 0.1, MeOH). IR (CHCl$_3$) ν_{max} 3400, 2923, 1657, 1601, 1386, 1333, 1273, 1149, 1033 cm^{-1}. ^{1}H NMR (400 MHz, CD$_3$OD): δ 7.88 (d, J = 4 Hz, 1H), 7.49 (d, J = 4 Hz, 1H), 5.92 (m, 1H), 5.83 (m, 1H), 4.07 (brs, 1H), 3.94–2.98 (m, 6H of piperidine), 2.71 (s, 3H), 2.23 (s, 3H), 1.46 (m, 1H). ^{13}C NMR (CD$_3$OD, 100 MHz): δ 181.9, 174.1, 166.1, 156.2, 151.2, 147.7, 128.4, 127.7, 127.0, 112.1, 107.8, 106.4, 99.4, 68.1, 66.4, 60.7, 55.4, 42.2, 35.6, 22.0, 18.7. ESIMS: m/z 463.1 [M + H]$^+$. HR-ESIMS: m/z 463.1172 [M + H]$^+$ (calcd for C$_{21}$H$_{23}$N$_2$O$_8$S, 463.1169).

(1'R,2'S)-3-((3-Bromo-4-methoxyphenyl)(hydroxy)methyl)-5,7-dihydroxy-8-(3-hydroxy-1-methylpiperidin-4-yl)-2-methyl-4H-chro-

men-4-one (10i). Cream colored solid (64 mg, 40% yield); mp 203–207 °C; HPLC t_R = 5.04 min (99% purity); [α]^{20}$_D$ +10.0 (c 0.1, MeOH). IR (CHCl$_3$) ν_{max} 3400, 2928, 1659, 1602, 1552, 1494, 1468, 1397, 1271, 1121, 1042 cm^{-1}. ^{1}H NMR (400 MHz, CD$_3$OD): δ 7.65 (m, 1H), 7.39 (m, 1H), 6.89 (m, 1H), 6.97 (m, 1H), 5.88 (m, 1H), 4.0 (brs, 1H), 3.42–2.78 (m, 7H), 3.20 (s, 3H), 3.28 (s, 3H), 2.61 (s, 3H), 1.46 (m, 1H). ^{13}C NMR (100 MHz, CD$_3$OD): δ 183.5, 167.1, 160.2, 157.4, 156.9, 155.8, 141.1, 137.7, 135.0, 132.7, 128.0, 113.2, 111.7, 109.3, 107.7, 101.1, 77.8, 77.4, 62.7, 57.0, 46.1, 37.7, 31.8, 24.1, 20.2. ESIMS: m/z 520.0 [M + H]$^+$. HR-ESIMS: m/z 520.0918 [M + H]$^+$ (calcd for C$_{24}$H$_{27}$BrNO$_7$, 520.0915).

(1'R,2'S)-3-((3,5-Difluorophenyl)(hydroxy)methyl)-5,7-dihydroxy-8-(3-hydroxy-1-methylpiperidin-4-yl)-2-methyl-4H-chromen-4-one (10j). White solid (64 mg, 44% yield); mp 202–206 °C; HPLC t_R = 5.13 min (98% purity); [α]^{20}$_D$ −14.8 (c 0.1, MeOH). IR (CHCl$_3$) ν_{max} 3391, 2924, 1659, 1557, 1465, 1388, 1272, 1113 cm^{-1}. ^{1}H NMR (CD$_3$OD, 400 MHz): δ 6.94 (m, 2H), 6.58 (m, 1H), 5.91 (m, 1H), 5.83 (m, 1H), 4.03 (m, 1H), 3.68–2.91 (m, 6H), 2.74 (s, 3H), 2.23 (s, 3H), 1.48 (m, 1H). ^{13}C NMR (CD$_3$OD): δ 181.9, 173.7, 166.0, 163.8 (d, $^1J_{CF}$ = 198 Hz), 161.7, 156.3, 155.4, 150.9, 112.7, 108.3 (d, $^3J_{CF}$ = 20 Hz), 107.6, 100.7 (d, $^2J_{CF}$ = 41 Hz), 99.6, 68.8, 68.1, 60.6, 55.4, 44.2, 35.5, 21.9, 18.8. ESIMS: m/z 448.6 [M + H]$^+$. HR-ESIMS: m/z 448.1534 [M + H]$^+$ (calcd for C$_{23}$H$_{24}$F$_2$NO$_6$, 448.1561).

(1'R,2'S)-3-((2-Bromo-5-ethoxyphenyl)(hydroxy)methyl)-5,7-dihydroxy-8-(3-hydroxy-1-methylpiperidin-4-yl)-2-methyl-4H-chromen-4-one (10k). Cream colored solid (75 mg, 43% yield); mp 203–206 °C; HPLC t_R = 5.36 min (99% purity); [α]^{20}$_D$ +3.0 (c 0.1, MeOH). IR (CHCl$_3$) ν_{max} 3391, 2924, 1657, 1590, 1470, 1414, 1387, 1273, 1122, 1040 cm^{-1}. ^{1}H NMR (400 MHz, CD$_3$OD): δ 7.34–7.14 (m, 2H), 6.75 (m, 1H), 6.33 (m, 1H), 5.81 (m, 1H), 3.95 (m, 3H), 3.50–3.21 (m, 9H), 2.35 (s, 3H), 1.55–1.50 (m, 4H). ^{13}C NMR (100 MHz, CD$_3$OD): δ 182.2, 166.3, 156.9, 155.8, 155.5, 134.3, 131.3, 130.7, 128.7, 125.9, 114.3, 113.3, 111.7, 107.2, 106.6, 67.9, 64.9, 63.7, 60.8, 55.7, 42.6, 35.7, 22.0, 18.5, 13.7. ESIMS: m/z 534.6 [M + H]$^+$. HR-ESIMS: m/z 534.1109 [M + H]$^+$ (calcd for C$_{25}$H$_{29}$BrNO$_7$, 534.1121).

(1'R,2'S)-3-((2,3-Dichlorophenyl)(hydroxy)methyl)-5,7-dihydroxy-8-(3-hydroxy-1-methylpiperidin-4-yl)-2-methyl-4H-chromen-4-one (10l). White crystalline powder (66 mg, 42% yield); mp 218–220 °C; HPLC t_R = 5.35 min (97% purity); [α]^{20}$_D$ −9.0 (c 0.1, MeOH). IR (CHCl$_3$) ν_{max} 3400, 2923, 1658, 1556, 1466, 1387, 1242, 1101 cm^{-1}. ^{1}H NMR (400 MHz, CD$_3$OD): δ 7.45–7.35 (m, 2H), 7.15 (m, 1H), 6.50 (m, 1H), 5.95 (brs, 1H), 4.25 (brs, 1H), 3.68–3.32 (m, 6H of piperidine), 2.88 (s, 3H), 2.39 (s, 3H), 1.78 (m, 1H). ^{13}C NMR (CD$_3$OD, 125 MHz): δ 182.0, 166.0, 157.0, 155.4, 144.3, 132.3, 132.0, 128.7, 128.2, 127.4, 126.8, 110.9, 107.3, 106.8, 100.1, 68.4, 68.02, 60.7, 55.4, 43.0, 35.6, 22.0, 18.8. HR-ESIMS: m/z 480.0947 [M + H]$^+$ (calcd for C$_{23}$H$_{24}$Cl$_2$NO$_6$, 480.0975).

(1'R,2'S)-3-((E)-Dodec-1-enyl)-5,7-dihydroxy-8-(3-hydroxy-1-methylpiperidin-4-yl)-2-methyl-4H-chromen-4-one (10m). White crystalline solid (70 mg, 45% yield); mp 185–192 °C; HPLC t_R = 4.80 min (99% purity); [α]^{20}$_D$ +14.0 (c 0.1, MeOH). IR (CHCl$_3$) ν_{max} 2921, 1657, 1576, 1425, 1272, 1040 cm^{-1}. ^{1}H NMR (400 MHz, CD$_3$OD): δ 6.56 (m, 1H), 5.83 (s, 1H), 4.05 (brs, 1H), 3.49–2.80 (m, 6H of piperidine), 2.63 (s, 3H), 2.24 (s, 3H), 2.14 (m, 2H), 1.39 (m, 1H), 1.20 (brs, 16H), 0.81 (m, 3H). ^{13}C NMR (100 MHz, CD$_3$OD): δ 183.4, 167.0, 159.3, 155.7, 134.1, 122.2, 112.7, 108.5, 107.9, 69.8, 62.5, 57.1, 44.7, 37.2, 36.0, 33.0, 31.1, 30.7, 30.7, 30.7, 30.4, 23.8, 23.7, 20.1, 14.4. HR-ESIMS: m/z 472.3013 [M + H]$^+$ (calcd for C$_{28}$H$_{42}$NO$_5$, 472.3058).

(1'R,2'S)-3-((4-Fluorophenyl)(hydroxy)methyl)-5,7-dihydroxy-8-(3-hydroxy-1-methylpiperidin-4-yl)-2-methyl-4H-chromen-4-one (10n). White needles (65 mg, 46% yield); mp 196–200 °C; HPLC t_R = 7.38 min (99% purity); [α]^{20}$_D$ −4.0 (c 0.1, MeOH). IR (CHCl$_3$) ν_{max} 3400, 2927, 1658, 1602, 1549, 1462, 1388, 1272, 1155, 1027 cm^{-1}. ^{1}H NMR (400 MHz, DMSO-d_6): δ 7.41 (m, 2H), 6.97 (m, 2H), 5.80 (m, 1H), 5.7 (m, 1H), 3.94 (m, 1H), 3.22–2.71 (m, 6H of piperidine), 2.68 (s, 3H), 2.32 (s, 3H), 1.29 (m, 1H). ^{13}C NMR (100 MHz, DMSO-d_6): δ 181.2, 166.3, 161.3 (d, $^1J_{CF}$ = 195 Hz), 157.4, 157.5, 136.8, 126.9 (d, $^3J_{CF}$ = 7 Hz), 112.8 (d, $^2J_{CF}$ = 24 Hz), 110.2, 105.9, 105.7, 106.9, 99.9, 73.8, 75.4, 66.9, 54.7, 54.5, 42.0, 38.3, 35.2,

28.2, 21.4, 17.8. ESIMS: m/z 430.1 [M + H]⁺. HR ESIMS: m/z 430.1664 [M + H]⁺ (calcd for C₂₅H₂₅FNO₃⁺, 430.1660).

Synthesis of Styryl Derivatives 11a–i. The solution of rohitukine (1, 100 mg, 0.328 mmol) in methanol or ethanol (10 mL) was stirred with substituted aryl aldehyde (0.394 mmol) in the presence of 15% aqueous KOH (few drops) as a catalyst (10 equiv). The reaction mixture was continuously stirred for 10–15 h. An intense yellow colored band was separated using preparative TLC to get styryl derivatives 11a–i.

The styryl derivative 11d was synthesized in large quantity for testing in animal models. For large scale synthesis, a slightly modified protocol was used. Briefly, 30 g of rohitukine (0.09804 mol) was dissolved in a solution of 500 mL of methanol containing 38.5 g (0.69 mol, 7 equiv) of KOH. To this mixture was added 17.19 g (0.098 mol) of 2,6-dichlorobenzaldehyde, and the resultant mixture was stirred at 100 °C for 3–4 h. After completion of the reaction, the mixture was cooled and neutralized with 6 N HCl. The precipitate was filtered and washed with 50 mL of methanol/water (30:70) to remove the unreacted aldehyde and further washed with acetone. Finally, it was recrystallized using methanol/chloroform (20:80) to get styryl derivative 11d in 62% yield (28 g). Using this protocol, total 270 g (HPLC purity >99%) of 11d was synthesized.

(1′R,2′S)-5,7-Dihydroxy-8-(3-hydroxy-1-methylpiperidin-4-yl)-2-styryl-4H-chromen-4-one (11d). Yellow solid (60 mg, 47% yield), mp 198–200 °C; HPLC tₑ = 7.07 min (99% purity), [α]²⁵_D −2.4 (c 0.1, MeOH). IR (CHCl₃): νₘₐₓ 3400, 2921, 1652, 1584, 1381, 1276, 1187, 1085 cm⁻¹. ¹H NMR (500 MHz, DMSO-d₆): δ 7.61 (m, 2H), 7.41 (d, J = 16 Hz, 1H), 7.30 (m, 3H), 6.92 (d, J = 16 Hz, 1H), 6.09 (s, 1H), 5.91 (s, 1H), 4.17 (brs, 1H), 3.61 (m, 1H), 3.41 (m, 1H), 3.29 (m, 1H), 3.26 (m, 1H), 3.03 (m, 2H), 2.75 (s, 3H), 1.58 (m, 1H). ¹³C NMR (125 MHz, Pyr-d₅): δ 184.8, 169.4, 164.0, 163.3, 157.6, 138.9, 132.7, 131.4, 130.3, 122.9, 110.6, 110.6, 106.6, 103.8, 100.6, 71.2, 64.7, 59.0, 47.7, 40.4, 27.1. ESIMS: m/z 394.1 [M + H]⁺. HR ESIMS: m/z 394.1646 [M + H]⁺ (calcd for C₂₃H₂₄NO₅⁺, 394.1649).

(1′R,2′S)-2-(4-Chlorostyryl)-5,7-dihydroxy-8-(3-hydroxy-1-methylpiperidin-4-yl)-4H-chromen-4-one (11b). Yellow solid (85 mg, 61% yield), mp 190–192 °C; HPLC tₑ = 9.31 min (99% purity), [α]²⁵_D −4.0 (c 0.1, MeOH). IR (CHCl₃): νₘₐₓ 3890, 2925, 2854, 1651, 1584, 1463, 1408, 1384, 1149, 1090 cm⁻¹. ¹H NMR (400 MHz, DMSO-d₆): δ 7.48–7.42 (m, J = 8 Hz, 2H), 7.39–7.32 (m, 3H), 7.16 (d, J = 16 Hz, 1H), 6.16 (s, 1H), 5.71 (s, 1H), 4.04 (brs, 1H), 3.84–2.84 (m, 6H), 2.62 (s, 3H), 1.44 (m, 1H). ¹³C NMR (100 MHz, DMSO-d₆): δ 180.7, 171.5, 159.5, 155.3, 154.6, 133.6, 133.2, 129.4, 129.1, 127.2, 126.4, 121.7, 107.3, 106.2, 100.5, 67.9, 60.7, 55.1, 43.8, 35.9, 22.9. ESIMS: m/z 428.2 [M + H]⁺. HR ESIMS: m/z 428.1259 [M + H]⁺ (calcd for C₂₃H₂₃ClNO₅⁺, 428.1259).

(1′R,2′S)-2-(3-Chlorostyryl)-5,7-dihydroxy-8-(3-hydroxy-1-methylpiperidin-4-yl)-4H-chromen-4-one (11c). Yellow solid (64 mg, 46% yield), mp 185–189 °C; HPLC tₑ = 7.3 min (99% purity), [α]²⁵_D −3.5 (c 0.1, MeOH). IR (CHCl₃): νₘₐₓ 3391, 2921, 2357, 1733, 1699, 1652, 1575, 1388, 1046 cm⁻¹. ¹H NMR (500 MHz, DMSO-d₆): δ 12.84 (s, 1H), 7.75 (s, 1H), 7.56–7.56 (m, 3H), 7.29 (d, J = 16 Hz, 1H), 7.22 (d, J = 16 Hz, 1H), 6.06 (s, 1H), 5.52 (s, 1H), 3.84 (brs, 1H), 3.19 (m, 1H), 2.97 (m, 1H), 2.89 (m, 1H), 1.77 (m, 1H), 2.26 (s, 3H), 2.20 (m, 2H), 1.19 (m, 1H). ¹³C NMR (100 MHz, DMSO-d₆): δ 179.1, 177.0, 159.6, 158.6, 154.5, 137.3, 133.7, 132.2, 130.7, 128.6, 126.4, 126.4, 123.0, 109.2, 108.2, 102.4, 99.4, 66.5, 62.7, 56.7, 45.8, 38.0, 22.3. ESIMS: m/z 428.3 [M + H]⁺. HR ESIMS: m/z 428.1232 [M + H]⁺ (calcd for C₂₃H₂₃ClNO₅⁺, 428.1259).

(1′R,2′S)-2-(2,6-Dichlorostyryl)-5,7-dihydroxy-8-(3-hydroxy-1-methylpiperidin-4-yl)-4H-chromen-4-one (11d). Yellow solid (90 mg, 60% yield), mp 193–196 °C; HPLC tₑ = 12.9 min (99% purity), [α]²⁵_D +5.0 (c 0.1, MeOH). IR (CHCl₃): νₘₐₓ 3435, 2922, 1652, 1577, 1463, 1380, 1318, 1171, 1064 cm⁻¹. ¹H NMR (500 MHz, CDCl₃): δ 7.66 (d, J = 12 Hz, 1H), 7.43 (d, J = 8 Hz, 2H), 7.23 (m, 1H), 7.10 (d, J = 16 Hz, 1H), 6.33 (s, 1H), 6.21 (s, 1H), 4.22 (brs, 1H), 3.63 (m, 1H), 3.49 (m, 1H), 3.08 (m, 2H), 2.44 (m, 1H), 2.43 (s, 3H), 2.35 (m, 1H), 1.64 (d, J = 12 Hz, 1H). ¹³C NMR (125 MHz, DMSO-d₆): δ 182.6, 163.9, 160.8, 160.0, 154.5, 134.9, 131.7, 129.83, 129.80, 129.7, 129.2, 129.19, 128.3, 110.5, 106.9, 105.3, 101.7, 68.9, 62.1, 56.2, 45.8,

37.7, 24.8. ESIMS: m/z 462.2 [M + H]⁺. HR ESIMS: m/z 462.0873 [M + H]⁺ (calcd for C₂₃H₂₂Cl₂NO₅⁺, 462.0869).

(1′R,2′S)-5,7-Dihydroxy-8-(3-hydroxy-1-methylpiperidin-4-yl)-2-(2,3,4,5,6-pentafluorostyryl)-4H-chromen-4-one (11e). Yellow solid (74 mg, 47% yield), mp 185–190 °C; HPLC tₑ = 7.19 min (99% purity), [α]²⁵_D −4.8 (c 0.1, MeOH). IR (CHCl₃): νₘₐₓ 3400, 2922, 2356, 1652, 1475, 1366, 1279, 1116, 1035 cm⁻¹. ¹H NMR (400 MHz, DMSO-d₆): δ 7.56 (d, J = 16 Hz, 1H), 7.31 (d, J = 16 Hz, 1H), 6.41 (s, 1H), 5.91 (s, 1H), 4.05 (m, 1H), 4.03–3.17 (m, 6H of piperidine), 2.51 (s, 3H), 1.55 (m, 1H). ¹³C NMR (125 MHz, DMSO-d₆): δ 184.1, 163.6 (d, ¹J_CF = 167 Hz), 156.3, 147.9, 145.9, 144.9, 144.8, 140.5, 127.6, 125.6, 117.7, 110.1, 107.8, 106.0, 69.0, 63.4, 63.3, 57.6, 45.9, 38.0, 24.2. ESIMS: m/z 484.9 [M + H]⁺.

(1′R,2′S)-2-((E)-2-(Anthracen-10-yl)vinyl)-5,7-dihydroxy-8-(3-hydroxy-1-methylpiperidin-4-yl)-4H-chromen-4-one (11f). Red solid (75 mg, 46% yield), mp 193–196 °C; HPLC tₑ = 5.45 min (99% purity), [α]²⁵_D +2.0 (c 0.1, MeOH). IR (CHCl₃): νₘₐₓ 3391, 2922, 2851, 2357, 1732, 1651, 1557, 1456, 1385, 1273, 1030 cm⁻¹. ¹H NMR (500 MHz, DMSO-d₆): δ 8.68 (s, 1H), 8.34 (m, 3H), 8.16 (m, 2H), 7.61 (m, 4H), 7.00 (d, J = 16 Hz, 1H), 6.33 (s, 1H), 5.56 (s, 1H), 3.9 (brs, 1H), 2.94–2.50 (m, 6H of piperidine), 2.05 (s, 3H), 1.28 (m, 1H). ¹³C NMR (125 MHz, DMSO-d₆): δ 183.8, 174.7, 162.2, 158.3, 155.9, 136.5, 133.9, 131.7, 131.4, 131.2, 110.1, 109.6, 103.8, 103.3, 70.3, 63.4, 57.9, 51.1, 38.9, 22.5. ESIMS: m/z 494.1 [M + H]⁺. HR ESIMS: m/z 494.1922 [M + H]⁺ (calcd for C₃₁H₂₈NO₅⁺, 494.1942).

(1′R,2′S)-2-(3-Fluorostyryl)-5,7-dihydroxy-8-(3-hydroxy-1-methylpiperidin-4-yl)-4H-chromen-4-one (11g). Yellow solid (60 mg, 45% yield), mp 187–192 °C; HPLC tₑ = 5.58 min (99% purity), [α]²⁵_D −9.8 (c 0.1, MeOH). IR (CHCl₃): νₘₐₓ 3400, 2922, 2356, 1652, 1475, 1366, 1279, 1116, 1035 cm⁻¹. ¹H NMR (400 MHz, DMSO-d₆): δ 13.0 (s, 1H), 7.68–7.59 (m, 3H), 7.48 (d, J = 16 Hz, 1H), 7.32 (m, 1H), 7.27 (d, J = 16 Hz, 1H), 6.55 (s, 1H), 5.79 (s, 1H), 4.20 (brs, 1H), 4.03–3.10 (m, 6H of piperidine), 2.71 (s, 3H), 1.52 (m, 1H). ¹³C NMR (125 MHz, DMSO-d₆): δ 180.9, 172.1, 159.8 (d, ¹J_CF = 254 Hz), 157.3, 154.7, 131.2, 129.2, 128.2, 127.1, 125.0, 123.3, 120.7, 116.1, 111.8, 108.5 (d, ²J_CF = 74 Hz), 101.0, 67.5, 61.3, 55.7, 44.9, 37.3, 23.3. ESIMS: m/z 412.4 [M + H]⁺. HR ESIMS: m/z 412.1523 [M + H]⁺ (calcd for C₂₃H₂₃FNO₅⁺, 412.1552).

(1′R,2′S)-2-(2-Fluorostyryl)-5,7-dihydroxy-8-(3-hydroxy-1-methylpiperidin-4-yl)-4H-chromen-4-one (11h). Yellow solid (78 mg, 58% yield), mp 191–193 °C; HPLC tₑ = 8.7 min (98% purity), [α]²⁵_D −6.0 (c 0.1, MeOH). IR (CHCl₃): νₘₐₓ 3400, 2922, 1651, 1587, 1463, 1382, 1276, 1151, 1046 cm⁻¹. ¹H NMR (500 MHz, DMSO-d₆): δ 7.88 (m, 1H), 7.52 (d, J = 16, 1H), 7.05–7.54 (m, 3H), 7.20 (d, J = 16, 1H), 6.05 (s, 1H), 5.32 (s, 1H), 3.92 (brs, 1H), 3.10–2.50 (m, 6H of piperidine), 2.05 (s, 3H), 1.14 (m, 1H). ¹³C NMR (125 MHz, DMSO-d₆): δ 180.5, 172.0, 159.8 (d, ¹J_CF = 262 Hz), 154.7, 131.2, 129.1, 129.2, 127.1, 124.9, 123.3, 120.7, 116.1, 111.8, 107.8 (d, ²J_CF = 74 Hz), 101.1, 67.6, 61.3, 55.7, 44.9, 37.3, 23.3. ESIMS: m/z 412.2 [M + H]⁺. HR ESIMS: m/z 412.1523 [M + H]⁺ (calcd for C₂₃H₂₃FNO₅⁺, 412.1552).

(1′R,2′S)-2-(2-Chlorostyryl)-5,7-dihydroxy-8-(3-hydroxy-1-methylpiperidin-4-yl)-4H-chromen-4-one (11i). Yellow solid (70 mg, 52% yield), mp 193–197 °C; HPLC tₑ = 9.44 min (99% purity), [α]²⁵_D −8.2 (c 0.1, MeOH). IR (CHCl₃): νₘₐₓ 3390, 2925, 2854, 1651, 1584, 1490, 1384, 1273, 1090, 1042 cm⁻¹. ¹H NMR (400 MHz, DMSO-d₆): δ 13.22 (s, 1H), 7.85 (m, 1H), 7.81 (d, J = 16 Hz, 1H), 7.52–7.32 (m, 2H), 7.20 (d, J = 16 Hz, 1H), 6.25 (s, 1H), 4.49 (brs, 1H), 3.88–3.10 (m, 6H), 2.35 (s, 3H), 1.41 (m, 1H). ¹³C NMR (101 MHz, DMSO-d₆): δ 181.3, 171.9, 160.2, 158.1, 155.6, 133.4, 132.8, 131.8, 129.9, 127.7, 127.5, 127.0, 123.4, 110.8, 108.4, 106.4, 101.6, 67.0, 59.8, 55.4, 44.1, 36.5, 21.0. HR ESIMS: m/z 428.1259 [M + H]⁺ (calcd for C₂₃H₂₃ClNO₅⁺, 428.1259).

General Protocol for Kinase Assay. All assays were carried out using a radioactive (³³P-ATP) filter binding assay at International Centre for Kinase Profiling (ICKP), U.K. The general protocol for Cdk-2 is as follows: Cdk 2/cyclin A (5–20 mU diluted in 50 mM Hepes pH 7.5, 1 mM DTT, 0.02% Brij35, 100 mM NaCl) was assayed against Histone III in a final volume of 25.5 μL containing 50 mM Hepes pH 7.5, 1 mM DTT, 0.02% Brij35, 100 mM NaCl, Histone III

(1 mg/mL), 10 mM magnesium acetate, and 0.02 mM $[^{33}P\gamma\text{-ATP}]$ (500–1000 cpm/pmole) and incubated for 30 min at room temperature. Assays were stopped by addition of 5 μL of 0.5 M (3%) ortho phosphoric acid and then harvested onto P81 Unifilter plates with a wash buffer of 50 mM ortho phosphoric acid. Cdk 9/cyclin T1 (5–20 mU) diluted in 50 mM Tris pH 7.5, 0.1 mM EGTA, 1 mg/mL BSA, 0.1% mercaptoethanol) was assayed against a substrate peptide (YSPTSPSYSPTSPSYSPTSPKKK) in a final volume of 25.5 μL containing 50 mM Tris pH 7.5, 0.1 mM EDTA, 10 mM DTT, 1 mg/mL BSA, 0.3 mM YSPTSPSYSPTSPSYSPTSPKKK, 10 mM magnesium acetate, and 0.05 mM $[^{33}P\gamma\text{-ATP}]$ (50–1000 cpm/pmole) and incubated for 30 min at room temperature. Assays were stopped by the addition of 5 μL of 0.5 M (3%) ortho phosphoric acid and then harvested onto P81 Unifilter plates with a wash buffer of 50 mM ortho phosphoric acid.

The kinase profiling of 11d was performed at DiscoverX corporation USA using their KINOMEscan Profiling Service. Compound 11d was screened at 0.5 μM, and results for primary screen binding interactions are reported as % Ctrl, where lower numbers indicate stronger hits in the matrix diagram. The selectivity score (S-score) was calculated by dividing the number of kinases that compounds bind to by the total number of distinct kinases tested, excluding mutant variants. This value was calculated using % Ctrl as a potency threshold. The three S-scores, S(35), S(10), and S(1), were computed using the following formulas:

$$S(35) = \frac{\text{number of nonmutant kinases with \% Ctrl} < 35}{\text{number of nonmutant kinases tested}}$$

$$S(10) = \frac{\text{number of nonmutant kinases with \% Ctrl} < 10}{\text{number of nonmutant kinases tested}}$$

$$S(1) = \frac{\text{number of nonmutant kinases with \% Ctrl} < 1}{\text{number of nonmutant kinases tested}}$$

Cellular Antiproliferative Activity. Cancer cell lines were procured from National Cancer Institute, USA and normal epithelial cell line fR2 was purchased from Sigma Aldrich (ECACC type). Cells were grown in appropriate growth medium in a CO_2 incubator (Thermocin Electron Corporation, Houston, TX) at 37 °C with 95% humidity and 5% CO_2 gas environment. The stock solution of test compounds was prepared in DMSO of appropriate strength so that the final DMSO concentration during treatment in cells is <0.2%. Cells were seeded in 96 well plates and exposed to tested compounds at various concentrations for 48 h time interval. MTT dye (2.5 mg/mL in PBS) was added 4 h prior to experiment termination. The plates were then centrifuged at 1500 rpm for 15 min, and the supernatant was discarded, and MTT formazan crystals were dissolved in 150 μL of DMSO. The OD measured at 570 nm with a reference wavelength of 620 nm. The percentages of cell viability and growth inhibition were calculated using formulae:

$$\% \text{ cell viability} = \frac{\text{absorbance of treated cells} - \text{absorbance of blank}}{\text{absorbance of control cells} - \text{absorbance of blank}} \times 100$$

$$\% \text{ growth inhibition} = 100 - \% \text{ cell viability}$$

Cell Cycle Analysis by Flow Cytometry. Cells were incubated with 11d at indicated concentrations for 24 h. In total, 400 μg of cells was collected, washed with ice-cold PBS, and fixed with ice cold 70% ethanol for overnight at 4 °C. Next day, cells were incubated with RNase at a concentration of 0.2 mg/mL at 37 °C for 1 h and stained with propidium iodide (10 μg/mL) for 30 min in the dark. Cells were analyzed on flow cytometer (FACS Calibur, Becton Dickinson), and data were collected in list mode on 10,000 events for FL2-A vs FL2-W. Resulting DNA distributions were analyzed by Modfit (Verity Software House Inc., Topsham, ME) for the proportions of cells in apoptosis, G_1 phase, S-phase, and G_2/M phase of the cell cycle.

Scanning Electron Microscopic (SEM) Analysis. To assess the mechanism of cell death, the cells were processed for SEM studies. MIAPaCa-2 cells were seeded in a six well tissue culture plate and

treated with different concentrations of 11d for 24 h. The cells on a coverslip were fixed with 2.5% glutaraldehyde in 0.1 M phosphate buffer (pH 7.2) at 4 °C for 24 h, postfixed with 1% osmium tetroxide in the same buffer for 4 h, dehydrated with graded ethanol solution, dried in a critical point drier using HMDS, and coated with gold using a sputter coater (Joel JEC-3000 FC). The specimens were examined with an electron microscope (JEOL JSM-IT300) with ASID at 20 kV.

Western-Blot Analysis. Protein was measured employing Bio Rad protein assay kit using bovine serum albumin as standard. Proteins aliquots (70 μg) were resolved on SDS-PAGE and then electrotransferred to PVDF membrane overnight at 4 °C at 30 V. Nonspecific binding was blocked by incubation with 5% nonfat milk in Tris buffered saline containing 0.1% Tween-20 (TBST) for 1 h at room temperature. The blots were probed with respective primary antibodies (Sigma and CST) for 2–4 h and washed three times with TBST. The blots were then incubated with horseradish peroxidase conjugated antimouse secondary antibodies for 1 h, followed by washing with TBST. The signals were detected then by using ECL plus chemiluminescence's kit on X-ray film.

Molecular Docking. Cdk 9/cylin T flavopiridol complex was retrieved from the protein data bank (PDB ID: 3BLH) and prepared by the protein preparation wizard in Maestro at pH 6.2. The site of molecular docking was defined by constructing the grid considering flavopiridol as the centroid of grid box. All docking calculations were done using GLIDE XP docking, and ΔG of inhibitors binding to Cdk 9/cyclin T1 complex was carried out by Prime using end-point MM-GB/SA method. The validation of the docking protocol was done by performing docking of the flavopiridol and comparing it with the binding pattern with the cocrystallized structure.

Human Cytochrome P450 (CYP450) Isoenzymes Assay. The cytochrome P450 isoenzymes were aliquoted as per the total concentration required to conduct the study and stored at −70 °C until use. Total assay volume was adjusted to 200 μL containing three components: cofactors, inhibitor/vehicle, and enzyme substrate (ES) mix. The 50 μL of working cofactor stock solution was dispensed to all the specified wells in a black nunc microtiter polypropylene plate. The 50 μL of diluted working concentrations of 11d/positive control inhibitors/vehicle was dispensed in triplicate to the specified wells as per the plate map design. Reaction plate with a cofactor and test item was preincubated at 37 °C ± 1 °C shaking incubator for 10 min. Simultaneously, ES mix was prepared by mixing the CYP P450 isoenzymes. Remaining volume was made up with the buffer and preincubated for 10 min at 37 ± 1 °C. One hundred microliters of ES mix was dispensed per well as per the plate map design and incubated at 37 ± 1 °C with shaking for a predetermined time. A set of controls was incubated with CYP P450 isoenzymes and substrate without test or reference item. A set of blanks were incubated with substrate and test or reference item, in the absence of CYP P450 isoenzymes. The reaction was terminated by adding specific quenching solutions (for CYP2C19 and CYP3A4, 75 μL of 100% acetonitrile; for CYP2C9, 20 μL of 0.25 M Tris in 60% methanol; for CYP2D6, 75 μL of 0.25 M Tris in 60% methanol). The reaction was quenched by thoroughly mixing the final contents of the wells by repeated pipetting using a multichannel pipet. The product fluorescence per well was measured using a fluorimeter at excitation and emission wavelength for respective CYP P450 isoenzyme fluorogenic metabolites. Data was analyzed by using an Excel spreadsheet, and the % inhibition was calculated.

Determination of Solubility, Lipophilicity, and Partition Coefficient. The thermodynamic equilibrium solubility in water, PBS, SGF, and SIF was determined using miniaturized shake-flask method, wherein the supernatant was analyzed by HPLC. Log P, log D, and pK_a were determined using our published protocols. The chemical stability of 11d in different pH buffers and biological media was performed as reported earlier.

Caco-2 Permeability Assay. Permeability study was conducted with the Caco-2 monolayer cultured for 21 days (>500 cm2 in each well) and by adding an appropriate volume of buffer (HBSS buffer containing 10 mM HEPES) containing test compounds to apical chamber. The test sample was taken from both apical and basolateral

chambers at 0 and 90 min after incubation at 37 °C and analyzed by LC–MS/MS. The same experiment was repeated by adding an appropriate volume of buffer (HBSS buffer containing 10 mM HEPES) containing test compound to the basolateral chamber. The AUC defined the net influx and outflow of the test compound across the Caco-2 cell monolayer.

Plasma Protein Binding Studies. This was done by equilibrium dialysis method. An aliquot of 150 μL respective matrices (n = 3) containing test compound (5 μM final concentration) was added to the first half (plasma side) of the well of the 96 well microequilibrium dialysis device. An aliquot of 150 μL of 0.1 M sodium phosphate buffer pH 7.4 (blank) (n = 3) was added in the second half (buffer side) of the same well of the above plate. The plate containing plasma and buffer was equilibrated at 37 ± 1 °C for 5 h, with a constant rotation of 130 rpm on an orbital shaker. After equilibration time is over, 10 μL of plasma sample was taken out from the first half of the well to a vial/plate containing 200 μL of acetonitrile (containing internal standard, 200 ng/mL), and 50 μL of blank buffer was added. Similarly, 50 μL of buffer sample was taken out from the buffer half of the wells to a vial containing 200 μL of acetonitrile (containing internal standard, 200 ng/mL), and 10 μL of blank plasma was added. Samples were centrifuged at 14000 rpm for 5 min at 4 °C. The supernatant was transferred to LC–MS/MS vials and injected on to the column for analysis. Two reference controls were used, viz. warfarin for high bound and naltrexone for low bound.

Metabolic Stability in Liver Microsomes. Microsomal stability studies were performed with mouse, rat, dog, monkey, and human liver microsomes at 0.5 mg/mL protein concentration. Briefly, the liver microsomal protein (25 μL), NADPH (100 μL), and phosphate buffer (870 μL) was coincubated (preincubation) in a deep 96 well plate in an orbital incubator (10 min, 37 °C). The reaction was initiated by the addition of 5 μL of 100 μM working stock solutions of 11d. Aliquots (50 μL) were withdrawn from the reaction tube at 0, 3, 6, 9, 12, 15, 18, 24, 27, and 30 min, and the reaction was immediately terminated by transferring to a deep 96 well plate containing 50 μL of acetonitrile. NADPH free control incubation was performed by mixing liver microsomes (25 μL) and phosphate buffer (970 μL) and incubating at 37 °C for 10 min. Reaction was initiated by addition of 5 μL of 11d. Aliquots (50 μL) were withdrawn at 0 and 30 min, and reaction was terminated with 50 μL of acetonitrile. The reaction and control experiments were performed in duplicate. Diclofenac was used as positive control in human and rat liver microsomes, and verapamil was used as positive control in mouse, dog, and monkey liver microsomes. To the quenched samples, internal standard was added and vortex mixed followed by centrifugation at 4000 rpm for 10 min, and an aliquot of supernatant was taken for LC–MS/MS analysis. The experimental sample was analyzed by employing a suitable multiple reaction monitoring method developed on LC–MS/MS to estimate the area ratio (analyte peak area/internal standard peak area). The data was fitted to the one-phase exponential decay equation using GraphPad Prism software. The half life ($t_{1/2}$) generated by the software was reported.

Metabolic Stability in Hepatocytes. The hepatocytes were incubated with naloxone, imipramine, and 11d (1 μM final concentrations) at 37 °C. Samples were removed at the appropriate time points (0, 60, 120, and 180 min) into acetonitrile containing internal standard to terminate the reaction. Following centrifugation, the supernatant was analyzed by LC–MS/MS. The disappearance of test compound was monitored over a 180 min time period.

Metabolic Stability in S9 Liver Fraction. The S9 fractions of different species was suspended in potassium phosphate buffer (pH 7.4) in the propylene tube. The test compound was added to this mixture. This mixture was then divided in to four tubes labeled as T_0, T_5, T_{15}, and T_{30}. The experiment was performed in duplicate. All the tubes were preincubated at 37 ± 1 °C for 5 min in shaking water bath. Tubes of NADPH solution (10 mM) were similarly preincubated. After preincubation, 20 μL of NADPH solution (10 mM) was added to the T_0, T_{15}, and T_{30} tubes, and 20 μL of buffer was added to the T_0 tube. At the end of the incubation period (0, 5, 15, and 30 min) of respective tubes, an aliquot of 290 μL of quenching solution was added

to each tube to stop the reaction. Resulting samples were centrifuged for 20 min. The supernatant (200 μL) from each reaction tube was taken for LC–MS/MS analysis.

Pharmacokinetics Studies. Oral and intravenous (IV) pharmacokinetic studies of compound 11d were carried out in BALB/c male mice of age 4–6 weeks, by administering 11d orally and IV at a dose of 10 mg/kg for oral and 1 mg/kg for IV. Plasma samples were collected at appropriate time points between the range of 0–24 h and analyzed by LC–MS/MS. Mean plasma concentration was calculated, and data was further analyzed to determine PK parameters using WinNonlin 5.3 software package. Similarly, the dose dependent and tissue distribution PK studies were carried out in BALB/c mice and SD rats.

The PK studies were carried out at Jubilant Biosys Bangalore on a commercial basis. These experiments were approved by the Jubilant Biosys Institutional Animal Ethics Committee, Bangalore, India (IAEC/JDC/2012/27), and were in accordance with the Committee for the Purpose of Control and Supervision of Experiments on Animals (CPCSEA), Ministry of Social Justice and Environment, Government of India.

In Vivo Activity in Ehrlich Solid Tumor Model. Ehrlich Ascites Carcinoma (EAC) cells were collected from the peritoneal cavity of the Swiss mice weighing 18–23 g, harboring 8–10 days old ascitic tumor. One × 10^7 EAC cells were injected intramuscularly in the right thigh of Swiss male mice selected for the experiment on day 0. The next day, animals were randomized and divided into different groups. The treatment groups contained seven animals each, and the control group contained 10 animals. One of the treatment group was treated with 5-fluorouracil (22 mg/kg, i.p.) from days 1–9, and it served as positive control. The control group was similarly administered normal saline (0.2 mL, i.p. and p.o.) from days 1–9. On day 9 and 13, tumor bearing thigh of each animal was shaved, and longest and shortest diameters of the tumor were measured with the help of vernier caliper. The percent tumor growth inhibition was calculated on day 13 by comparing the average values of treated groups with that of the control group. Tumor growth in saline treated control animals was taken to be 100%.

In Vivo Efficacy Studies in Xenograft Models. The xenograft was generated by subcutaneous injection of human cancer cell line MIAPaCa-2 in CD1 nude mice. The tumor size was measured by taking the longest length and shortest width of the tumor with a digital caliper. The tumor volume was calculated with the formula (width² × length)/2. Animals were randomized into five groups (vehicle control, standard drug, test compound: two doses), and treatment was started when average tumor size was 130 mm³. The body weight was checked before dosing or alternate day as required. The size of the tumor was measured every alternate day. Blood (35–40 μL) was drawn, and plasma separated on day 0 (before treatment). On the last day (25th day), maximum blood was collected and plasma separated after final dosing. Carbon dioxide overdosing was done to euthanize the animals at the end of the experiment. Tumor isolation was done and snap frozen in liquid nitrogen and was stored at −80 °C for further studies. Complete liver and lung tissue was isolated and snap frozen. Other two xenograft studies were also done using a similar protocol.

Data is expressed as the mean of one of three similar experiments unless otherwise indicated. Comparisons were made between control and treated groups or the entire intra group using one way ANOVA with post Bonferroni test through GraphPad Prism 5.00.288 statistical analysis software. *p values < 0.05 were considered significant.

hERG Competitive Binding Assay. hERG competitive binding assay was performed using membranes obtained from HEK293 cells expressing the hERG K^+ channel (PerkinElmer Catalog # RBHERGM400UA). The hERG competitive binding assay was performed at a radioligand [³H] Astemizole concentration of 5 nM and membrane concentration of 3 μg per well. The test item and reference item Astemizole were dissolved in 100% DMSO to make the stock concentrations of 10 mM and 6 mM, respectively. Five times intermediate concentrations of test/reference item was prepared by dilution with assay buffer. Eight serial dilutions of the test/reference item were prepared with starting highest test concentration of 50000 nM (50 μM) for IIIM-290 and 30000 nM (30 μM) for Astemizole.

The binding assay was performed in a total volume of 100 μL, which includes 60 μL of membrane, 20 μL of test item/reference item/ vehicle, and 20 μL of radioligand. Nonspecific binding was determined in the presence of 100 μM Astemizole. The plate was incubated for 90 min at 27 °C. During incubation, Filtermat A was presoaked in 0.3% polyethylenimine. After incubation, binding reaction mixture was transferred to the filter plate and washed eight times with wash buffer. The plate was dried and radioactive counts were measured using the top count. The percent inhibition of the compounds was calculated using the formula

$$\% \ inhibition = 100 \times \left(1 - \frac{F(test \ compound)}{F(vehicle \ control)}\right)$$

where F(test compound) is CPM of test compound and F(vehicle control) is CPM of vehicle control.

AMES Test. This study was performed to evaluate compound 11d for its possible mutagenic activity, by the bacterial reverse mutation test, using five histidine deficient (his−) mutant tester strains of Salmonella typhimurium, viz., TA1537, TA1535, TA98, TA100, and TA102 maintained at Jubilant Biosys Limited. Liver microsomal enzyme (S-9) homogenate was prepared in-house. This has been evaluated along with known mutagens (positive controls), sodium azide (SA), 9-aminoacridine (9-AA), 2-nitrofluorene (2-NF), and mitomycin C (MMC) in the absence and 2-aminoanthracene (2-AA) in the presence of metabolic activation system. The treatments were performed by plate incorporation technique both in the absence and presence of metabolic activation (S9 mix). The S9 mix of 5% v/v (Trial I) and 10% v/v (Trial II) included S9 fraction supplemented with essential cofactors. Before conducting the mutagenicity test, compound 11d was evaluated for its possible cytotoxicity in strain TA100, both in the absence and presence of S9 mix (5%, v/v). The solubility test was performed in water and DMSO. Cytotoxicity to the tester strain TA100 was tested at concentrations of 0.03906, 0.078125, 0.15625, 0.3125, 0.625, 1.25, 2.5, and 5 mg/plate both in the presence (5%, v/v S9 mix) and absence of the metabolic activation system. Cytotoxicity is characterized by inhibition of the background bacterial lawn and/or reduction in the number of revertant colonies. Based on the results of the cytotoxicity study, compound 11d was evaluated for its possible mutagenic effect in five strains of Salmonella typhimurium at dose levels of 1.5625, 3.125, 6.25, 12.5, 25, and 50 μg/ plate in Trial I and 0.512, 1.28, 3.2, 8, 20, and 50 μg/plate in Trial II both in the absence and presence of metabolic activation. This study was performed as per OECD 1997 guidelines.

In Vitro Micronucleus Test. The test system used for the in vitro mammalian cell micronucleus test was human peripheral blood lymphocytes, as recommended by the OECD and other regulatory authorities. Liver microsomal enzyme (S-9) homogenate was prepared in-house. Cyclophosphamide (V0 μg/mL) was used as a positive control agent, clastogen, in the presence of metabolic activation, which demonstrates both the activity of the metabolic activation system and the responsiveness of the test system. For long term treatment, mitomycin-C was used as an aneugenic agent in the absence of metabolic activation system. Positive controls were maintained in duplicate and run with all experiments. The precipitation and pH of 11d culture medium was assessed and considered for the selection of the highest concentration for treatment. Based on the precipitation and pH of compound 11d, the test concentrations was determined. Treatment was performed in two phase (phase I, short term treatment; phase II, long term treatment). In phase I, the cells were exposed to the compound both with and without metabolic activation for 3–6 h (usually 4 h). Cells were washed with the culture medium after treatment to remove compound 11d. If required, a second wash with culture medium was given to remove traces of treatment medium. After washing, cells were placed into complete medium with cytochalasin B and sampled at about 24 h from the beginning of the treatment. In Phase II, the cells were exposed to compound 11d without metabolic activation with continuous treatment in the presence of cytochalasin B for about 24 h. Cultures were harvested after completion of the treatment period. Each culture was harvested

and processed separately for the preparation of chromosomes. A minimum of two slides per treatment group were prepared, one was used for scoring and the other was kept as reserve. All slides were coded before microscopic scoring and decoded after completion of scoring. Slides were randomly observed under a microscope, and a minimum of 2000 binucleated cells per concentration (equally divided in replicates) were counted in different fields for micronucleus frequencies. The proportions of binucleated cells and multinucleated cells were determined for each culture by counting a minimum of 500 cells per culture.

Single-Dose Acute Oral Toxicity in Rats. This study was performed as per OECD423 guidelines. To determine the acute oral toxicity, a stepwise procedure was employed with the use of three animals of a single sex (females) at each step. The test item was administered orally at one of the defined doses. Absence or presence of compound-related mortality of the animals dosed at one step was used to determine the dose at the next step. The study outcomes were used to determine the LD₅₀ value of the test compound.

■ ASSOCIATED CONTENT

⊙ Supporting Information

The Supporting Information is available free of charge on the ACS Publications website at DOI: 10.1021/acs.jmedchem.7b01765.

> ¹H, ¹³C, DEPT NMR, HRMS, and HPLC scans of all compounds; results of in vivo efficacy in murine models; additional molecular modeling details; kinase profiling data (PDF)
> Molecular formula strings (CSV)

■ AUTHOR INFORMATION

Corresponding Authors

*Tel: +91 191 2569006, Fax: +91 191 2569333, E-mail: sbharate@iiim.ac.in.
*Tel: +91 191 2569111, Fax: +91 191 2569333, E-mail: ram@iiim.ac.in.

ORCID

Sandip B. Bharate: 0000-0001-6081-5787
Ram A. Vishwakarma: 0000-0002-0752-6238

Author Contributions

Contributed equally to this work as co-first authors. S.B.B. and R.A.V. designed, executed, and coordinated this whole study; V.K. and S.B.B. designed and executed large-scale isolation protocol for rohitukine; V.K., V.K.N., and M.S. synthesized IIIM-290 in bulk quantity; S.K.J. synthesized rohitukine derivatives; M.J.M. and D.M.M. designed and performed in vivo efficacy study in murine models and Molt-4 xenograft; S.K.G. and S.B. designed and performed cellular antiproliferative activity experiments; V.K. and S.S.B. performed experimental physicochemical characterization and solution-state stability studies of the lead; S.G.G. collected and authenticated D. binectariferum plant material required for this study; S.B.B. and R.A.V. contributed to manuscript writing.

Notes

The authors declare no competing financial interest.
IIIM publication number: IIIM/2165/2017.

■ ACKNOWLEDGMENTS

■ ABBREVIATIONS USED

AAG, alpha-acid glycoprotein; ADH, alcohol dehydrogenase; ADME, absorption, distribution, metabolism, and excretion; AUC_{0-t}, the area under the plasma concentration–time curve from 0 to last measurable time point; $AUC_{0-\infty}$, area under the plasma concentration–time curve from time zero to infinity; BALB/c mice, albino, laboratory-bred strain of the house mouse; C_{max}, maximum observed plasma concentration; C_0, extrapolated concentration at zero time point; CL, clearance; CL_{int}, intrinsic clearance; CPT, camptothecin; CYP3A4, cytochrome P450 3A4; CYP2D6, cytochrome P450 2D6; CYP2C9, cytochrome P450 2C9; CYP2C19, cytochrome P450 2C19; CPM, counts per minute; DABCO, 1,4-diazabicyclo-[2.2.2]octane; DAPI, 4′,6-diamidino-2-phenylindole; DCM, dichloromethane; %F, percentage bioavailability; fR2, normal epithelial tissue; GST, glutathione S-transferase; hERG, human ether-a-go-go-related gene; HCT-116, human colon carcinoma cell lines; HRMS, high resolution mass spectroscopy; HSA, human serum albumin; IR, infrared spectroscopy; MMC, mitomycin C; NAT, N-acetyltransferase; NADPH, nicotinamide adenine dinucleotide phosphate; PBS, phosphate buffer saline; PARP, poly(ADP-ribose) polymerase; PDB, Protein Data Bank; PRKCE, protein kinase C epsilon; PO, oral route; RoS, rule of five; SD, standard deviation; SD rats, Sprague–Dawley rats; SGF, simulated gastric fluid; SIF, simulated intestinal fluid; SULT, sulfotransferase; THF, tetrahydrofuran; TGI, tumor growth inhibition; T_{last}, time at which last concentration was found; $t_{1/2,0}$ terminal half-life; V_d, volume of distribution; V_{ss}, volume of distribution at steady state; XO, xanthine oxidase.

■ REFERENCES

(1) Ingham, M.; Schwartz, G. K. Cell-cycle therapeutics come of age. J. Clin. Oncol. 2017, 35, 2949–2959.

(2) Abou Zahr, A.; Borthakur, G. Emerging cell cycle inhibitors for acute myeloid leukemia. Expert Opin. Emerging Drugs 2017, 22, 137–148.

(3) Michalides, R.; van Veelen, N.; Hart, A.; Loftus, B.; Wientjens, E.; Balm, A. Overexpression of cyclin D1 correlates with recurrence in a group of forty-seven operable squamous cell carcinomas of the head and neck. Cancer Res. 1995, 55, 975–978.

(4) Roskoski, R., Jr. Cyclin dependent protein kinase inhibitors including palbociclib as anticancer drugs. Pharmacol. Res. 2016, 107, 249–275.

(5) Burki, T. K. Palbociclib improves survival in advanced breast cancer. Lancet Oncol. 2017, 18, e1.

(6) Zerdes, I.; Zingas, D. E.; Lykoudis, E. G.; Roukos, D. H. Palbociclib: an approval at last for HER2 negative breast cancer. Future Oncol. 2016, 12, 1097–1100.

(7) Palanisamy, R. P. Palbociclib: A new hope in the treatment of breast cancer. J. Cancer Res. Ther. 2016, 12, 1220–1221.

(8) Gupta, A. K.; Sharma, S.; Dahiya, N.; Brashier, D. B. Palbociclib: A breakthrough in breast carcinoma in women. Med. J. Armed Forces India 2016, 72, 537–542.

(9) Ribociclib (Kisqali). https://www.fda.gov/drugs/informationondrugs/approveddrugs/ucm546438.htm (accessed on July 11, 2017).

(10) Torres-Guzman, R.; Calsina, B.; Hermoso, A.; Baquero, C.; Alvarez, B.; Amat, J.; McNulty, A. M.; Gong, X.; Boehnke, K.; Du, J.; de Dios, A.; Beckmann, R. P.; Buchanan, S.; Lallena, M. J. Preclinical

characterization of abemaciclib in hormone receptor positive breast cancer. Oncotarget 2017, 8, 69493–69507.

(11) Sledge, G. W.; Toi, M.; Neven, P.; Sohn, J.; Inoue, K.; Pivot, X.; Burdaeva, O.; Okera, M.; Masuda, N.; Kaufman, P. A.; Koh, H.; Grischke, E. M.; Frenzel, M.; Lin, Y.; Barriga, S.; Smith, I. C.; Bourayou, N.; Llombart-Cussac, A. MONARCH 2: Abemaciclib in combination with fulvestrant in women with HR+/HER2 advanced breast cancer who had progressed while receiving endocrine therapy. J. Clin. Oncol. 2017, 35, 2875–2884.

(12) Patnaik, A.; Rosen, L. S.; Tolaney, S. M.; Tolcher, A. W.; Goldman, J. W.; Gandhi, L.; Papadopoulos, K. P.; Beeram, M.; Rasco, D. W.; Hilton, J. F.; Nasir, A.; Beckmann, R. P.; Schade, A. E.; Fulford, A. D.; Nguyen, T. S.; Martinez, R.; Kulanthaivel, P.; Li, L. Q.; Frenzel, M.; Cronier, D. M.; Chan, E. M.; Flaherty, K. T.; Wen, P. Y.; Shapiro, G. I. Efficacy and safety of abemaciclib, an inhibitor of CDK4 and CDK6, for patients with breast cancer, non-small cell lung cancer, and other solid tumors. Cancer Discovery 2016, 6, 740–753.

(13) https://clinicaltrials.gov (accessed on August 23, 2017).

(14) Rahaman, M. H.; Kumarasiri, M.; Mekonnen, L. B.; Yu, M.; Diab, S.; Albrecht, H.; Milne, R. W.; Wang, S. Targeting CDK9: a promising therapeutic opportunity in prostate cancer. Endocr. Relat. Cancer 2016, 23, T211–T226.

(15) Sonawane, Y. A.; Taylor, M. A.; Napoleon, J. V.; Rana, S.; Contreras, J. I.; Natarajan, A. Cyclin dependent kinase 9 inhibitors for cancer therapy. J. Med. Chem. 2016, 59, 8667–8684.

(16) Morales, F.; Giordano, A. Overview of CDK9 as a target in cancer research. Cell Cycle 2016, 15, 519–527.

(17) Shao, H.; Shi, S.; Huang, S.; Hole, A. J.; Abbas, A. Y.; Baumli, S.; Liu, X.; Lam, F.; Foley, D. W.; Fischer, P. M.; Noble, M.; Endicott, J. A.; Pepper, C.; Wang, S. Substituted 4-(thiazol-5-yl)-2-(phenylamino)-pyrimidines are highly active CDK9 inhibitors: synthesis, X-ray crystal structures, structure-activity relationship, and anticancer activities. J. Med. Chem. 2013, 56, 640–659.

(18) Nemeth, G.; Greff, Z.; Sipos, A.; Varga, Z.; Szekely, R.; Sebestyen, M.; Jaszay, Z.; Beni, S.; Nemes, Z.; Pirat, J. L.; Volle, J. N.; Virieux, D.; Gyuris, A.; Kelemenics, K.; Ay, E.; Minarovits, J.; Szathmary, S.; Keri, G.; Orfi, L. Synthesis and evaluation of phosphorus containing, specific CDK9/CycT1 inhibitors. J. Med. Chem. 2014, 57, 3939–3965.

(19) Li, Y.; Guo, Q.; Zhang, C.; Huang, Z.; Wang, T.; Wang, X.; Wang, X.; Xu, G.; Liu, Y.; Yang, S.; Fan, Y.; Xiang, R. Discovery of a highly potent, selective and novel CDK9 inhibitor as an anticancer drug candidate. Bioorg. Med. Chem. Lett. 2017, 27, 3231–3237.

(20) Tong, Z.; Chatterjee, D.; Deng, D.; Veeranki, O.; Mejia, A.; Ajani, J. A.; Hofstetter, W.; Lin, S.; Guha, S.; Kopetz, S.; Krishnan, S.; Maru, D. Antitumor effects of cyclin dependent kinase 9 inhibition in esophageal adenocarcinoma. Oncotarget 2017, 8, 28696–28710.

(21) Yeh, Y. Y.; Chen, R.; Hessler, J.; Mahoney, E.; Lehman, A. M.; Heerema, N. A.; Grever, M. R.; Plunkett, W.; Byrd, J. C.; Johnson, A. J. Up-regulation of CDK9 kinase activity and Mcl-1 stability contributes to the acquired resistance to cyclin dependent kinase inhibitors in leukemia. Oncotarget 2015, 6, 2667–2679.

(22) Chen, R.; Keating, M. J.; Gandhi, V.; Plunkett, W. Transcription inhibition by flavopiridol: mechanism of chronic lymphocytic leukemia cell death. Blood 2005, 106, 2513–2519.

(23) Harmon, A. D.; Weiss, U. The structure of rohitukine, the main alkaloid of Amoora rohituka (Syn. Aphanamixis polystachya) (Meliaceae). Tetrahedron Lett. 1979, 20, 721–724.

(24) Naik, R. G.; Kattige, S. L.; Bhat, S. V.; Alreja, B.; de Souza, N. J.; Rupp, R. H. An antiinflammatory cum immunomodulatory piperidinylbenzopyranone from dysoxylum binectariferum: isolation, structure and total synthesis. Tetrahedron 1988, 44, 2081–2086.

(25) Mohanakumara, P.; Sreejayan, N.; Priti, V.; Ramesha, B. T.; Ravikanth, G.; Ganeshaiah, K. N.; Vasudeva, R.; Mohan, J.; Santhoshkumar, T. R.; Mishra, P. D.; Vishwakarma, R. A.; Uma Shaanker, R. Dysoxylum binectariferum Hook.f (Meliaceae), a rich source of rohitukine. Fitoterapia 2010, 81, 145–148.

(26) Kumar, V.; Guru, S. K.; Jain, S. K.; Joshi, P.; Gandhi, S. G.; Bharate, S. B.; Bhushan, S.; Bharate, S. S.; Vishwakarma, R. A. A

chromatography free isolation of rohitukine from leaves of *Dysoxylum binectariferum*: Evaluation for in vitro cytotoxicity, Cdk inhibition and physicochemical properties. *Bioorg. Med. Chem. Lett.* **2016**, 26, 3457–3463.

(27) Mahajan, V.; Sharma, N.; Kumar, S.; Bhardwaj, V.; Ali, A.; Khajuria, R. K.; Bedi, Y. S.; Vishwakarma, R. A.; Gandhi, S. G. Production of rohitukine in leaves and seeds of *Dysoxylum binectariferum*: an alternate renewable resource. *Pharm. Biol.* **2015**, 53, 446–450.

(28) Li, Y.; Tanaka, K.; Li, X.; Okada, T.; Nakamura, T.; Takasaki, M.; Yamamoto, S.; Oda, Y.; Tsuneyoshi, M.; Iwamoto, Y. Cyclin-dependent kinase inhibitor, flavopiridol, induces apoptosis and inhibits tumor growth in drug-resistant osteosarcoma and Ewing's family tumor cells. *Int. J. Cancer* **2007**, 121, 1212–1218.

(29) Lanasa, M. C.; Andritsos, L.; Brown, J. R.; Gabrilove, J.; Caligaris-Cappio, F.; Ghia, P.; Larson, R. A.; Kipps, T. J.; Leblond, V.; Milligan, D. W.; Janssens, A.; Johnson, A. J.; Heerema, N. A.; Buhler, A.; Stilgenbauer, S.; Devin, J.; Hallek, M.; Byrd, J. C.; Grever, M. R. Final results of EFC6663: a multicenter, international, phase 2 study of alvocidib for patients with fludarabine-refractory chronic lymphocytic leukemia. *Leuk. Res.* **2015**, 39, 495–500.

(30) Lin, T. S.; Ruppert, A. S.; Johnson, A. J.; Fischer, B.; Heerema, N. A.; Andritsos, L. A.; Blum, K. A.; Flynn, J. M.; Jones, J. A.; Hu, W.; Moran, M. E.; Mitchell, S. M.; Smith, L. L.; Wagner, A. J.; Raymond, C. A.; Schaaf, L. J.; Phelps, M. A.; Villalona-Calero, M. A.; Grever, M. R.; Byrd, J. C. Phase II study of flavopiridol in relapsed chronic lymphocytic leukemia demonstrating high response rates in genetically high-risk disease. *J. Clin. Oncol.* **2009**, 27, 6012–6018.

(31) Phelps, M. A.; Lin, T. S.; Johnson, A. J.; Hurh, E.; Rozewski, D. M.; Farley, K. L.; Wu, D.; Blum, K. A.; Fischer, B.; Mitchell, S. M.; Moran, M. E.; Brooker-McEldowney, M.; Heerema, N. A.; Jarjoura, D.; Schaaf, L. J.; Byrd, J. C.; Grever, M. R.; Dalton, J. T. Clinical response and pharmacokinetics from a phase 1 study of an active dosing schedule of flavopiridol in relapsed chronic lymphocytic leukemia. *Blood* **2009**, 113, 2637–2645.

(32) Zeidner, J.; Foster, M.; Blackford, A.; Litzow, M. R.; Morris, L. E.; Strickland, S. A.; Lancet, J. E.; Bose, P.; Levy, M. Y.; Tibes, R.; Gojo, I.; Gocke, C. D.; Rosner, G. L.; Little, R. F.; Wright, J. J.; Doyle, L. A.; Smith, B. D.; Karp, J. E. Randomized multicenter phase II study of flavopiridol (alvocidib), cytarabine, and mitoxantrone (FLAM) versus cytarabine/daunorubicin (7 + 3) in newly diagnosed acute myeloid leukemia. *Haematologica* **2015**, 100, 1172–1179.

(33) Karp, J. E.; Garrett-Mayer, E.; Estey, E. H.; Rudek, M. A.; Smith, B. D.; Greer, J. M.; Drye, D. M.; Mackey, K.; Dorcy, K. S.; Gore, S. D.; Levis, M. J.; McDevitt, M. A.; Carraway, H. E.; Pratz, K. W.; Gladstone, D. E.; Showel, M. M.; Othus, M.; Doyle, L. A.; Wright, J. J.; Pagel, J. M. Randomized phase II study of two schedules of flavopiridol given as timed sequential therapy with cytosine arabinoside and mitoxantrone for adults with newly diagnosed, poor-risk acute myelogenous leukemia. *Haematologica* **2012**, 97, 1736–1742.

(34) Zeidner, J. F.; Karp, J. E. Clinical activity of alvocidib (flavopiridol) in acute myeloid leukemia. *Leuk. Res.* **2015**, 39, 1312–1318.

(35) Wiernik, P. H. Alvocidib (flavopiridol) for the treatment of chronic lymphocytic leukemia. *Expert Opin. Invest. Drugs* **2016**, 25, 729–734.

(36) Shirsath, N. P.; Manohar, S. M.; Joshi, K. S. P276-00, a cyclin-dependent kinase inhibitor, modulates cell cycle and induces apoptosis in vitro and in vivo in mantle cell lymphoma cell lines. *Mol. Cancer* **2012**, 11, 77.

(37) Joshi, K. S.; Rathos, M. J.; Mahajan, P.; Wagh, V.; Shenoy, S.; Bhatia, D.; Chile, S.; Sivakumar, M.; Maier, A.; Fiebig, H. H.; Sharma, S. P276-00, a novel cyclin-dependent inhibitor induces G1 G2 arrest, shows antitumor activity on cisplatin-resistant cells and significant in vivo efficacy in tumor models. *Mol. Cancer Ther.* **2007**, 6, 926–934.

(38) Joshi, K. S.; Rathos, M. J.; Joshi, R. D.; Sivakumar, M.; Mascarenhas, M.; Kamble, S.; Lal, B.; Sharma, S. In vitro antitumor properties of a novel cyclin-dependent kinase inhibitor, P276-00. *Mol. Cancer Ther.* **2007**, 6, 918–925.

(39) Rathos, M. J.; Joshi, K.; Khanwalkar, H.; Manohar, S. M.; Joshi, K. S. Molecular evidence for increased antitumor activity of gemcitabine in combination with a cyclin-dependent kinase inhibitor, P276-00 in pancreatic cancers. *J. Transl. Med.* **2012**, 10, 161.

(40) Manohar, S. M.; Padgaonkar, A. A.; Jalota-Badhwar, A.; Rao, S. V.; Joshi, K. S. Cyclin-dependent kinase inhibitor, P276-00, inhibits HIF-1α and induces G2/M arrest under hypoxia in prostate cancer cells. *Prostate Cancer Prostatic Dis.* **2012**, 15, 15–27.

(41) Raje, N.; Hideshima, T.; Mukherjee, S.; Raab, M.; Vallet, S.; Chhetri, S.; Cirstea, D.; Pozzi, S.; Mitsiades, C.; Rooney, M.; Kiziltepe, T.; Podar, K.; Okawa, Y.; Ikeda, H.; Carrasco, R.; Richardson, P. G.; Chauhan, D.; Munshi, N. C.; Sharma, S.; Parikh, H.; Chabner, B.; Scadden, D.; Anderson, K. C. Preclinical activity of P276-00, a novel small-molecule cyclin-dependent kinase inhibitor in the therapy of multiple myeloma. *Leukemia* **2009**, 23, 961–970.

(42) Cassaday, R. D.; Goy, A.; Advani, S.; Chawla, P.; Nachankar, R.; Gandhi, M.; Gopal, A. K. A phase II, single-arm, open-label, multicenter study to evaluate the efficacy and safety of P276-00, a cyclin-dependent kinase inhibitor, in patients with relapsed or refractory mantle cell lymphoma. *Clin. Lymphoma Myeloma Leuk.* **2015**, 15, 392–397.

(43) Vishwakarma, R. A.; Bharate, S. B.; Bhushan, S.; Mundhe, D. M.; Jain, S. K.; Meena, S.; Guru, S. K.; Pathania, A. S.; Kumar, S.; Behl, A.; Mintoo, M. J.; Bharate, S. S.; Joshi, P. Rohitukine Analogs as Cyclin-dependent Kinase Inhibitors and a Process for the Preparation Thereof. WO2014170914A1, US20160052915, EP2986605, CA2908084, IN201303E01142, October 23, 2014.

(44) Huwe, A.; Mazitschek, R.; Giannis, A. Small molecules as inhibitors of cyclin-dependent kinases. *Angew. Chem., Int. Ed.* **2003**, 42, 2122–2138.

(45) Baumli, S.; Lolli, G.; Lowe, E. D.; Troiani, S.; Rusconi, L.; Bullock, A. N.; Debreczeni, J. E.; Knapp, S.; Johnson, L. N. The structure of P-TEFb (CDK9/cyclin T1), its complex with flavopiridol and regulation by phosphorylation. *EMBO J.* **2008**, 27, 1907–1918.

(46) Jain, S. K.; Bharate, S. B.; Vishwakarma, R. A. Cyclin-dependent kinase inhibition by flavoalkaloids. *Mini-Rev. Med. Chem.* **2012**, 12, 632–649.

(47) De Azevedo, W. F., Jr.; Mueller-Dieckmann, H. J.; Schulze-Gahmen, U.; Worland, P. J.; Sausville, E.; Kim, S. H. Structural basis for specificity and potency of a flavonoid inhibitor of human CDK2, a cell cycle kinase. *Proc. Natl. Acad. Sci. U. S. A.* **1996**, 93, 2735–2740.

(48) Kim, K. S.; Sack, J. S.; Tokarski, J. S.; Qian, L.; Chao, S. T.; Leith, L.; Kelly, Y. F.; Misra, R. N.; Hunt, J. T.; Kimball, S. D.; Humphreys, W. G.; Wautlet, B. S.; Mulheron, J. G.; Webster, K. R. Thio- and oxoflavopiridols, cyclin-dependent kinase 1 selective inhibitors: synthesis and biological effects. *J. Med. Chem.* **2000**, 43, 4126–4134.

(49) Murthi, K. K.; Dubay, M.; McClure, C.; Brizuela, L.; Boisclair, M. D.; Worland, P. J.; Mansuri, M. M.; Pal, K. Structure-activity relationship studies of flavopiridol analogues. *Bioorg. Med. Chem. Lett.* **2000**, 10, 1037–1041.

(50) Schoepfer, J.; Fretz, H.; Chaudhuri, B.; Muller, L.; Seeber, E.; Meijer, L.; Lozach, O.; Vangrevelinghe, E.; Furet, P. Structure-based design and synthesis of 2-benzylidene-benzofuran-3-ones as flavopiridol mimics. *J. Med. Chem.* **2002**, 45, 1741–1747.

(51) Ahn, Y. M.; Vogeti, L.; Liu, C. J.; Santhapuram, H. K.; White, J. M.; Vasandani, V.; Mitscher, L. A.; Lushington, G. H.; Hanson, P. R.; Powell, D. R.; Himes, R. H.; Roby, K. F.; Ye, Q.; Georg, G. I. Design, synthesis, and antiproliferative and CDK2-cyclin a inhibitory activity of novel flavopiridol analogues. *Bioorg. Med. Chem.* **2007**, 15, 702–713.

(52) Jain, S. K.; Meena, S.; Singh, B.; Bharate, J. B.; Joshi, P.; Singh, V. P.; Vishwakarma, R. A.; Bharate, S. B. KF/alumina catalyzed regioselective benzylation and benzoylation using solvent-free grind stone chemistry. *RSC Adv.* **2012**, 2, 8929–8933.

(53) Kang, C.; Qin, J.; Osei, W.; Hu, K. Regulation of protein kinase C-epsilon and its age-dependence. *Biochem. Biophys. Res. Commun.* **2017**, 482, 1201–1206.

(54) Fabiani, R.; Rosignoli, P.; De Bartolomeo, A.; Fuccelli, R.; Morozzi, G. Inhibition of cell cycle progression by hydroxytyrosol is

associated with upregulation of cyclin-dependent protein kinase inhibitors p21(WAF1/Cip1) and p27(Kip1) and with induction of differentiation in HL60 cells. *J. Nutr.* **2008**, *138*, 42−48.

(55) Xie, S.; Jiang, H.; Zhai, X. W.; Wei, F.; Wang, S. D.; Ding, J.; Chen, Y. Antitumor action of CDK inhibitor LS-007 as a single agent and in combination with ABT-199 against human acute leukemia cells. *Acta Pharmacol. Sin.* **2016**, *37*, 1481−1489.

(56) Evers, B. M.; Ko, T. C.; Li, J.; Thompson, E. A. Cell cycle protein suppression and p21 induction in differentiating Caco-2 cells. *Am. J. Physiol.* **1996**, *271*, G722−G727.

(57) Bharate, S. S.; Kumar, V.; Vishwakarma, R. A. Determining partition coefficient (Log P), distribution coefficient (Log D) and ionization constant (pKa) in early drug discovery. *Comb. Chem. High Throughput Screening* **2016**, *19*, 461−469.

(58) Bharate, S. S.; Vishwakarma, R. A. Thermodynamic equilibrium solubility measurements in simulated fluids by 96-well plate method in early drug discovery. *Bioorg. Med. Chem. Lett.* **2015**, *25*, 1561−1567.

(59) Fabian, M. A.; Biggs, W. H.; Treiber, D. K.; Atteridge, C. E.; Azimioara, M. D.; Benedetti, M. G.; Carter, T. A.; Ciceri, P.; Edeen, P. T.; Floyd, M.; Ford, J. M.; Galvin, M.; Gerlach, J. L.; Grotzfeld, R. M.; Herrgard, S.; Insko, D. E.; Insko, M. A.; Lai, A. G.; Lelias, J. M.; Mehta, S. A.; Milanov, Z. V.; Velasco, A. M.; Wodicka, L. M.; Patel, H. K.; Zarrinkar, P. P.; Lockart, D. J. A small molecule kinase interaction map for clinical kinase inhibitors. *Nat. Biotechnol.* **2005**, *23*, 329−336.

(60) Baumli, S.; Lolli, G.; Lowe, E. D.; Troiani, S.; Rusconi, L.; Bullock, A. N.; Debreczeni, J. E.; Knapp, S.; Johnson, L. N. The structure of P-TEFb (CDK9/cyclin T1), its complex with flavopiridol and regulation by phosphorylation. *EMBO J.* **2008**, *27*, 1907−1918.

(61) Crespi, C. L.; Miller, V. P.; Penman, B. W. Microtiter plate assays for inhibition of human, drug-metabolizing cytochromes P450. *Anal. Biochem.* **1997**, *248*, 188−190.

(62) Kumar, V.; Bharate, S. S.; Vishwakarma, R. A. Modulating lipophilicity of rohitukine via prodrug approach: Preparation, characterization, and in vitro enzymatic hydrolysis in biorelevant media. *Eur. J. Pharm. Sci.* **2016**, *92*, 203−211.

Design, Synthesis, and Pharmacological Evaluation of Embelin–Aryl/alkyl Amine Hybrids as Orally Bioavailable Blood–Brain Barrier Permeable Multitargeted Agents with Therapeutic Potential in Alzheimer's Disease: Discovery of SB-1448

Vijay K. Nuthakki, Sushil Choudhary, Chilakala N. Reddy, Shipra Bhatt, Ashiya Jamwal, Anshika Jotshi, Rinky Raghuvanshi, Ankita Sharma, Shikha Thakur, Hemant R. Jadhav, Sonali S. Bharate, Utpal Nandi, Ajay Kumar, and Sandip B. Bharate*

ABSTRACT: The complex and multifaceted nature of Alzheimer's disease has brought about a pressing demand to develop ligands targeting multiple pathways to combat its outrageous prevalence. Embelin is a major secondary metabolite of *Embelia ribes* Burm f., one of the oldest herbs in Indian traditional medicine. It is a micromolar inhibitor of cholinesterases (ChEs) and β-site amyloid precursor protein cleaving enzyme 1 (BACE-1) with poor absorption, distribution, metabolism, and excretion (ADME) properties. Herein, we synthesize a series of embelin–aryl/alkyl amine hybrids to improve its physicochemical properties and therapeutic potency against targeted enzymes. The most active derivative, 9j (SB-1448), inhibits human acetylcholinesterase (hAChE), human butyrylcholinesterase (hBChE), and human BACE-1 (hBACE-1) with IC$_{50}$ values of 0.15, 1.6, and 0.6 μM, respectively. It inhibits both ChEs noncompetitively with k_i values of 0.21 and 1.3 μM, respectively. It is orally bioavailable, crosses blood–brain barrier (BBB), inhibits Aβ self-aggregation, possesses good ADME properties, and protects neuronal cells from scopolamine induced cell death. The oral administration of 9j at 30 mg/kg attenuates the scopolamine-induced cognitive impairments in C57BL/6J mice.

KEYWORDS: embelin, Alzheimer's disease, cholinesterase, β-secretase, blood–brain barrier, MTDL.

INTRODUCTION

Dementia is one of the leading causes of death among seniors (aged 65 and above), which has already affected more than 55 million people worldwide, of which Alzheimer's disease (AD) alone contributes to 60–70% of cases.[1,2] AD is the main form of dementia and is an unfathomable multifactorial neurodegenerative disorder that progresses via degeneration of the brain cells, worsening cognitive and behavioral skills and resulting in the loss of brain function, eventually leading to death.[3,4] Unfortunately, no disease-modifying therapy is available for AD; all available drugs only alleviate symptoms associated with AD. In 2021, there was a controversial approval of a monoclonal antibody, aducanumab, by the Food and Drug Administration (FDA).[5] Aducanumab has been assumed to

treat AD by acting on Aβ, whereas its therapeutic efficacy is still ambiguous.[6,7] This lack of curative therapeutics has brought about a dire need to develop molecules capable of dealing with the underlying pathology of AD. The enigmatic multifactorial pathophysiology of AD led researchers to develop ligands targeting multiple pathways.[9,10] Researchers
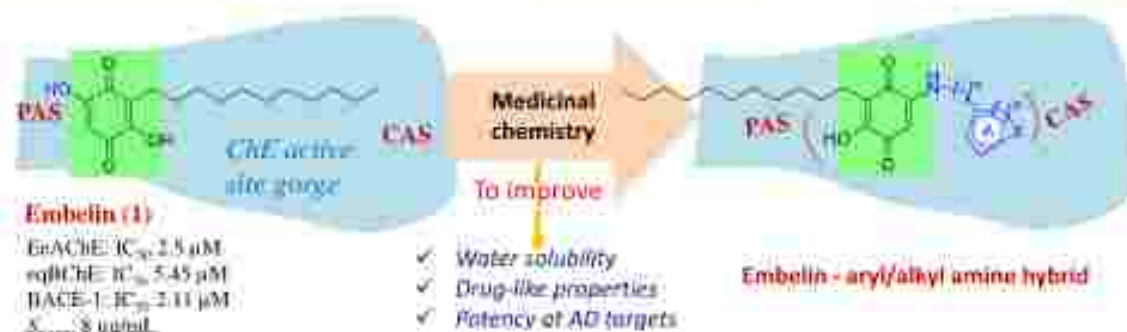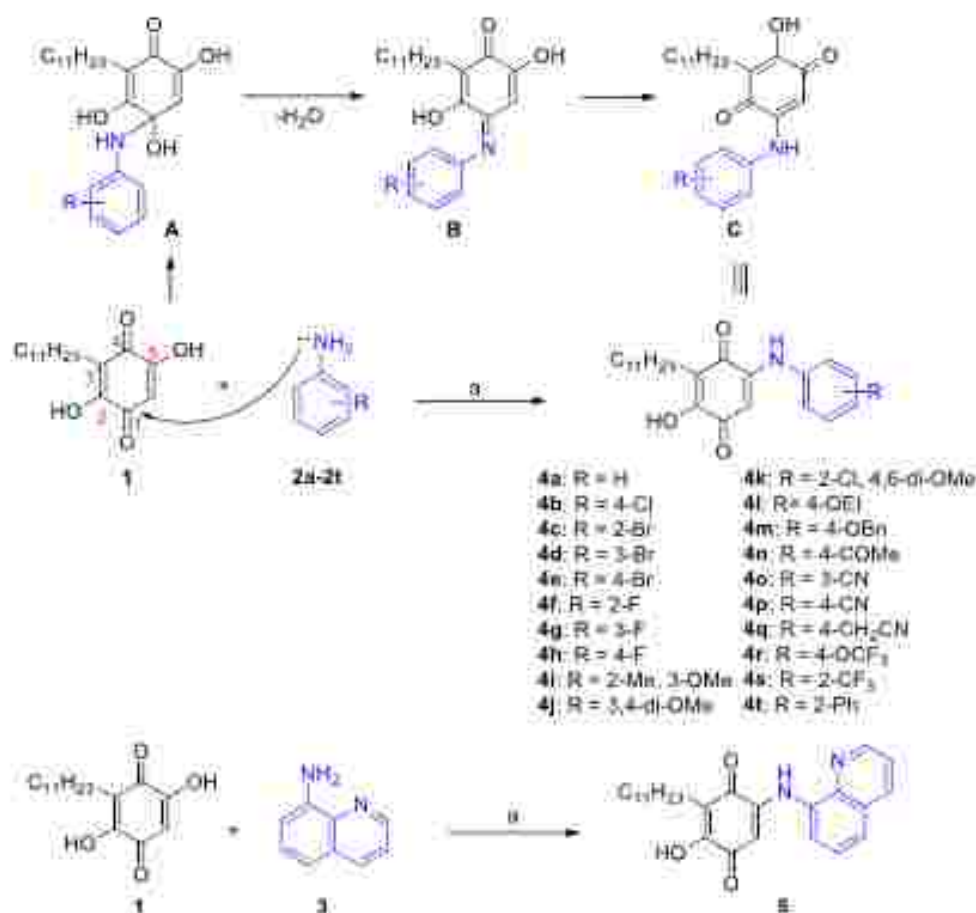
Figure 1. Proposed series of embelin derivatives to improve its physicochemical/ ADME properties and efficacy against targets.

Scheme 1. Synthesis of Embelin Derivatives 4a–t and 5[a]

4a: R = H	4k: R = 2-Cl, 4,6-di-OMe
4b: R = 4-Cl	4l: R = 4-OEt
4c: R = 2-Br	4m: R = 4-OBn
4d: R = 3-Br	4n: R = 4-COMe
4e: R = 4-Br	4o: R = 3-CN
4f: R = 2-F	4p: R = 4-CN
4g: R = 3-F	4q: R = 4-CH₂CN
4h: R = 4-F	4r: R = 4-OCF₃
4i: R = 2-Me, 3-OMe	4s: R = 2-CF₃
4j: R = 3,4-di-OMe	4t: R = 2-Pr

[a]Reagents and conditions: (a) acetic acid, reflux, 2 h, 68–89%.

have proposed three hypotheses, viz. amyloid, cholinergic, and tau hypotheses, which constitute the core pathology of AD.[15] These hypotheses collectively state that neurodegeneration in AD starts with a plunge in synaptic acetylcholine (ACh) levels and further progresses with the extracellular deposition of misfolded amyloid β (Aβ) in senile plaques and intracellular aggregation of the hyperphosphorylated tau protein in neurofibrillary tangles (NFTs).[12,13] These senile plaques and NFTs constitute AD's major pathological markers, which further cause neurotoxicity and eventually result in cell death.[14,15] Nevertheless, the etiology of AD has not been fully understood; palliative therapies have emerged following the conventional cholinergic approach by restoring the synaptic ACh levels via inhibiting the function of cholines-

terases (ChEs), acetylcholinesterase (AChE), and/or butyrylcholinesterase (BChE).[16–18] According to the amyloid hypothesis, there is consensus that Aβ is the major pathological hallmark of AD, which is formed by sequential proteolysis of the amyloid precursor protein (APP) by β-secretase (BACE-1) and γ-secretase.[19,20] This complex and multifactorial etiology of AD has created an urgent need to develop multitargeted drug ligands (MTDLs) to combat its dreadful ubiquity among the elderly.[21] MTDLs are constructed by merging two or more different pharmacophores into one. Since the strategy of MTDLs by virtue of its hypothesis is likely to modulate the disease progression, there has been a growing consensus that MTDLs can effectively combat neurodegenerative disorders like AD.[22,23]

There is an incredible contribution of natural products (NPs) to drug discovery in general and particularly in the CNS domain (84% of the marketed drugs in the CNS domain are either pure NPs or NP-inspired molecules).[24-26] In continuation to our continuous efforts on exploring natural products for CNS diseases,[27-39] herein, the hydroxybenzoquinone natural product, embelin (1), was pursued for medicinal chemistry lead optimization in search of optimized MTDL for AD. Embelin (1) is an MTDL showing inhibition of AChE, BChE, and BACE-1 with respective IC$_{50}$ values of 2.5, 5.45, and 2.11 μM[29] and also has an ability to bind Aβ and prevent its accumulation.[36,37] The ameliorating potential of embelin against scopolamine-induced amnesia[38] and streptozotocin-induced cognitive impairment[39] was proved in rat models. Embelin (1) also significantly inhibits electroshock and pentylenetetrazole-induced seizures with an anticonvulsant potential similar to phenytoin and diazepam.[40] Besides, embelin also has antioxidant properties.[41,42] These reports showcase the scope and potential of the embelin scaffold to be explored further in the CNS domain, particularly in AD drug discovery. Traditionally, embelin (1) is effective against fevers and inflammation,[43,44] gastrointestinal diseases, and has analgesic properties.[45,46] Embelin (1) is a highly lipophilic molecule with low aqueous solubility accounting for its poor oral pharmacokinetics (PK).[47] The poor oral exposure is also likely attributed to its metabolic instability. Moreover, the therapeutic potency of embelin (1) against all three enzymes (AChE, BChE, and BACE-1) has to be improved. In this work, we aim to address these problems by synthesizing hybrids of embelin with amines/drug-like functionalities. To improve the aqueous solubility of the embelin scaffold, we planned to introduce oxygen and nitrogen-containing substituents. The introduction of nitrogen-containing heterocyclic fragments has the potential to boost cholinesterase inhibition.[48] In these lines, we have synthesized forty-five derivatives of embelin by condensation with various aliphatic, aromatic, and heterocyclic amines. A detailed preclinical characterization is carried out for the optimized compound, SB-1448.

RESULTS AND DISCUSSION

Design and Synthesis of Embelin Derivatives. Embelin (1) is an 11-carbon-long alkyl chain linked to dihydroxyquinone, which binds with the peripheral binding site of ChEs. The hydroxyquinone framework stays at the peripheral anionic site (PAS), whereas its long aliphatic chain remains suspended inside the cavity without showing any interaction. The catalytic site of cholinesterases contains an anionic site that interacts with the quaternary nitrogen of ligands. Interaction with the anionic site significantly contributes to the enzyme inhibition activity. Thus, the introduction of polar functionalities containing nitrogen-bearing linkers or nitrogen heterocycles is likely to create interaction with the anionic site of catalytic anionic site (CAS) in the ChE binding pocket. Thus, we planned to prepare hybrid structures of embelin with various aryl or alkyl amines, as depicted in Figure 1. Incorporating polar functionalities is also likely to improve the physicochemical and absorption, distribution, metabolism, and excretion (ADME) properties of the embelin scaffold.

The scheme followed for synthesizing proposed embelin–amine hybrids is illustrated in Scheme 1. Embelin (1) was used as a starting material in synthesizing these derivatives. The extraction of dried berries of *Embelia ribes* with dichloromethane, followed by crystallization, provided orange crystals

of embelin (1). The isolated compound was characterized by comparing its NMR data with literature values.[49] It was interesting to note that none of the oxygen-linked carbons appeared in the ^{13}C NMR spectrum. This is because of the fluxional effect caused by intramolecular H-bonding.[49]

Treatment of embelin (1) with aniline (2a) in the presence of acetic acid under reflux conditions yielded the condensation product, 4a, in 78% yield. The ^{1}H NMR of 4a showed the presence of aromatic CH peaks for five protons at δ 7.44–7.23 ppm, whereas the aryl CH (C$_e$–H) of the embelin core is intact with a singlet at δ 6.00 ppm. This indicated the condensation of aniline with one of the OH/–C=O groups. Mechanistically, the reaction proceeds via imine formation with the C1-carbonyl group, followed by tautomerization to form 4a. Treatment of embelin with substituted anilines 2b–t yielded the corresponding aniline-fused embelin derivatives, 4b–t, in good yields. The reaction of embelin with aminoquinoline also produced the corresponding product, 5, in 85% yield (Scheme 1).
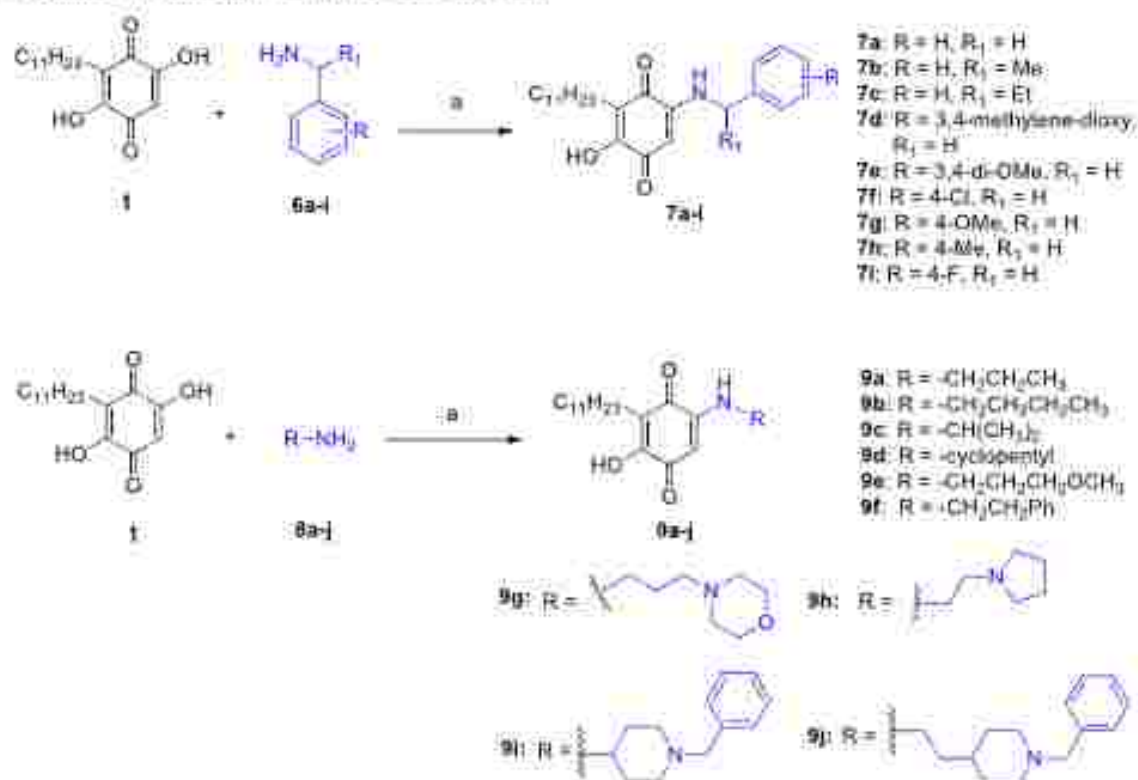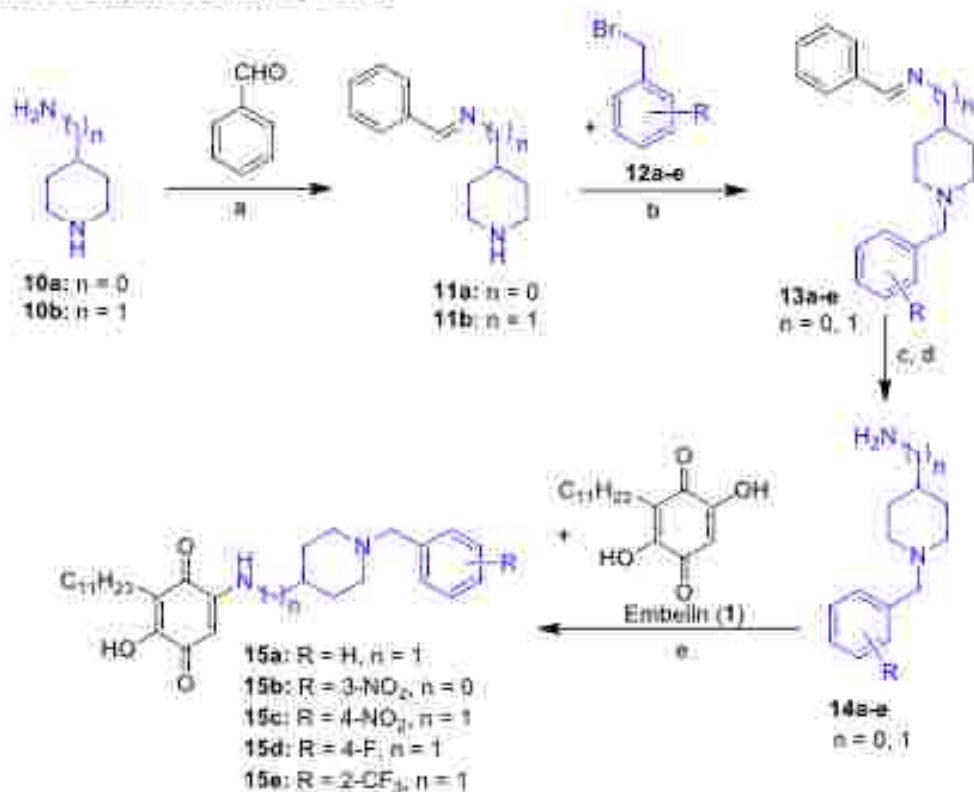
The condensation of embelin with aniline has two possibilities, as depicted in Figure 2. The ^{13}C NMR of these
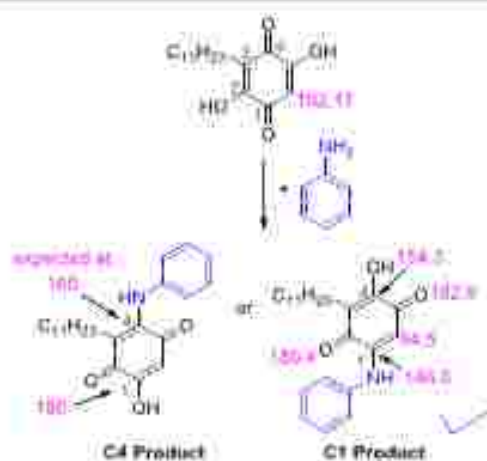
Figure 2. Two possible products for the condensation of embelin with aniline. The expected/obtained ^{13}C NMR signals for selected carbons are shown in pink color. The values for C4 product are expected values based on the ChemDraw predictions. The chemical shift values for embelin and the C1 product are experimental values.
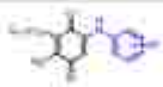
two possible products would be quite different, particularly the C1 and C4 carbon signals. Based on the obtained ^{13}C NMR for 4a (and rest of the products), the obtained product is assigned as C1-coupled. The formation of the C1 product was further confirmed via two-dimensional (2D)-NMR (heteronuclear single quantum coherence (HSQC), heteronuclear multiple bond correlation (HMBC), and nuclear Overhauser enhancement spectroscopy (NOESY)) analysis (spectra provided in Section S4 of the Supporting information).

To build the structure–activity relationship (SAR), other amines, such as benzylamines and aliphatic amines, were also investigated for reaction with embelin. The treatment of embelin (1) with benzylamine (6a) also smoothly yielded the corresponding product, 7a, in 82% yield. Similarly, other benzylamines provided products, 7b–l, in good yields. The aliphatic amine, such as n-propyl amine (8a), also provided a corresponding derivative 9a in good yield (79%). The aliphatic amines connected with various saturated heterocycles, such as

Scheme 2. Synthesis of Embelin Derivatives 7a–i and 9a–j[a]

7a: R = H, R₁ = H
7b: R = H, R₁ = Me
7c: R = H, R₁ = Et
7d: R = 3,4-methylene-dioxy, R₁ = H
7e: R = 3,4-di-OMe, R₁ = H
7f: R = 4-Cl, R₁ = H
7g: R = 4-OMe, R₁ = H
7h: R = 4-Me, R₁ = H
7i: R = 4-F, R₁ = H

9a: R = -CH₂CH₂CH₃
9b: R = -CH₂CH₂CH₂CH₃
9c: R = -CH(CH₃)₂
9d: R = -cyclopentyl
9e: R = -CH₂-CH₂CH₂OCH₃
9f: R = -CH₂CH₂Ph

9g: R = [structure with morpholine]
9h: R = [structure with pyrrolidine]
9i: R = [structure with benzylpiperazine]
9j: R = [structure with benzylpiperidine]

[a]Reagents and conditions: (a) acetic acid, reflux, 2 h, 67–86%.

Scheme 3. Synthesis of Embelin Derivatives, 15a–e.[a]

10a: n = 0
10b: n = 1

11a: n = 0
11b: n = 1

13a-e
n = 0, 1

14a-e
n = 0, 1

15a: R = H, n = 1
15b: R = 3-NO₂, n = 0
15c: R = 4-NO₂, n = 1
15d: R = 4-F, n = 1
15e: R = 2-CF₃, n = 1

[a]Reagents and conditions: (a) toluene, rt, 4 h; (b) NaH, dimethylformamide (DMF), rt, 6 h; (c) 4 N HCl, rt, 2 h; (d) neutralize with NaHCO₃; (v) acetic acid, reflux, 2 h, 64–72%.

Table 1. *In Vitro* Inhibitory Activities of Embelin Derivatives with Aromatic Amine Substitution against Three Targets, Antioxidant Activity, BBB Permeability, and Aqueous Solubility[a]

Entry	R	AD targets, IC_{50} (μM) $\pm$ SD[b]			Antioxidant activity IC_{50} (μM) $\pm$ SD[c]		BBB permeability $(Pe \times 10^{-6}\ cm/s) \pm$ SD[d] (CNS +/-)	Aqueous solubility (μg/mL) $\pm$ SD
		AChE	BChE	BACE-1	ABTS	DPPH		
4a	H	2.95 ± 0.48	4.08 ± 0.23	>10	44.16 ± 0.77	>100	12.18 ± 0.73 (CNS+)	16.81 ± 6.29
4b	4-Cl	7.42 ± 0.89	>10	5.36 ± 0.87	71.24 ± 0.09	>100	4.86 ± 0.27 (CNS+)	40 ± 1.26
4c	2-Br	>10	>10	4.89 ± 0.87	>100	>100	5.04 ± 0.63 (CNS+)	40 ± 8.42
4d	3-Br	2.1 ± 0.4	>10	5.41 ± 0.56	16.7 ± 1.82	49.28 ± 4.39	4.06 ± 0.34 (CNS+)	71.22 ± 1.79
4e	4-Br	1.59 ± 0.11	>10	7.87 ± 0.45	84.85 ± 2.59	24.36 ± 2.51	5.83 ± 0.62 (CNS+)	20.95 ± 0.9
4f	2-F	1.04 ± 0.05	9.50 ± 0.29	4.08 ± 0.5	>100	>100	5.76 ± 0.37 (CNS+)	11.12 ± 1.55
4g	3-F	3.08 ± 0.55	>10	4.87 ± 1.17	55.93 ± 8.85	>100	6.53 ± 0.07 (CNS+)	20.57 ± 0.43
4h	4-F	2.82 ± 0.43	>10	2.27 ± 0.12	>100	>100	7.71 ± 1.29 (CNS+)	35.63 ± 4.32
4i	2-Me, 3-OMe	1.93 ± 0.21	>10	3.97 ± 0.41	>100	>100	6.50 ± 0.34 (CNS+)	14.99 ± 2.45
4j	3,4-dimethoxy	4.58 ± 0.08	>10	>10	33.47 ± 3.2	>100	4.10 ± 0.06 (CNS+)	19.95 ± 1.17
4k	3-Cl, 4,6-dimethoxy	2.9 ± 0.25	2.29 ± 0.62	>10	15.07 ± 0.55	>100	10.35 ± 2.02 (CNS+)	409.5 ± 131.04
4l	4-OH	4.95 ± 0.1	>10	4.36 ± 1.13	4.51 ± 1.39	54.03 ± 2.25	5.86 ± 0.34 (CNS+)	13.53 ± 3.86
4m	4-OMe	8.04 ± 9.69	>10	>10	>100	>100	8.92 ± 0.79 (CNS+)	52.45 ± 5.64
4n	4-COMe	5.15 ± 0.5	>10	4.3 ± 0.31	99.55 ± 5.3	>100	4.89 ± 0.06 (CNS+)	150.23 ± 53.24
4o	3-CN	2.60 ± 0.1	2.63 ± 0.76	>10	>100	>100	7.02 ± 1.28 (CNS+)	21.66 ± 5.34
4p	4-CN	3.07 ± 0.07	5.56 ± 1.7	>10	>100	>100	12.25 ± 0.99 (CNS+)	488.89 ± 18.17
4q	4-CH₂CN	4.53 ± 0.62	>10	9.69 ± 1.75	40.23 ± 2.79	>100	7.30 ± 0.46 (CNS+)	43.38 ± 5.52
4r	4-OCF₃	4.23 ± 0.1	8.25 ± 1.23	4.25 ± 0.56	20.97 ± 7.07	35.11 ± 1.97	4.24 ± 0.39 (CNS+)	15.44 ± 0.6
4s	2-CF₃	3.34 ± 0.1	9.25 ± 1.00	3.25 ± 0.25	>100	>100	6.99 ± 0.26 (CNS+)	27.29 ± 1.1
4t	2-Br	1.15 ± 0.03	>10	>10	>100	>100	4.21 ± 0.18 (CNS+)	22.35 ± 1.57
5		1.72 ± 0.40	>10	6.31 ± 0.08	>100	>100	3.08 ± 1.21 (CNS+)	16.21 ± 9.20
Embelin (1)		2.90 ± 0.08	5.45 ± 0.19	2.51 ± 0.33	7.52 ± 0.01	19.02 ± 0.53	4.54 ± 0.18 (CNS+)	8.02 ± 2.23
Donepezil		0.025 ± 0.001	4.5 ± 0.56	nd[e]	nd	nd	13.8 ± 1.64 (CNS+)	nd
Ascorbic acid		nd	nd	nd	21.39 ± 0.54	68.62 ± 2.02	nd	nd

[a]Values are expressed as mean ± standard deviation (SD) of at least three experiments (n = 3). [b]IC_{50} inhibitory concentration of compounds against *E. electricus* AChE, equine serum BChE, and human recombinant BACE-1. [c]*In vitro* antioxidant activity by 2,2′-azino-bis(3-ethylbenzothiazoline-6-sulfonic acid) (ABTS) and 2,2-diphenyl-1-picrylhydrazyl (DPPH) methods. [d]Permeability values from the parallel artificial membrane permeability assay (PAMPA)–BBB assay. [e]nd: not determined.

Table 2. *In Vitro* Inhibitory Activities of Embelin Derivatives with Benzylic/Alkyl–Aryl Amine Substitution against Three Targets, Antioxidant Activity, BBB Permeability, and Aqueous Solubility[a]

Entry	R1	R2	AD targets, IC_{50} (μM) $\pm$ SD[b]			Antioxidant activity IC_{50} (μM) $\pm$ SD[c]		BBB permeability $(Pe \times 10^{-6}\ cm/s) \pm$ SD[d] (CNS +/-)	Aqueous solubility (μg/mL) $\pm$ SD
			AChE	BChE	BACE-1	ABTS	DPPH		
7a	H	H	>10	>10	9.2 ± 0.75	96.85 ± 1.86	97.70 ± 4.71	5.51 ± 0.33 (CNS+)	27.52 ± 14.92
7b	H	4-OH	>10	>10	>10	>100	>100	4.76 ± 1.68 (CNS+)	11.30 ± 3.16
7c	H	4-F	>10	>10	>10	17.51 ± 1.06	36.79 ± 3.33	5.71 ± 0.31 (CNS+)	21.54 ± 7.06
7d	3,4-methylenedioxy	H	7.82 ± 0.39	>10	>10	>100	>100	6.99 ± 1.21 (CNS+)	33.79 ± 3.34
7e	3,4-dimethoxy	H	>10	>10	>10	21.04 ± 0.88	19.16 ± 2.31	2.89 ± 0.06 (CNS+)	40 ± 6.9
7f	4-Cl	H	>10	>10	>10	54.83 ± 4.89	>100	2.89 ± 0.18 (CNS+)	32.44 ± 2.2
7g	4-OMe	H	>10	>10	>10	78.82 ± 4.82	>100	1.35 ± 0.12 (CNS+)	40 ± 1.47
7h	4-Me	H	7.08 ± 0.95	>10	>10	18.33 ± 1.23	>100	4.72 ± 0.27 (CNS+)	40.29 ± 13.57
7i	4-F	H	8.52 ± 0.08	8.25 ± 0.19	5.34 ± 0.6	88.54 ± 5.44	58.87 ± 2.64	4.49 ± 0.91 (CNS+)	21.58 ± 3.18
Embelin (1)			2.90 ± 0.08	5.45 ± 0.16	2.51 ± 0.33	7.52 ± 0.01	19.02 ± 0.53	4.54 ± 0.18 (CNS+)	8.02 ± 2.23
Donepezil			0.025 ± 0.001	4.5 ± 0.56	nd[e]	nd	nd	13.8 ± 1.64 (CNS+)	nd
Ascorbic acid			nd	nd	nd	21.39 ± 0.54	68.62 ± 2.02	nd	nd
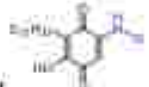
[a]Values are expressed as mean ± standard deviation (SD) of at least three experiments (n = 3). [b]IC_{50} inhibitory concentration of compounds against *E. electricus* AChE, equine serum BChE, and human recombinant BACE-1. [c]*In vitro* antioxidant activity by ABTS and DPPH methods. [d]Permeability values from the PAMPA–BBB assay. [e]nd: not determined.

morpholine, pyrrolidine, and piperidine, produced the corresponding products, 9g–i, in good yield (Scheme 2).

Further, to build SAR in piperidinyl-linked analogues (9i, 9j series), the substituted piperidine amines 14a–e were prepared following Scheme 3 starting from piperidine amines 10a or

Table 3. *In Vitro* Inhibitory Activities of Embelin Derivatives with Aliphatic Amine or Heteroaryl Amine Substitution against Three Targets, Antioxidant Activity, BBB Permeability, and Aqueous Solubility[a]

Entry	-R	AD targets, IC_{50} (μM) ± SD[b]			Antioxidant activity IC_{50} (μM) ± SD[c]		BBB permeability $[Pe \times 10^{-7} \text{ cm/s}] \pm SD^{d}$ (CNS+/-)	Aqueous solubility (μg/mL ± SD)
		AChE	BChE	BACE-1	ABTS	DPPH		
9a	-CH₂CH₂CH₃	>10	>10	>10	15.75 ± 3.02	68.98 ± 6.65	2.99 ± 0.04 (CNS+)	24.05 ± 6
9b	-CH(CH₃CH₂CH₃)	>10	>10	4.02 ± 0.39	82.87 ± 0.84	26.44 ± 3.3	2.89 ± 0.01 (CNS+/-)	40 ± 2.22
9c	-CH(CF₃)₂	>10	>10	>10	14.9 ± 1.01	41.75 ± 3.67	2.92 ± 0.1 (CNS+/-)	29.07 ± 2.64
9d	Cyclopentyl	>10	>10	>10	>100	>100	5.29 ± 0.45 (CNS+)	40 ± 5.4
9e	-CH₂CH₂CH₂OCH₃	>10	>10	>10	4.81 ± 0.54	36.06 ± 2.2	1.87 ± 0.77 (CNS+)	27.53 ± 4.76
9f	-CH₂CH₂Ph	1.81 ± 0.31	>10	>10	>100	>100	8.96 ± 0.94 (CNS+)	19.06 ± 1.98
9g		>10	>10	>10	>100	>100	6.44 ± 0.01 (CNS+)	226.76 ± 55.21
9h		>10	>10	>10	>100	>100	7.81 ± 0.09 (CNS+)	94.10 ± 2.40
Embelin (1)		2.90 ± 0.08	7.43 ± 0.16	2.11 ± 0.33	7.52 ± 0.01	19.92 ± 6.55	4.54 ± 0.38 (CNS+)	8.02 ± 2.23
Donepezil		0.026 ± 0.001	4.5 ± 0.56	nd[e]	nd	nd	15.8 ± 1.64 (CNS+)	nd
Ascorbic acid		nd	nd	nd	21.39 ± 0.54	68.62 ± 2.02	nd	nd

[a]Values are expressed as mean ± standard deviation (SD) of at least three experiments (n = 3). [b]IC_{50} inhibitory concentration of compounds against *E. electricus* AChE, equine serum BChE, and human recombinant BACE-1. [c]*In vitro* antioxidant activity by ABTS and DPPH methods. [d]Permeability values from the PAMPA–BBB assay. [e]nd: not determined.

Table 4. *In Vitro* Inhibitory Activities of Embelin Derivatives with *N*-Benzylpiperidine Substitution against Three Targets, Antioxidant Activity, BBB Permeability, and Aqueous Solubility[a]

| Entry	n	R	AD targets, IC_{50} (μM) ± SD[b]			Antioxidant activity IC_{50} (μM) ± SD[c]		BBB permeability $[Pe \times 10^{-7} \text{ cm/s}] \pm SD^{d}$ (CNS+/-)	Aqueous solubility (μg/mL ± SD)
			AChE	BChE	BACE-1	ABTS	DPPH		
9i	0	H	4.79 ± 0.19	6.53 ± 0.92	8.75 ± 0.03	>100	>100	8.29 ± 0.37 (CNS+)	18.63 ± 1.17
9j	2	H	0.42 ± 0.07	0.89 ± 0.02	0.6 ± 0.02	19.09 ± 1.72	37.41 ± 1.32	8.39 ± 0.48 (CNS+)	26.21 ± 2.49
17a	1	H	9.66 ± 0.42	7.23 ± 0.58	9.81 ± 0.50	13.07 ± 1.65	19.86 ± 2.29	7.17 ± 0.33 (CNS+)	12.26 ± 0.62
15b	0	3-NO₂	>10	>10	>10	28.09 ± 1.49	43.1 ± 3.54	15.0 ± 0.61 (CNS+)	3.0 ± 0.10
15c	1	4-NO₂	>10	>10	>10	25.47 ± 0.78	23.46 ± 1.42	10.27 ± 1.78 (CNS+)	5.2 ± 0.47
15d	1	4-F	>10	>10	9.31 ± 0.21	30.66 ± 2.80	20.77 ± 1.8	11.52 ± 1.01 (CNS+)	5.36 ± 0.47
15e	1	2-CF₃	>10	>10	5.28 ± 0.6	11.88 ± 2.1	20.67 ± 1.97	8.71 ± 1.84 (CNS+)	6.49 ± 0.47
Embelin (1)			2.90 ± 0.08	8.48 ± 0.16	2.11 ± 0.33	7.52 ± 0.01	19.92 ± 0.59	4.54 ± 0.38 (CNS+)	8.02 ± 2.23
Donepezil			0.026 ± 0.001	4.5 ± 0.56	nd	nd	nd	15.8 ± 1.64 (CNS+)	nd
Ascorbic acid			nd	nd	nd	21.39 ± 0.54	68.62 ± 2.02	nd	nd

[a]Values are expressed as means ± standard deviation (SD) of at least three experiments (n = 3). [b]IC_{50} inhibitory concentration of compounds against *E. electricus* AChE, equine serum BChE, and human recombinant BACE-1. [c]*In vitro* antioxidant activity by ABTS and DPPH methods. [d]Permeability values from the PAMPA–BBB assay. [e]Embelin inhibits hAChE and hBChE with IC_{50} values of 7.9 and >100 μM, respectively. SB-1448 (9j) inhibits these two enzymes with IC_{50} values of 0.45 and 1.61 μM. Compound 9j is an optimized lead for further studies. [f]nd: not determined.

10b. The piperidine amines 10a or 10b were converted to their corresponding imines 11a or 11b by stirring with benzaldehyde in toluene at room temperature (rt). These obtained imines were reacted with substituted benzyl bromides 12a–e to form intermediates 13a–e, which were stirred in 4 N HCl, followed by neutralization with sodium bicarbonate to yield the desired piperidine amines 14a–e. The synthesized substituted piperidine amines 14a–e were condensed with embelin (1) in acetic acid to yield the corresponding products, 15a–e, in good yields (Scheme 3).

In Vitro Inhibition of ChEs and BACE-1. ChEs from different species, *Electrophorus electricus* AChE (EeAChE) and equine serum BChE (eqBChE), are frequently used for *in vitro* enzyme inhibition studies as suitable models for the corresponding recombinant human enzymes owing to their better stability.[30–32] Moreover, EeAChE and eqBChE share a sequence identity of 87 and 93.4% with their human counterparts.[33,34] Thus, these enzymes were employed for

ChE inhibition studies. The blood–brain barrier (BBB) permeability and aqueous solubility were also determined for all synthesized compounds. ChE/BACE-1 inhibition, BBB permeability, and solubility results for three different series are shown in Tables 1–4. The derivatization of embelin with aniline (derivative 4a) provided improved water solubility with the same level of ChE inhibition; however, the BACE-1 inhibition activity was compromised. Most other aniline-substituted compounds inhibited AChE and BACE-1 enzymes with IC_{50} values in the low micromolar range. However, only a few derivatives, 4a, 4f, 4k, 4o, 4p, 4r, and 4s, inhibited BChE with the IC_{50} value <10 μM. The 3,4-dimethoxy substitution on the phenyl ring did not turn out to be fruitful, whereas compound 4k with 2-chloro-4,6-dimethoxyphenyl substitution has shown dual cholinesterase inhibition with IC_{50} values of 2.9 and 2.3 μM against AChE and BChE, respectively. Moreover, 4k has also shown a tremendous increase in aqueous solubility (405 μg/mL) compared with embelin (1).
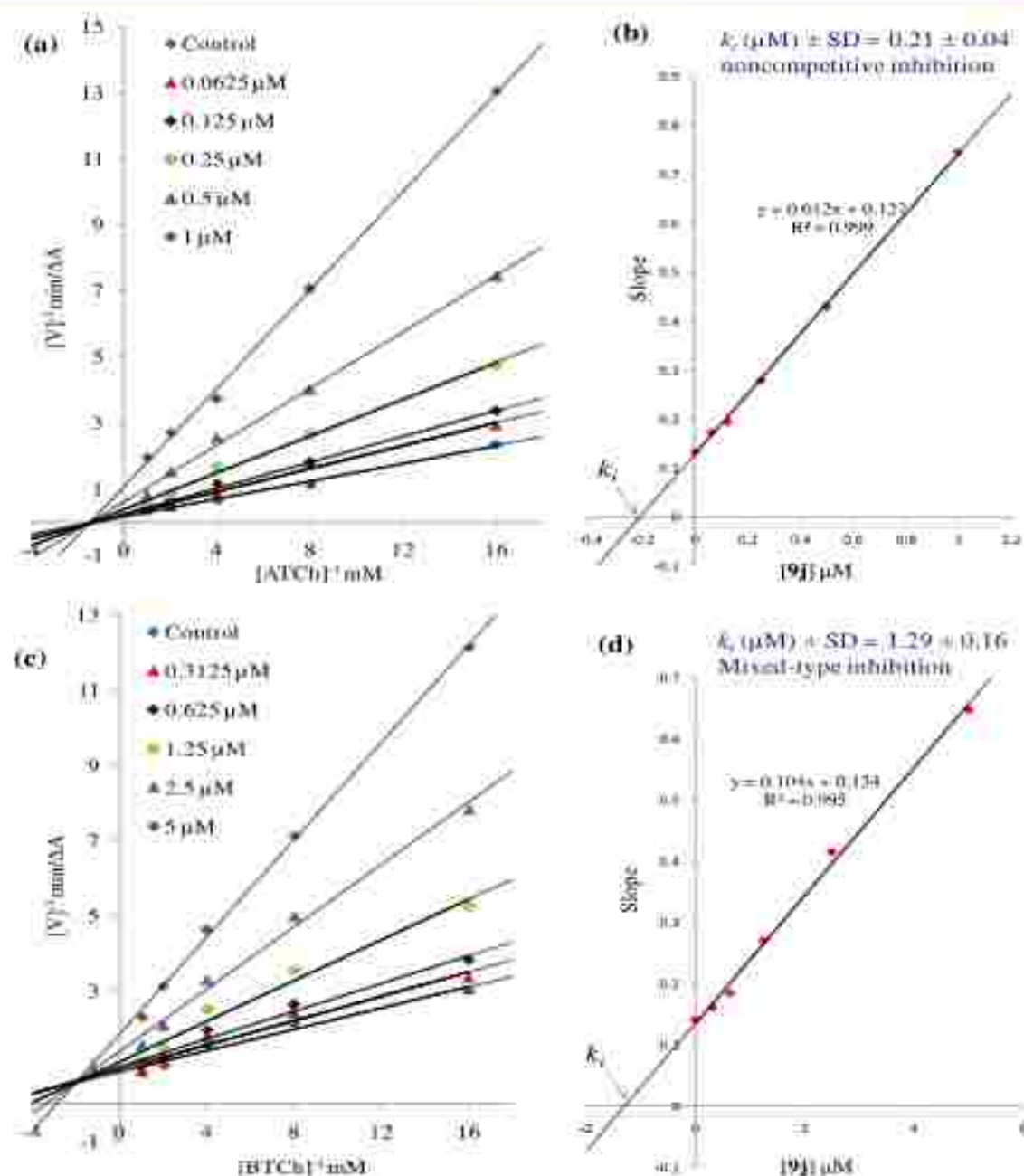
Figure 3. Enzyme kinetics of 9j with human AChE and human BChE. (a) The LB plot for the inhibition of hAChE by 9j; (b) a replot of slopes of the LB plot versus 9j concentration to determine the k_i value for AChE inhibition; (c) the LB plot for the inhibition of hBChE by 9j; and (d) a replot of the LB plot versus 9j concentration slopes to determine the k_i value for BChE inhibition.

Phenyl amine linkers with cyano groups (4o and 4p) also resulted in dual cholinesterase inhibition. The 4-fluorophenyl-substituted derivative, 4h, inhibits AChE and BACE-1 with respective IC_{50} values of 2.62 and 2.27 μM. It is evident that compounds with halogen-substituted phenyl amine linkers, particularly fluoro and bromo substitution, show significant AChE and BACE-1 inhibition. The aminoquinoline derivative, 5, inhibits AChE and BACE-1 with IC_{50} values of 1.72 and 4.31 μM, respectively, with 5-fold better aqueous solubility than embelin (8 versus 39 μg/mL). 4-Acetyl and 4-cyano substitution on the phenyl rings (4n and 4p) boosts the aqueous solubility of these compounds (Table 1). Interestingly, 4p also display high BBB permeability ($P_e = 12 \times 10^{-6}$ cm/s). The aminoquinoline derivative 5 is the best compound

from this series, with a balanced gain in ChE inhibition activity and significantly better (5-fold) water solubility.

The introduction of the methylene unit between NH and the phenyl ring in compound 4a led to the loss in ChE inhibition activity (analogue 4a versus 7a). Most of the benzylic amine derivatives were weak inhibitors of ChEs and BACE-1; however, the 4-fluoro-substituted benzylamino derivative 7i exhibited 2.5-fold superior AChE inhibition activity over embelin. The analogue 7i inhibit all three enzymes, AChE, BChE, and BACE-1, with IC_{50} values of 0.92, 4.75, and 3.74 μM, respectively, with excellent BBB permeability ($P_e = 6.5 \times 10^{-6}$ cm/s) and improved water solubility (21 μg/mL) (Table 2).
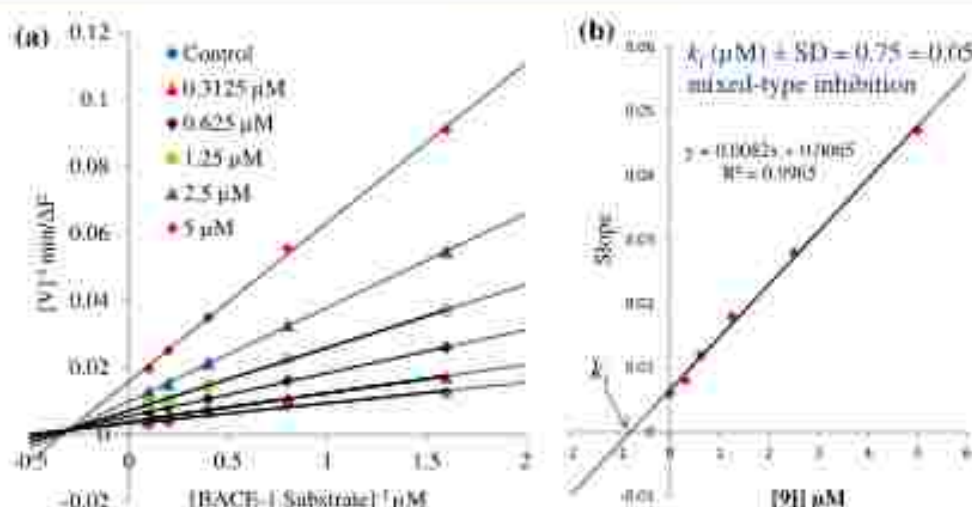
Figure 4. Kinetics of BACE-1 inhibition by 9j. (a) The LB plot for the inhibition of BACE-1 by 9j; (b) a replot of the LB plot versus 9j concentration slopes to determine the k_i value for BACE-1 inhibition.

Among embelin derivatives with aliphatic substituents, the analogue with a butyl amine linker, 9b, alone display an IC_{50} value of 4.02 μM against BACE-1, whereas other aliphatic linker compounds from the series did not show significant inhibition of ChEs and BACE-1. The introduction of a phenyl group on the ethyl linker resulted in compound 9f, which inhibits AChE with an IC_{50} value of 3.81 μM. This compound also had improved BBB permeability ($P_e = 6.9 \times 10^{-6}$ cm/s) and 2-fold better water solubility. Morpholine and pyrrolidine substitution (compounds 9g and 9h) resulted in multiple-fold improvement in the aqueous solubility of the compounds, but their therapeutic potency against the targeted enzymes was compromised. The derivatives 9i and 9j with the N-benzylpiperidine moiety were inhibitors of all three enzymes, along with improved water solubility. Compound 9j display the best inhibitory potential against AChE, BChE, and BACE-1 with IC_{50} values of 0.42, 0.85, and 0.6 μM, respectively. Analogue 9j also inhibits human AChE (hAChE) and human BChE (hBChE) with IC_{50} values of 0.147 and 1.61 μM, respectively. Compared with embelin (1), compound 9j achieved multifold increased therapeutic potency against all three targeted enzymes (Table 4). Further optimization by introducing substituents on the benzyl ring of N-benzylpiperidine was done to obtain five new compounds. The introduction of nitro and fluoro substituents on the phenyl group of N-benzylpiperidine in 15b to 15e drastically reduced the compounds' cholinesterase and β-secretase inhibitory potential, though there is a considerable increase in the PAMPA–BBB permeability. The introduction of nitro or halogen atoms on benzyl imparts lipophilicity gain and thus there was no improvement in water solubility compared to embelin (Table 4).

Antioxidant Activity. Embelin is known to exhibit antioxidant activity.[11,43,55] Thus, it was evident to test all its derivatives for antioxidant activity. Antioxidants play a vital role in delaying the onset and slowing down the progression of AD.[56] The typical free radical scavenging assays like ABTS and DPPH serve as rapid and reliable techniques to determine the antioxidant/free radical scavenging capability of compounds. ABTS•+ and DPPH•+ are stable free radicals that transform into stable molecules by accepting an electron or a hydrogen radical.[57,58] The free radical scavenging activity of the

compounds was determined by ABTS and DPPH assays, and the IC_{50} values of the compounds are shown in Tables 1–4. Ascorbic acid was used as a positive control in both assays, which displayed respective IC_{50} values of 21.39 and 68.62 μM in ABTS and DPPH assays. Embelin [1] shows radical scavenging activity with IC_{50} values of 7.52 and 19.92 μM in ABTS and DPPH assays, respectively. Embelin was previously reported to scavenge ABTS and DPPH free radicals with IC_{50} values of 0.3 and 28 μM, respectively.[55] Compounds 4l (4-ethoxyphenylamino substitution) and 9e (3-methoxypropyla-mino substitution) have shown good radical scavenging activity with IC_{50} values of 4.51 and 4.81 μM in the ABTS assay (Tables 1 and 3). Most of the synthesized embelin derivatives have shown moderate antioxidant activity. Compound 9j, the most active ChE and BACE-1 inhibitor, also offered a radical scavenging potential with IC_{50} values of 19.09 and 37.41 μM in ABTS and DPPH assays, respectively (Table 4).

Mode of Inhibition of ChEs and BACE-1 by 9j. The mode of inhibition of hAChE and hBChE by compound 9j was determined by performing the kinetic study. The velocity of enzyme activity was determined by varying the substrate and inhibitor concentrations, and the obtained results were used to construct Lineweaver–Burk (LB) double reciprocal plots (Figure 3). The velocity of hAChE was determined at five different concentrations of ATChI (0.0625–1 mM) and five different concentrations of 9j (0.0625–1 μM), whereas the velocity of hBChE was determined at five different concentrations of S-butyrylthiocholine iodide (BTChI) (0.0625–1 mM) and five different concentrations of 9j (0.3125–5 μM). The reciprocal of enzyme velocity (1/V) was plotted against the reciprocal of substrate concentration (1/[S]) to generate LB plots from which the mode of inhibition of the enzymes by compound 9j was determined. The LB plot constructed for hAChE showed a gradual decrease in the V_{max} of the enzyme with an increase in inhibitor concentration, leaving the K_m value constant, which is a characteristic feature of the noncompetitive mode of inhibition. In the LB plot constructed for hBChE, with an increase in the concentration of compound 9j, the V_{max} of the enzyme gradually decreased while the K_m value gradually increased. From this pattern, it is confirmed that compound 9j
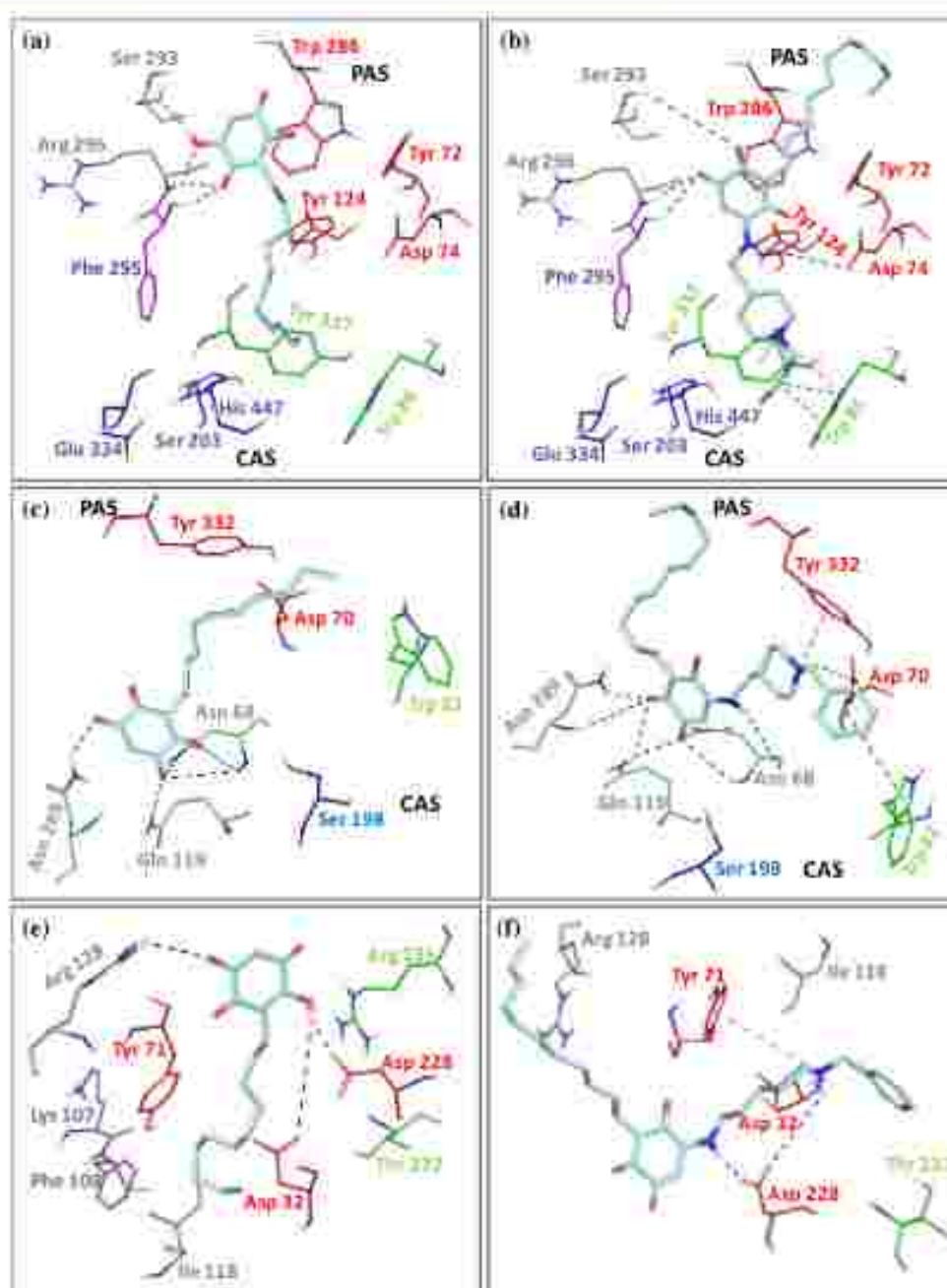
Figure 5. Molecular docking of 1 and 9j with human AChE (PDB ID: 4EY7), human BChE (PDB ID: 6EP4), and BACE-1 (PDB ID: 1W51). (a) Interaction of 1 with the active site of hAChE. (b) Interaction of 9j with the active site of hAChE. (c) Interaction of 1 with the active site of hBChE. (d) Interaction of 9j with the active site of hBChE. (e) Interaction of 1 with the active site of hBACE-1. (f) Interaction of 9j with the active site of hBACE-1. The blue, green, and pink dotted lines indicate H-bonding, π−π bonding, and cation−π interactions, respectively.

displayed a mixed-type inhibition against human BChE. The inhibition rate constant (k_i) for the enzyme−inhibitor complex was determined by plotting the slopes of the LB plot against the inhibitor concentration. The intersection point of the line on the X-axis is k_i, which can also be calculated by dividing the intercept of the line by its slope. The k_i values of 9j for hAChE and hBChE were found to be 0.21 and 1.29 μM, respectively.

Further, a BACE-1 kinetic study was performed at different substrate concentrations (0.625–10 μM) and compound 9j (0.3125–5 μM) to determine the type of inhibition. With an increase in inhibitor concentration, we have observed a decrease in V_{max} and an increase in K_m values from the LB plot constructed for BACE-1 inhibition. This pattern shows

that compound 9j is a mixed-type inhibitor of the human BACE-1 enzyme. Plotting slopes of the LB plot against the 9j concentrations showed that the k_i value of 9j for human BACE-1 was 0.75 μM (Figure 4).

To further investigate and understand the superior inhibitory potential of compound 9j in comparison to embelin (1), docking studies were performed with hAChE (Protein Data Bank (PDB): 4EY7),[59,60] hBChE (PDB: 6EP4),[61] and hBACE-1 (PDB: 1W51)[62] using the Glide module of Schrödinger molecular modeling software. Docking poses of embelin (1) and 9j with all three enzymes are presented in Figure 5. The crystal structures, 4EY7,[63−65] 6EP4,[64,67] and 1W51,[68,69] were previously employed for docking studies by
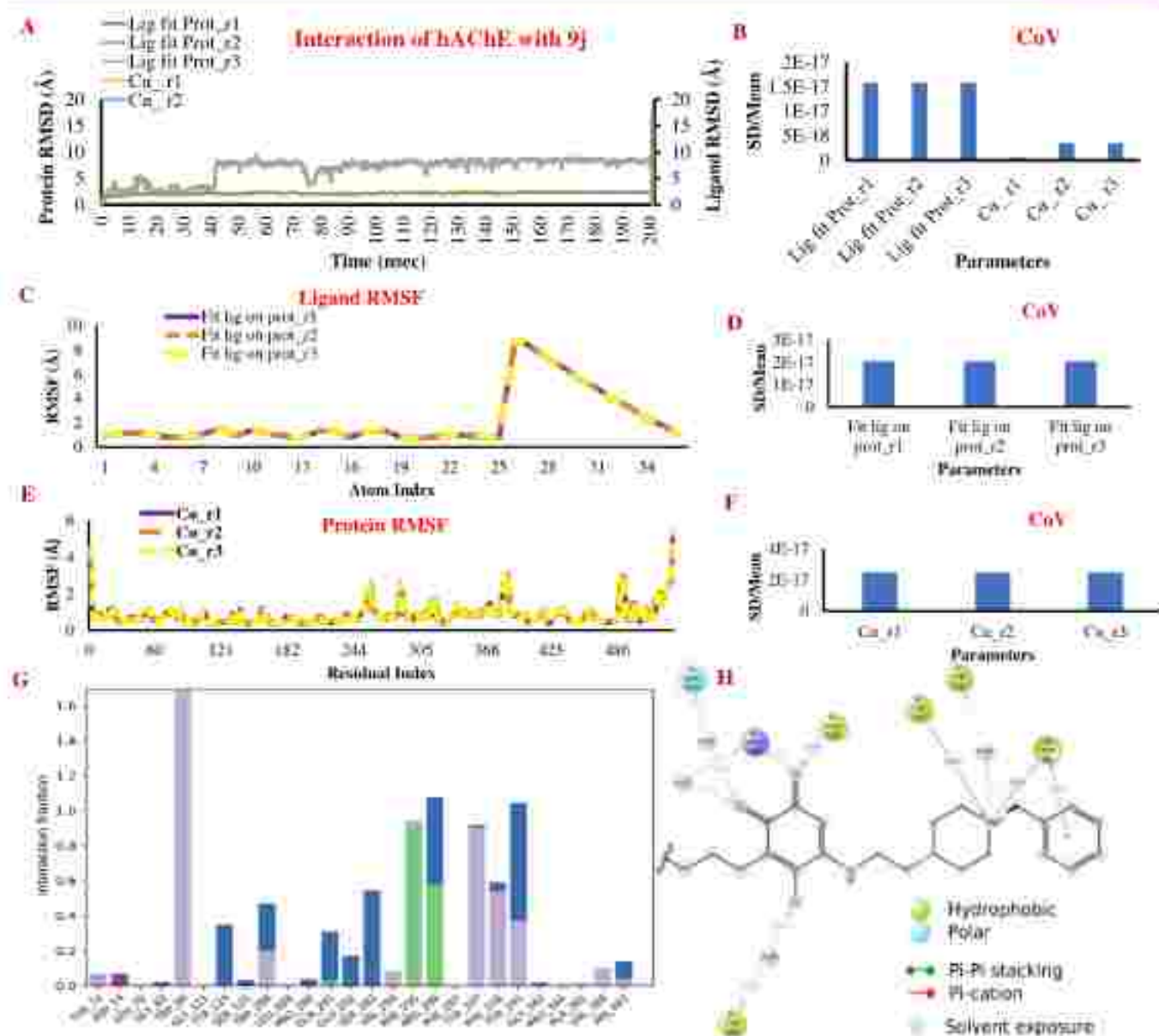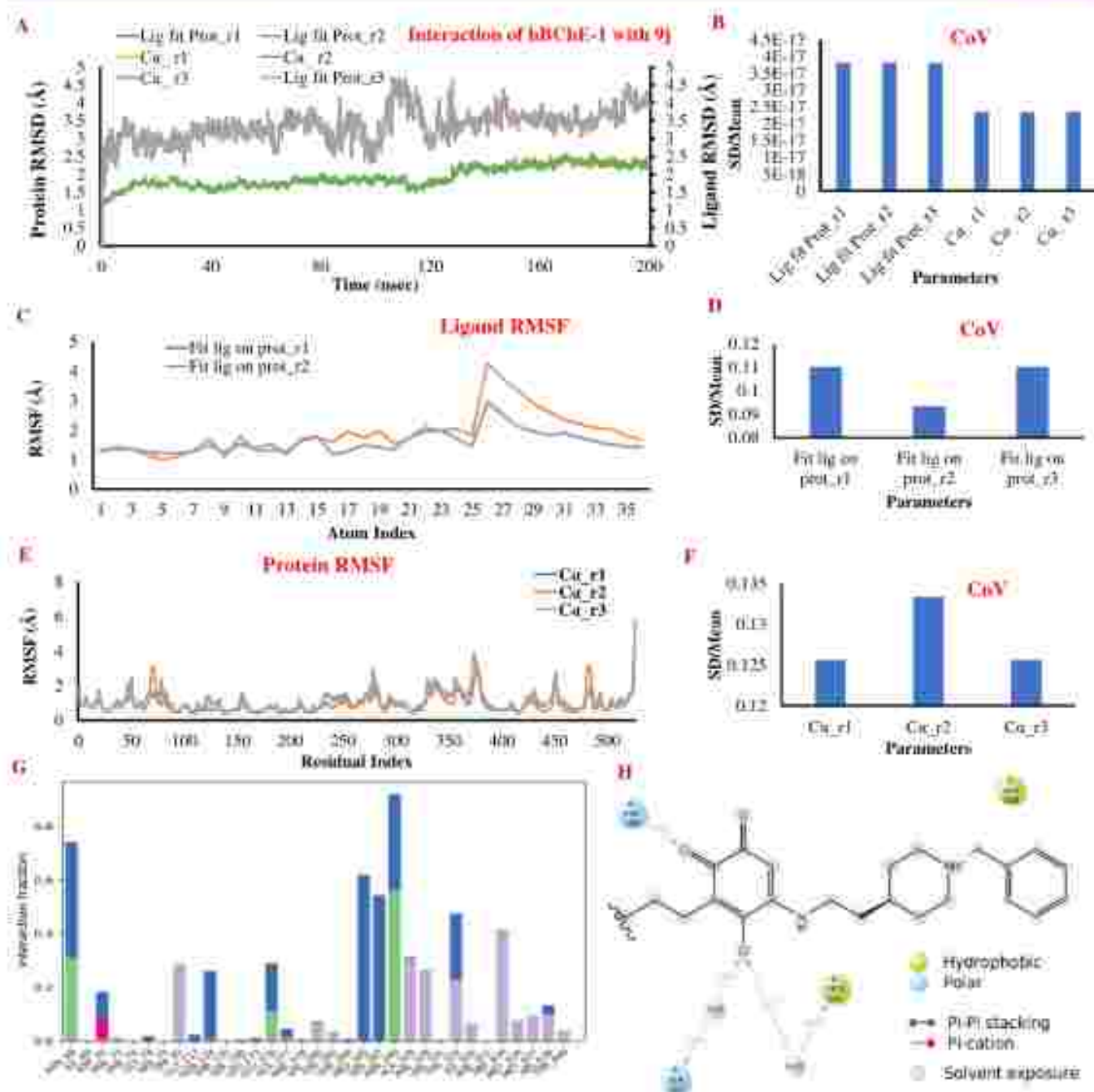
Figure 6. MD simulation study of 9j in complex with hAChE (PDB: 4EY7). (A) The plot of protein and ligand RMSD values with a function of time. Protein RMSD is at the left Y-axis, and the ligand RMSD is at the right Y-axis. (B) Coefficient of variation of protein and ligand. (C) Ligand RMSF; (D) coefficient of variation of ligand RMSF; (E) protein RMSF; (F) coefficient of variation of protein RMSF; (G) bar charts of protein interaction with ligands throughout the simulation (green—H-bonding; gray—hydrophobic; blue—water bridges; pink—ionic interactions); (H) ligand interactions with the key amino acid residues in the 2D diagram.

several groups. The substitution of embelin at C1 carbonyl with the N-benzylpiperidine ring resulted in the 1,4-benzoquinone ring turning 180° inside the active site gorge of ChEs. Embelin (1) occupies the active site of hAChE with its 1,4-benzoquinone ring positioned at the PAS and the 11-carbon aliphatic chain entering deep into the active site gorge, reaching closer to His 447 (4.13 Å) of CAS. The 4-keto and 5-OH groups of the 1,4-benzoquinone ring display H-bonding interactions with residues of the acyl binding pocket and the allosteric site [4-keto group with Phe 295 (2.07 Å) and Arg 296 (2.81 Å), 5-OH with Ser 293 (2.16 Å) and Arg 296 (2.38 Å)]. However, embelin does not interact with the key residues of CAS (Trp 86 and Tyr 337) and PAS (Trp 286). Interaction with Tyr 337 is crucial for the potent inhibition of human AChE.[70] The N-benzylpiperidine ring of 9j enters deep into the active site gorge by displaying vital interactions with Trp 86

and Tyr 337 of CAS. This has resulted in the 1,4-benzoquinone ring flipping 180° around with the 11-carbon aliphatic chain positioned toward PAS. Despite this turn-around, H-bonding interactions with residues of the acyl binding pocket and the allosteric site are retained by 1-keto and 2-OH groups, but with higher distance. The 1-keto group interacted with Arg 296 (3.45 Å) and Phe 295 (3.23 Å) through H-bonding interactions similar to those displayed by the indanone keto group of donepezil, Arg 296 (3.53 Å) and Phe 295 (1.78 Å). Additionally, the NH linked to C-5 of the benzoquinone ring display a loose H-bonding interaction with Asp 74 at the lining of the gorge. Unlike embelin, compound 9j show similar orientation and interactions as displayed by donepezil inside the active site of hAChE. Moreover, the key interactions with Trp 86 and Tyr 337 might be the plausible reason for the superior inhibitory potential of 9j over embelin
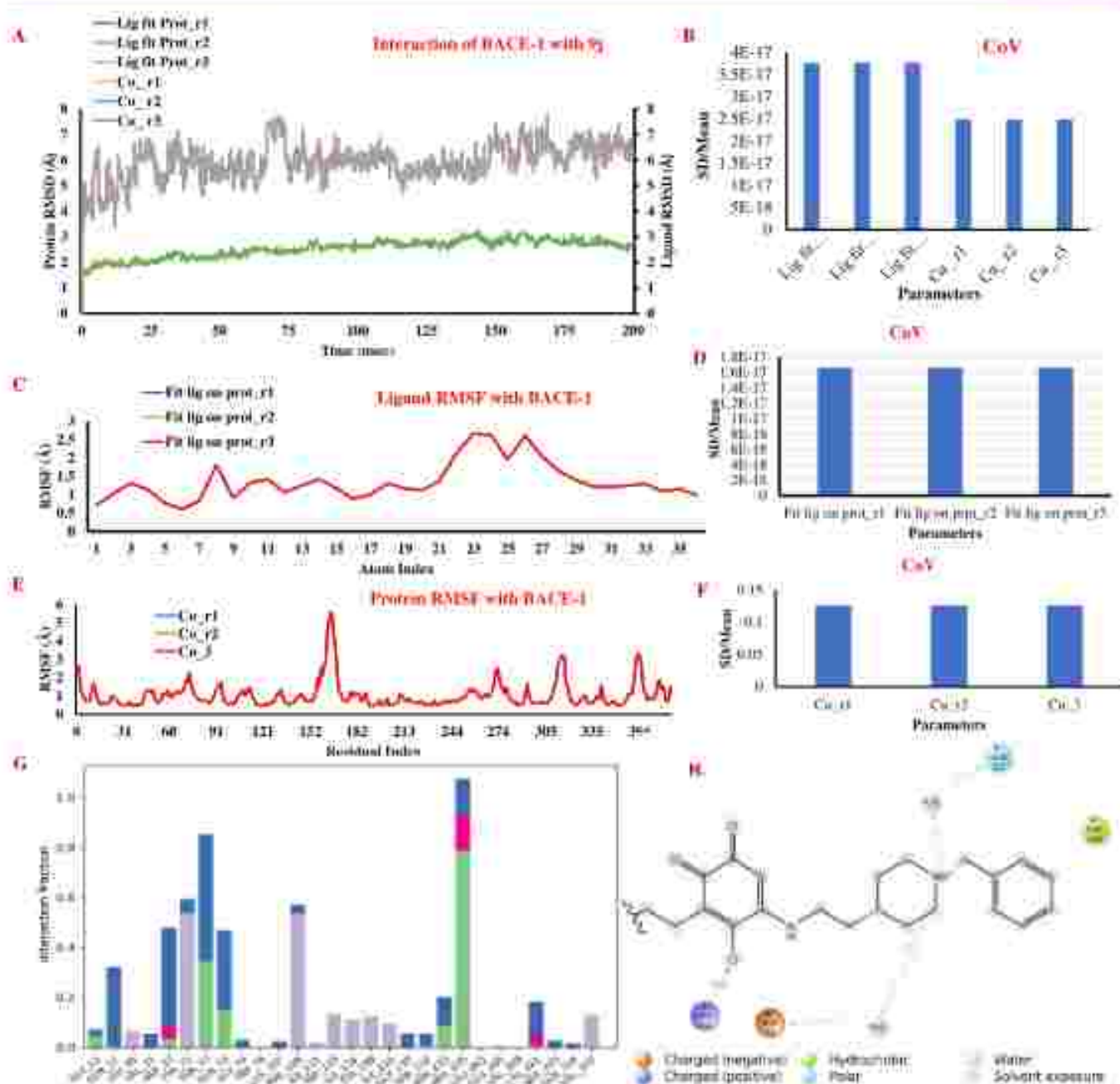
Figure 7. MD simulation study of 9j in complex with hBChE (PDB: 6EP4). (A) The plot of protein and ligand RMSD values with a function of time. Protein RMSD is at the left Y-axis, and the ligand RMSD is at the right Y-axis. (B) Coefficient of variation of protein and ligand; (C) ligand RMSF; (D) coefficient of variation of ligand RMSF; (E) protein RMSF; (F) coefficient of variation of protein RMSF; (G) bar charts of protein interaction with ligands throughout the simulation (green—H-bonding; gray—hydrophobic; blue—water bridges; pink—ionic interactions); and (H) ligand interactions with the key amino acid residues in the 2D diagram.

against hAChE. After examining the interaction patterns displayed by embelin and 9j with hBChE, it was found that the benzoquinone ring of embelin interacts via H-bonding with Asn 68, Gln 119, and Asn 289 only. Due to the undecyl aliphatic carbon chain orientation near Asp 70, embelin does not interact with important amino acids like Tyr 332, Asp 70, and Trp 82. On the contrary, 9j interacts with Asp 70 through the nitrogen of piperidine via a 3.67 Å long H-bond, and the N-benzylpiperidine substituent of 9j displays H-bonding between piperidine NH and Asp 70, resulting in the benzoquinone ring to flip 180° inside the active site of

BChE. Despite the flip, 9j retains the H-bonding interactions of the benzoquinone ring with Asn 68, Gln 119, and Asn 289. Improved inhibitory potential of 9j against BACE-1 can be attributed to the strong H-bonding interaction of 1.71 Å between C-5 NH and Asp 228 (critical catalytic site residue) as well as a cation–π interaction between piperidinyl NH and the flip modifying residue Tyr 71. Embelin also interacts with Asp 228 through a 2.03 Å H-bond, but the interaction with Tyr 71 is absent owing to the orientation of the 11-carbon aliphatic chain toward the catalytic site.

Figure 8. MD simulation study of 9j in complex with hBACE-1 (PDB: 1W51). (A) The plot of protein and ligand RMSD values with a function of time. Protein RMSD is at the left Y-axis, and the ligand RMSD is at the right Y-axis. (B) Coefficient of variation of protein and ligand. (C) ligand RMSF; (D) coefficient of variation of Ligand RMSF; (E) protein RMSF; (F) coefficient of variation of protein RMSF; (G) bar charts of protein interaction with ligands throughout the simulation (green—H-bonding; gray—hydrophobic; blue—water bridges; pink—ionic interactions); and (H) ligand interactions with the key amino acid residues in the 2D diagram.

To investigate the stability of the ligand–protein complex, we performed molecular dynamics (MD) studies on ligand 9j with three separate proteins viz. BACE-1 (PDB ID: 1W51), hAChE (PDB ID: 4EY7), and hBChE (PDB ID: 6EP4). The simulations were performed in triplicate, and the trajectory of stability between ligand–protein complexes was monitored for an extended duration of 200 ns. In the simulation of hAChE with 9j, the root-mean-square deviation (RMSD) plot depicted that all three simulations were stabilized throughout 200 ns (Figure 6A) with a high degree of agreement for coefficient of variation (CoV) (Figure 6B). The RMSD value of the protein was in the range of 2–4 Å. The "Lig fit Prot" plot (Figure 6A)

shows that after 40 ns updrift in ligand initially, it was found to be stable throughout the simulation with RMSD in the range of 2–9 Å. Considering the root-mean-square fluctuation (RMSF) of both the ligand (Figure 6C) and protein (Figure 6E), a stable complex was observed throughout the simulation with only atoms 25–30 fluctuating with RMSF of up to 8 Å. The percentage of ligand interaction diagram shows (Figure 6G,H) that the amino acids Phe 295 (85%) and Arg 296 (47%) were involved in the H-bonding with carbonyl groups of the ligand. Tyr 337 showed π–cation interaction for 84% of time, and Trp 86 showed hydrophobic interaction with the phenyl ring and also interacted with ligand nitrogen

throughout 200 ns. The time-frame analysis is presented in Section S3 of the Supporting information.

The simulation study between ligand 9j with hBChE suggested a similar pattern of results as obtained with the MD study of hAChE with 9j. The RMSD plot depicted (Figure 7A) the RMSD value of the protein in the range of 1–2.5 Å. The CoV indicated that the protein active site was stable throughout the simulation (Figure 7B). The Lig fit Prot plot shows ligand fluctuations from 100 to 120 ns and later stable up to 200 ns with RMSD in the range of 2–4 Å. Considering the RMSF parameters, the ligand RMSF plot (Figure 7C) indicated that the ligand was stable throughout the course of the simulation, with only atoms 25–29 showing fluctuation. When run in triplicate, there was a difference in run 2. The difference in run 2 compared to run 1 and run 3 can be attributed to the ligand's interactions with specific amino acids. The percentage of ligand interaction diagram (Figure 7G,H) shows that the amino acids Asn 289 (58%) and Ser 287 (50%) were involved in the H-bonding with carbonyl groups of ligands. The time-frame analysis is presented in the Supporting Information.

The simulation of BACE-1 indicated that the protein was stable throughout 200 ns with the RMSD range of 1–3 Å (Figure 8A). The coefficient of variation (CoV) for the three runs was almost the same (Figure 8B), indicating that the side chains for active site residues are stable in all three simulations. The RMSD value for BACE with 9j was in the range of 3–7 Å with slight fluctuation near 75 ns (Figure 8A). Further, as dynamics also involve protein chain perturbations, we calculated the RMSF that determines the changes occurring in the protein residues throughout the simulation to analyze the impact. The ligand-based RMSF analysis (Figure 8C) revealed the ligand's stability during the simulation. Only atoms 23–27 fluctuated with RMSF in the range of 1–2.5 Å. The CoV of the analysis (Figure 8D) reveals a high degree of correlation between runs. The percentage of ligand interaction diagram (Figure 8G,H) portrayed that Arg 235 is involved in H-bonding with the hydroxy group of 9j for the entire 200 ns duration. The time-frame analysis is presented in the Supporting Information.

Anti-amyloid Aggregation Activity of 9j. The inhibitory potential of embelin (1) and 9j against the self-aggregation of Aβ42 was determined in vitro using a Thioflavin T-based fluorometric assay. The reference compound, curcumin, display aggregation inhibition of 61.3% at 10 μM. Compounds 1 and 9j inhibited the spontaneous self-aggregation of Aβ42 with EC_{50} values of 0.24 and 0.26 μM, respectively. The dose–response curves are shown in Figure 9. The inhibitory activity of curcumin is associated with its ability to interact with the key residues of the Aβ42 peptide monomer that is involved in the aggregation process. Asp 23 is a key amino acid of the Aβ42 monomer involved in intermolecular salt-bridge formation during the aggregation process.[71] Phe 19 is another crucial hydrophobic residue that connects two β-strands of Aβ monomers for initiating oligomerization.[72] The OH of curcumin forms a very close H-bonding with the carbonyl oxygen of Asp 23 (2.03 Å) and the carbonyl oxygen of Phe 19 (3.55 Å). The embelin derivative 9j also forms a strong H-bonding with these two crucial residues. The protonated piperidinium nitrogen forms H-bonding with Asp 23 (2.29 Å) and the carbonyl oxygen of Phe 19 (2.43 Å) (Figure 10A–C). Curcumin also binds to the Aβ₁–42 fibrils.[73] The interaction of curcumin and 9j with the Aβ₁–42 fibrils[74]
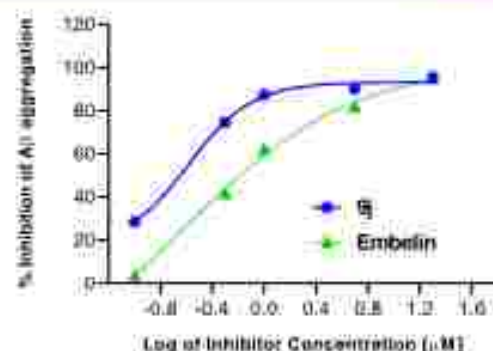

Figure 9. Inhibition of self-aggregation of Aβ42 by embelin (EC_{50} = 0.24 μM) and its derivative 9j (EC_{50} = 0.26 μM).

was also studied (Figure 10D–F). The embelin derivative binds at a similar binding site like curcumin. These interactions likely contribute to the strong inhibitory activity of curcumin and 9j for Aβ self-aggregation.

The peripheral anionic site of AChE is known to interact with Aβ peptide and promote its aggregation.[75−77] The affinity of embelin (1) and 9j for the PAS of AChE was assessed by the propidium iodide displacement method using donepezil as a reference compound. Propidium iodide, a PAS-specific ligand of AChE, enhances its fluorescence intensity up to eightfold after binding to AChE. Therefore, the affinity of compounds for PAS is measured by the decrease in fluorescence intensity as it is directly proportional to the respective compound's potential to displace propidium iodide. At 10 and 50 μM, compound 9j displaces propidium iodide by 22 and 31%, respectively. This is similar to the displacement exhibited by donepezil (23 and 31% displacement at 10 and 50 μM, respectively). On the other hand, embelin (1) exhibit a slightly lower displacement of 14 and 27% at respective test concentrations of 10 and 50 μM.

Embelin Derivative 9j Reverses Scopolamine-induced Toxicity in Human and Mouse Neuroblastoma Cells. The effect of 9j on the viability of SH-SY5Y and N2a cells was assessed by treating cells at a range of concentrations from 0.19 to 25 μM. The analogue 9j displays statistically significant toxicity at 12.5 μM in SH-SH5Y cells and at 25 μM in N2a cells (Figure 11A,D), whereas below these concentrations, the compound is nontoxic in these cells. Next, the protective effect of 9j against scopolamine-induced cytotoxicity in both cells was determined. Treatment with scopolamine (2 mM) resulted in highly significant cell death compared with the control (untreated cells). The co-treatment with compound 9j (1, 0.5, 0.25, 0.125, 0.0625, 0.031, and 0.015 μM) was investigated to attenuate the toxicity induced by scopolamine (2 mM) in SH-SY5Y and N2a cells (Figure 11B,E). Compound 9j was most effective in preventing the scopolamine cytotoxicity at the 0.5–0.125 μM concentration range. Scopolamine (2 mM) co-treated with embelin derivative 9j, 0.5 μM, resulted in better SH-SY5Y cell viability (78%) versus scopolamine-alone treated cells (55%). A similar trend was observed in mouse neuroblastoma N2a cells. The scopolamine (2 mM) co-treated with embelin derivative 9j, 1.0 or 0.5 μM, resulted in better N2a cell viability (>95%) versus scopolamine-alone treated cells (72%). Donepezil also displayed a similar profile for attenuating scopolamine-induced toxicity in SH-SY5Y and N2a cells (Figure 11C,F).

ADME Profile of 9j. The metabolic stability study of embelin (1) and 9j was performed in human liver microsomes
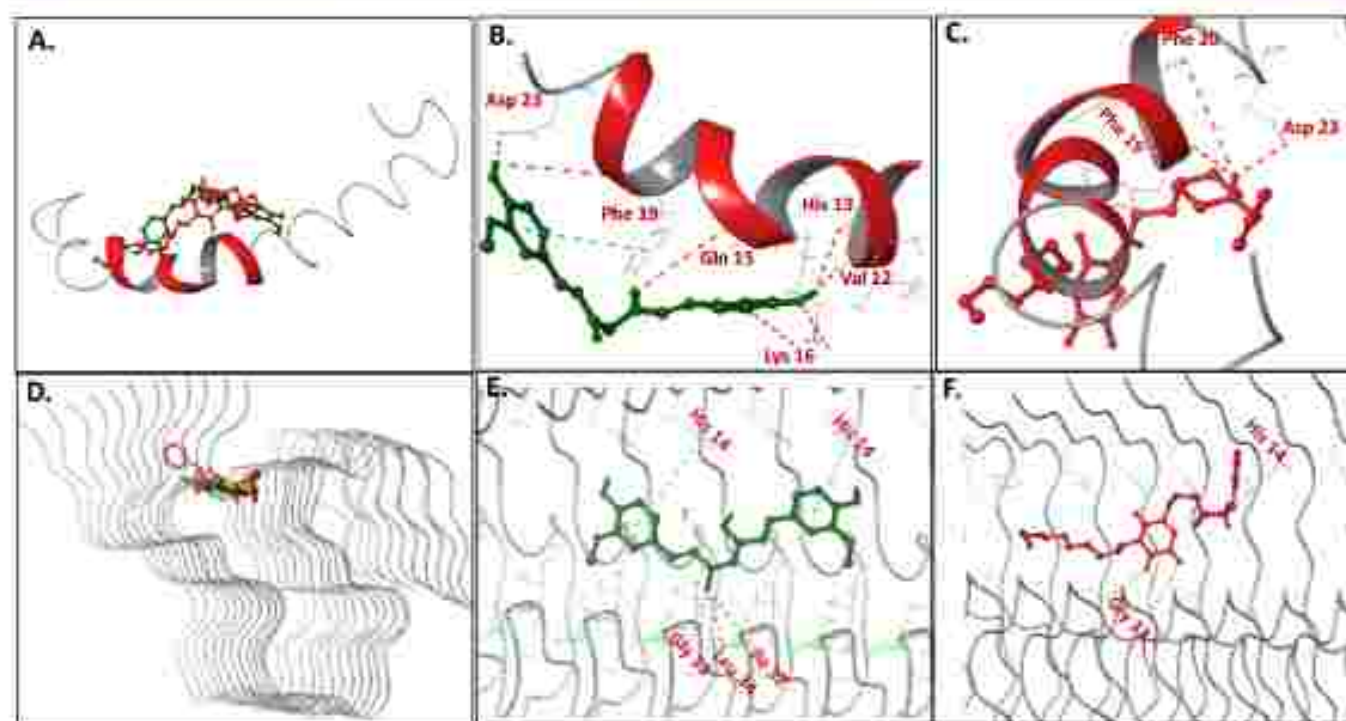
Figure 10. Molecular docking of curcumin (green) and 9j (red) with the amyloid-β 42 monomer and amyloid-β 42 fibrils. (A–C) Molecular graphic images of the lowest energy binding mode curcumin and 9j with the amyloid-β 42 monomer (PDB: 1Z0Q). (D–F) Molecular graphic images of the lowest energy binding mode curcumin and 9j with amyloid-β 42 fibrils (PDB: 2MXU).

(HLM) and mouse liver microsomes (MLM) using a substrate depletion method. Embelin gets metabolized very fast, with >75% of the drug disappearing within 15 min in HLM as well as MLM. Thus, the results dictate the metabolically unstable nature of embelin (1). However, the derivative 9j is highly stable in both microsomes, with <20% of the drug disappearing in 15 min (Figure 12a). From the in vitro extrapolation results, embelin (1) was found to be a high intrinsic clearance molecule in the HLM and MLM (>47 μL/min/mg of protein). However, 9j has low intrinsic clearance in HLM (<8.8 μL/min/mg of protein) and moderate intrinsic clearance in MLM (between 8.8 and 48 μL/min/mg of protein) (Figure 12b). The in vitro half-life of embelin (1) is low (9 min) in both microsomes. On the other hand, the in vitro half-life of 9j was significantly enhanced (>1 h) in both the microsomes, with HLM showing a high in vitro half-life compared to MLM. On extrapolating the in vitro results for predicting in vivo behavior, 9j is found to be a low (<0.3) and moderate (0.3–0.7) hepatic extraction category of molecules in humans and mice, respectively. On the other hand, embelin (1) belongs to the high (>0.7) hepatic extraction ratio molecule.[78,79] Based on in vitro data, the oral bioavailability of 9j is predicted to be 54 and 71% in mice and humans, respectively. Therefore, the new analog 9j is expected to have better metabolic stability and pharmacokinetic profile in in vivo than embelin (1).

Further, we carried out cytochrome P450 (CYP) inhibition studies of 9j in HLM using FDA-recommended CYP substrates for specific CYP isoforms. The obtained results (IC$_{50}$ values) for particular positive controls are as follows: fluvoxamine (0.31 μM), ticlopidine (0.86 μM), quercetin (9.3 μM), sulfaphenazole (1.17 μM), tranylcypromine (12.4 μM), quinidine (0.23 μM), and ketoconazole (0.02 μM) for CYP1A2, CYP2B6, CYP2C8, CYP2C9, CYP2C19, CYP2D6, and CYP3A4, respectively. Results for individual standard

inhibitors corroborate with the reported value in the literature.[80−82] Compound 9j was screened against these CYP isoforms in the concentration range of 0.1−100 μM. The calculated IC$_{50}$ values of 9j for particular CYP isoforms are as follows: CYP1A2 (>50 μM), CYP2B6 (10.9 μM), CYP2C8 (2.2 μM), CYP2C9 (>50 μM), CYP2C19 (17.8 μM), CYP2D6 (20.3 μM), and CYP3A4 (12.1 μM). Compound 9j showed significant inhibition of CYP2C8 and belonged to the moderate inhibitor category (1 μM < IC$_{50}$ ≤ 10 μM). On the contrary, 9j displayed negligible inhibitory action on other CYP isoforms (CYP1A2, CYP2B6, CYP2C9, CYP2C19, CYP2D6, and CYP3A4) and can be categorized into weak inhibitor or noninhibitor (IC$_{50}$ ≥ 10 μM). Overall results suggest that 9j is devoid of any CYP liability, except for CYP2C8, where concomitant administration of 9j with substrate drugs of CYP2C8 should be avoided. In this context, already marketed anti-Alzheimer drugs like donepezil, galantamine, rivastigmine, and memantine are the substrates of mainly CYP2D6 and CYP3A4. Therefore, 9j is less likely to cause any drug interaction upon co-administration.

The ADME properties of embelin and 9j were also computed using the in silico QikProp module of Schrödinger (Table S3; Supporting Information). All of the calculated properties of embelin and 9j fall in the recommended range. The total solvent accessible surface area is significantly higher in 9j than embelin, primarily contributed by the higher hydrophilic component. The analogue 9j has higher H-bond acceptors than embelin.

The in vivo pharmacokinetic study was conducted for 9j in Swiss Albino mice (SAM). The mean concentration versus time profile and calculated pharmacokinetic parameters of 9j in plasma are depicted in Figure 13a. Administration of 9j at 30 mg/kg to the SAM by oral route resulted in the C$_{max}$ of >14 μM with rapid absorption (T$_{max}$ ~ 1.2 h). The overall plasma
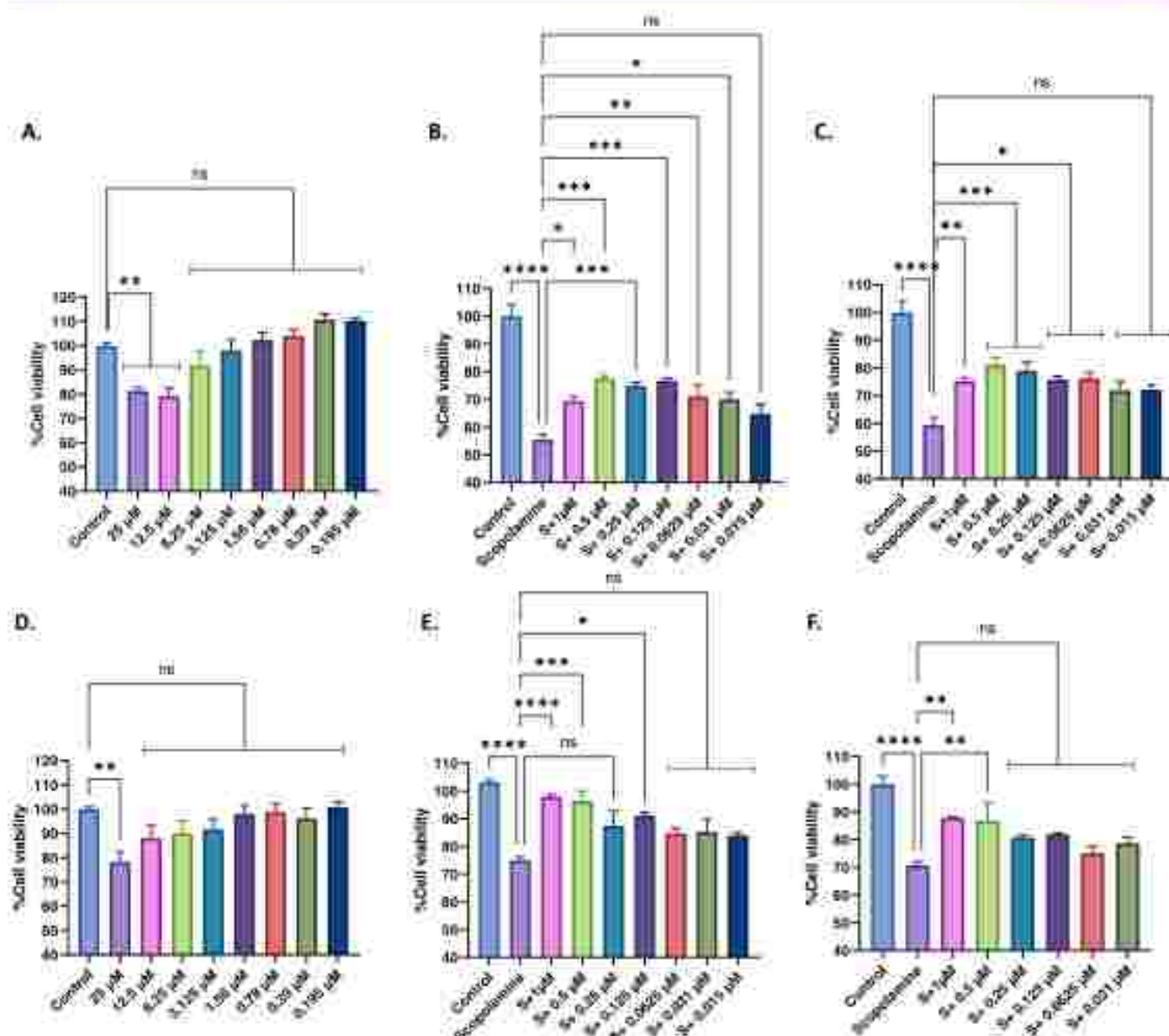
Figure 11. Effect of 9j on cell viability of SH-SY5Y and N2a cells. (A) Cell viability of SH-SY5Y cells after 9j treatment. (B) Prevention of scopolamine (S)-induced cytotoxicity in SH-SY5Y cells by 9j co-treatment at various concentrations. (C) Prevention of scopolamine-induced cytotoxicity in SH-SY5Y cells by donepezil co-treatment at various concentrations. (D) Cell viability of N2a cells after 9j treatment. (E) Prevention of scopolamine-induced cytotoxicity in N2a cells by 9j co-treatment at various concentrations. (F) Prevention of scopolamine-induced cytotoxicity in N2a cells by donepezil co-treatment at various concentrations. Data are expressed as the mean ± standard error of the mean (SEM) ($n = 3$), the "*" and "ns" represent the p-value by one-way analysis of variance (ANOVA) followed by Tukey's multiple comparisons test, ****$p < 0.0001$, ***p between 0.0001 and 0.001, **p between 0.001 and 0.01, *p between 0.01 and 0.05; and ns, $p > 0.05$.

exposure (area under curve (AUC)$_{0-t}$ or AUC$_{0-\infty}$) reached over 97 μM h (48 μg h/mL) with an excellent $T_{1/2}$ of 2.9 h. This result corroborates with the in vitro observations. The level of 9j in brain tissues was also measured. The mean concentration versus time profile and pharmacokinetic parameters of 9j in the brain are represented in Figure 13b. Results illustrate that 9j reaches the brain with a C_{max} of 403 ng/g, AUC$_{0-t}$ of 1677 ng h/g, and AUC$_{0-\infty}$ of 1763 ng h/g. Although it reached the brain relatively slower ($T_{max} \sim 3$ h), it showed a higher $T_{1/2}$ (5.9 h) in the brain compared to plasma. The brain–blood concentration ratio (Kp) determined using C_{max} and AUC$_{0-t}$ were 0.053 and 0.034, respectively. Considering an average mice brain density of 1.04 g/mL[67,68] and a 9j molecular weight of 494, the achieved maximum brain

concentration (C_{max}) and total brain levels (AUC$_{0-t}$) of 9j are 0.85 and 3.5 μM, respectively. The in vitro IC$_{50}$ of 9j against AD targets, AChE, BChE, and BACE-1 ranges between 0.15 and 1.6 μM. This indicated that the dose of 30 mg/kg is able to achieve the desired levels in the brain required for inhibiting ChEs and BACE-1. These results advocate that 9j crosses the BBB and attains the desired concentration at 30 mg/kg dose.

In Vivo Anti-dementia Effect of 9j in Mice. The ability of 9j to improve learning and spatial memory in scopolamine-induced memory-impaired C57BL/6J mice was investigated. Based on pharmacokinetic results, the doses of 15 and 30 mg/kg were chosen for the anti-dementia study. All animals were subjected to the Morris Water Maze (MWM) test followed by scopolamine administration (except for control group animals)

(a).

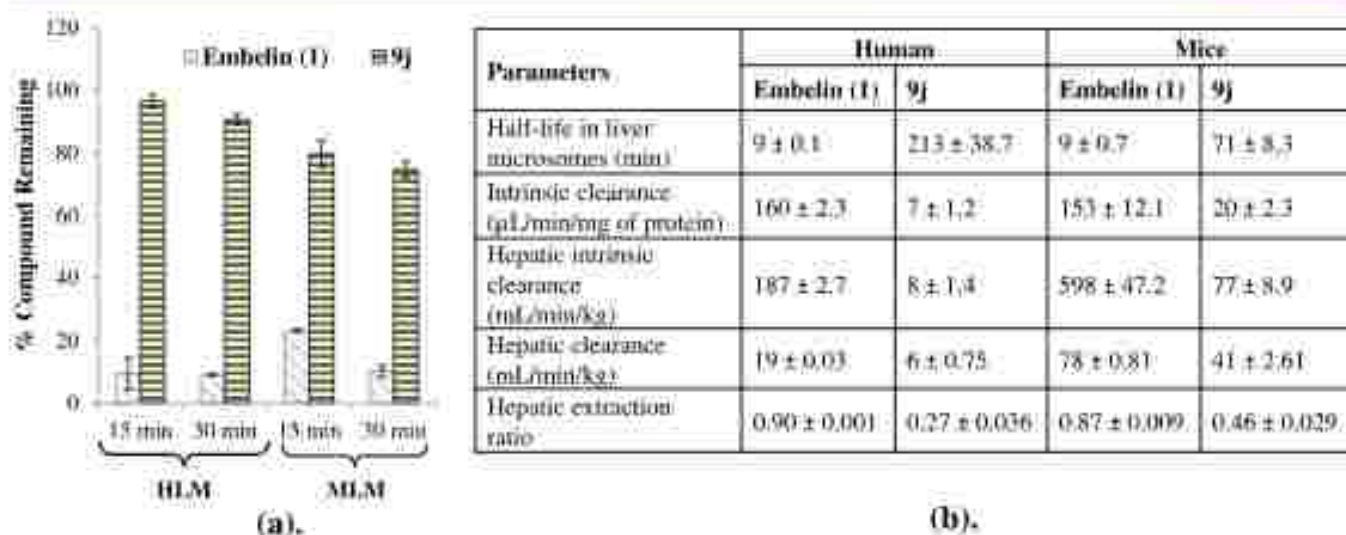| Parameters	Human		Mice	
	Embelin (1)	9j	Embelin (1)	9j
Half-life in liver microsomes (min)	9 ± 0.1	213 ± 38.7	9 ± 0.7	71 ± 8.3
Intrinsic clearance (µL/min/mg of protein)	160 ± 2.3	7 ± 1.2	153 ± 12.1	20 ± 2.3
Hepatic intrinsic clearance (mL/min/kg)	187 ± 2.7	8 ± 1.4	598 ± 47.2	77 ± 8.9
Hepatic clearance (mL/min/kg)	19 ± 0.03	6 ± 0.75	78 ± 0.81	41 ± 2.61
Hepatic extraction ratio	0.90 ± 0.001	0.27 ± 0.036	0.87 ± 0.009	0.46 ± 0.029

(b).

Figure 12. Comparative metabolic stability and predicted in vivo behavior of embelin (1) and 9j. (a) Metabolic stability of embelin (1) and 9j in HLM and MLM in the presence of 1.2 mM dihydronicotinamide adenine dinucleotide phosphate (NADPH). (b) Prediction of in vivo behavior of embelin (1) and 9j from in vitro data. Data are represented as mean ± SD (n = 2).

(a)

Parameters	Plasma
C_{max} (ng/mL)	7298 ± 1019
T_{max} (h)	1.2 ± 0.1
$T_{1/2}$ (h)	2.9 ± 0.2
AUC_{0-t} (ng.h/mL)	47837 ± 3565
$AUC_{0-\infty}$ (ng.h/mL)	48067 ± 3895
MRT	5.5 ± 0.2
V_d/F (L/kg)	2.6 ± 0.2
Cl/F (L/h/kg)	0.64 ± 0.05

(b)

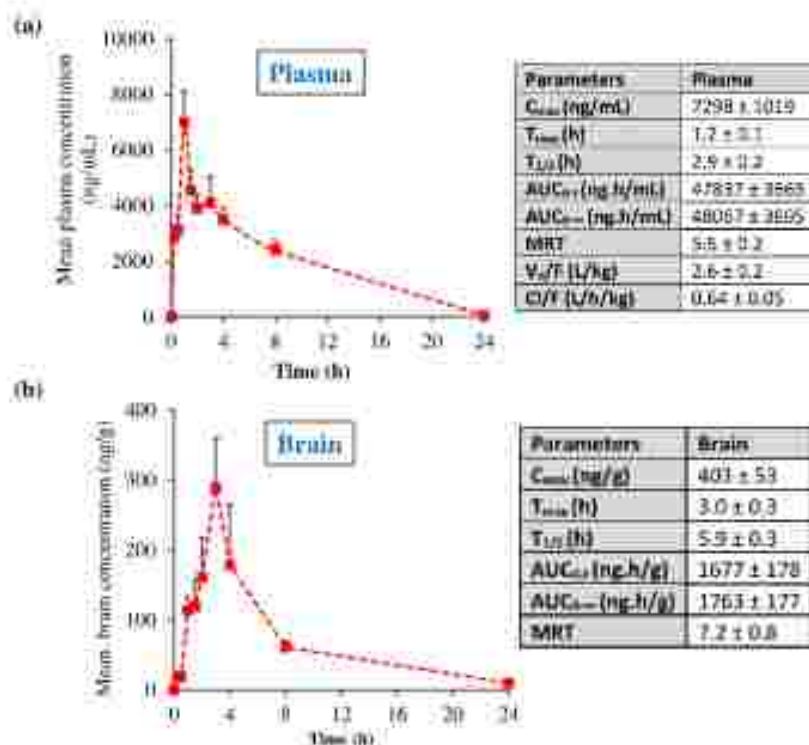| Parameters	Brain
C_{max} (ng/g)	403 ± 53
T_{max} (h)	3.0 ± 0.3
$T_{1/2}$ (h)	5.9 ± 0.3
AUC_{0-t} (ng.h/g)	1677 ± 178
$AUC_{0-\infty}$ (ng.h/g)	1763 ± 177
MRT	7.2 ± 0.8

Figure 13. Mean plasma concentration versus time profile of 9j in plasma (a) and brain (b) after oral administration in SAM at 30 mg/kg dose. Data are represented as mean ± SEM (n = 5). C_{max}, maximum plasma concentration; T_{max}, time to reach C_{max}; AUC_{0-t} and $AUC_{0-\infty}$, AUC for plasma concentration from zero to the last measurable plasma sample time and infinity, respectively; $T_{1/2}$, elimination half-life; MRT, mean residence time; V_d/F, the volume of distribution after oral administration; and CL/F, clearance after oral administration.

for six consecutive days to impair the cognitive abilities of the mice. Latency to find the hidden platform is a measure of the learning abilities of the animals. Scopolamine treatment significantly increased the latency time compared with the control. Treatment with compound 9j at doses 15 and 30 mg/kg QD for three consecutive days gradually recovered the spatial memory of mice, as indicated by the substantial reduction in the time taken by the animals to locate the hidden platform. The donepezil (1 mg/kg)-treated group was taken as a reference standard. The anti-dementia effect of compound 9j

at both doses is similar to that of the donepezil group, which clearly shows the potential of 9j in restoring mice's memory and learning abilities (Figure 14). Further, brain AChE levels were estimated using supernatants from brain homogenates post-animal sacrifice and brain isolation. Elevated levels of AChE were observed in the scopolamine-treated group compared with the control group.[85] Treatment with 9j (15 mg/kg) caused a significant reduction in AChE activity. In groups treated with donepezil (1 mg/kg) and 9j (30 mg/kg), a
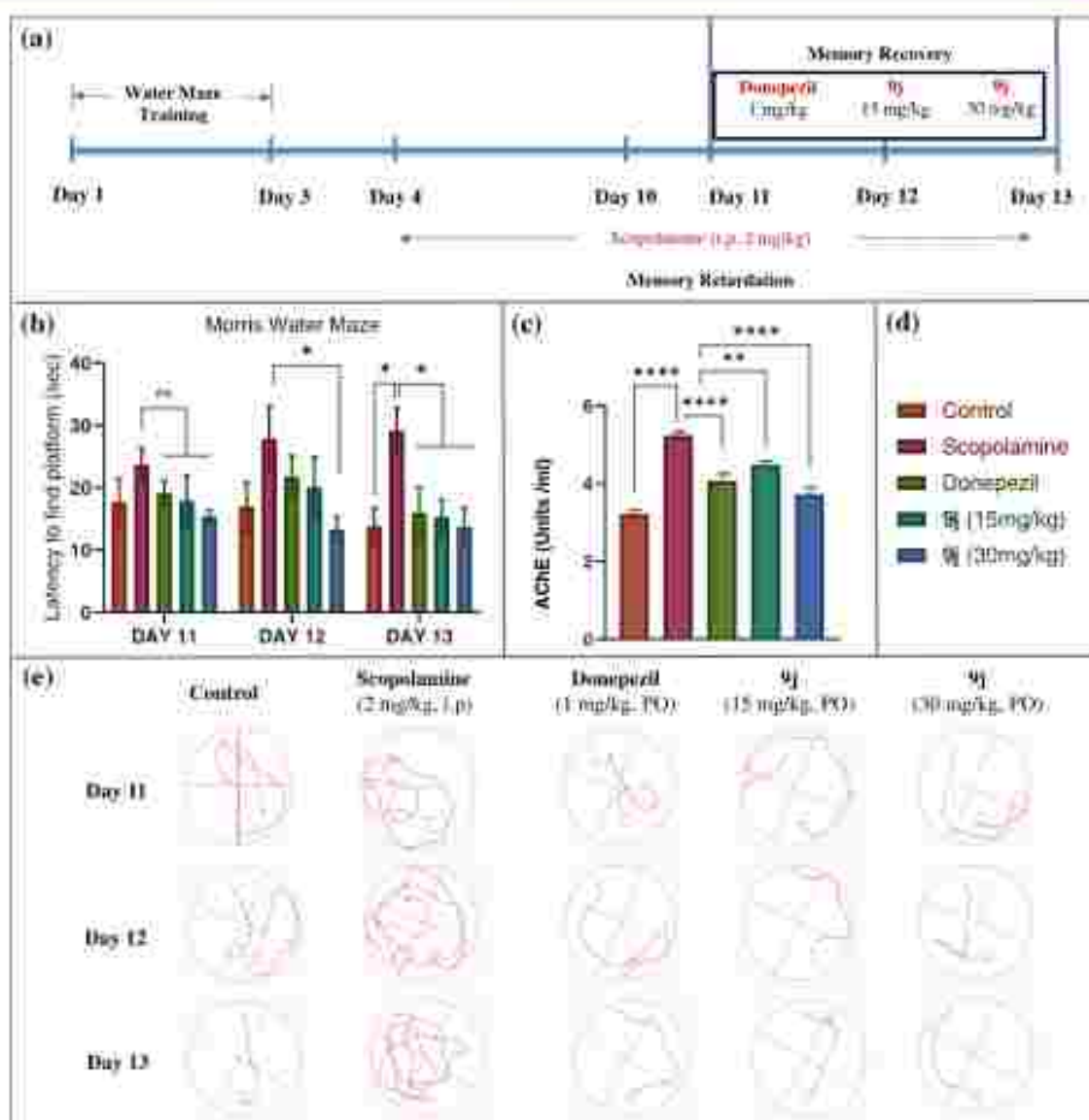
Figure 14. Recovery of spatial memory by 9j in scopolamine-induced memory-impaired C57BL/6J mice. (a) MWM experimental design. (b) Effect of 9j on scopolamine-induced amnesia by the MWM test. (c) Effect of 9j on brain AChE levels. (d) Color coding for different bars in (b) and (c). (e) Track plots representing animals swimming in the MWM test. Data are expressed as the mean ± SEM ($n = 7$), the * and ns represent the p-value by one-way ANOVA followed by Tukey's multiple comparisons test, ****$p < 0.0001$, ***p between 0.0001 and 0.001, **p between 0.001 and 0.01, *p between 0.01 and 0.05; and ns, $p > 0.05$. This study was performed in 30 C57BL/6J mice that were distributed into five groups (six mice per group).

highly significant decrease in AChE activity was observed (Figure 14c).

■ CONCLUSIONS

Our efforts have resulted in identifying a BBB-permeable MTDL, 9j, with multifold increased potency compared with embelin. Compound 9j inhibits hAChE, hBChE, and hBACE-1 with IC$_{50}$ values of 0.15, 1.6, and 0.6 μM, respectively. Enzyme kinetics revealed that 9j is a noncompetitive inhibitor of hAChE with a k_i value of 0.21 μM; and a mixed-type inhibitor of hBChE and hBACE-1 with respective k_i values of 1.3 and 0.75 μM. Analogue 9j also inhibits the Aβ42 self-aggregation and exhibits antioxidant activity. Overall, there is a significant improvement (fold-change summarized in Table 5) in anticholinesterase, anti-BACE-1, water solubility, and BBB

permeability of embelin via incorporation of amino acid alkyl appendage in 9j.

The in silico studies of lead compound affirmed its consensual binding interactions with CAS and PAS of ChEs, aspartate dyad of BACE-1, and Asp 23 of Aβ monomer. Analogue 9j effectively attenuated the scopolamine-induced cytotoxicity in SH-SY5Y and N2a cells at nontoxic concentrations. Compound 9j displayed good metabolic stability in HLM and MLM, no CYP liability, and possessed high passive BBB permeability potential (8.39×10^{-6} cm/s). Compound 9j showed an excellent oral PK profile in Swiss albino mice with good distribution (C_{max} of 7298 ng/mL and 403 ng/g) and high MRT of 5.5 and 7.2 h in plasma and brain, respectively. Further, the Morris Water Maze test determined the anti-dementia potential of 9j in C57BL/6J mice. Compound 9j effectively restored the scopolamine-induced

Table 5. Fold Improvement in the *In Vitro* Activity, Water Solubility, and BBB Permeability of Embelin (1)

target/parameter	embelin (1)	9j.1443 (9j)	fold improvement
hAChE (IC$_{50}$ μM)	7.9	0.15	52.67
hBChE (IC$_{50}$ μM)	>100	1.61	62.11
hBACE-1 (IC$_{50}$ μM)	2.11	0.6	3.52
Aβ$_{1-42}$ aggregation (IC$_{50}$ μM)	0.24	0.26	0.92
DPPH (IC$_{50}$ μM)	7.52	19	0.40
ABTS (IC$_{50}$ μM)	19.92	37	0.54
S_{max} (μM)	8	26	3.25
BBB, P$_e$ × 10^{-6} cm/s	4.54	8.4	1.85

memory impairment at both the test doses (15 and 30 mg/kg), displaying a similar activity profile to the donepezil-treated group. Finally, the brain AChE levels were significantly reduced by 9j treatment at levels comparable with the donepezil treatment. The data presented herein warrants a detailed investigation of 9j for AD.

■ EXPERIMENTAL SECTION

General. All chemicals, reagents, and solvents were purchased from TCI, Sigma-Aldrich, or Merck and used as received. Enzymes and reagents used in biological assays were the same as described earlier.[ ] The instruments used to record ^{1}H, ^{13}C, IR, mass, high-performance liquid chromatography (HPLC), and melting point data were the same as described earlier.[ ] The chemical shift values in ^{1}H and ^{13}C spectra were reported downfield to tetramethylsilane (TMS) in parts per million. NADPH was purchased from Cayman. Dulbecco's modified Eagle's medium (DMEM, #11600034), phosphate buffer saline (#21600005), 3-(4,5-dimethylthiazol-2-yl)-2,5-diphenyl tetrazolium bromide (MTT) (# M5655), and fetal bovine serum (# A4736401) were purchased from Gibco.

Chlorzoxazone, diazepam, flumazenil maleate, ticlopidine hydrochloride, quercetin dihydrate, sulfaphenazole, quinidine, phosphate-buffered solution (PBS), and dihydronicotinamide adenine dinucleotide phosphate (NADPH) were procured from Sigma-Aldrich. Tranylcypromine sulfate was obtained from United States Pharmacopoeia. HLM (lot no # PL050E-D) and MLM (lot no# MS035-A) were obtained from Gibco. Magnesium chloride was purchased from Rankem. HLM (pool of 50 donors; lot no# PL050F-A) was procured from Gibco. Ketoconazole and dextromethorphan hydrobromide were purchased from HiMedia Laboratories and Indian Pharmacopoeia Commission, respectively. MS grade acetonitrile, formic acid, methanol, ammonium formate, and water (LC-MS grade) were received from Thermo Fisher Scientific. All other reagents/solvents/chemicals were of analytical grade or above. All compounds are >95% pure by HPLC analysis. HPLC or high-resolution mass spectrometry (HRMS) data is recorded for all compounds; data is provided below, and scans are included in the Supporting Information. Compound 9j was studied in *ex vivo*, for which HPLC and HRMS data are recorded, and traces are included in the Supporting Information.

Isolation of Embelin from *E. ribes*. Ten grams of embelin (1) was isolated from the dried fruits (1 kg) of *E. ribes* following the procedure described in our previous publication.[ ]

2,5-Dihydroxy-3-undecylcyclohexa-2,5-diene-1,4-dione (1). Orange solid; m.p. 142–144 °C; IR (ν$_{max}$): 3308, 2921, 2848, 1614, 1360, 1327, 1308, 1281, 1194 cm^{-1}. ^{1}H NMR (400 MHz, CDCl$_3$) δ 7.67 (s, 2H, 2 × OH), 6.01 (s, 1H, 6-CH), 2.45 (t, *J* = 8.0 Hz, 2H, 1'-CH$_2$), 1.46 (m, 2H, 10' CH$_2$), 1.36–1.22 (m, 16H), 0.87 (t, *J* = 8.0 Hz, 3H, 11'-CH$_3$). ^{13}C NMR (101 MHz, CDCl$_3$) δ 116.98, 102.17, 31.92, 29.65, 29.62, 29.55, 29.38, 29.34, 27.95, 22.70, 22.53, 14.14. HRMS (TOF, ES–) calcd for C$_{17}$H$_{24}$O$_4$ H', 293.1758; found, 293.1740.

General Procedure for the Synthesis of Embelin Derivatives 4a–t, 5, 7a–i, and 9a–j. To a solution of 0.1 mmol embelin (1) in

acetic acid, 0.1 mmol primary amine [anilines (2a–t) or quinidine amine (3) or benzylic/alkyl–aryl amines (6a–i) or aliphatic and heterocyclic amines (8a–j)] was added and refluxed for 2 h. After 2 h of reflux, the reaction mixture was poured into excess water and extracted thrice using ethyl acetate. The ethyl acetate layers were pooled, concentrated, and loaded onto 100–200 mesh silica and purified using hexane/ethyl acetate (4:1) as a mobile phase to get the targeted compounds 4a–t, 5, 7a–i, 9a–j in 65–90% yield.

2-Hydroxy-5-(phenylamino)-3-undecylcyclohexa-2,5-diene-1,4-dione (4a).[ ] Yield: 78%; wine-red solid; m.p. 186–188 °C; IR (ν$_{max}$): 3309, 3237, 2916, 2849, 1643, 1589, 1505, 1441, 1380, 1217, 1174 cm^{-1}. ^{1}H NMR (400 MHz, CDCl$_3$) δ 7.96 (brs, 2H, OH, NH), 7.42 (t, *J* = 7.7 Hz, 2H), 7.25–7.23 (m, 3H), 6.00 (s, 1H), 2.45 (t, *J* = 7.6 Hz, 2H), 1.49 (m, 2H), 1.37–1.27 (m, 16H), 0.88 (t, *J* = 6.6 Hz, 3H). ^{13}C NMR (101 MHz, CDCl$_3$) δ 182.94, 180.39, 154.34, 146.04, 136.93, 129.75, 126.32, 122.82, 116.33, 94.50, 31.95, 29.71, 29.66, 29.63, 29.50, 29.38, 28.12, 22.82, 22.72, 14.16. HRMS (TOF, AP+) calcd for C$_{23}$H$_{31}$NO$_3$ + H', 370.2377; found, 370.2398.

5-((4-Chlorophenyl)amino)-2-hydroxy-3-undecylcyclohexa-2,5-diene-1,4-dione (4b).[ ] Yield: 81%; wine-red solid; m.p. 182–184 °C; IR (ν$_{max}$): 3318, 3248, 2921, 2852, 1645, 1598, 1569, 1503, 1487, 1577, 1217 cm^{-1}. ^{1}H NMR (400 MHz, CDCl$_3$) δ 7.91 (brs, 2H, OH, NH), 7.39 (d, *J* = 8.3 Hz, 2H), 7.18 (d, *J* = 8.3 Hz, 2H), 5.94 (s, 1H), 2.45 (t, *J* = 7.6 Hz, 2H), 1.48 (q, *J* = 7.6 Hz, 2H), 1.31–1.26 (m, 16H), 0.88 (t, *J* = 6.7 Hz, 3H). ^{13}C NMR (101 MHz, CDCl$_3$) δ 182.75, 180.47, 154.19, 145.71, 135.53, 131.66, 129.92, 124.01, 116.53, 94.88, 31.95, 29.71, 29.67, 29.62, 29.49, 29.38, 28.11, 22.81, 22.73, 14.17. HRMS (TOF, AP+) calcd for C$_{23}$H$_{30}$ClNO$_3$ + H', 404.1987; found, 404.2004.

5-((2-Bromophenyl)amino)-2-hydroxy-3-undecylcyclohexa-2,5-diene-1,4-dione (4c). Yield: 85%; wine-red solid; m.p. 119–120 °C; IR (ν$_{max}$): 3254, 2921, 2852, 1637, 1589, 1570, 1502, 1465, 1440, 1376, 1211, 1032 cm^{-1}. ^{1}H NMR (400 MHz, CDCl$_3$) δ 8.14 (s, 1H), 7.84 (s, 1H), 7.67 (d, *J* = 8.0 Hz, 1H), 7.42–7.35 (m, 2H), 7.11 (t, *J* = 7.7 Hz, 1H), 5.96 (s, 1H), 2.47 (t, *J* = 7.7 Hz, 2H), 1.51 (t, *J* = 7.5 Hz, 2H), 1.33–1.27 (m, 16H), 0.88 (t, *J* = 6.7 Hz, 3H). ^{13}C NMR (101 MHz, CDCl$_3$) δ 182.68, 180.84, 153.99, 145.26, 135.49, 133.77, 128.44, 127.21, 123.52, 118.20, 116.84, 95.51, 31.96, 29.70, 29.66, 29.63, 29.48, 29.38, 28.11, 22.90, 22.72, 14.13. HRMS (TOF, AP+) calcd for C$_{23}$H$_{30}$BrNO$_3$ + H', 448.1482; found, 448.1488.

5-((3-Bromophenyl)amino)-2-hydroxy-3-undecylcyclohexa-2,5-diene-1,4-dione (4d). Yield: 86%; wine-red solid; m.p. 156–158 °C; IR (ν$_{max}$): 3263, 2921, 2850, 1637, 1598, 1572, 1511, 1380, 1220 cm^{-1}. ^{1}H NMR (400 MHz, CDCl$_3$) δ 7.91 (s, 1H), 7.87 (s, 1H), 7.44 (s, 1H), 7.37 (d, *J* = 7.9 Hz, 1H), 7.29 (d, *J* = 8.0 Hz, 1H), 7.17 (d, *J* = 8.0 Hz, 1H), 6.01 (s, 1H), 2.45 (t, *J* = 7.6 Hz, 2H), 1.48 (q, *J* = 7.2 Hz, 2H), 1.31–1.26 (m, 16H), 0.88 (t, *J* = 6.7 Hz, 3H). ^{13}C NMR (101 MHz, CDCl$_3$) δ 182.75, 180.70, 154.11, 145.51, 138.51, 130.99, 129.21, 125.66, 123.35, 121.27, 116.73, 95.47, 31.95, 29.70, 29.66, 29.61, 29.47, 29.36, 28.08, 22.83, 22.71, 14.11. HRMS (TOF, AP+) calcd for C$_{23}$H$_{30}$BrNO$_3$ + H', 448.1482; found, 448.1475.

5-((4-Bromophenyl)amino)-2-hydroxy-3-undecylcyclohexa-2,5-diene-1,4-dione (4e). Yield: 88%; wine-red solid; m.p. 169–171 °C; IR (ν$_{max}$): 3313, 3249, 2921, 2852, 1641, 1594, 1570, 1505, 1487, 1376, 1217 cm^{-1}. ^{1}H NMR (400 MHz, CDCl$_3$) δ 7.89 (s, 2H), 7.54 (d, *J* = 8.2 Hz, 2H), 7.12 (d, *J* = 8.4 Hz, 2H), 5.96 (s, 1H), 2.45 (t, *J* = 7.6 Hz, 2H), 1.48 (q, *J* = 7.5 Hz, 2H), 1.31–1.27 (m, 16H), 0.88 (t, *J* = 6.7 Hz, 3H). ^{13}C NMR (101 MHz, CDCl$_3$) δ 182.73, 180.49, 154.17, 145.63, 136.15, 132.86, 124.22, 119.32, 116.60, 95.07, 31.90, 29.65, 29.61, 29.57, 29.43, 29.32, 28.04, 22.78, 22.66, 14.06. HPLC: 99.9% purity (t$_R$ 13.06 min).

5-((2-Fluorophenyl)amino)-2-hydroxy-3-undecylcyclohexa-2,5-diene-1,4-dione (4f).[ ] Yield: 75%; wine-red solid; m.p. 124–126 °C; IR (ν$_{max}$): 3254, 2923, 2848, 1438, 1574, 1517, 1479, 1456, 1376, 1307, 1212, 1114 cm^{-1}. ^{1}H NMR (400 MHz, CDCl$_3$) δ 7.92 (s, 2H), 7.37 (t, *J* = 6.7 Hz, 1H), 7.20 (q, *J* = 4.8, 3.2 Hz, 3H), 5.90 (s, 1H), 2.45 (t, *J* = 7.6 Hz, 2H), 1.51–1.46 (m, 2H), 1.37–1.27 (m, 16H), 0.88 (t, *J* = 6.7 Hz, 3H). ^{13}C NMR (101 MHz, CDCl$_3$) δ 182.67, 180.72, 154.23, 153.98, 145.67, 127.30 (d, *J* = 7.6 Hz), 125.33, 124.84 (d, *J* = 4.0 Hz), 123.80, 116.74 (d, *J* = 5.0 Hz), 116.52, 95.69, 31.96,

29.71, 29.66, 29.63, 29.49, 29.38, 28.12, 22.83, 22.72, 14.13. HRMS (TOF, AP+) calcd for $C_{23}H_{30}FNO_3$ + H⁺, 388.2282; found, 388.2305.

5-((3-Fluorophenyl)amino)-2-hydroxy-3-undecylcyclohexa-2,5-diene-1,4-dione (4g). Yield: 84%; wine-red solid; m.p. 169−171 °C; IR (ν_{max}): 3254, 2923, 2848, 1638, 1574, 1517, 1479, 1456, 1378, 1307, 1212, 1114 cm⁻¹. ¹H NMR (400 MHz, CDCl₃) δ 7.93 (s, 1H), 7.86 (s, 1H), 7.38 (q, J = 7.6 Hz, 1H), 7.03−6.92 (m, 3H), 6.04 (s, 1H), 2.45 (t, J = 7.6 Hz, 2H), 1.48 (q, J = 7.3 Hz, 2H), 1.37−1.27 (m, 16H), 0.88 (t, J = 6.6 Hz, 3H). ¹³C NMR (101 MHz, CDCl₃) δ 182.74, 180.67, 164.15, 154.07, 145.38, 138.65, 131.04 (d, J = 8.8 Hz), 118.20, 116.67, 113.03 (d, J = 21.4 Hz), 109.87 (d, J = 24.1 Hz), 95.47, 31.93, 29.68, 29.64, 29.59, 29.46, 29.35, 28.07, 22.80, 22.70, 14.11. HRMS (TOF, AP+) calcd for $C_{23}H_{30}FNO_3$ + H⁺, 388.2282; found, 388.2307.

5-((4-Fluorophenyl)amino)-2-hydroxy-3-undecylcyclohexa-2,5-diene-1,4-dione (4h). Yield: 87%; wine-red solid; m.p. 200−202 °C; IR (ν_{max}): 3236, 2920, 2848, 1572, 1499, 1219 cm⁻¹. ¹H NMR (400 MHz, CDCl₃) δ 7.90 (s, 1H), 7.84 (s, 1H), 7.22 (dd, J = 8.9, 4.6 Hz, 2H), 7.12 (t, J = 8.3 Hz, 2H), 5.85 (s, 1H), 2.45 (t, J = 7.7 Hz, 2H), 1.49 (t, J = 7.4 Hz, 2H), 1.37−1.27 (m, 16H), 0.88 (t, J = 6.6 Hz, 3H). ¹³C NMR (101 MHz, CDCl₃) δ 182.81, 180.31, 160.67 (d, J = 247.9 Hz), 154.33, 146.55, 132.84, 125.09 (d, J = 8.4 Hz), 116.73 (d, J = 22.9 Hz), 116.37, 94.23, 77.35, 77.03, 76.71, 31.94, 29.69, 29.65, 29.61, 29.48, 29.37, 28.10, 22.78, 22.71, 14.14. HRMS (TOF, AP+) calcd for $C_{23}H_{30}FNO_3$ + H⁺, 388.2282; found, 388.2299.

2-Hydroxy-5-((3-methoxy-2-methylphenyl)amino)-3-undecylcyclohexa-2,5-diene-1,4-dione (4i). Yield: 88%; wine-red solid; m.p. 109−111 °C; IR (ν_{max}): 3272, 2923, 1642, 1599, 1564, 1502, 1462, 1375, 1261, 1216 cm⁻¹. ¹H NMR (400 MHz, CDCl₃) δ 7.95 (s, 1H), 7.75 (s, 1H), 7.21 (t, J = 8.1 Hz, 1H), 6.83 (dd, J = 10.8, 8.2 Hz, 2H), 5.56 (s, 1H), 3.86 (s, 3H), 2.45 (t, J = 7.7 Hz, 2H), 2.11 (s, 3H), 1.50 (t, J = 7.4 Hz, 2H), 1.38−1.27 (m, 16H), 0.88 (t, J = 6.6 Hz, 3H). ¹³C NMR (101 MHz, CDCl₃) δ 183.05, 180.10, 158.74, 154.59, 147.44, 135.87, 127.03, 122.24, 116.90, 116.15, 109.02, 94.39, 77.36, 77.05, 76.73, 55.78, 31.96, 29.71, 29.68, 29.64, 29.50, 29.38, 28.15, 22.82, 22.72, 14.13, 10.42. HRMS (TOF, AP+) calcd for $C_{25}H_{35}NO_4$ + H⁺, 414.2639; found, 414.2644.

5-((3,4-Dimethoxyphenyl)amino)-2-hydroxy-3-undecylcyclohexa-2,5-diene-1,4-dione (4j). Yield: 80%; wine-red solid; m.p. 146−148 °C; IR (ν_{max}): 3248, 2919, 2850, 1645, 1570, 1521, 1507, 1377, 1261, 1228, 1214 cm⁻¹. ¹H NMR (400 MHz, CDCl₃) δ 7.97 (s, 1H), 7.88 (s, 1H), 6.90 (d, J = 8.5 Hz, 1H), 6.81 (dd, J = 8.6, 2.5 Hz, 1H), 6.74 (d, J = 2.5 Hz, 1H), 5.88 (s, 1H), 3.89 (d, J = 8.7 Hz, 6H), 2.45 (t, J = 7.6 Hz, 2H), 1.51−1.45 (m, 2H), 1.36−1.27 (m, 16H), 0.88 (t, J = 6.7 Hz, 3H). ¹³C NMR (101 MHz, CDCl₃) δ 184.33, 181.41, 156.01, 151.27, 149.23, 148.19, 131.31, 117.34, 117.09, 115.22, 108.76, 95.30, 57.59, 57.56, 31.33, 31.08, 31.04, 31.00, 30.87, 30.74, 29.50, 24.17, 24.08, 15.48. HRMS (TOF, AP+) calcd for $C_{25}H_{35}NO_5$ + H⁺, 430.2588; found, 430.2599.

5-((5-Chloro-2,4-dimethoxyphenyl)amino)-2-hydroxy-3-undecylcyclohexa-2,5-diene-1,4-dione (4k). Yield: 69%; wine-red solid; m.p. 98−100 °C; IR (ν_{max}): 3278, 2924, 2853, 1650, 1595, 1523, 1465, 1394, 1336, 1207, 1029 cm⁻¹. ¹H NMR (400 MHz, CDCl₃) δ 8.13 (s, 1H), 8.02 (s, 1H), 7.33 (s, 1H), 6.56 (s, 1H), 5.92 (s, 1H), 3.91 (d, J = 5.2 Hz, 6H), 2.44 (t, J = 7.5 Hz, 2H), 1.48 (q, J = 7.4 Hz, 2H), 1.37−1.27 (m, 16H), 0.88 (t, J = 6.6 Hz, 3H). ¹³C NMR (101 MHz, CDCl₃) δ 182.85, 180.13, 154.41, 153.48, 151.49, 145.13, 123.15, 119.51, 116.35, 113.72, 97.02, 94.23, 56.59, 56.19, 31.95, 29.70, 29.66, 29.63, 29.50, 29.38, 28.13, 22.85, 22.72, 14.16. HRMS (TOF, AP+) calcd for $C_{25}H_{34}ClNO_5$ + H⁺, 464.2198; found, 464.2216.

5-((4-Ethoxyphenyl)amino)-2-hydroxy-3-undecylcyclohexa-2,5-diene-1,4-dione (4l). Yield: 69%; wine-red solid; m.p. 166−168 °C; IR (ν_{max}): 3241, 2921, 2851, 1569, 1508, 1499, 1374, 1228 cm⁻¹. ¹H NMR (400 MHz, CDCl₃) δ 7.98 (s, 1H), 7.87 (s, 1H), 7.15 (d, J = 8.6 Hz, 2H), 6.92 (d, J = 8.5 Hz, 2H), 5.84 (s, 1H), 4.04 (q, J = 7.0 Hz, 2H), 2.44 (t, J = 7.6 Hz, 2H), 1.48 (t, J = 7.4 Hz, 2H), 1.43 (t, J = 7.0 Hz, 3H), 1.33−1.27 (m, 16H), 0.88 (t, J = 6.6 Hz, 3H). ¹³C NMR (101 MHz, CDCl₃) δ 182.97, 179.90, 157.44, 154.67, 146.38, 129.41, 124.69, 116.05, 115.46, 93.60, 63.83, 31.91, 29.67, 29.63, 29.60, 29.47,

29.33, 28.09, 22.75, 22.68, 14.74, 14.09. HRMS (TOF, AP+) calcd for $C_{25}H_{35}NO_4$ + H⁺, 414.2639; found, 414.3652.

5-((4-(Benzyloxy)phenyl)amino)-2-hydroxy-3-undecylcyclohexa-2,5-diene-1,4-dione (4m). Yield: 89%; wine-red solid; m.p. 150−152 °C; IR (ν_{max}): 3248, 2916, 2850, 1642, 1565, 1515, 1490, 1418, 1376, 1284, 1212 cm⁻¹. ¹H NMR (400 MHz, CDCl₃) δ 7.87 (s, 1H), 7.44−7.34 (m, 5H), 7.16 (d, J = 8.5 Hz, 2H), 7.01 (d, J = 8.5 Hz, 2H), 5.84 (s, 1H), 5.09 (s, 2H), 2.44 (t, J = 7.6 Hz, 2H), 1.48 (q, J = 7.5 Hz, 2H), 1.37−1.27 (m, 16H), 0.88 (t, J = 6.6 Hz, 3H). ¹³C NMR (101 MHz, CDCl₃) δ 182.98, 179.99, 157.27, 154.63, 146.87, 136.55, 129.90, 128.70, 128.19, 127.47, 124.73, 116.15, 116.01, 93.76, 70.45, 31.94, 29.70, 29.65, 29.62, 29.49, 29.36, 28.11, 22.79, 22.70, 14.10. HRMS (TOF, AP+) calcd for $C_{30}H_{37}NO_4$ + H⁺, 476.2795; found, 476.2832.

5-((4-Acetylphenyl)amino)-2-hydroxy-3-undecylcyclohexa-2,5-diene-1,4-dione (4n). Yield: 76%; wine-red solid; m.p. 170−172 °C; IR (ν_{max}): 3311, 3240, 2916, 2848, 1652, 1572, 1516, 1492, 1360, 1270, 1221 cm⁻¹. ¹H NMR (400 MHz, CDCl₃) δ 8.09 (s, 1H), 8.02 (d, J = 8.3 Hz, 2H), 7.82 (s, 1H), 7.32 (d, J = 8.2 Hz, 2H), 6.19 (s, 1H), 2.61 (s, 3H), 2.46 (t, J = 7.7 Hz, 2H), 1.48 (q, J = 7.7 Hz, 2H), 1.37−1.27 (m, 16H), 0.88 (t, J = 6.7 Hz, 3H). ¹³C NMR (101 MHz, CDCl₃) δ 197.75, 184.10, 182.33, 155.31, 145.90, 142.93, 135.49, 131.56, 122.74, 118.37, 98.03, 33.32, 31.07, 31.03, 30.98, 30.84, 30.73, 29.46, 27.84, 24.24, 24.08, 15.48. HPLC: 98.3% purity (t_R, 10.82 min).

3-((4-Hydroxy-3,6-dioxo-5-undecylcyclohexa-1,4-dien-1-yl)amino)benzonitrile (4o). Yield: 72%; wine-red solid; m.p. 176−178 °C; IR (ν_{max}): 3242, 2929, 2848, 1643, 1568, 1490, 1212 cm⁻¹. ¹H NMR (400 MHz, CDCl₃) δ 7.93 (s, 1H), 7.80 (s, 1H), 7.55−7.47 (m, 4H), 6.01 (s, 1H), 2.46 (t, J = 7.6 Hz, 2H), 1.48 (q, J = 7.4 Hz, 2H), 1.37−1.27 (m, 16H), 0.88 (t, J = 6.7 Hz, 3H). ¹³C NMR (101 MHz, CDCl₃) δ 182.50, 180.83, 153.89, 145.03, 138.24, 130.75, 129.28, 126.72, 125.56, 117.64, 117.01, 114.13, 95.91, 31.91, 29.66, 29.62, 29.57, 29.42, 29.33, 28.03, 22.79, 22.67, 14.09. HPLC: 96.6% purity (t_R, 7.42 min).

4-((4-Hydroxy-3,6-dioxo-5-undecylcyclohexa-1,4-dien-1-yl)amino)benzonitrile (4p). Yield: 68%; wine-red solid; m.p. 220−222 °C; IR (ν_{max}): 3238, 2919, 2848, 1645, 1565, 1487, 1228 cm⁻¹. ¹H NMR (400 MHz, CDCl₃) δ 8.05 (s, 1H), 7.71 (d, J = 10.2 Hz, 2H), 7.33 (s, 2H), 6.17 (s, 1H), 2.47 (s, 2H), 1.49 (s, 2H), 1.35−1.26 (m, 16H), 0.88 (s, 3H). ¹³C NMR (101 MHz, CDCl₃) δ 182.54, 181.05, 153.75, 144.10, 141.51, 133.86, 121.83, 117.30, 114.52, 108.82, 97.26, 31.94, 29.68, 29.65, 29.60, 29.45, 29.35, 28.06, 22.87, 22.70, 14.09. HPLC: 98.4% purity (t_R, 9.22 min).

2-(4-((4-Hydroxy-3,6-dioxo-5-undecylcyclohexa-1,4-dien-1-yl)amino)phenyl)acetonitrile (4q). Yield: 74%; dark purple solid; m.p. 217−219 °C; IR (ν_{max}): 3244, 2920, 2850, 1646, 1566, 1519, 1491, 1375, 1225 cm⁻¹. ¹H NMR (400 MHz, CDCl₃) δ 7.94 (s, 1H), 7.88 (s, 1H), 7.40 (t, J = 8.2 Hz, 2H), 7.29−7.25 (m, 2H), 6.00 (d, J = 8.9 Hz, 1H), 3.78 (d, J = 8.0 Hz, 2H), 2.47 (q, J = 8.0 Hz, 2H), 1.51−1.47 (m, 2H), 1.37−1.27 (m, 16H), 0.89 (q, J = 8.1, 7.6 Hz, 3H). ¹³C NMR (101 MHz, CDCl₃) δ 182.77, 180.54, 154.15, 145.69, 137.12, 129.36, 127.76, 125.28, 117.24, 116.61, 95.12, 31.91, 29.66, 29.62, 29.57, 29.43, 29.32, 28.05, 23.20, 22.79, 22.66, 14.05. HPLC: 96.5% purity (t_R, 7.0 min).

2-Hydroxy-5-((4-(trifluoromethoxy)phenyl)amino)-3-undecylcyclohexa-2,5-diene-1,4-dione (4r). Yield: 70%; dark purple solid; m.p. 105−107 °C; IR (ν_{max}): 3315, 3242, 2916, 2849, 1647, 1568, 1517, 1498, 1377, 1286, 1218 cm⁻¹. ¹H NMR (400 MHz, CDCl₃) δ 7.90 (s, 2H), 7.28 (s, 4H), 5.95 (s, 1H), 2.45 (t, J = 7.6 Hz, 2H), 1.49 (t, J = 7.4 Hz, 2H), 1.36−1.27 (m, 16H), 0.88 (t, J = 6.7 Hz, 3H). ¹³C NMR (101 MHz, CDCl₃) δ 182.73, 180.55, 154.17, 146.77, 145.87, 135.60, 124.20, 122.38, 120.39 (d, J = 257.9 Hz), 116.62, 94.92, 31.91, 29.66, 29.62, 29.58, 29.44, 29.33, 28.05, 22.77, 22.67, 14.08. HRMS (TOF, AP+) calcd for $C_{24}H_{30}F_3NO_4$ + H⁺, 454.2200; found, 454.2226.

2-Hydroxy-5-((2-(trifluoromethyl)phenyl)amino)-3-undecylcyclohexa-2,5-diene-1,4-dione (4s). Yield: 71%; maroon solid; m.p. 174−176 °C; IR (ν_{max}): 3249, 2922, 2848, 1648, 1591, 1576, 1500, 1487, 1378, 1321, 1137 cm⁻¹. ¹H NMR (400 MHz, CDCl₃) δ 8.02 (s, 1H), 7.74 (dd, J = 7.9, 1.5 Hz, 1H), 7.64−7.60 (m, 1H), 7.49 (d, J = 8.0

Hz, 1H), 7.38 (t, J = 7.7 Hz, 1H), 5.83 (s, 1H), 2.48–2.44 (m, 2H), 1.50 (q, J = 7.3 Hz, 2H), 1.37–1.27 (m, 16H), 0.88 (t, J = 6.8 Hz, 3H). ^{13}C NMR (101 MHz, CDCl$_3$) δ 182.43, 180.85, 153.89, 146.46, 135.17, 133.00, 127.39 (d, J = 5.3 Hz), 126.54, 125.72, 116.79, 95.54, 31.93, 29.70, 29.67, 29.63, 29.60, 29.44, 29.35, 28.06, 22.85, 22.69, 14.10. HRMS (TOF, AP+) calcd for C$_{29}$H$_{36}$F$_2$NO$_2$ + H$^+$, 438.2251; found, 438.2258.

5-([1,1′-Biphenyl]-2-ylamino)-2-hydroxy-3-undecylcyclohexa-2,5-diene-1,4-dione (4t). Yield: 88%; dark purple solid; m.p. 89–91 °C; IR (ν_{max}): 3292, 2924, 2853, 1646, 1580, 1514, 1382, 1217 cm^{-1}. ^{1}H NMR (400 MHz, CDCl$_3$) δ 7.90 (s, 1H), 7.84 (s, 1H), 7.46–7.39 (m, 6H), 7.34–7.30 (m, 3H), 5.86 (s, 1H), 2.38 (t, J = 7.6 Hz, 2H), 1.43 (q, J = 7.3 Hz, 2H), 1.31–1.27 (m, 16H), 0.88 (t, J = 6.7 Hz, 3H). ^{13}C NMR (101 MHz, CDCl$_3$) δ 182.65, 180.28, 154.30, 146.27, 137.47, 136.58, 134.40, 131.32, 128.97, 128.93, 128.47, 128.16, 126.73, 123.54, 116.27, 94.59, 31.94, 29.68, 29.65, 29.63, 29.46, 29.35, 28.04, 22.78, 22.70, 14.10. Purity: 97.1% purity (t_R: 15.37 min).

2-Hydroxy-5-(quinolin-8-ylamino)-3-undecylcyclohexa-2,5-diene-1,4-dione (5). Compound 5 was synthesized by condensing embelin (1) with quinoline amine (3) following the above-mentioned general procedure for synthesis. Yield: 85%; wine-red solid; m.p. 129–131 °C; IR (ν_{max}): 3282, 2920, 2852, 1590, 1569, 1529, 1486, 1387, 1300, 1226, 1198 cm^{-1}. ^{1}H NMR (400 MHz, CDCl$_3$) δ 10.61 (s, 1H), 8.93 (d, J = 4.3 Hz, 1H), 8.18 (d, J = 8.3 Hz, 1H), 7.87 (s, 1H), 7.66 (d, J = 6.7 Hz, 1H), 7.59–7.50 (m, 3H), 6.45 (s, 1H), 2.51 (t, J = 7.8 Hz, 2H), 1.61–1.53 (m, 2H), 1.38–1.27 (m, 16H), 0.88 (t, J = 6.6 Hz, 3H). ^{13}C NMR (101 MHz, CDCl$_3$) δ 183.17, 181.40, 153.84, 149.28, 143.83, 140.50, 136.30, 134.51, 128.63, 126.69, 123.10, 122.38, 117.15, 116.08, 96.98, 31.94, 29.70, 29.65, 29.63, 29.50, 29.36, 28.16, 23.04, 22.70, 14.09. HRMS (TOF, AP+) calcd for C$_{26}$H$_{32}$N$_2$O$_3$ + H$^+$, 421.2488; found, 421.2510.

5-(Benzylamino)-2-hydroxy-3-undecylcyclohexa-2,5-diene-1,4-dione (7a). Yield: 82%; maroon solid; m.p. 151–153 °C; IR (ν_{max}): 3286, 2921, 2851, 1646, 1568, 1506, 1438, 1383, 1356, 1210 cm^{-1}. ^{1}H NMR (400 MHz, CDCl$_3$) δ 8.03 (brs, 1H), 7.40–7.33 (m, 3H), 7.28 (d, J = 7.6 Hz, 2H), 6.67 (s, 1H), 5.42 (s, 1H), 4.34 (d, J = 5.7 Hz, 2H), 2.39 (t, J = 7.5 Hz, 2H), 1.30–1.26 (m, 16H), 0.88 (t, J = 6.6 Hz, 3H). ^{13}C NMR (101 MHz, CDCl$_3$) δ 182.53, 179.09, 154.81, 149.36, 135.25, 129.08, 128.32, 127.68, 115.95, 93.54, 47.01, 31.92, 29.67, 29.63, 29.59, 29.46, 29.34, 28.07, 22.69, 22.64, 14.13. HRMS (TOF, AP+) calcd for C$_{24}$H$_{34}$NO$_3$ + H$^+$, 384.2533; found, 384.2542.

2-Hydroxy-5-((1-phenylethyl)amino)-3-undecylcyclohexa-2,5-diene-1,4-dione (7b). Yield: 81%; red solid; m.p. 106–108 °C; IR (ν_{max}): 3296, 2925, 2854, 1649, 1582, 1506, 1454, 1385, 1222, 1132 cm^{-1}. ^{1}H NMR (400 MHz, CDCl$_3$) δ 7.97 (brs, 1H), 7.37–7.23 (m, 5H), 6.64 (d, J = 6.7 Hz, 1H), 5.21 (s, 1H), 4.50–4.44 (m, 1H), 2.38 (t, J = 7.6 Hz, 2H), 1.60 (d, J = 6.7 Hz, 3H), 1.43 (q, J = 7.4 Hz, 2H), 1.32–1.26 (m, 11H), 0.88 (t, J = 6.6 Hz, 3H). ^{13}C NMR (101 MHz, CDCl$_3$) δ 182.75, 179.01, 154.73, 148.42, 141.37, 129.09, 127.98, 125.77, 115.93, 93.56, 53.07, 31.92, 29.66, 29.62, 29.58, 29.44, 29.33, 28.06, 23.15, 22.67, 14.07. HRMS (TOF, AP+) calcd for C$_{25}$H$_{36}$NO$_3$ + H$^+$, 398.2690; found, 398.2694.

2-Hydroxy-5-((1-phenylpropyl)amino)-3-undecylcyclohexa-2,5-diene-1,4-dione (7c). Yield: 70%; wine-red sticky solid; IR (ν_{max}): 3297, 2925, 2854, 1645, 1583, 1506, 1385, 1354, 1219 cm^{-1}. ^{1}H NMR (400 MHz, CDCl$_3$) δ 8.07 (s, 1H), 7.36–7.29 (m, 3H), 7.21 (d, J = 7.3 Hz, 2H), 6.75 (s, 1H), 5.22 (s, 1H), 4.22–4.17 (m, 1H), 2.39 (t, J = 7.6 Hz, 2H), 1.92–1.85 (m, 2H), 1.47–1.43 (m, 2H), 1.30 (m, 6H), 1.26 (m, 10H), 0.94 (t, J = 7.3 Hz, 3H), 0.88 (t, J = 6.7 Hz, 3H). ^{13}C NMR (101 MHz, CDCl$_3$) δ 182.83, 179.00, 154.92, 148.71, 140.11, 128.98, 128.00, 126.41, 115.93, 93.46, 59.27, 31.96, 30.29, 29.74, 29.71, 29.67, 29.63, 29.50, 29.39, 28.12, 22.73, 22.71, 14.15, 10.62. HRMS (TOF, AP+) calcd for C$_{26}$H$_{38}$NO$_3$ + H$^+$, 412.2846; found, 412.2857.

5-((Benzo[d][1,3]dioxol-5-ylmethyl)amino)-2-hydroxy-3-undecylcyclohexa-2,5-diene-1,4-dione (7d). Yield: 77%; red solid; m.p. 179–181 °C; IR (ν_{max}): 3285, 2919, 2850, 1642, 1570, 1501, 1449, 1381, 1367, 1328, 1211 cm^{-1}. ^{1}H NMR (400 MHz, CDCl$_3$) δ 8.01 (brs, 1H), 6.82–6.75 (m, 3H), 6.59 (s, 1H), 5.99 (d, J = 2.9 Hz, 2H),

5.41 (d, J = 2.8 Hz, 1H), 4.24 (s, 2H), 2.39 (t, J = 7.6 Hz, 2H), 1.44 (s, 2H), 1.30 (s, 6H), 1.26 (s, 10H), 0.88 (t, J = 3.5 Hz, 3H). ^{13}C NMR (101 MHz, CDCl$_3$) δ 182.58, 179.15, 154.83, 149.29, 148.36, 147.72, 129.01, 121.29, 116.03, 108.69, 108.17, 101.36, 92.80, 46.92, 31.94, 29.69, 29.65, 29.60, 29.47, 29.35, 28.08, 22.70, 22.67, 14.11. HRMS (TOF, AP+) calcd for C$_{25}$H$_{34}$NO$_5$ + H$^+$, 428.2431; found, 428.2440.

5-((3,4-Dimethoxybenzyl)amino)-2-hydroxy-3-undecylcyclohexa-2,5-diene-1,4-dione (7e). Yield: 80%; red solid; m.p. 132–134 °C; IR (ν_{max}): 3287, 2920, 2851, 1642, 1566, 1505, 1442, 1381, 1260, 1205 cm^{-1}. ^{1}H NMR (400 MHz, CDCl$_3$) δ 8.06 (brs, 1H), 6.85 (s, 2H), 6.77 (s, 1H), 6.60 (s, 1H), 5.43 (s, 1H), 4.26 (d, J = 5.3 Hz, 2H), 3.88 (s, 6H), 2.39 (t, J = 7.6 Hz, 2H), 1.48–1.41 (m, 2H), 1.31–1.28 (m, 6H), 1.25 (m, 10H), 0.87 (t, J = 6.6 Hz, 3H). ^{13}C NMR (101 MHz, CDCl$_3$) δ 183.98, 180.48, 156.34, 150.94, 150.72, 150.57, 129.11, 121.74, 117.38, 112.95, 112.43, 93.88, 57.39, 48.36, 33.52, 31.07, 31.03, 31.00, 30.86, 30.74, 29.47, 24.09, 24.05, 15.51. HPLC: 99.3% purity (t_R: 7.70 min).

5-((4-Chlorobenzyl)amino)-2-hydroxy-3-undecylcyclohexa-2,5-diene-1,4-dione (7f). Yield: 73%; wine-red solid; m.p. 154–156 °C; IR (ν_{max}): 3291, 2923, 2852, 1645, 1583, 1572, 1507, 1382, 1357, 1209 cm^{-1}. ^{1}H NMR (400 MHz, CDCl$_3$) δ 7.99 (brs, 1H), 7.35 (d, J = 8.1 Hz, 2H), 7.21 (d, J = 8.0 Hz, 2H), 6.65 (s, 1H), 5.37 (s, 1H), 4.32 (d, J = 5.8 Hz, 2H), 2.39 (t, J = 7.6 Hz, 2H), 1.43 (t, J = 8.0 Hz, 2H), 1.30–1.28 (m, 6H), 1.25 (m, 10H), 0.88 (t, J = 6.6 Hz, 3H). ^{13}C NMR (101 MHz, CDCl$_3$) δ 182.50, 179.23, 154.71, 149.24, 134.36, 133.82, 129.29, 128.92, 116.15, 92.87, 46.31, 31.93, 29.67, 29.63, 29.59, 29.45, 29.34, 28.06, 22.69, 22.66, 14.10. HRMS (TOF, AP+) calcd for C$_{24}$H$_{33}$ClNO$_3$ + H$^+$, 418.2143; found, 418.2192.

2-Hydroxy-5-((4-methoxybenzyl)amino)-3-undecylcyclohexa-2,5-diene-1,4-dione (7g). Yield: 72%; red solid; m.p. 135–137 °C; IR (ν_{max}): 3286, 2921, 2851, 1644, 1566, 1505, 1441, 1383, 1356, 1247, 1208 cm^{-1}. ^{1}H NMR (400 MHz, CDCl$_3$) δ 8.06 (s, 1H), 7.20 (d, J = 8.5 Hz, 2H), 6.90 (d, J = 8.6 Hz, 2H), 6.60 (s, 1H), 5.42 (s, 1H), 4.26 (d, J = 5.6 Hz, 2H), 3.81 (s, 3H), 2.39 (t, J = 7.6 Hz, 2H), 1.43 (q, J = 7.2 Hz, 2H), 1.31–1.28 (m, 6H), 1.25 (m, 10H), 0.88 (t, J = 6.6 Hz, 3H). ^{13}C NMR (101 MHz, CDCl$_3$) δ 183.97, 180.46, 161.08, 156.30, 150.73, 130.57, 128.68, 117.34, 115.91, 93.81, 56.75, 47.98, 33.53, 31.07, 31.03, 30.99, 30.86, 30.74, 29.47, 24.09, 24.05, 15.49. HRMS (TOF, AP+) calcd for C$_{25}$H$_{36}$NO$_4$ + H$^+$, 414.2639; found, 414.2664.

2-Hydroxy-5-((4-methylbenzyl)amino)-3-undecylcyclohexa-2,5-diene-1,4-dione (7h). Yield: 76%; red solid; m.p. 150–152 °C; IR (ν_{max}): 3286, 2921, 2852, 1643, 1568, 1507, 1356, 1212 cm^{-1}. ^{1}H NMR (400 MHz, CDCl$_3$) δ 8.02 (s, 1H), 7.19–7.15 (m, 4H), 6.63 (s, 1H), 5.41 (s, 1H), 4.30 (d, J = 5.8 Hz, 2H), 2.39 (t, J = 7.6 Hz, 2H), 2.36 (s, 3H), 1.46–1.40 (m, 2H), 1.31–1.28 (m, 6H), 1.25 (m, 10H), 0.88 (t, J = 6.7 Hz, 3H). ^{13}C NMR (101 MHz, CDCl$_3$) δ 182.56, 179.08, 154.86, 149.42, 138.16, 132.30, 129.74, 127.69, 115.95, 92.49, 46.84, 31.91, 29.65, 29.61, 29.57, 29.43, 29.32, 28.04, 22.66, 22.64, 22.07, 14.05. HRMS (TOF, AP+) calcd for C$_{25}$H$_{36}$NO$_3$ + H$^+$, 398.2690; found, 398.2694.

5-((4-Fluorobenzyl)amino)-2-hydroxy-3-undecylcyclohexa-2,5-diene-1,4-dione (7i). Yield: 73%; red solid; m.p. 150–152 °C; IR (ν_{max}): 3290, 2923, 2853, 1645, 1573, 1506, 1443, 1383, 1356, 1208 cm^{-1}. ^{1}H NMR (400 MHz, CDCl$_3$) δ 7.97 (s, 1H), 7.27–7.24 (m, 2H), 7.07 (t, J = 8.6 Hz, 2H), 6.59 (s, 1H), 5.39 (s, 1H), 4.31 (d, J = 5.8 Hz, 2H), 2.41–2.37 (m, 2H), 1.45–1.41 (m, 2H), 1.29 (m, 6H), 1.25 (m, 10H), 0.88 (t, J = 6.8 Hz, 3H). ^{13}C NMR (101 MHz, CDCl$_3$) δ 182.52, 179.19, 162.59 (d, J = 247.5 Hz), 154.77, 149.24, 131.08 (d, J = 3.4 Hz), 129.82 (d, J = 8.4 Hz), 116.13 (d, J = 6.5 Hz), 115.94, 92.71, 77.33, 77.01, 76.70, 46.30, 31.91, 29.69, 29.66, 29.62, 29.58, 29.44, 29.33, 28.05, 22.68, 22.66, 14.09. HRMS (TOF, AP+) calcd for C$_{24}$H$_{33}$FNO$_3$ + H$^+$, 402.2439; found, 402.2480.

2-Hydroxy-5-(propylamino)-3-undecylcyclohexa-2,5-diene-1,4-dione (9a). Yield: 79%; wine-red solid; m.p. 100–102 °C; IR (ν_{max}): 3276, 2956, 2918, 2851, 1645, 1567, 1507, 1468, 1384, 1213 cm^{-1}. ^{1}H NMR (400 MHz, CDCl$_3$) δ 8.12 (s, 1H), 6.43 (s, 1H), 5.35 (s, 1H), 3.13 (q, J = 6.8 Hz, 2H), 2.39 (t, J = 7.6 Hz, 2H), 1.70 (q, J = 7.3 Hz, 2H), 1.44 (q, J = 7.3 Hz, 2H), 1.32–1.29 (m, 6H), 1.25 (s, 10H), 1.01 (t, J = 7.3 Hz, 3H), 0.88 (t, J = 6.7 Hz, 3H). ^{13}C NMR (101

MHz, CDCl$_3$) δ 183.97, 180.11, 156.57, 151.18, 117.11, 92.97, 45.91, 33.33, 31.07, 31.03, 30.99, 30.86, 30.74, 29.47, 24.09, 24.05, 22.94, 15.50, 12.85. HRMS (TOF, AP+) calcd for C$_{22}$H$_{33}$NO$_3$ + H$^+$, 336.2533; found, 336.2547.

5-(Butylamino)-2-hydroxy-3-undecylcyclohexa-2,5-diene-1,4-dione (**9b**). Yield: 80%; maroon solid; m.p. 100−102 °C; IR (ν_{max}): 3271, 2955, 2919, 2850, 1642, 1564, 1506, 1467, 1368, 1210 cm^{-1}. ^{1}H NMR (400 MHz, CDCl$_3$) δ 8.13 (s, 1H), 6.44 (s, 1H), 5.34 (s, 1H), 3.15 (q, J = 6.7 Hz, 2H), 2.37 (t, J = 7.6 Hz, 2H), 1.68−1.61 (m, 2H), 1.45−1.38 (m, 6H), 1.30−1.27 (m, 4H), 1.24 (s, 10H), 0.95 (t, J = 7.4 Hz, 3H), 0.86 (t, J = 6.7 Hz, 3H). ^{13}C NMR (101 MHz, CDCl$_3$) δ 182.56, 178.68, 155.23, 149.76, 115.70, 91.53, 42.54, 31.93, 30.18, 29.67, 29.63, 29.59, 29.47, 29.34, 28.08, 22.69, 22.64, 20.16, 14.10, 13.63. HRMS (TOF, AP+) calcd for C$_{21}$H$_{35}$NO$_3$ + H$^+$, 350.2690; found, 350.2698.

2-Hydroxy-5-(isobutylamino)-3-undecylcyclohexa-2,5-diene-1,4-dione (**9c**). Yield: 83%; maroon solid; m.p. 102−104 °C; IR (ν_{max}): 3276, 2955, 2920, 2850, 1643, 1571, 1505, 1467, 1384, 1361, 1241 cm^{-1}. ^{1}H NMR (400 MHz, CDCl$_3$) δ 8.14 (s, 1H), 6.51 (s, 1H), 5.34 (s, 1H), 2.98 (t, J = 6.4 Hz, 2H), 2.38 (t, J = 7.6 Hz, 2H), 2.02−1.93 (m, 1H), 1.44 (q, J = 6.2, 5.0 Hz, 2H), 1.33−1.28 (m, 6H), 1.25 (s, 10H), 0.99 (d, J = 6.7 Hz, 6H), 0.87 (t, J = 6.7 Hz, 3H). ^{13}C NMR (101 MHz, CDCl$_3$) δ 182.55, 178.69, 155.28, 149.88, 115.68, 91.61, 50.30, 31.91, 29.66, 29.62, 29.59, 29.44, 29.33, 28.06, 27.71, 22.67, 22.65, 20.26, 14.08. HRMS (TOF, AP+) calcd for C$_{21}$H$_{35}$NO$_3$ + H$^+$, 350.2690; found, 350.2699.

5-(Cyclopentylamino)-2-hydroxy-3-undecylcyclohexa-2,5-diene-1,4-dione (**9d**). Yield: 75%; maroon solid; m.p. 94−96 °C; IR (ν_{max}): 3276, 2956, 2921, 2851, 1646, 1572, 1511, 1393, 1363, 1343, 1221 cm^{-1}. ^{1}H NMR (400 MHz, CDCl$_3$) δ 8.16 (s, 1H), 6.38 (s, 1H), 5.37 (s, 1H), 3.78−3.70 (m, 1H), 2.37 (t, J = 7.6 Hz, 1H), 2.07−1.99 (m, 2H), 1.77−1.57 (m, 6H), 1.46−1.41 (m, 2H), 1.28 (s, 6H), 1.28 (s, 10H), 0.87 (t, J = 6.7 Hz, 3H). ^{13}C NMR (101 MHz, CDCl$_3$) δ 182.65, 178.52, 155.24, 149.15, 115.68, 92.18, 54.15, 32.74, 31.94, 29.69, 29.64, 29.60, 29.48, 29.35, 28.09, 24.08, 22.70, 22.66, 14.11. HRMS (TOF, AP+) calcd for C$_{22}$H$_{35}$NO$_3$ + H$^+$, 362.2690; found, 362.2704.

2-Hydroxy-5-((2-methoxyethyl)amino)-3-undecylcyclohexa-2,5-diene-1,4-dione (**9e**). Yield: 72%; maroon solid; m.p. 93−95 °C; IR (ν_{max}): 3282, 2921, 2849, 1645, 1566, 1504, 1463, 1384, 1365, 1214 cm^{-1}. ^{1}H NMR (400 MHz, CDCl$_3$) δ 8.05 (s, 1H), 6.64 (s, 1H), 5.36 (s, 1H), 3.60 (t, J = 5.2 Hz, 2H), 3.39 (s, 3H), 3.32 (q, J = 5.5 Hz, 2H), 2.39 (t, J = 7.6 Hz, 2H), 1.43 (q, J = 7.3 Hz, 2H), 1.28 (s, 6H), 1.25 (s, 10H), 0.88 (t, J = 6.6 Hz, 3H). ^{13}C NMR (101 MHz, CDCl$_3$) δ 182.40, 178.94, 154.60, 149.72, 115.87, 91.83, 77.35, 77.03, 76.72, 69.25, 59.02, 42.42, 31.93, 29.68, 29.64, 29.61, 29.59, 29.48, 29.36, 28.08, 22.71, 22.65, 14.14. HPLC: 99.2% purity (t_R 7.79 min).

2-Hydroxy-5-(phenethylamino)-3-undecylcyclohexa-2,5-diene-1,4-dione (**9f**). Yield: 78%; maroon solid; m.p. 132−134 °C; IR (ν_{max}): 3270, 2920, 2850, 1641, 1566, 1499, 1459, 1362, 1116 cm^{-1}. ^{1}H NMR (400 MHz, CDCl$_3$) δ 8.07 (s, 1H), 7.36−7.28 (m, 3H), 7.25−7.19 (m, 2H), 6.44 (s, 1H), 5.39 (s, 1H), 3.42 (q, J = 6.7 Hz, 2H), 2.95 (t, J = 7.2 Hz, 2H), 2.37 (t, J = 7.6 Hz, 2H), 1.43 (q, J = 7.4 Hz, 2H), 1.32−1.28 (m, 6H), 1.26 (s, 10H), 0.88 (t, J = 6.7 Hz, 3H). ^{13}C NMR (101 MHz, CDCl$_3$) δ 182.45, 178.90, 154.99, 149.49, 137.46, 129.01, 128.60, 127.13, 115.87, 91.89, 43.93, 34.35, 31.95, 29.69, 29.66, 29.62, 29.48, 29.36, 28.08, 22.71, 22.67, 14.12. HRMS (TOF, AP+) calcd for C$_{25}$H$_{35}$NO$_3$ + H$^+$, 398.2690; found, 398.2705.

2-Hydroxy-5-((3-morpholinopropyl)amino)-3-undecylcyclohexa-2,5-diene-1,4-dione (**9g**). Yield: 67%; wine-red sticky solid; IR (ν_{max}): 3284, 2924, 2855, 1711, 1580, 1464, 1114 cm^{-1}. ^{1}H NMR (400 MHz, CDCl$_3$) δ 7.99 (s, 1H), 5.31 (s, 1H), 3.82 (t, J = 4.7 Hz, 4H), 3.24 (q, J = 5.7 Hz, 2H), 2.54−2.48 (m, 6H), 2.37 (t, J = 7.5 Hz, 2H), 1.86−1.80 (m, 2H), 1.45−1.40 (m, 2H), 1.30−1.28 (m, 6H), 1.24 (s, 10H), 0.87 (t, J = 6.6 Hz, 3H). ^{13}C NMR (101 MHz, CDCl$_3$) δ 182.44, 178.70, 155.32, 150.41, 115.75, 91.23, 66.56, 57.45, 55.71, 42.78, 31.93, 29.69, 29.64, 29.60, 29.49, 29.35, 29.21, 28.11, 23.43, 22.69, 22.63, 14.11. HPLC: 98.9% purity (t_R 2.74 min).

2-Hydroxy-5-((2-(pyrrolidin-1-yl)ethyl)amino)-3-undecylcyclohexa-2,5-diene-1,4-dione (**9h**). Yield: 68%; wine-red sticky solid; IR

(ν_{max}): 3284, 2924, 2854, 1712, 1635, 1458, 1377, 1219 cm^{-1}. ^{1}H NMR (400 MHz, CDCl$_3$) δ 7.49 (s, 1H), 7.05 (s, 1H), 5.30 (s, 1H), 3.29 (s, 2H), 2.86 (t, J = 6.1 Hz, 2H), 2.68 (d, J = 6.1 Hz, 4H), 2.35 (t, J = 7.6 Hz, 2H), 1.84−1.81 (m, 4H), 1.40 (q, J = 7.3 Hz, 2H), 1.30−1.25 (m, 6H), 1.24 (s, 10H), 0.86 (t, J = 6.7 Hz, 3H). ^{13}C NMR (101 MHz, CDCl$_3$) δ 181.72, 179.62, 179.54, 157.35, 150.20, 150.17, 115.74, 91.88, 53.99, 53.11, 40.80, 40.78, 31.94, 29.71, 29.66, 29.54, 29.36, 28.23, 23.52, 22.76, 22.70, 14.10. HPLC: 99.1% purity (t_R 2.74 min).

5-((1-Benzylpiperidin-4-yl)amino)-2-hydroxy-3-undecylcyclohexa-2,5-diene-1,4-dione (**9i**). Yield: 74%; wine-red sticky solid; IR (ν_{max}): 3252, 2925, 2853, 1627, 1582, 1538, 1489, 147, 1456, 1365, 1218 cm^{-1}. ^{1}H NMR (400 MHz, CDCl$_3$) δ 7.33 (q, J = 6.2 Hz, 5H), 6.39 (s, 1H), 5.35 (s, 1H), 3.57 (s, 2H), 3.29 (s, 1H), 2.88 (d, J = 11.5 Hz, 1H), 2.38 (t, J = 7.6 Hz, 2H), 2.30 (t, J = 7.6 Hz, 1H), 2.23 (t, J = 11.3 Hz, 2H), 1.99 (d, J = 11.9 Hz, 2H), 1.70−1.87 (m, 2H), 1.43 (q, J = 7.2 Hz, 2H), 1.33−1.29 (m, 6H), 1.26 (s, 10H), 0.88 (t, J = 6.7 Hz, 3H). ^{13}C NMR (101 MHz, CDCl$_3$) δ 178.89, 177.47, 155.51, 148.52, 129.28, 128.37, 127.41, 115.84, 91.84, 62.88, 51.42, 34.56, 31.92, 30.65, 29.68, 29.61, 29.60, 29.53, 29.47, 29.36, 29.27, 28.10, 25.12, 22.89, 14.13. HRMS (TOF, ES+) calcd for C$_{29}$H$_{42}$N$_2$O$_3$ + H$^+$, 467.3268; found, 467.3271.

5-((2-(1-Benzylpiperidin-4-yl)ethyl)amino)-2-hydroxy-3-undecylcyclohexa-2,5-diene-1,4-dione (**9j**). Yield: 75%; wine-red solid; HPLC purity: 98%; m.p. 109−111 °C; IR (ν_{max}): 3275, 2924, 2853, 1649, 1591, 1533, 1486, 1377, 1217 cm^{-1}. ^{1}H NMR (400 MHz, CDCl$_3$) δ 7.33 (d, J = 3.8 Hz, 5H), 6.37 (s, 1H), 5.31 (s, 1H), 3.64 (s, 2H), 3.17 (q, J = 6.8 Hz, 2H), 3.02 (s, 2H), 2.37 (t, J = 7.6 Hz, 2H), 2.09 (s, 2H), 1.70−1.62 (m, 4H), 1.42 (s, 5H), 1.32−1.27 (m, 6H), 1.25 (s, 10H), 0.88 (t, J = 6.8 Hz, 3H). ^{13}C NMR (101 MHz, CDCl$_3$) δ 181.64, 179.32, 157.49, 150.02, 129.88, 128.50, 127.93, 115.54, 91.57, 62.51, 52.96, 40.15, 34.34, 32.82, 31.92, 30.93, 29.69, 29.64, 29.52, 29.36, 28.21, 22.70, 14.14. HRMS (TOF, AP+) calcd for C$_{31}$H$_{46}$N$_2$O$_3$ + H$^+$, 495.3581; found, 495.3592.

General Procedure for the Synthesis of Embelin Derivatives 15a–e. Benzaldehyde (1 mmol) was added to a stirring solution of 1 mmol of aminopiperidines 10a or 10b in toluene and stirred for 4 h. Toluene was removed under vacuum, and the solid was dissolved in DMF and stirred. To the stirring solution, sodium hydride (1.5 equiv) was added in portions, followed by the addition of 1 equiv of substituted benzyl bromides 12a–e and stirred for 6 h. The reaction mixture was acidified using 4 N HCl and further stirred for 2 h. Finally, the reaction mixture was neutralized using sodium bicarbonate and extracted thrice using ethyl acetate. The ethyl acetate fractions were pooled together, and concentrated to dryness to yield substituted piperidine amines 14a–e, which were used for further synthesis without purification. The obtained amines 14a–e were refluxed with embelin (1) in acetic acid for 2 h to yield the targeted compounds 15a–e.

5-((1-Benzylpiperidin-4-yl)methylamino)-2-hydroxy-3-undecylcyclohexa-2,5-diene-1,4-dione (**15a**). Yield: 72%; wine-red solid; m.p. 95−97 °C; IR (ν_{max}): 3424, 2924, 2853, 2345, 1594, 1533, 1490, 1457, 1384, 1118 cm^{-1}. ^{1}H NMR (400 MHz, CDCl$_3$) δ 7.35−7.28 (m, 5H), 6.58 (s, 1H), 5.31 (s, 1H), 3.74 (s, 2H), 3.13 (s, 2H), 3.06 (s, 2H), 2.36 (t, J = 7.5 Hz, 1H), 2.17 (s, 2H), 1.72 (d, J = 11.3 Hz, 1H), 1.44−1.38 (m, 4H), 1.33−1.27 (m, 6H), 1.24 (s, 10H), 0.87 (t, J = 6.6 Hz, 3H). ^{13}C NMR (101 MHz, CDCl$_3$) δ 182.15, 179.13, 156.34, 149.98, 130.06, 128.67, 127.09, 115.85, 91.92, 61.98, 52.57, 48.04, 34.36, 32.01, 29.78, 29.73, 29.71, 29.58, 29.44, 28.91, 28.22, 22.78, 22.76, 14.23. HRMS (TOF, ES+) calcd for C$_{30}$H$_{44}$N$_2$O$_3$ + H$^+$, 481.3425; found, 481.3434.

2-Hydroxy-5-((1-(3-nitrobenzyl)piperidin-4-yl)amino)-3-undecylcyclohexa-2,5-diene-1,4-dione (**15b**). Yield: 68%; wine-red solid; m.p. 100−102 °C; IR (ν_{max}): 3435, 2923, 2852, 1638, 1599, 1530, 1497, 1384, 1221, 1087 cm^{-1}. ^{1}H NMR (400 MHz, CDCl$_3$) δ 8.20 (s, 1H), 8.12 (d, J = 8.3 Hz, 1H), 7.66 (d, J = 7.9 Hz, 1H), 7.50 (t, J = 7.9 Hz, 1H), 6.36 (d, J = 8.1 Hz, 1H), 5.36 (s, 1H), 3.61 (s, 2H), 3.31 (d, J = 8.0 Hz, 1H), 2.83 (d, J = 12.1 Hz, 2H), 2.39−2.34 (m, 2H), 2.22 (t, J = 10.4 Hz, 2H), 2.00 (d, J = 9.9 Hz, 2H), 1.68−1.61 (m, 2H), 1.43 (t, J = 7.6 Hz, 2H), 1.32−1.27 (m, 6H), 1.24 (s, 10H), 0.88−

0.85 (m, 3H). ^{13}C NMR (101 MHz, CDCl$_3$) δ 182.58, 178.88, 155.11, 148.50, 148.46, 140.70, 134.92, 129.35, 123.69, 122.45, 116.00, 91.99, 61.97, 51.77, 49.67, 32.00, 30.96, 29.76, 29.71, 29.67, 29.54, 29.43, 28.16, 22.78, 22.76, 14.22. HRMS (TOF, ES+) calcd for C$_{29}$H$_{41}$N$_3$O$_4$ + H$^+$, 512.3119; found, 512.3127.

2-Hydroxy-5-(((1-(4-nitrobenzyl)piperidin-4-yl)methyl)amino)-3-undecylcyclohexa-2,5-diene-1,4-dione (15c). Yield: 62%; wine-red sticky solid; IR (ν_{max}): 3432, 2924, 2851, 1590, 1530, 1497, 1384, 1221, 1081 cm^{-1}. ^{1}H NMR (400 MHz, CDCl$_3$) δ 8.16 (d, J = 8.4 Hz, 2H), 7.49 (d, J = 8.4 Hz, 2H), 6.52 (t, J = 6.1 Hz, 1H), 5.33 (s, 1H), 3.99 (s, 2H), 3.07 (t, J = 6.2 Hz, 2H), 2.88 (d, J = 11.1 Hz, 2H), 2.38–2.34 (m, 2H), 2.02 (t, J = 11.9 Hz, 2H), 1.71 (d, J = 12.3 Hz, 3H), 1.44–1.34 (m, 4H), 1.31–1.25 (m, 6H), 1.23 (s, 10H), 0.87–0.84 (m, 3H). ^{13}C NMR (101 MHz, CDCl$_3$) δ 182.48, 178.92, 155.46, 149.87, 147.25, 146.27, 129.57, 123.62, 115.87, 91.86, 62.32, 53.31, 48.41, 35.07, 31.99, 30.10, 29.75, 29.71, 29.68, 29.54, 29.42, 28.16, 22.77, 22.73, 14.21. HRMS (TOF, ES+) calcd for C$_{29}$H$_{41}$N$_3$O$_5$ + H$^+$, 526.3275; found, 526.3284.

5-(((1-(4-Fluorobenzyl)piperidin-4-yl)methyl)amino)-2-hydroxy-3-undecylcyclohexa-2,5-diene-1,4-dione (15d). Yield: 70%; wine-red solid; m.p. 92–94 °C; IR (ν_{max}): 3435, 2924, 2853, 1592, 1384, 1227 cm^{-1}. ^{1}H NMR (400 MHz, CDCl$_3$) δ 7.27 (t, J = 7.1 Hz, 2H), 7.00 (t, J = 8.7 Hz, 2H), 6.51 (s, 1H), 5.32 (s, 1H), 3.52 (s, 2H), 3.06 (t, J = 6.2 Hz, 2H), 2.95 (d, J = 11.3 Hz, 2H), 2.39–2.35 (m, 2H), 2.01 (t, J = 11.7 Hz, 2H), 1.71 (d, J = 12.3 Hz, 3H), 1.44–1.37 (m, 4H), 1.32–1.27 (m, 6H), 1.24 (s, 10H), 0.87 (t, J = 6.7 Hz, 3H). ^{13}C NMR (101 MHz, CDCl$_3$) δ 181.66, 179.57, 162.70 (d, J = 247.3 Hz), 157.55, 150.26, 132.08, 132.00, 129.56, 115.84, 115.71, 115.50, 91.97, 60.94, 52.05, 47.90, 34.26, 31.99, 29.76, 29.71, 29.59, 29.42, 28.48, 28.27, 22.76, 14.21. HRMS (TOF, ES+) calcd for C$_{29}$H$_{41}$FN$_2$O$_3$ + H$^+$, 499.3336; found, 499.3338.

2-Hydroxy-5-(((1-(2-(trifluoromethyl)benzyl)piperidin-4-yl)methyl)amino)-3-undecylcyclohexa-2,5-diene-1,4-dione (15e). Yield: 71%; wine-red solid; m.p. 96–98 °C; IR (ν_{max}): 3351, 2924, 2853, 1594, 1456, 1384, 1313, 1220, 1172, 1121 cm^{-1}. ^{1}H NMR (400 MHz, CDCl$_3$) δ 7.73 (s, 1H), 7.64 (d, J = 7.8 Hz, 1H), 7.53 (t, J = 7.9 Hz, 1H), 7.38 (t, J = 7.4 Hz, 1H), 6.54 (s, 1H), 5.34 (s, 1H), 3.85 (s, 2H), δ 3.06 (d, J = 6.5 Hz, 3H), δ 2.37 (t, J = 7.6 Hz, 2H), 2.22 (d, J = 11.7 Hz, 2H), 1.70 (d, J = 12.7 Hz, 3H), 1.47–1.39 (m, 3H), 1.32–1.28 (m, 6H), 1.24 (s, 10H), 0.87 (t, J = 6.8 Hz, 3H). ^{13}C NMR (101 MHz, CDCl$_3$) δ 182.48, 178.90, 155.27, 149.82, 132.33, 130.82, 128.09, 126.61 (d, J = 124.8 Hz), 116.48, 115.92, 115.66, 91.91, 57.97, 53.23, 48.10, 52.01, 29.79, 29.76, 29.72, 29.69, 29.60, 29.55, 29.44, 28.35, 28.17, 22.78, 22.74, 14.22. HRMS (TOF, ES+) calcd for C$_{31}$H$_{41}$F$_3$N$_2$O$_3$ + H$^+$, 549.3299; found, 549.3304.

In Vitro AChE and BChE Inhibition Assay. Inhibition of EeAChE, hAChE, eqBChE, and hBChE by test compounds was determined using the Ellman assay[27] as described in our earlier publications.[29,30] Mode of inhibition and enzyme inhibitory constants for inhibition of hAChE and hBChE were determined by performing kinetic studies as described earlier.[29,30]

Fluorescence Resonance Energy Transfer (FRET) Assay for hBACE-1 Inhibition. The inhibitory potential of the test compounds against the recombinant human hBACE-1 enzyme was determined by a fluorescence-based FRET assay, as described in our earlier publications.[29,30]

DPPH Radical Scavenging Activity. Methanolic solutions of 20 μL of test compound and 180 μL of 80 μM DPPH were mixed in a 96-well plate and incubated in the dark for 30 min at room temperature. The absorbance of the wells was recorded at 517 nm using a microplate reader, and the percentage scavenging effect was determined using the equation $100[(A_c - A_t)/A_c]$, where A_c and A_t represent the absorbance of untreated DPPH and test compound-treated wells, respectively.[30]

ABTS Radical Scavenging Activity. Aqueous ABTS solution (7 mM) was prepared and reacted with 2.45 mM of potassium persulfate solution, followed by incubation in the dark at room temperature for 14 h. One milliliter of this solution was diluted with 60 mL of methanol to obtain an absorbance of 0.706 ± 0.001 units at 734 nm. Then, 100 μL of test compound solution was added to 100 μL of

reagent solution in a 96-well plate, shaken for 10 s, and incubated for 7 min in the dark at room temperature. The absorbance of the wells was recorded at 734 nm using a microplate reader, and the percentage scavenging effect was determined using the equation $100[(A_c - A_t)/A_c]$, where A_c and A_t represent the absorbance of the control and test compound-treated wells, respectively.[31]

In Vitro BBB Permeability Assay. Passive BBB permeability of the test compounds was performed by parallel artificial membrane permeability assay (PAMPA). The stock solutions of test compounds in dimethyl sulfoxide (DMSO) (5 mg/mL) were further diluted with PBS (pH 7.4) to get 100 μg/mL concentration. Four milliliters of 20 mg/mL PBL in dodecane was coated on the filter membranes of a donor plate and was carefully placed on the acceptor plate, which was filled with 0.3 mL of PBS in each well to form a sandwich. Then, 0.2 mL of test compound solution was added to the donor plate wells, and the entire setup was left undisturbed for 18 h at 25 °C. The absorbance of both plates was recorded using a microplate reader, and the effective permeability was calculated as described earlier.[33]

Aqueous Solubility. As described earlier, the solubility of the synthesized compounds in water was determined by the miniaturized shake flask method.[30,33]

Aβ42 Self-Aggregation Inhibition Assay. The potential of the test compounds to inhibit the self-aggregation of amyloid β 1–42 rat peptide was determined following the same protocol described in our earlier publication.[35] The dose–response was performed using five test concentrations (0.1, 0.5, 1, 5, and 20 μM) of embelin and 9j, and EC$_{50}$ was determined using GraphPad Prism 8.0.2 software.

Molecular Docking, MD Simulation, and QikProp Properties. The docking studies were performed as described earlier[35,34] using the crystal structures of human AChE (PDB ID: 4EY7), human BChE (PDB ID: 6EP4), human BACE-1 (PDB ID: 1W51), and the amyloid β monomer (PDB ID: 1Z0Q) retrieved from RCSB-PD. Further, MD simulation studies were performed for a period of 200 ns using Desmond software (v3.8) under default conditions in the same way as described earlier.[30,35] The ADME properties of ligands were calculated using the QikProp module of Schrödinger software.

In Vitro Cytotoxicity Studies. The colorimetric MTT assay was used to determine cell viability. SH-SY5Y and N2a cells were purchased from ATCC. Cells were seeded in 96-well plates at the density of 7 × 10^3 cells per well and cultured at 37 °C in a 5% CO$_2$ and 95% humidified incubator using DMEM as a nutrient medium. Compound 9j was dissolved in a mixture of 1-methyl-2-pyrrolidinone (NMP) and purified water and further diluted with a fresh culture medium. After 24 h, media was removed from cultured cells, replaced with new media containing different concentrations of test compounds, and incubated for another 24 h. The final concentration of NMP in every well in the final dilution was less than 0.1%, including the control. The cells were incubated with the 0.5 mg/mL MTT dye for 4 h. After removing MTT from the wells, the formazan crystals were dissolved in DMSO and shook the plate for 15 min. To calculate the amount of dissolved formazan, absorbance readings were recorded at 570 nm using a TECAN plate reader. Further, the protective effect of 9j against scopolamine-induced cytotoxicity was determined.[36,37] Cells were co-treated with scopolamine (2 mM) and different concentrations of 9j (1, 0.5, 0.25, 0.125, 0.0625, 0.031, and 0.015 μM). Cell viability was measured following the above-mentioned procedure. Similarly, the protective effect of donepezil was also determined. Cell viability was expressed as the percentage of viable cells versus control cells. Data were subjected to one-way ANOVA followed by Tukey's multiple comparison test using GraphPad Prism 9.0 Software.

Metabolic Stability Study of Embelin (1) and 9j (In Vitro). The metabolic stability study of compounds 1 and 9j was performed in HLM and MLM by employing a substrate depletion approach using our earlier reported protocol.[30,39] The stock solutions of embelin (1) and 9j were prepared in methanol and chloroform, respectively. Further dilutions for both compounds were done in methanol. Briefly, phosphate buffer (0.1 M, pH 7.4) containing magnesium chloride (3.3 mM) and microsomal protein (HLM or MLM, 0.5 mg/mL) was preincubated (5 min) in a preheated shaking

water bath at 37 °C. The preincubated mixture was then spiked with the substrate (1 or 9j, 5 μM) and NADPH (1.2 mM) and incubated again in a preheated shaking water bath at 37 °C for 0, 15, and 30 min. Incubations were carried out in duplicate. Samples without NADPH at 0 and 30 min were considered as a negative control. The incubation was stopped by placing samples in a precooled thermal block and adding chilled acetonitrile (100 μL) containing chlorzoxazone (1000 ng/mL) as the internal standard (IS) for embelin (1) and diazepam (62.5 ng/mL) as IS for 9j. The samples were then vortexed for 2 min and centrifuged for 15 min at 3000 rpm. The samples were then decanted into the vials for analysis by liquid chromatography with tandem mass spectrometry (LC-MS/MS) (Table S2 of the Supporting Information). The percent substrate remaining in the samples was calculated by comparing the data obtained at 0 min and considering it as 100% of the substrate. Then, the concentration data obtained at each time point was utilized for log-linear plotting to determine various parameters for the prediction of in vivo behavior using standard equations.[103,104]

Cytochrome P450 Inhibition Studies. CYP inhibition study of 9j was performed using USFDA-recommended CYP substrates, which are phenacetin (CYP1A2), bupropion (CYP2B6), amodiaquine (CYP2C8), diclofenac (CYP2C9), S-mephenytoin (CYP2C19), dextromethorphan (CYP2D6), and testosterone (CYP3A4) using earlier reported protocols.[92,105] The positive controls were fluvoxamine (0.0025–5 μM), ticlopidine (0.01–25 μM), quercetin (0.1–25 μM), sulfaphenazole (0.025–2.5 μM), tranylcypromine (0.1–50 μM), quinidine (0.01–10 μM), and ketoconazole (0.005–10 μM) for CYP1A2, CYP2B6, CYP2C8, CYP2C9, CYP2C19, CYP2D6, and CYP3A4, respectively. The reaction mixture consisted of phosphate buffer, MgCl₂, substrate (CYP specific), positive control (CYP specific) or 9j, protein (HLM), and NADPH. The reaction was started by adding NADPH and incubating it in a shaking water bath at 37 °C for a specific time. After the particular incubation time, quenching of the reaction was done by placing the sample tubes in the thermal block and adding ice-cold acetonitrile (100 μL) with or without an internal standard. Samples were vortex mixed, centrifuged (3000 rpm, 15 min), decanted into inner vials, and quantified by LC-MS/MS using a matrix match calibration curve for individual metabolites. The study protocol for individual CYP inhibition studies is described in Table S1. The reaction was carried out in triplicate. Data were fitted into software (GraphPad Prism) for the calculation of the inhibitory potential of 9j.

Pharmacokinetic and Brain Distribution Study of 9j (In Vivo). The pharmacokinetic study of 9j was performed in male Swiss albino mice following our previously reported protocols.[103,104] The approval to carry out the in vivo study was taken prior from our Institutional Animal Ethics Committee (IAEC No. 255/79/8/2021). A total of 50 animals were fasted overnight (10 h) with free access to water, and on the day of the experiment, these were randomly allocated to 10 groups to cover all of the sampling time points. Each group was composed of five animals (n = 5). 9j was administered at the dose level and dose volume of 30 mg/kg and 10 mL/kg, respectively. The dose was prepared freshly with 2% 1-methyl-2-pyrrolidinone, 30% solutol HS-15, and 68% purified water (v/v). The dose was administered orally. Blood was retrieved from the retro-orbital plexus of mice into the tubes with an anticoagulant at 0 (predose), 0.25, 0.5, 1, 1.5, 2, 3, 4, 8, and 24 h. Plasma was separated by centrifugation (8000 rpm, 10 min) and stored (−80 °C). Immediately after the blood was collected, the animals were sacrificed using carbon dioxide euthanasia, followed by cervical dislocation. The animals at each time point were dissected, and the brain was obtained. The brain was cleaned using washing with ice-cold normal saline, dried using blotting paper, and stored (−80 °C). The individual brain homogenate was prepared in phosphate buffer (10 mM, pH 7.4) at a level of 250 mg/mL. Plasma or brain homogenate samples (50 μL) were processed using diethyl ether (200 μL) containing diazepam (62.5 ng/mL) as IS, and estimation of 9j was done in LC-MS/MS using the matrix match calibration curve, which was prepared by spiking known concentration of 9j in the blank plasma and blank brain homogenate. All of the obtained concentration data were used

further to calculate the PK parameters by a noncompartmental method using PK Solution software. The LC-MS conditions are listed in Table S2 of the Supporting Information.

The brain-to-plasma concentration ratio was calculated using the formula

$$Kp, \text{brain} = C_{\text{brain}}/(C_{\text{plasma}} \times \rho_{\text{brain}})$$

where C_{brain} and C_{plasma} are the concentration of the molecule in the brain and blood. ρ_{brain} is the density of brain tissue = 1.04 g/mL.[103,104]

In Vivo Anti-dementia Study in C57BL/6J Mice. The Morris Water Maze (MWM) test was carried out in C57BL/6J mice. The approval to carry out the in vivo study was taken prior from our Institutional Animal Ethics Committee (IAEC No. 287/303/2/2022). Before starting the experiment, 30 mice were trained for 3 days, having three trials per day to reach the hidden platform. After completing the training, animals were randomized according to their body weight into five groups (six animals per group), i.e., control, scopolamine, donepezil, 9j (15 mg/kg), and 9j (30 mg/kg) for the experiments. Except for the control group, all four groups were given the i.p. dose of scopolamine (2 mg/kg) 30 min before the trial for six consecutive days. On the 7 day, the control group was given a vehicle, and the groups, i.e., donepezil (1 mg/kg), 9j (15 mg/kg), and 9j (30 mg/kg), were administered orally with the dosing volume of 10 mL/kg 3 h before the trial. Scopolamine (2 mg/kg) was administered to all of the groups except for the control group. Thirty minutes post scopolamine administration, animals were subjected to the Morris Water Maze and recorded the movement of animals with automated ANY-maze software using a camera. A similar experiment was conducted on the eighth and ninth days. After the MWM experiment, animals from all of the groups were sacrificed by cervical dislocation, and the brains were quickly isolated and washed with cold saline. Brains were homogenized using 0.1 M phosphate buffer, pH 7.2 (10% w/v), centrifuged for 10 min at 4500 rpm, and the supernatants were collected and used to measure the activity of AChE in units/mL (U/mL) using the Ellman method. The statistical significance of the data was determined by GraphPad software 9.0.0 (121), Tukey's multiple comparisons test. Mean ± SEM, the * and ns represent the p-value by Tukey's multiple comparisons test, *p < 0.05; ns p > 0.05.

■ ASSOCIATED CONTENT

⦿ Supporting Information

The Supporting Information is available free of charge at https://pubs.acs.org/doi/10.1021/acschemneuro.3c00030.

> Scanned copies of ¹H, ¹³C, DEPT135 NMR spectra and HRMS (or) HPLC purity of all compounds (Section S1); protocols for CYP inhibition studies of SB-1448 (9j) (Section S2; Table S1); time-frame analysis in MD simulation (Section S3; Figure S1); time-frame analysis at different intervals for AChE interaction (Figure S2), time-frame analysis for BChE interaction (Figure S3); time-frame analysis at different intervals for BACE-1 interaction; 2D NMR data of 4a (Section S4); molecular modeling image showing the orientation of embelin and 9j in the AChE active site (Section S5); main LC and MS conditions for quantification of SBN-61 (1) and SB-1448 (9j) in in vitro (metabolic stability) or in vivo (pharmacokinetics) study samples (Section S6; Table S2); and in silico ADME properties of embelin and 9j (Section S7; Table S3) (PDF)

■ AUTHOR INFORMATION

Corresponding Author

Sandip B. Bharate − Natural Products & Medicinal Chemistry Division, CSIR-Indian Institute of Integrative Medicine, Jammu 180001, India; Academy of Scientific & Innovative Research (AcSIR), Ghaziabad 201002, India;

• orcid.org/0000-0001-6081-5787; Phone: +91-191-2586333; Email: sbharate@iiim.res.in, sandipbharate@gmail.com

Authors

Vijay K. Nuthakki – *Natural Products & Medicinal Chemistry Division, CSIR-Indian Institute of Integrative Medicine, Jammu 180001, India; Academy of Scientific & Innovative Research (AcSIR), Ghaziabad 201002, India;* • orcid.org/0000-0002-7454-1948

Sushil Choudhary – *Pharmacology Division, CSIR-Indian Institute of Integrative Medicine, Jammu 180001, India; Academy of Scientific & Innovative Research (AcSIR), Ghaziabad 201002, India*

Chilakala N. Reddy – *Natural Products & Medicinal Chemistry Division, CSIR-Indian Institute of Integrative Medicine, Jammu 180001, India; Academy of Scientific & Innovative Research (AcSIR), Ghaziabad 201002, India*

Shipra Bhatt – *Pharmacology Division, CSIR-Indian Institute of Integrative Medicine, Jammu 180001, India; Academy of Scientific & Innovative Research (AcSIR), Ghaziabad 201002, India*

Ashiya Jamwal – *Pharmacology Division, CSIR-Indian Institute of Integrative Medicine, Jammu 180001, India; Academy of Scientific & Innovative Research (AcSIR), Ghaziabad 201002, India*

Anshika Jotshi – *Pharmacology Division, CSIR-Indian Institute of Integrative Medicine, Jammu 180001, India*

Rinky Raghuvanshi – *Natural Products & Medicinal Chemistry Division, CSIR-Indian Institute of Integrative Medicine, Jammu 180001, India; Academy of Scientific & Innovative Research (AcSIR), Ghaziabad 201002, India*

Ankita Sharma – *Natural Products & Medicinal Chemistry Division, CSIR-Indian Institute of Integrative Medicine, Jammu 180001, India; Academy of Scientific & Innovative Research (AcSIR), Ghaziabad 201002, India*

Shikha Thakur – *Department of Pharmacy, Birla Institute of Technology and Sciences Pilani, Pilani 333031 Rajasthan, India*

Hemant R. Jadhav – *Department of Pharmacy, Birla Institute of Technology and Sciences Pilani, Pilani 333031 Rajasthan, India*

Sonali S. Bharate – *Shobhaben Pratapbhai Patel School of Pharmacy & Technology Management, SVKM's NMIMS, Mumbai 400056, India;* • orcid.org/0000-0001-7267-5080

Utpal Nandi – *Pharmacology Division, CSIR-Indian Institute of Integrative Medicine, Jammu 180001, India; Academy of Scientific & Innovative Research (AcSIR), Ghaziabad 201002, India;* • orcid.org/0000-0002-7868-0240

Ajay Kumar – *Pharmacology Division, CSIR-Indian Institute of Integrative Medicine, Jammu 180001, India; Academy of Scientific & Innovative Research (AcSIR), Ghaziabad 201002, India*

Complete contact information is available at:
https://pubs.acs.org/10.1021/acschemneuro.3c00030

Author Contributions

S.B.B. designed, executed, and coordinated this study; V.K.N. and C.N.R. synthesized compounds; V.K.N., R.R., and A.S. performed *in vitro* biological evaluations and molecular docking; S.T. performed MD simulation studies, and H.R.J. monitored and interpreted MD results. S.S.B. performed solubility studies; U.N. designed and monitored metabolic stability and PK studies; S.B. and A. Jamwal carried out metabolic stability and PK studies; A.K. designed and monitored cell line and *in vivo* anti-dementia studies; S.C. and A. Jotshi performed cell line and *in vivo* anti-dementia studies; V.K.N. and S.B.B. contributed to the manuscript writing.

Notes

The authors declare no competing financial interest.

■ ABBREVIATIONS USED

$A\beta$, amyloid β; ABTS, 2,2'-azino-bis(3-ethylbenzothiazoline-6-sulfonic acid); AChE, acetylcholinesterase; ACh, acetylcholine; AD, Alzheimer's disease; ANOVA, analysis of variance; ATChI, acetyl thiocholine iodide; AUC, area under curve; BACE-1, β-site amyloid precursor protein clearing enzyme 1; BBB, blood–brain barrier; BChE, butyrylcholinesterase; BTChI, S-butyrylthiocholine iodide; CAS, catalytic anionic site; CIs, cholinesterase inhibitors; Cl, clearance; C_{max}, maximum concentration; DMEM, Dulbecco's modified Eagle's medium; DPPH, 2,2-diphenyl-1-picrylhydrazyl; EeAChE, acetylcholinesterase from *Electrophorus electricus* (electric eel); eqBChE, equine serum butyrylcholinesterase; HLM, human liver microsomes; K_m, Michaelis–Menten constant; k_i, inhibition constant; MLM, mouse liver microsomes; MRT, mean residence time; MTDLs, multitarget directed ligands; MWM, Morris water maze; NPs, natural products; NFTs, neurofibrillary tangles; PAMPA, parallel artificial membrane permeability assay; PAS, peripheral anionic site; PDB, Protein Data Bank; PK, pharmacokinetics; hAChE, recombinant human acetylcholinesterase; SAM, Swiss albino mice; SD, standard deviation; $T_{1/2}$, half-life; T_{max}, time to peak drug concentration; V_d, volume of distribution; V_{max}, maximum rate of reaction (the rate of reaction when the enzyme is saturated with the substrate)

■ REFERENCES

(1) Dementia Fact Sheet, 2022. https://www.who.int/news-room/fact-sheets/detail/dementia.

(2) GBD 2019 Collaborators. Global mortality from dementia: Application of a new method and results from the Global Burden of Disease Study 2019. *Alzheimer's Dementia* **2021**, 7, No. e12200.

(3) Scheltens, P.; De Strooper, B.; Kivipelto, M.; Holstege, H.; Chételat, G.; Teunissen, C. E.; Cummings, J.; van der Flier, W. M. Alzheimer's disease. *Lancet* **2021**, 397, 1577–1590.

(4) Knopman, D. S.; Amieva, H.; Petersen, R. C.; Chételat, G.; Holtzman, D. M.; Hyman, B. T.; Nixon, R. A.; Jones, D. T. Alzheimer disease. *Nat. Rev. Dis. Primers* **2021**, 7, No. 33.

(5) Karran, E.; De Strooper, B. The amyloid hypothesis in Alzheimer disease: new insights from new therapeutics. *Nat. Rev. Drug Discovery* **2022**, 21, 306–318.

(6) Rabinovici, G. D. Controversy and Progress in Alzheimer's Disease - FDA Approval of Aducanumab. *N. Engl. J. Med.* **2021**, 385, 771–774.

(7) Alexander, G. C.; Karlawish, J. The Problem of Aducanumab for the Treatment of Alzheimer Disease. *Ann. Intern. Med.* **2021**, 174, 1303–1304.

(8) Petersen, R. C.; Aduncumah; What about the Patient? Ann. Neurol. 2021, 90, 334—335.

(9) de Freitas Silva, M.; Dias, K. S. T.; Gontijo, V. S.; Ortiz, C. J. C.; Viegas, C., Jr. Multi-Target Directed Drugs as a Modern Approach for Drug Design Towards Alzheimer's Disease: An Update. Curr. Med. Chem. 2018, 25, 3491—3525.

(10) González, J. F.; Alcántara, A. R.; Doadrio, A. L.; Sánchez-Montero, J. M. Developments with multi-target drugs for Alzheimer's disease: an overview of the current discovery approaches. Expert Opin. Drug Discovery 2019, 14, 879—891.

(11) Dos Santos Picanco, L. C.; Ozela, P. F.; de Fatima de Brito Brito, M.; Pinheiro, A. A.; Padilha, E. C.; Braga, F. S.; de Paula da Silva, C. H. T.; Dos Santos, C. B. R.; Rosa, J. M. C.; da Silva Hage-Melim, L. I. Alzheimer's Disease: A Review from the Pathophysiology to Diagnosis, New Perspectives for Pharmacological Treatment. Curr. Med. Chem. 2018, 25, 3141—3159.

(12) Selkoe, D. J. Treatments for Alzheimer's disease emerge. Science 2021, 373, 624—626.

(13) Golde, T. E.; DeKosky, S. T.; Galasko, D. Alzheimer's disease: The right drug, the right time. Science 2018, 362, 1250—1251.

(14) Arnsten, A. F. T.; Datta, D.; Del Tredici, K.; Braak, H. Hypothesis: Tau pathology as an initiating factor in sporadic Alzheimer's disease. Alzheimer's Dementia 2021, 17, 115—124.

(15) Kumar, A.; Singh, A.; Ekavali. A review on Alzheimer's disease pathophysiology and its management: an update. Pharmacol. Rep. 2015, 67, 195—203.

(16) Marucci, G.; Buccioni, M.; Ben, D. D.; Lambertucci, C.; Volpini, R.; Amenta, F. Efficacy of acetylcholinesterase inhibitors in Alzheimer's disease. Neuropharmacology 2021, 190, No. 108352.

(17) Terry, A. V., Jr.; Buccafusco, J. J. The cholinergic hypothesis of age and Alzheimer's disease-related cognitive deficits: recent challenges and their implications for novel drug development. J. Pharmacol. Exp. Ther. 2003, 306, 821—827.

(18) Ferreira-Vieira, T. H.; Guimaraes, I. M.; Silva, F. R.; Ribeiro, F. M. Alzheimer's disease: Targeting the Cholinergic System. Curr. Neuropharmacol. 2016, 14, 101—115.

(19) Chen, G.-f.; Xu, T.-h.; Yan, Y.; Zhou, Y.-r.; Jiang, Y.; Melcher, K.; Xu, H. E. Amyloid beta: structure, biology and structure-based therapeutic development. Acta Pharmacol. Sin. 2017, 38, 1205—1235.

(20) Hardy, J.; Selkoe, D. J. The amyloid hypothesis of Alzheimer's disease: progress and problems on the road to therapeutics. Science 2002, 297, 353—356.

(21) Rossi, M.; Freschi, M.; de Camargo Nascente, L.; Salerno, A.; de Melo Viana Teixeira, S.; Nachon, F.; Chantegreil, F.; Soukup, O.; Prchal, L.; Malaguti, M.; Bergamini, C.; Bartolini, M.; Angeloni, C.; Hrelia, S.; Soares Romeiro, L. A.; Bolognesi, M. L. Sustainable Drug Discovery of Multi-Target-Directed Ligands for Alzheimer's Disease. J. Med. Chem. 2021, 64, 4972—4990.

(22) Ramalakshmi, N.; Remya, R. S.; Nalini, C. N. Multitarget Directed Ligand Approaches for Alzheimer's Disease: A Comprehensive Review. Mini Rev. Med. Chem. 2021, 21, 2361—2388.

(23) Maramai, S.; Benchekroun, M.; Gabr, M. T.; Yahiaoui, S. Multitarget Therapeutic Strategies for Alzheimer's Disease: Review on Emerging Target Combinations. Biomed. Res. Int. 2020, 2020, No. 5120230.

(24) Bharate, S. S.; Mignani, S.; Vishwakarma, R. A. Why Are the Majority of Active Compounds in the CNS Domain Natural Products? A Critical Analysis. J. Med. Chem. 2018, 61, 10345—10374.

(25) Bocci, A.; Runfola, M.; Sestito, S.; Rapposelli, S. Beyond Antioxidant Effects: Nature-Based Templates Unveil New Strategies for Neurodegenerative Diseases. Antioxidants 2021, 10, No. 367.

(26) Atanasov, A. G.; Zotchev, S. B.; Dirsch, V. M.; International Natural Product Sciences Taskforce, T.; Supuran, C. T. Natural products in drug discovery: advances and opportunities. Nat. Rev. Drug Discovery 2021, 20, 200—216.

(27) Wani, A.; Al Rihani, S. B.; Sharma, A.; Weadick, B.; Govindarajan, R.; Khan, S. U.; Sharma, P. R.; Dogra, A.; Nandi, U.; Reddy, C. N.; Bharate, S. S.; Singh, G.; Bharate, S. B.; Vishwakarma, R. A.; Kaddoumi, A.; Kumar, A. Crocetin promotes clearance of

amyloid-beta by inducing autophagy via the STK11/LKB1-mediated AMPK pathway. Autophagy 2021, 17, 3813—3832.

(28) Augustin, N.; Nuthakki, V. K.; Abdullaha, M.; Hassan, Q. P.; Gandhi, S. G.; Bharate, S. B. Discovery of Helminthosporin, an Anthraquinone Isolated from Rumex abyssinicus Jacq as a Dual Cholinesterase Inhibitor. ACS Omega 2020, 5, 1616—1624.

(29) Nuthakki, V. K.; Sharma, A.; Kumar, A.; Bharate, S. B. Identification of embelin, a 3-undecyl-1,4-benzoquinone from Embelia ribes as a multitargeted anti-Alzheimer agent. Drug Dev. Res. 2019, 80, 655—565.

(30) Yadav, R. R.; Sharma, S.; Joshi, P.; Wani, A.; Vishwakarma, R. A.; Kumar, A.; Bharate, S. B. Meridianin derivatives as potent Dyrk1A inhibitors and neuroprotective agents. Bioorg. Med. Chem. Lett. 2015, 25, 2948—2952.

(31) Bharate, S. S.; Kumar, V.; Singh, G.; Singh, A.; Gupta, M.; Singh, D.; Kumar, A.; Vishwakarma, R. A.; Bharate, S. B. Preclinical Development of Crocus sativus-Based Botanical Lead IIIM-141 for Alzheimer's Disease: Chemical Standardization, Efficacy, Formulation Development, Pharmacokinetics, and Safety Pharmacology. ACS Omega 2018, 3, 9572—9585.

(32) Sharma, A.; Nuthakki, V. K.; Gairola, S.; Singh, B.; Bharate, S. B. A Coumarin-Donepezil Hybrid as a Blood-Brain Barrier Permeable Dual Cholinesterase Inhibitor: Isolation, Synthetic Modifications, and Biological Evaluation of Natural Coumarins. ChemMedChem 2022, 17, No. e202200300.

(33) Nuthakki, V. K.; Yadav Bheemanaboina, R. R.; Bharate, S. B. Identification of aplysinopsin as a blood-brain barrier permeable scaffold for anti-cholinesterase and anti-BACE-1 activity. Bioorg. Chem. 2021, 107, No. 104568.

(34) Raghuvanshi, R.; Jamwal, A.; Nandi, U.; Bharate, S. B. Multitargeted C9-substituted ester and ether derivatives of berberrubine for Alzheimer's disease: Design, synthesis, biological evaluation, metabolic stability, and pharmacokinetics. Drug Dev. Res. 2023, 84, 121—140.

(35) Raghuvanshi, R.; Nuthakki, V. K.; Singh, L.; Singh, B.; Bharate, S. S.; Bhatti, R.; Bharate, S. B. Identification of plant-based multitargeted leads for Alzheimer's disease: In-vitro and in-vivo validation of Woodfordia fruticosa (L.) Kurz. Phytomedicine 2021, 91, No. 153659.

(36) Bhuvanendran, S.; Hanapi, N. A.; Ahemad, N.; Othman, I.; Yusof, S. R.; Shaikh, M. F. Embelin, a Potent Molecule for Alzheimer's Disease: A Proof of Concept From Blood-Brain Barrier Permeability, Acetylcholinesterase Inhibition and Molecular Docking Studies. Front. Neurosci. 2019, 13, No. 495.

(37) Bhuvanendran, S.; Pandel, Y. N.; Kumari, Y.; Othman, I.; Shaikh, M. F. Embelin prevents amyloid-beta accumulation via modulation of SOD1 in a Streptozotocin-induced AD-like condition: An evidence from in vitro investigation. Curr. Res. Neurobiol. 2022, 3, No. 100032.

(38) Bhuvanendran, S.; Kumari, Y.; Othman, I.; Shaikh, M. F. Amelioration of Cognitive Deficit by Embelin in a Scopolamine-Induced Alzheimer's Disease-Like Condition in a Rat Model. Front. Pharmacol. 2018, 9, No. 665.

(39) Aniza, R.; Deshmukh, B. Embelin Attenuates Intracerebroventricular Streptozotocin-Induced Behavioral, Biochemical, and Neurochemical Abnormalities in Rats. Mol. Neurobiol. 2017, 54, 6670—6680.

(40) Mahendran, S.; Thippeswamy, B. S.; Veerapur, V. P.; Badami, S. Anticonvulsant activity of embelin isolated from Embelia ribes. Phytomedicine 2011, 18, 186—188.

(41) Joshi, R.; Kamat, J. P.; Mukherjee, T. Free radical scavenging reactions and antioxidant activity of embelin: biochemical and pulse radiolytic studies. Chem. Biol. Interact. 2007, 167, 125—134.

(42) Caruso, F.; Rossi, M.; Kaur, S.; Garcia-Villar, E.; Molasky, N.; Belli, S.; Sitek, J. D.; Gionfra, F.; Pedersen, J. Z.; Incerpi, S. Antioxidant Properties of Embelin in Cell Culture. Electrochemistry and Theoretical Mechanism of Scavenging. Potential Scavenging of Superoxide Radical through the Cell Membrane. Antioxidants 2020, 9, No. 382.

(43) Silva, R. L.; Demarque, D. P.; Dusi, R. G.; Sousa, J. P. B.; Albernaz, L. C.; Espindola, L. S. Residual Larvicidal Activity of Quinones against Aedes aegypti. Molecules 2020, 25, No. 3978.

(44) Khare, T.; Palakurthi, S. S.; Shah, B. M.; Palakurthi, S.; Khare, S. Natural Product-Based Nanomedicine in Treatment of Inflammatory Bowel Disease. Int. J. Mol. Sci. 2020, 21, No. 3956.

(45) Sheng, Z.; Ge, S.; Gao, M.; Jian, R.; Chen, X.; Xu, X.; Li, D.; Zhang, K.; Chen, W. H. Synthesis and Biological Activity of Embelin and its Derivatives: An Overview. Mini Rev. Med. Chem. 2020, 20, 396−407.

(46) Badu, N. J.; Basavarajaiah, S. M.; Baskaran, S.; Kumar, P. A comprehensive insight on the biological potential of embelin and its derivatives. Nat. Prod. Res. 2022, 36, 3054−3068.

(47) Li, Z.; Chen, S. J.; Yu, X. A.; Li, J.; Gao, X. M.; He, J.; Chang, Y. X. Pharmacokinetic and Bioavailability Studies of Embelin after Intravenous and Oral Administration to Rats. Evidence-Based Complementary Altern. Med. 2019, 2019, No. 9682495.

(48) Obaid, R. J.; Naeem, N.; Mughal, E. U.; Al-Rooqi, M. M.; Sadiq, A.; Jassas, R. S.; Moussa, Z.; Ahmed, S. A. Inhibitory potential of nitrogen, oxygen and sulfur containing heterocyclic scaffolds against acetylcholinesterase and butyrylcholinesterase. RSC Adv. 2022, 12, 19764−19855.

(49) Midiwo, J. O.; Arot, L. M. New Dialkyl Benzoquinones from Fruits of Myrsine africana L. and Maesa lanceolata. Fresh. Nat. Prod. Lett. 1996, 8, 11−14.

(50) Dighe, S. N.; Deora, G. S.; De la Mora, E.; Nachon, F.; Chan, S.; Parat, M. O.; Brazzolotto, X.; Ross, B. P. Discovery and Structure-Activity Relationships of a Highly Selective Butyrylcholinesterase Inhibitor by Structure-Based Virtual Screening. J. Med. Chem. 2016, 59, 7683−7689.

(51) Heller, L.; Kahnt, M.; Loesche, A.; Grabandt, P.; Schwarz, S.; Brandt, W.; Csuk, R. Amino derivatives of platanic acid act as selective and potent inhibitors of butyrylcholinesterase. Eur. J. Med. Chem. 2017, 126, 652−668.

(52) Singh, J. V.; Thakur, S.; Kumar, N.; Singh, H.; Mithu, V. S.; Singh, H.; Bhagat, K.; Gulati, H. K.; Sharma, A.; Singh, H.; Sharma, S.; Bedi, P. M. S. Donepezil-Inspired Multitargeting Indanone Derivatives as Effective Anti-Alzheimer's Agents. ACS Chem. Neurosci. 2022, 13, 733−750.

(53) Salih, E.; Chishti, S. B.; Vicedomine, P.; Cohen, S. G.; Chiara, D. C.; Cohen, J. B. Active-site peptides of acetylcholinesterase of Electrophorus electricus: labelling of His-440 by 1-bromo-[2-14C]-pinacolone and Ser-200 by tritiated diisopropyl fluorophosphate. Biochim. Biophys. Acta, Protein Struct. Mol. Enzymol. 1994, 1208, 324−331.

(54) Moorad, D.; Chunyuan, L.; Ashima, S.; Bhupendra, D.; Gregory, G. Purification and determination of the amino acid sequence of equine serum butyrylcholinesterase. Toxicol. Methods 1999, 9, 219−227.

(55) Mahendran, S.; Badami, S.; Ravi, S.; Thippeswamy, B. S.; Veerapur, V. P. Synthesis and evaluation of analgesic and anti-inflammatory activities of most active free radical scavenging derivatives of embelin-A structure-activity relationship. Chem. Pharm. Bull. 2011, 59, 913−919.

(56) Singru, B.; Minov, J.; Ochner, C. Alzheimer's Disease, Inflammation, and the Role of Antioxidants. J. Alzheimer's Dis. Rep. 2020, 4, 175−183.

(57) Kedare, S. B.; Singh, R. P. Genesis and development of DPPH method of antioxidant assay. J. Food Sci. Technol. 2011, 48, 412−422.

(58) More, G. K.; Makola, R. T. In vitro analysis of free radical scavenging activities and suppression of LPS induced ROS production in macrophage cells by Solanum aculeastrum extracts. Sci. Rep. 2020, 10, No. 6493.

(59) Cheung, J.; Rudolph, M. J.; Burshteyn, F.; Cassidy, M. S.; Gary, E. N.; Love, J.; Franklin, M. C.; Height, J. J. Structures of human acetylcholinesterase in complex with pharmacologically important ligands. J. Med. Chem. 2012, 55, 10282−10286.

(60) Wang, N.; Liu, W.; Zhou, L.; Liu, W.; Liang, X.; Liu, X.; Xu, Z.; Zhong, T.; Wu, Q.; Jiao, X.; Chen, J.; Ning, X.; Jiang, X.; Zhao, Q.

Design, Synthesis, and Biological Evaluation of Neopterol Derivatives as Triple Inhibitors of AChE/BACE1/GSK3β for the Treatment of Alzheimer's Disease. ACS Omega 2022, 7, 32131−32152.

(61) Rosenberry, T. L.; Brazzolotto, X.; Macdonald, I. R.; Wandhammer, M.; Trovaslet-Leroy, M.; Darvesh, S.; Nachon, F. Comparison of the Binding of Reversible Inhibitors to Human Butyrylcholinesterase and Acetylcholinesterase: A Crystallographic, Kinetic and Calorimetric Study. Molecules 2017, 22, No. 2098.

(62) Patel, S.; Vuillard, L.; Cleasby, A.; Murray, C. W.; Yon, J. Apo and Inhibitor Complex Structures of BACE (β-secretase). J. Mol. Biol. 2004, 343, 407−416.

(63) Yazdani, M.; Edraki, N.; Badri, R.; Khoshneviszadeh, M.; Iraji, A.; Firuzi, O. 5,6-Diphenyl triazine-thio methyl triazole hybrid as a new Alzheimer's disease modifying agents. Mol. Diversity 2020, 24, 641−654.

(64) Jang, C.; Yadav, D. K.; Subedi, L.; Venkatesan, R.; Venkanna, A.; Afzal, S.; Lee, E.; Yoo, J.; Ji, E.; Kim, S. Y.; Kim, M. H. Identification of novel acetylcholinesterase inhibitors designed by pharmacophore-based virtual screening, molecular docking and bioassay. Sci. Rep. 2018, 8, No. 14921.

(65) Fang, J.; Wu, P.; Yang, R.; Gao, L.; Li, C.; Wang, D.; Wu, S.; Liu, A. L.; Du, G. H. Inhibition of acetylcholinesterase by two genistein derivatives: kinetic analysis, molecular docking and molecular dynamics simulation. Acta Pharm. Sin. B 2014, 4, 430−437.

(66) Sharma, V.; Sharma, N.; Mahajan, S.; Kapoor, K. K.; Gupta, V. K. Synthesis, Characterization, Crystal Structure, Molecular Docking Analysis and Other Physico-Chemical Properties of (E)-2-(3,4-Dimethoxyphenyl)Quinoline. Polycyclic Aromat. Compd. 2022, 42, 7155−7177.

(67) Mahajan, S.; Slathia, N.; Nuthakki, V. K.; Bharate, S. B.; Kapoor, K. K. Malononitrile-activated synthesis and anti-cholinesterase activity of styrylquinoxalin-2(1H)-ones. RSC Adv. 2020, 10, 15966−15975.

(68) Liu, S.; Fu, R.; Cheng, X.; Chen, S. P.; Zhou, L. H. Exploring the binding of BACE-1 inhibitors using comparative binding energy analysis (COMBINE). BMC Struct. Biol. 2012, 12, No. 21.

(69) Craig, I. R.; Essex, J. W.; Spiegel, K. Ensemble docking into multiple crystallographically derived protein structures: an evaluation based on the statistical analysis of enrichments. J. Chem. Inf. Model. 2010, 50, 511−524.

(70) Ashani, Y.; Grunwald, J.; Kronman, C.; Velan, B.; Shafferman, A. Role of tyrosine 337 in the binding of huperzine A to the active site of human acetylcholinesterase. Mol. Pharmacol. 1994, 45, 555−560.

(71) Luhrs, T.; Ritter, C.; Adrian, M.; Riek-Loher, D.; Bohrmann, B.; Dobeli, H.; Schubert, D.; Riek, R. 3D structure of Alzheimer's amyloid-beta(1-42) fibrils. Proc. Natl. Acad. Sci. U.S.A. 2005, 102, 17342−17347.

(72) Hayne, D. J.; Lim, S.; Donnelly, P. S. Metal complexes designed to bind to amyloid-beta for the diagnosis and treatment of Alzheimer's disease. Chem. Soc. Rev. 2014, 43, 6701−6715.

(73) Jakubowski, J. M.; Orr, A. A.; Le, D. A.; Tamamis, P. Interactions between Curcumin Derivatives and Amyloid-beta Fibrils: Insights from Molecular Dynamics Simulations. J. Chem. Inf. Model. 2020, 60, 289−305.

(74) Xiao, Y.; Ma, B.; McElheny, D.; Parthasarathy, S.; Long, F.; Hoshi, M.; Nussinov, R.; Ishii, Y. Abeta(1-42) fibril structure illuminates self-recognition and replication of amyloid in Alzheimer's disease. Nat. Struct. Mol. Biol. 2015, 22, 499−505.

(75) Inestrosa, N. C.; Alarcón, R. Molecular interactions of acetylcholinesterase with senile plaques. J. Physiol. 1998, 92, 341−344.

(76) Inestrosa, N. C.; Alvarez, A.; Pérez, C. A.; Moreno, R. D.; Vicente, M.; Linker, C.; Casanueva, O. I.; Soto, C.; Garrido, J. Acetylcholinesterase accelerates assembly of amyloid-beta-peptides into Alzheimer's fibrils: possible role of the peripheral site of the enzyme. Neuron 1996, 16, 881−891.

(77) Johnson, G.; Moore, S. W. The peripheral anionic site of acetylcholinesterase: structure, functions and potential role in rational drug design. Curr. Pharm. Des. 2006, 12, 217−225.

(78) Brahmankar, D. M.; Jaiswal, S. N. Biopharmaceutics and Pharmacokinetics—A Treatise, 3rd ed.; Vallabh Prakashan Publications, 2015; pp 269–270.

(79) Gibaldi, M. Biopharmaceutics and Clinical Pharmacokinetics, 4th ed.; Pharmamed Press Publications, 2005; pp 155–156.

(80) Hu, H. Z.; Smith, K.; Mage, L.; Tetelbaum, P. High-throughput cytochrome P450 inhibition screening via cassette probe dosing strategy. IV. Validation of a direct injection on-line guard cartridge extraction/tandem mass spectrometry method for simultaneous CYP3A4, 2D6 and 2E1 inhibition assessment. Rapid Commun. Mass Spectrom. 2000, 14, 1943–1948.

(81) Lee, K. S.; Kim, S. K. Direct and metabolism-dependent cytochrome P450 inhibition assays for evaluating drug-drug interactions. J. Appl. Toxicol. 2013, 33, 100–108.

(82) Walsky, R. L.; Obach, R. S. Validated assays for human cytochrome P450 activities. Drug Metab. Dispos. 2004, 32, 647–660.

(83) Bothe, H. W.; Bodsch, W.; Hossmann, K. A. Relationship between specific gravity, water content, and serum protein extravasation in various types of vasogenic brain edema. Acta Neuropathol. 1984, 64, 37–42.

(84) Leithner, C.; Muller, S.; Fuchtemeier, M.; Lindauer, U.; Dirnagl, U.; Royl, G. Determination of the brain-blood partition coefficient for water in mice using MRI. J. Cereb. Blood Flow Metab. 2010, 30, 1821–1824.

(85) Yadang, F. S. A.; Nguezeye, Y.; Kom, C. W.; Betote, P. H. D.; Mamat, A.; Tchokouaha, L. R. Y.; Taiwe, G. S.; Agbor, G. A.; Bum, E. N. Scopolamine-Induced Memory Impairment in Mice: Neuroprotective Effects of Carissa edulis (Forssk.) Valh (Apocynaceae) Aqueous Extract. J. Alzheimer's Dis. 2020, 2020, No. 6372059.

(86) Nuthakki, V. K.; Mudududdla, R.; Sharma, A.; Kumar, A.; Bharate, S. B. Synthesis and biological evaluation of indoloquinoline alkaloid cryptolepine and its bromo-derivative as dual cholinesterase inhibitors. Bioorg. Chem. 2019, 90, No. 103062.

(87) Joshi, B. S.; Kamat, V. N. Benzoquinone derivatives Part II-Reaction of Primary Aromatic Amines with Embelin & Embelin di-methyl Ether. Ind. J. Chem. 1975, 13, 795–799.

(88) Joshi, B. S.; Kamat, V. N. Benzoquinone derivatives. Part I. Reactions of primary aliphatic amines with embelin (2,5-dihydroxy-3-undecyl-1,4-benzoquinone) and di-o-methylembelin. J. Chem. Soc., Perkin Trans. 1 1975, 327–332.

(89) Ellman, G. L.; Courtney, K. D.; Andres, V., Jr.; Feather-Stone, R. M. A new and rapid colorimetric determination of acetylcholinesterase activity. Biochem. Pharmacol. 1961, 7, 88–95.

(90) Patel, D. V.; Patel, N. R.; Kanhed, A. M.; Patel, S. P.; Sinha, A.; Kansara, D. D.; Mecwan, A. R.; Patel, S. B.; Upadhyay, P. N.; Patel, K. B.; Shah, D. B.; Prajapati, N. K.; Murumkar, P. R.; Patel, K. V.; Yadav, M. R. Novel Multitarget Directed Triazinoindole Derivatives as Anti-Alzheimer Agents. ACS Chem. Neurosci. 2019, 10, 3635–3661.

(91) Zheleva-Dimitrova, D.; Nedialkov, P.; Kitanov, G. Radical scavenging and antioxidant activities of methanolic extracts from Hypericum species growing in Bulgaria. Pharmacogn. Mag. 2010, 6, 74–78.

(92) Bharate, S. S.; Vishwakarma, R. A. Thermodynamic equilibrium solubility measurements in simulated fluids by 96-well plate method in early drug discovery. Bioorg. Med. Chem. Lett. 2015, 25, 1561–1567.

(93) Kumar, V.; Bharate, S. S.; Vishwakarma, R. A. Modulating lipophilicity of rohitukine via prodrug approach: Preparation, characterization, and in vitro enzymatic hydrolysis in biorelevant media. Eur. J. Pharm. Sci. 2016, 92, 203–211.

(94) Abdjullaha, M.; Nuthakki, V. K.; Bharate, S. B. Discovery of methoxy-naphthyl linked N-(1-benzylpiperidine) benzamide as a blood-brain permeable dual inhibitor of acetylcholinesterase and butyrylcholinesterase. Eur. J. Med. Chem. 2020, 207, No. 112761.

(95) Joshi, P.; McCann, G. J. P.; Sonawane, V. R.; Vishwakarma, R. A.; Chaudhuri, B.; Bharate, S. B. Identification of Potent and Selective CYP1A1 Inhibitors via Combined Ligand and Structure-Based Virtual Screening and Their in Vitro Validation in Sacchrosomes and Live Human Cells. J. Chem. Inf. Model. 2017, 57, 1309–1320.

(96) Puangmalai, N.; Thangnipon, W.; Soi-Ampornkul, R.; Suwanna, N.; Tuchinda, P.; Nobsathian, S. Neuroprotection of N-benzylcinnamide on scopolamine-induced cholinergic dysfunction in human SH-SY5Y neuroblastoma cells. Neural Regener. Res. 2017, 12, 1492–1498.

(97) Sutthprasertporn, N.; Mingchinda, N.; Fukunaga, K.; Thangnipon, W. Neuroprotection of SAK3 on scopolamine-induced cholinergic dysfunction in human neuroblastoma SH-SY5Y cells. Cytotechnology 2020, 72, 155–164.

(98) Dogra, A.; Kotwal, P.; Gour, A.; Bhatt, S.; Singh, G.; Mukherjee, D.; Nandi, U. Description of Druglike Properties of Safranal and Its Chemistry behind Low Oral Exposure. ACS Omega 2020, 5, 9885–9891.

(99) Manhas, D.; Gour, A.; Bhardwaj, N.; Sharma, D. K.; Sharma, K.; Vij, B.; Jain, S. K.; Singh, G.; Nandi, U. Pharmacokinetic Assessment of Rottlerin from Mallotus philippensis Using a Highly Sensitive Liquid Chromatography–Tandem Mass Spectrometry-Based Bioanalytical Method. ACS Omega 2021, 6, 32637–32646.

(100) Magotra, A.; Sharma, A.; Gupta, A. P.; Wazir, P.; Sharma, S.; Singh, P. P.; Tikoo, M. K.; Vishwakarma, R. A.; Singh, G.; Nandi, U. Development and validation of a highly sensitive LC-ESI-MS/MS method for estimation of IIIM-MCD-211, a novel nitrofuranyl methyl piperazine derivative with potential activity against tuberculosis: Application to drug development. J. Chromatogr. B: Anal. Technol. Biomed. Life Sci. 2017, 1060, 200–206.

(101) Magotra, A.; Gour, A.; Sharma, D. K.; Dash, A. K.; Singh, G.; Mukherjee, D.; Nandi, U. Pharmacokinetic evaluation of medicinally important synthetic N,N' diindolylmethane glucoside: Improved synthesis and metabolic stability. Bioorg. Med. Chem. Lett. 2019, 29, 1007–1011.

(102) Bhatt, S.; Manhas, D.; Kumar, V.; Gour, A.; Sharma, K.; Dogra, A.; Ojha, P. K.; Nandi, U. Effect of Myricetin on CYP2C8 Inhibition to Assess the Likelihood of Drug Interaction Using In Silico, In Vitro, and In Vivo Approaches. ACS Omega 2022, 7, 13260–13269.

(103) Magotra, A.; Sharma, A.; Singh, S.; Ojha, P. K.; Kumar, S.; Bekolla, N.; Wazir, P.; Sharma, S.; Khan, I. A.; Singh, P. P.; Vishwakarma, R. A.; Singh, G.; Nandi, U. Physicochemical, pharmacokinetic, efficacy and toxicity profiling of a potential nitrofuranyl methyl piperazine derivative IIIM-MCD-211 for oral tuberculosis therapy via in-silico-in-vitro-in-vivo approach. Pulm. Pharmacol. Ther. 2018, 48, 151–160.

(104) Sharma, A.; Magotra, A.; Dogra, A.; Rath, S. K.; Rayees, S.; Wazir, P.; Sharma, S.; Sangwan, P. L.; Singh, S.; Singh, G.; Nandi, U. Pharmacokinetics, pharmacodynamics and safety profiling of IS01957, a preclinical candidate possessing dual activity against inflammation and nociception. Regul. Toxicol. Pharmacol. 2017, 91, 216–225.